The determination of the parameters of non-linear equivalent circuits for synchronous machines and transformers

Thesis submitted for the degree of

Doctor of Philosophy,

University of London.

by

Narayan Gopal Swamy, B.E.

Department of Electrical Engineering

Imperial College of Science and Technology,

London.

August, 1964.

SYNOPSIS

The topological form of the equivalent circuit of a magnetic system can be derived from its magnetic circuit by the application of the concept of the duality of electric and magnetic circuits. This concept is employed in this thesis firstly to derive the equivalent Tee and Pi circuits of a two-winding transformer. These equivalent circuits are essentially composed of three reactances in association with an ideal transformer. In the Tee circuit, the pillar reactance is saturable while the flanking reactances are linear; in the Pi circuit, the pillar reactances are saturable while the spanning reactance is linear. Similar equivalent Tee and Pi circuits of the direct-axis of a synchronous machine are also derived.

The major part of this thesis is concerned with the experimental determination of the parameters of the two equivalent circuits of a transformer or a synchronous machine. The reactances can be determined from tests if the turns-ratios of the associated ideal transformers are specified. For the non-linear Tee circuit, the turns-ratio is unique, and can be experimentally evaluated. Novel methods of evaluating this unique turns-ratio are presented. These methods supplement the Potier method of determining the leakage reactance of an alternator. It is shown that the turns-ratio of the ideal transformer

associated with an equivalent Pi circuit can not be determined uniquely from tests. A valid equivalent Pi circuit may be determined for any specified value of turns-ratio.

The characteristics obtained by tests on an induction motor operated at stand-still as a transformer are used to illustrate the methods of derivation of the equivalent circuits. These equivalent circuits are also determined from characteristics obtained from tests on the machine used as an alternator. The relationship between the two sets of characteristics is explained.

Results of tests on a model synchronous machine, called the micro-machine, are discussed. These tests were performed using in turn cylindrical-rotor and salient-pole types of field systems, with the same stator. The effect of different distributions of the armature and field windings on the parameters of the equivalent circuits is discussed. It is seen that as a result of this effect, one reactance of the equivalent Tee circuit and the reactances of the equivalent Pi circuit can be only approximately determined from terminal measurements. The test results indicate that the advantage in accuracy of the Pi circuit representation of the direct-axis (of this micro-machine) over the Tee circuit is small.

Acknowledgement

The work described in this thesis was carried out under the supervision of Dr. D.G.O. Morris, D.Sc., M.I.E.E., Reader in Electrical Engineering, Imperial College of Science and Technology. The author wishes to express his profound gratitude to Dr. Morris for his helpful guidance, constant encouragement and keen interest.

The author also wishes to thank the Central Electricity Generating Board for providing financial assistance to the author to enable him to carry out the research work. The author acknowledges with gratitude the assistance rendered by the staff of the Electrical Engineering Department in carrying out the experimental work.

CONTENTS

List of Symbols

A, A', A_1, A_{d1}	air-gap flux-density distribution constants (chapter 5)
a	area of cross-section, m^2
B	air-gap flux-density
$\bar{B}$	average air-gap flux-density
B_{gf}	peak fundamental air-gap flux-density (equation 2.25)
B_{gm}	peak actual air-gap flux-density (equation 2.24)
B_{mn}	peak nth harmonic air-gap flux-density
C	capacitance
E_n	nth harmonic phase voltage
E_{fn}	fundamental phase voltage due to nth harmonic air-gap flux-density
e	instantaneous e.m.f.
F	instantaneous m.m.f.
F_m	maximum m.m.f.
F_a	peak fundamental armature-reaction m.m.f.
F_{ad}	component of F_a along direct-axis
F_{aq}	component of F_a along quadrature-axis
F_f	peak fundamental field m.m.f. (for cylindrical-rotor machine)

F_f	field m.m.f. (for salient-pole machine)
F_3	peak fundamental m.m.f. due to third harmonic current
g	slots per pole per phase
I	current
I_a	armature current
I_d, I_q	components of I_a along direct and quadrature-axis
I_f	field current
I_f'	peak alternating current in field winding (equations 5.4 to 5.8)
I_n	nth harmonic current (chapter 4, n = 3, 4, 5)
I_1, I_2	currents at terminals 1-1 and 2-2 of the equivalent circuits
i	instantaneous current
i_a	instantaneous armature current
i_f	instantaneous field current (chapter 5, eqn. 5.4)
K', K_1, K_ϕ	flux distribution constants (chapter 5)
K_w	fundamental winding factor of the field winding
K_{w1}	fundamental winding factor of the armature winding

K_{wn}	nth harmonic winding factor of the armature (chapter 5)
K_{wn}	nth harmonic winding factor of a stator phase (chapter 4)
K'_{wn}	nth harmonic winding factor of a rotor phase (chapter 4)
L_c	length of the core, m (equation A4)
L	inductance
l_g	effective length of the air-gap at the polar-axis, m
M	mutual inductance
N	number of turns
N_1, N_2	number of turns on windings 1 and 2 (Fig. 2.3)
N_f	number of turns on field winding
n	turns-ratio
P	number of poles
R	resistance
R'	equivalent iron-loss resistance
R_1, R_2	resistances of windings 1 and 2 (Fig. 2.3)
R_a	armature resistance per phase
S	reluctance
T_{ph}	turns per phase
t	time, sec

V_d, V_q	direct-axis and quadrature-axis voltages
V_1, V_1'	voltage across terminals 1-1 of the equivalent circuits
V_2, V_2'	voltage across terminals 2-2 of the equivalent circuits
V_{d1}	$= (V_1 - V_2)$ (appendix B)
V_{d2}	$= (V_2' - V_1)$ (appendix B)
X	reactance
X	$= (X_d' - X_{La})$ (section 5.6.1)
X_d, X_q	direct-axis and quadrature-axis synchronous reactances
X_d'	unsaturated transient reactance
X_{La}	armature leakage reactance
X_{Lf}	referred field leakage reactance
X_{sLf}	referred slot leakage reactance of the field winding
X_1, X_2, X_m	reactances of the equivalent Tee circuit
X_{uns}	unsaturated value of X_m
X_1', X_2', X_3	reactances of equivalent Pi circuit
Z_m	parallel combination of R' and X_m (Fig. 4.6)
δ	load angle
θ	phase angle (equations 2.5, 2.6; Fig. 5.23)

θ	angle measured in electrical degrees from inter-polar axis (equations 4.3, 5.1)
λ	$= F/d\dot{\phi}/dt$ (equation 2.3)
λ	specific slot permeance (equation A.4)
μ	permeability
μ_o	permeability of free space ($= 4\pi \times 10^{-7}$ H/metre)
ρ	$= \dot{\phi}/F$ (equation 2.1)
ϕ	instantaneous flux
ϕ_m	time-maximum flux
ϕ_a	mutual flux per pole due to fundamental direct-axis armature m.m.f. (equation 5.3)
ϕ_f'	mutual flux per pole due to field m.m.f. (equation 5.4)
ϕ_g	fundamental air-gap flux per pole (equation 5.7)
ϕ_{Lf}, ϕ'_{Lf}	field leakage flux per pole
ϕ_{sL}	peak armature slot leakage flux per phase
ϕ_{sLf}	field slot leakage flux per pole
$\dot{\phi}$	$= d\phi/dt$
ψ	phase shift (Fig. 5.23)
ω	angular frequency

Subscripts

a	armature
d, q	direct-axis, quadrature-axis
f	field
g	air-gap
L1, L2	limbs 1 and 2 (Figs. 2.2, 2.3)
La	armature leakage
Lf	field leakage
P	pole (Figs. 2.11, 2.12)
p, s	primary and secondary leakage paths (Figs. 2.2c, 2.3)
rc, sc	rotor core, stator core
rt, st	rotor teeth, stator teeth
sL	equivalent armature slot leakage
sLf	equivalent field slot leakage
Y	yoke (Fig. 2.12)
y_1, y_2	yoke (Figs. 2.2c, 2.3)
1,2	terminals 1-1; terminals 2-2
1, 2	winding 1; winding 2

CHAPTER 1

Introduction

The terminal properties of an air-cored transformer formed by two coils having negligible resistance are described by the self-inductances of the two coils L_1 and L_2, and their mutual inductance M. These parameters may be represented by an equivalent Tee circuit composed of the mutual inductance M and leakage inductances (L_1-M) and (L_2-M). Frequently, it is found convenient to represent the terminal properties by an alternative equivalent Tee circuit formed by three inductances in association with an ideal transformer of ratio n, as shown in Fig. 1.1. The choice of this ratio is arbitrary and hence any number of equivalent circuits can be derived from the measured inductances. For a single frequency of operation, even circuits in which one of the leakage inductances is negative can be practically realised by representing the inductance by a capacitance of a magnitude such that the inductive and capacitive reactances are equal.[1]

In practice, particular values of these ratios, e.g. the ratio of the terminal voltages on open-circuit, may be preferred to others mainly because they lead to equivalent circuits the parameters of which can be determined with greater ease and more accurately than

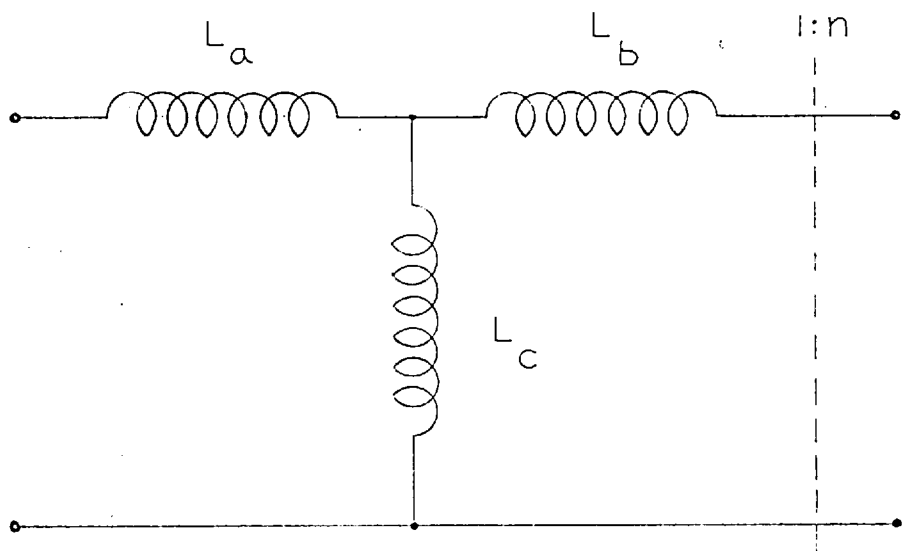

FIG. 1.1 TEE CIRCUIT OF INDUCTANCES

those associated with other ratios[2,3].

On exactly the same principles, a large number of equivalent circuits can also be derived to represent a loss-less, iron-cored transformer so long as the core is unsaturated. A useful circuit is obtained by making the assumption that the mutual flux is constrained to the iron core. This assumption is also largely correct for a practical transformer. The ratio n in an equivalent circuit based on this assumption will be equal to the ratio of the physical number of turns on the two windings. A transformer is very often represented by this circuit.

An explicit determination of the four parameters of this equivalent circuit is not possible. Methods of derivation of this circuit have been proposed in many papers on the assumption that the turns-ratio is known.[4,5,6] Some times the parameters are also determined by employing the open-circuit voltage ratio as the turns-ratio.[7]

Subject to certain additional approximations, discussed in chapter 2, a saturated transformer can be described by an equivalent Tee circuit in which the mutual reactance depends on the voltage across its terminals and the leakage reactances are of constant magnitudes. It is possible to determine explicitly the ratio n, and hence the other parameters of this circuit from terminal measurements. In addition to the three independent measurements that can be made at the terminals of a linear four-terminal network, the non-linear nature of the magnetisation characteristic of the core is utilised to provide the fourth measurement required for the derivation of the circuit. This derivation can be achieved in a number of ways. Two novel methods, called the transfer-impedance and self-impedance methods, are explained in chapter 3. The well-known Potier method[8] of determining the armature leakage reactance of a synchronous machine employs a similar approach.

A restricted similarity between a transformer and an alternator has long been recognised.[9] This similarity exists even when both the magnetic systems are saturated. To illustrate this similarity, it was necessary to choose for tests a machine that could be easily operated both as a transformer and as an alternator. Hence, an induction motor was employed as the test machine. Tests on this machine are described in chapter 4. The machine was tested both as a transformer and as an alternator. The characteristics obtained from tests on the machine as a transformer have been employed to demonstrate the novel methods of determining the reactances of the Tee circuit. Potier-type tests were performed on the machine both with the machine operating as a transformer and as an alternator. The relationship between the sets of characteristics obtained by these tests is also explained in chapter 4. This explanation brings out the basis for the similarity between a transformer and an alternator.

1.1 Need for a Pi circuit representation of synchronous machines

One of the assumptions made in the representation of a saturated transformer or a machine by the equivalent Tee circuit referred to above is that the leakage fluxes follow purely air paths. It has been pointed out in reference 10 that this assumption is not strictly correct for a transformer, and a suggestion has been made that the Pi circuit would be a more realistic representation of the transformer. The Pi circuit representation of a transformer has also been mentioned in references 11 and 12.

The fact that the representation of a synchronous machine by a Tee circuit is not completely justified is shown by the variable values of reactance that result from Potier tests on the machine, particularly if the machine is of the salient-pole type. The reactance is also found to be larger than the calculated armature leakage reactance.[13] The difference between the test and calculated reactances is large enough to make it necessary to distinguish between the two reactances. The measured reactance is called the Potier reactance.

The various factors that cause the Potier reactance to be different from the calculated armature leakage reactance have been discussed by Beckwith.[14] One of the contributory factors is saturation of the field system due to field leakage flux. The influence of this particular factor on Potier reactance has been studied by Saad Mikhail.[15] He has derived an expression relating Potier reactance to the armature leakage reactance. This expression is partly based on constants which can be determined from design data. In a recent publication, Schuisky[16] has developed an approximate method by which the influence of saturation due to field leakage flux is allowed for in the prediction of field excitation.

Although the assumptions made in the Potier method are not wholly correct, the Potier reactance is widely employed along with the open-circuit characteristic for the prediction of field excitation under various load conditions. The use of Potier reactance is justified on the grounds that the reactance can be easily determined and that the predicted performance is reasonably correct. The properties of a Pi circuit consisting of two non-linear "pillar" reactances spanned by a linear reactance have been examined in this thesis in an attempt to secure a more consistent representation of the machine. This Pi circuit representation is adopted for the direct-axis of the machine.

This thesis is mainly concerned with an examination of the possible methods of determining the parameters of the equivalent Tee and Pi circuits of a transformer and a synchronous machine. In the case of a synchronous machine, the equivalent circuits are most conveniently derived from the open-circuit and zero power factor characteristics of the machine. For this reason, attention has been mostly devoted to the study of an alternator operating at zero power factor.

In chapter 2, the equivalent Tee and Pi circuits are derived by the transformation of more elaborate networks. These networks are themselves obtained from a consideration of representative flux paths in the magnetic system. The approximations involved in the derivation of the equivalent Tee and Pi circuits are indicated in this chapter. Though a qualitative assessment of the relative merits of the Tee and Pi circuit representations is made in this chapter, the conclusions drawn are later modified in the light of experimental results discussed in chapters 4 and 5.

Chapter 3 sets out the test methods devised for the derivation of the Tee and Pi circuits. As stated previously, chapter 4 deals with the results of tests on an induction motor operated as a transformer and as an alternator.

Additional tests were performed on a model synchronous machine, called the micro-machine, employing both salient-pole and cylindrical-rotor field systems. The results of these tests are discussed in chapter 5. The difficulties in the determination of the parameters of the Pi circuit are pointed out and it is shown that these parameters can not be exactly determined from terminal tests.

The conclusions from all these tests are stated in chapter 6.

The following points are thought to represent the original contributions of the author.

1. The development of the transfer-impedance and self-impedance methods of determination of the parameters of the equivalent Tee circuit.

2. A demonstration of the impossibility of determining explicitly the turns-ratio of the ideal transformer associated with the equivalent Pi circuit, even when the pillar reactances are non-linear.

3. A study of the representation of the direct-axis of a synchronous machine by an equivalent Pi circuit.

CHAPTER 2

EQUIVALENT CIRCUITS OF TRANSFORMERS AND SYNCHRONOUS MACHINES

2.1. Scope.

The concept of topological duality of magnetic and electric circuits is explained and later employed to derive the equivalent circuits of a two-winding transformer. Equivalent circuits for saturated cylindrical-rotor and salient-pole synchronous machines supplying a balanced load are obtained, and the approximations involved in the representation of the machines by the Tee and Pi circuits are indicated.

2.2. Derivation of equivalent circuits of a magnetic system.

The process by which the equivalent circuits of a magnetic system are derived can be divided into two steps. These steps are the formulation of a lumped magnetic circuit of the distributed magnetic system, and the derivation of the equivalent electric circuit from the lumped magnetic circuit. The reduction of the magnetic system into a magnetic circuit is an approximate process. The approximations that are made depend upon the purpose of the equivalent circuit and the available data. Thus, very elaborate representations of the system are seldom necessary for the prediction of terminal characteristics. The need to determine the parameters from terminal measurements alone further limits the number of parameters that an equivalent circuit may contain.

Once the lumped magnetic circuit of a system has been derived, however, the equivalent electric circuit can be immediately obtained by applying the concept of topological duality of magnetic and electric circuits.[17,18,19] This concept is explained in the following sections.

2.3. Elements of a magnetic circuit and the dynamic and topological analogues of magnetic systems.

The concept of duality of magnetic and electric circuits has been formulated by Cherry[17,18] by a comparison of the equations describing the magnetic and electric constraints of an ideal transformer. Using a more general approach, Morris[19] has arrived at the concept of duality by deriving the elements of a magnetic circuit by analogy with the elements of an electric circuit. This approach is explained below.

The analogy between magnetic and electric circuits rests on Lenz's law, $e = -N\dot{\varnothing}$, and the relation $F = Ni$ (F represents instantaneous m.m.f.). These two equations relate the electric circuit quantities e and i to the corresponding quantities $\dot{\phi}$ and F in magnetic systems.

2.3.1. Ideal sources and passive elements in magnetic circuits.

Ideal sources in magnetic circuits are defined by analogy with the sources in electric circuits. Thus, the ideal m.m.f. and $\dot{\phi}$ sources are respectively defined as sources which maintain the m.m.f. and $\dot{\phi}$ in a magnetic system constant regardless of changes in the permeability of the system.

Since the m.m.f.s and fluxes in the magnetic systems considered here are set up by currents in various windings, the nature of magnetic sources is determined by the electric sources connected to different windings. Thus, the m.m.f. set up by the field winding of an alternator may be regarded as an ideal m.m.f. source if the excitation is derived from a current source. The excitation of the primary of an ideal transformer from a constant voltage supply can be looked upon as setting up an ideal flux source. For a constant frequency of operation, an ideal flux source is also an ideal $\dot{\phi}$ source. The ideal m.m.f. and $\dot{\phi}$ sources are symbolically represented as shown in Figs. 2.1(a) and (b).

Corresponding to the three passive elements, R, L and C in an electric circuit, three elements ρ , μ ,

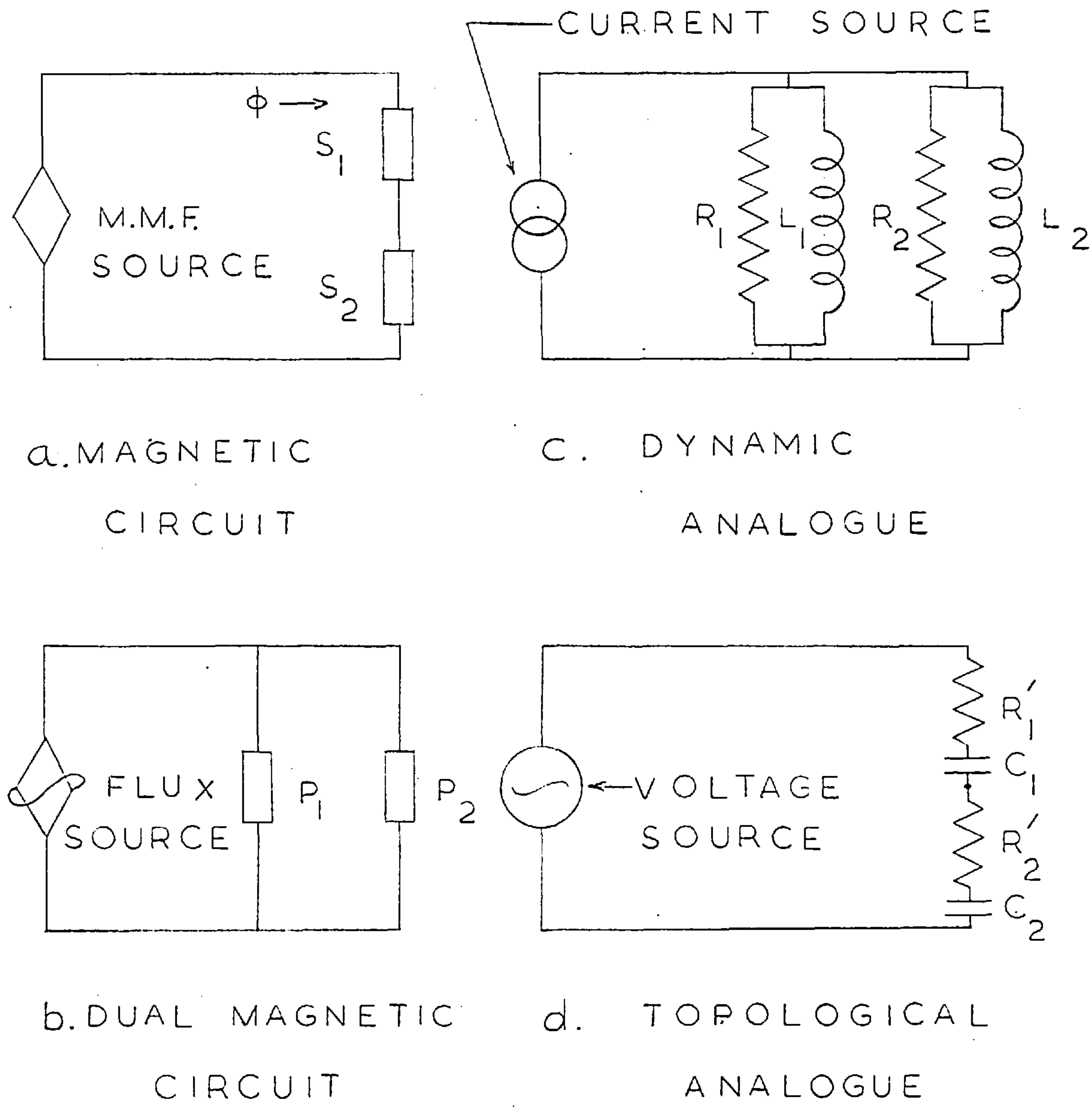

FIG. 2.1 REPRESENTATION OF TWO IRON CORES CARRYING THE SAME FLUX

and λ can be defined in magnetic circuits, the characteristics of all six elements being represented by the equations

$$R = e/i \ ; \ \rho = \frac{\dot{\phi}}{F} \tag{2.1}$$

$$L = \frac{\int e \, dt}{i} \ ; \ \mu = \frac{\int \dot{\phi} \, dt}{F} \tag{2.2}$$

$$\text{and } 1/C = \frac{de/dt}{i} \ ; \ 1/\lambda = \frac{d\dot{\phi}/dt}{F} \tag{2.3}$$

ρ and μ represent iron loss and the permeability of iron respectively. Iron does not exhibit the characteristic described by λ . The equivalent electrical analogues of the magnetic systems considered here are therefore networks of resistors and inductors alone. However, it must be pointed out that in the dual of these equivalent networks inductors would be replaced by capacitors.

2.3.2. Topological and dynamic analogues of a magnetic circuit.

A magnetic circuit consisting of ideal sources and passive elements can now be formed. As in electric circuits, the connection of passive elements in series or parallel constrains either of the two quantities $\dot{\phi}$ or F to be the same in the elements. Topologically these constraints could be represented by two graphs which are dual to each other. For example, two iron cores carrying the same uniformly distributed flux may be represented by either Fig. 2.1(a) or (b). Besides the topological duality of the two circuits, Figs. 2.1(a) and (b) also show the dual relationship of the ideal m.m.f. and flux sources. The electrical analogue of the magnetic circuit of Fig. 2.1(a) based on the analogy discussed in the previous section is shown in Fig. 2.1(c). Since an electric circuit can be replaced by its dual, the magnetic circuit can also be represented by the circuit of Fig. 2.1(d). Comparing the magnetic circuit with Fig. 2.1(d), voltage and current in the analogue (Fig. 2.1d) now represent m.m.f. and flux respectively in the magnetic circuit. The elements ρ and μ are represented by capacitive impedances.

Since Figs. 2.1(a) and (d) are topologically similar, the capacitive analogue is called the topological analogue of the magnetic circuit. As the analogy between magnetic and electrical driving sources is preserved in Fig. 2.1(c), the circuit is called the dynamic analogue of the system.

2.4. Representation of magnetic systems by electric circuits composed of linear circuit elements.

A complete representation of the non-linear magnetisation characteristic and hysteresis loop of iron by an electric circuit can only be achieved by employing circuit elements which have similar characteristics.

Consequently, if only linear circuit elements have to be employed, the electrical analogue forms only an approximate representation of the magnetic system. The approximations involved are brought out by considering the representation of an iron core carrying uniform flux.

Neglecting initial non-linearity, if the core is unsaturated and has no losses, the magnetisation characteristic reduces to a straight line. If a m.m.f. varying sinusoidally in time is applied to the core, the resulting flux is sinusoidal and in phase with the m.m.f. The permeability μ being the only property associated with the system, the electrical analogue will be an inductance. The analogy is exact.

If the core has hysteresis loss, a sinusoidal applied m.m.f. will no longer produce a sinusoidal flux. Since the harmonic components of flux are usually much smaller than the fundamental, attention is confined to the representation of the fundamental component alone. The applied m.m.f. being sinusoidal, the hysteresis loss is supplied by the fundamental components of flux and m.m.f. alone. This loss causes the fundamental component of flux to lag behind the m.m.f. by an angle θ. The two quantities are described by the equations

$$F = F_m \sin \omega t \qquad 2.4.$$

and $$\phi = \phi_m \sin (\omega t - \theta) \qquad 2.5.$$

From equation 2.5,

$$\dot{\phi} = \omega \phi_m \cos(\omega t - \theta) \quad 2.6$$

Assuming that the core has unit dimensions, the following expressions relating ϕ_m and F_m can be written down.

$$F_m \sin\theta = (1/\rho).\ \omega\phi_m \quad 2.7$$

$$\text{and } F_m \cos\theta = (1/\mu).\quad \phi_m \quad 2.8$$

The operating conditions in the core may be then represented by a magnetic circuit consisting of a m.m.f. source connected across the series combination of the elements $1/\rho$ and $1/\mu$. ϕ forms the mesh quantity in this magnetic circuit. The dynamic analogue of this magnetic circuit consists of a current source connected to the parallel combination of a resistance R and an inductance L. If the current i and voltage e in the analogue directly represent F and $\dot{\phi}$ respectively, the following expressions can be used to describe i and e.

$$i = F_m \sin\omega t \quad 2.9$$

$$e = \omega\phi_m \sin(\omega t + \psi) \quad 2.10$$

R and L are then given by the expressions

$$R = \frac{\omega\ \phi_m}{F_m \cos\psi} \quad 2.11$$

$$\text{and } \omega L = \frac{\omega\ \phi_m}{F_m \sin\psi} \quad 2.12$$

By comparing corresponding equations it can be seen that if ψ is made equal to ($\pi/2 - \theta$), R and L become respectively equal to ρ and μ. The passive elements in the dynamic analogue are hence inversely related to the corresponding elements in the magnetic circuit.

Instead of using a direct numerical relationship between corresponding sources in the magnetic circuit and the analogue, it is often convenient to use scale factors to relate these quantities. These scale factors also govern the relationship between the passive elements in the two circuits. The use of an ideal transformer in an equivalent circuit is an example of the use of a scale factor.

Since ρ is a function of the angular frequency ω, the resistance R in the dynamic analogue is frequency-dependent. This frequency-dependent nature of the analogue has been pointed out in reference 17.

When the dimensions of the core are other than unity, the quantities $1/\rho$ and $1/\mu$ in equations 2.7 and 2.8 are replaced by the corresponding reluctances. Both μ and ρ, and the associated reluctances, may be viewed as components of the vector permeability and vector reluctance respectively. This point of view has been developed by Macfadyen.[20]

The above development of the dynamic analogue is based on the simplifying assumption that the iron loss is supplied by the fundamental components of m.m.f. and flux alone. When the applied m.m.f. and flux are both non-sinusoidal, some of the iron loss is also supplied by the harmonic components of flux and m.m.f. For the same fundamental m.m.f. or flux, therefore, the total iron loss associated with the fundamental components of flux and m.m.f. will vary with the waveforms of the two quantities. The resistance R will be then waveform-dependent. As an approximation, R can be chosen to represent the total iron loss measured at a given fundamental m.m.f. with the flux sinusoidal. The total iron loss referred to also includes some eddy current loss.

2.5. Representation of a saturated magnetic system

2.5.1. Electrical analogue of a saturated iron core

When the iron core saturates, the permeability μ varies over a cycle of applied m.m.f. or flux. This variation results in further distortion of the waveform of either or both the flux and m.m.f. The variations of μ are accounted for by the concept of fundamental permeability. Fundamental permeability is defined as the ratio of the fundamental components of flux and m.m.f.[21] A fundamental magnetic circuit comprising the fundamental components of m.m.f., flux and the fundamental permeability can now be formed. This circuit is represented by a fundamental equivalent circuit which consists of a linear inductive impedance connected across a voltage or current source.

However, the fundamental permeability reduces with increasing fundamental flux. The inductance in the equivalent circuit must correspondingly decrease as the voltage across its terminals is increased. An example of this change in fundamental permeability is the reduction in the synchronous reactance of an alternator on saturation of the machine.

The influence of saturation on iron loss is approximately represented by a variable resistance in the equivalent circuit. This resistance is calculated by equating the total iron loss to the loss occurring in the resistance.

2.5.2. Influence of harmonic fluxes on fundamental permeability.

Apart from the reduction in fundamental permeability that accompanies an increase in fundamental flux, the fundamental permeability is also influenced by the harmonic components of flux and m.m.f. Thus, for the same fundamental component of flux, the fundamental permeability is minimum when flux is sinusoidal, and maximum when m.m.f. is sinusoidal.[21] This change in fundamental permeability can be ignored if the magnetic circuit operates in the region around the knee of the magnetisation characteristic. The change in permeability becomes significant when the magnetic circuit is highly saturated.

The influence of harmonic fluxes and m.m.f.s. on the fundamental permeability is also dependent on how the fundamental permeabilities for different waveforms of flux are compared. Thus, the fundamental permeability at a given fundamental m.m.f. is much less variable with the waveform of flux or m.m.f. than the permeability at a given fundamental flux. The decrease in the fundamental permeability of a saturated iron core at a given fundamental applied m.m.f. as the m.m.f. and flux become sinusoidal in turn is of the order of 5 to 10 per cent.[21, 22] The influence of harmonics on the fundamental permeability is discussed in detail in reference 21.

2.6. Representation of exciting currents and voltages

In the electrical analogues described so far, current and voltage sources represent m.m.f. and rate-of-change of flux, or flux. As mentioned in section 2.3.1, the m.m.f.s. and fluxes are established by currents and voltages in various windings in the system. In practice, these currents and voltages are of principal interest.

The currents and voltages at the terminals of the windings in a magnetic system are represented in an equivalent circuit by adopting an arrangement similar to that shown in Fig. 2.1 e. This figure shows the components of an equivalent circuit of a two-winding magnetic system. The ideal transformers 1 and 2 respectively couple the terminals of the dynamic analogue to the terminals 1-1 and 2-2 of the equivalent circuit. The terminals 1-1 and 2-2 correspond to the terminals of the windings on the magnetic system.

The number of ideal transformers in an equivalent circuit can be reduced to one less than the number of windings on the system. This reduction can be achieved by referring the elements of the dynamic analogue to the primary (or secondary, as appropriate) side of any one ideal transformer. Thus, ideal transformer 1 in Fig. 2.1e can be removed if the elements of the dynamic analogue are referred to the primary side of the transformer. Transformer-less equivalent circuits can also be obtained by replacing the ideal transformers with equivalent networks of impedances. The elements in these networks may not be realisable in themselves, but in some cases realisable components could be derived by suitable combination with other elements of the equivalent circuit.[23]

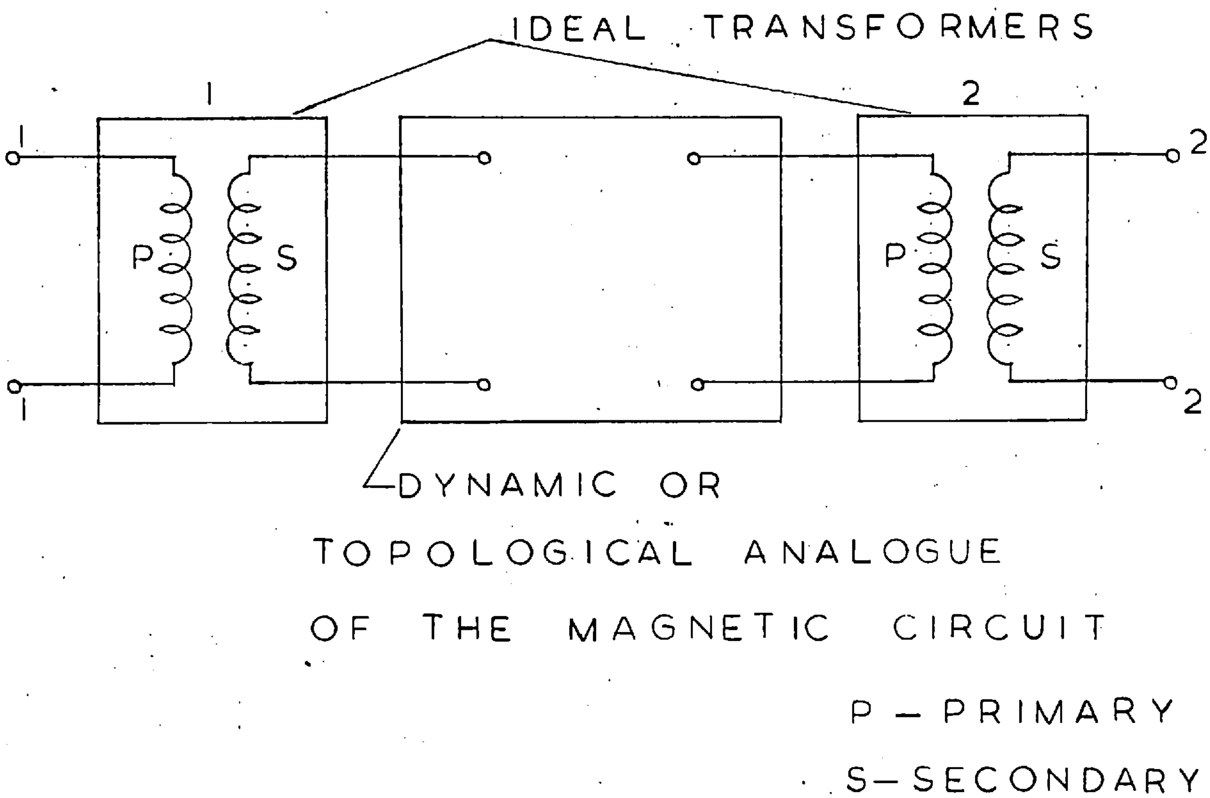

FIG. 2.1e COMPONENTS OF THE EQUIVALENT CIRCUIT OF A TWO-WINDING MAGNETIC SYSTEM

The turns-ratio of an ideal transformer in an equivalent circuit representing a physical coupled system is not defined by the physical number of turns on a winding (or the ratio of the physical number of turns on two windings). When the coupled system is a two-winding transformer, the turns-ratios of the two ideal transformers are equal to the fundamental (time) voltages induced in the corresponding windings by unit rate of change of the flux linking the windings. This definition of the turns-ratio satisfies the requirement that the currents and voltages at the terminals of an equivalent circuit should correspond to those at the terminals of the respective windings of the magnetic system. At the same time, the fluxes in the magnetic system are "correctly" represented in magnitude in the dynamic analogue section of the equivalent circuit. A modified definition of the turns-ratio is adopted in the case of a synchronous machine. For example, the turns-ratio of the field and armature windings of a cylindrical-rotor synchronous machine will be defined as the ratio of the currents in the two windings that produce the same fundamental m.m.f. in the magnetic circuit.

2.7. Representation of transformers and synchronous machines by equivalent circuits.

The concepts explained above are employed in the following sections to obtain the equivalent circuits of a two-winding transformer, and cylindrical-rotor and salient-pole synchronous machines. The magnetic circuits are derived in each case from a study of representative paths of flux in the system. Complete equivalent circuits are obtained from these magnetic circuits and transformed to yield more practical approximate forms. The approximations involved in each case are indicated.

2.8. Equivalent circuits of a two-winding transformer.

The two-winding transformer with uniform primary and secondary windings located on different limbs as shown in Fig. 2.2(a) forms an elementary magnetic system. A study of the procedure followed in the derivation of equivalent circuits of the system illustrates some of the points mentioned in previous sections.

With only one winding of the transformer excited, the total flux linking the winding can be divided into fluxes following an entirely iron path and fluxes following part-iron part-air paths. Representative paths of the two fluxes are shown in Fig. 2.2a. The part-air paths shown do not include paths which traverse

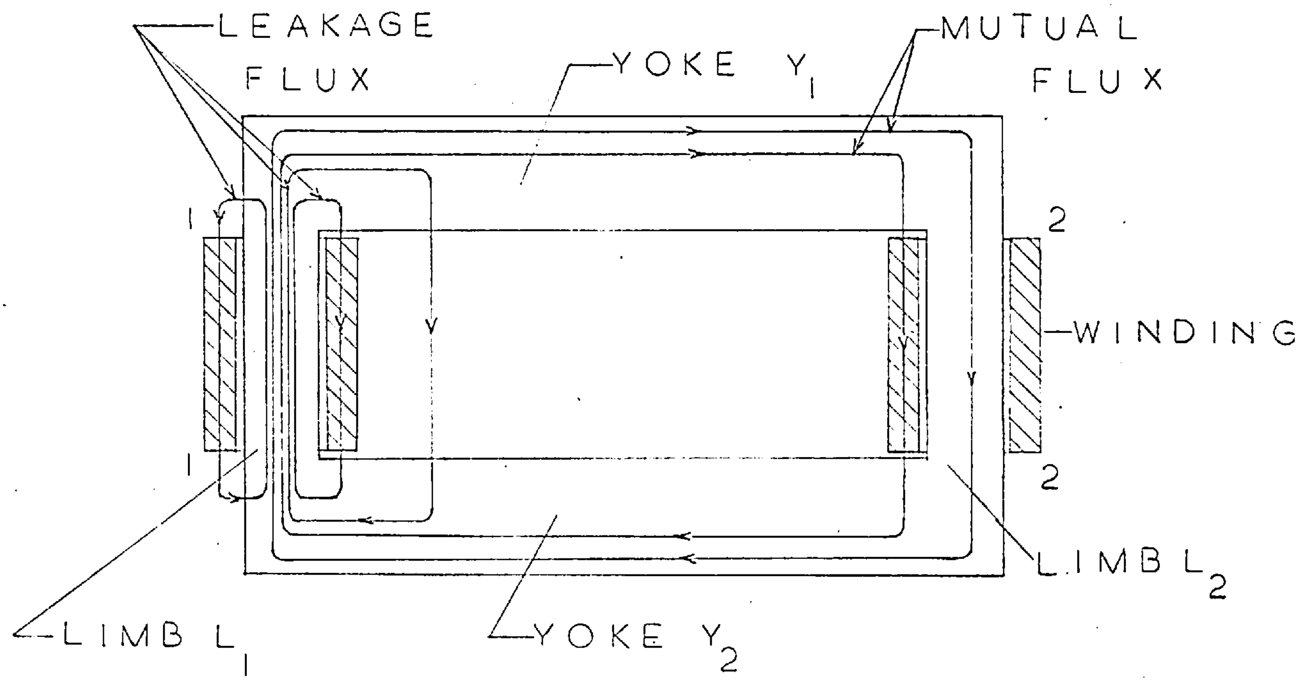

FIG. 2.2 a IDEALISED PATHS OF FLUX WHEN ONLY WINDING 1 IS EXCITED

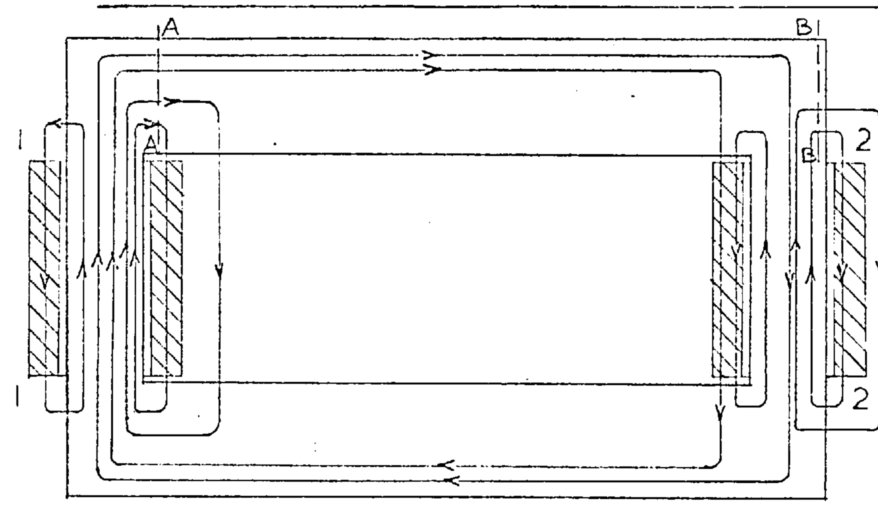

FIG. 2.2 b FLUX PATHS WHEN BOTH WINDINGS ARE EXCITED

only a part of the limb and link the excited winding partially. When the winding is uniformly distributed along the limb, the flux lines following such paths form only a small proportion of all the flux lines following part-air paths. They can be therefore neglected. While the flux lines following an entirely iron path wholly link both the windings, the lines following part-air paths link the two windings to varying extents. Some of these lines do not link the open-circuited winding at all. Such lines constitute a leakage flux associated with the excited winding and are responsible for the major part of the leakage reactance of the winding.

Since the two windings are identical, the flux produced by winding 2 (excited alone) follows paths similar to those described above. The principal components of the resultant flux when both the windings carry currents are shown in Fig. 2.2b. The major difference between Figs. 2.2a and b is the presence of flux paths linking winding 2 alone in Fig. 2.2b.

The simplified flux paths shown in Figs. 2.2 a and b are axial in the two limbs. The flux densities in different cross-sections taken at various points along the height of the limbs are then equal. The limbs can be therefore represented by two lumped reluctances in the magnetic circuit. Since the fluxes following part-air paths traverse different lengths of the yokes, the flux densities at various sections of the yokes differ. Thus, the flux density at the section AA [Fig. 2.2(b)] is a maximum while that at the section BB is a minimum. However, the fluxes following part-air paths are usually small in comparison to the flux following an entirely iron path and a detailed representation of the yokes is not normally necessary.

A simplified magnetic circuit is obtained by assuming that the yokes carry only the flux existing entirely in iron. Once this assumption is made, the two yokes may be represented by two lumped reluctances in the magnetic circuit. An additional simplification can be made by replacing the leakage fluxes linking the respective windings partially by equivalent fluxes linking the windings wholly. This simplification rests on the fact that the reluctance in the path of a leakage flux line mainly arises from the air path through the window. The reluctance in the path of all leakage flux lines is then nearly the same. This reluctance is also not significantly influenced by the level of saturation of the transformer core.

Fig. 2.2c shows the lumped magnetic circuit derived from the simplified view of the various fluxes. S_{L1} and S_{L2} are the reluctances of the two limbs; S_{y1}

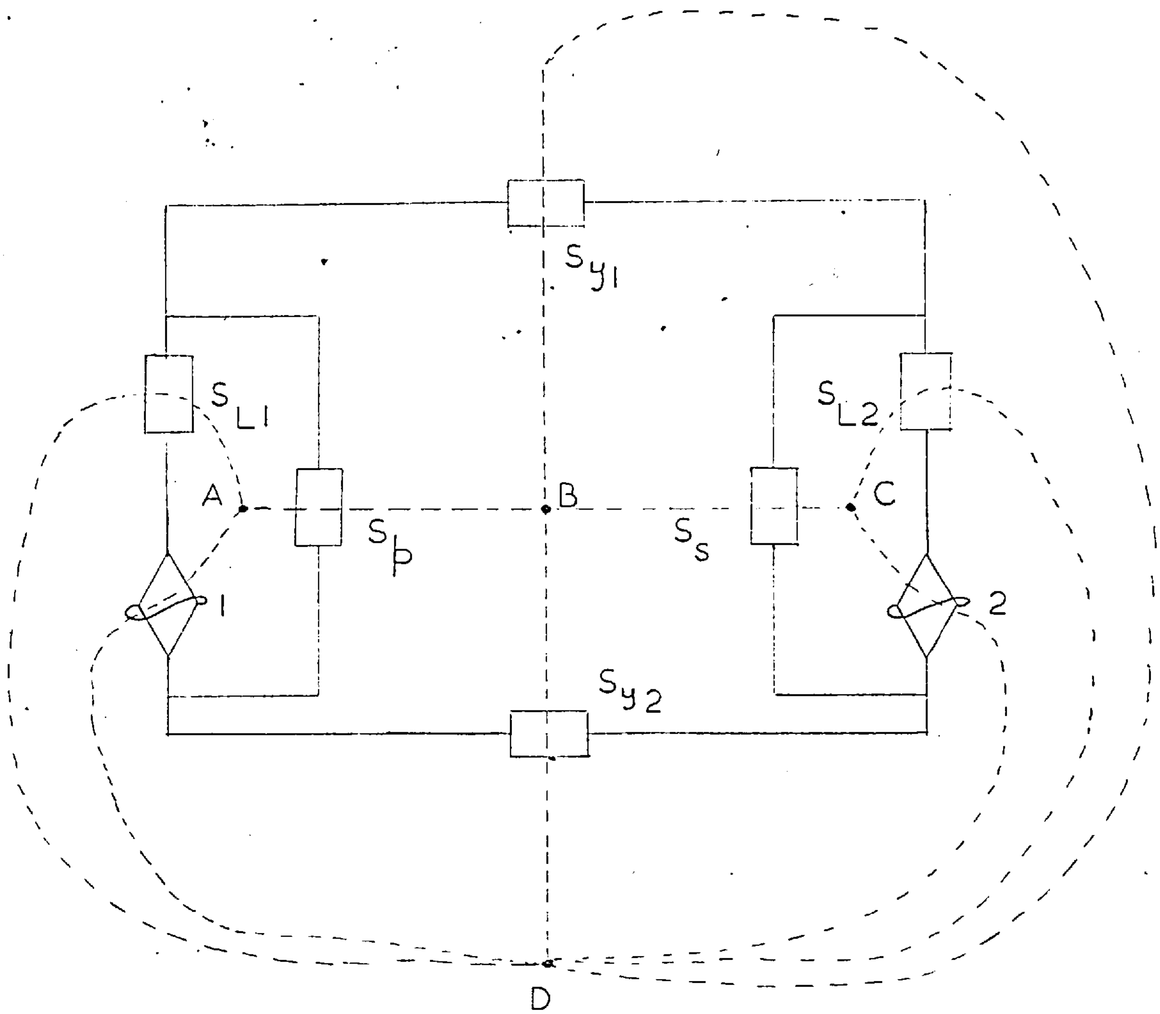

S_{L1}, S_{L2} RELUCTANCES OF THE LIMBS

S_{y1}, S_{y2} RELUCTANCES OF THE YOKES

S_p, S_s RELUCTANCES OF THE PRIMARY AND SECONDARY LEAKAGE FLUX (AIR) PATHS

FIG. 2.2 C MAGNETIC CIRCUIT AND ITS DUAL and S_{y2} are the reluctances of the yokes. (The term "reluctance" employed in connection with an iron path signifies both the "true" reluctance and the loss properties of iron.) S_p and S_s are reluctances of the air sections of the paths of the equivalent leakage fluxes.

2.8.1. Equivalent Electric circuit of the transformer.

The topological form of the dynamic analogue is derived by forming the dual of the lumped magnetic circuit. This dual is readily obtained by the graphical method illustrated in Fig. 2.2(c). The graphical method consists of joining nodes A, B and C placed within the three meshes of the magnetic circuit to the reference node D by lines crossing one element (of the magnetic circuit) each. The resulting graph, drawn dotted in Fig. 2.2(c), is the topological dual of the original graph. The dynamic analogue of the magnetic circuit is shown in Fig. 2.3(a). Iron losses in various parts of the magnetic circuit are represented by resistances in parallel with the corresponding inductances.

An equivalent circuit of the transformer is obtained by the addition of two ideal transformers to the analogue. This equivalent circuit is shown in Fig. 2.3(b). The two ideal transformers are represented by the dotted lines. The turns-ratios, N_1 and N_2, of

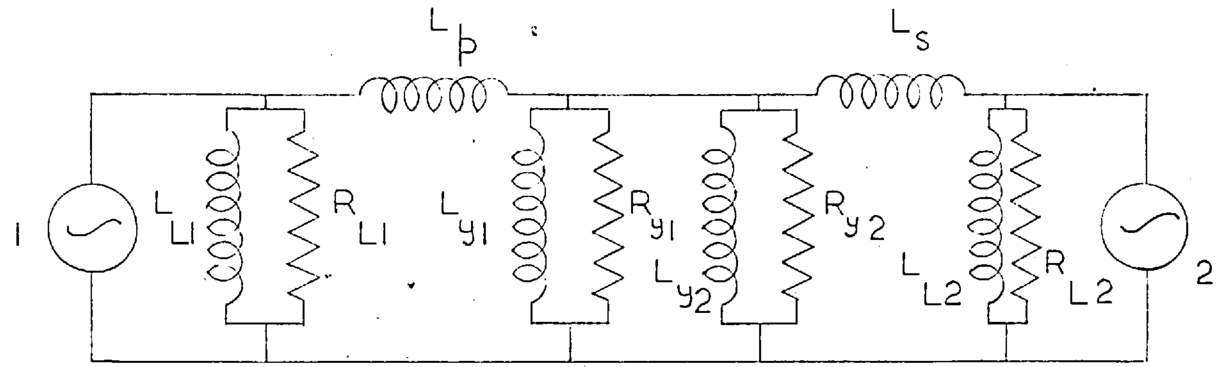

a. DYNAMIC ANALOGUE

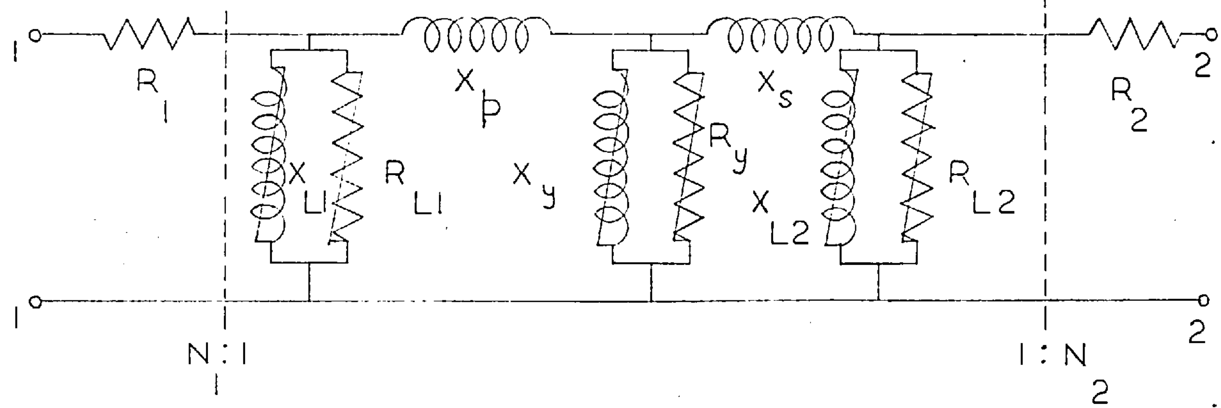

b. EQUIVALENT CIRCUIT

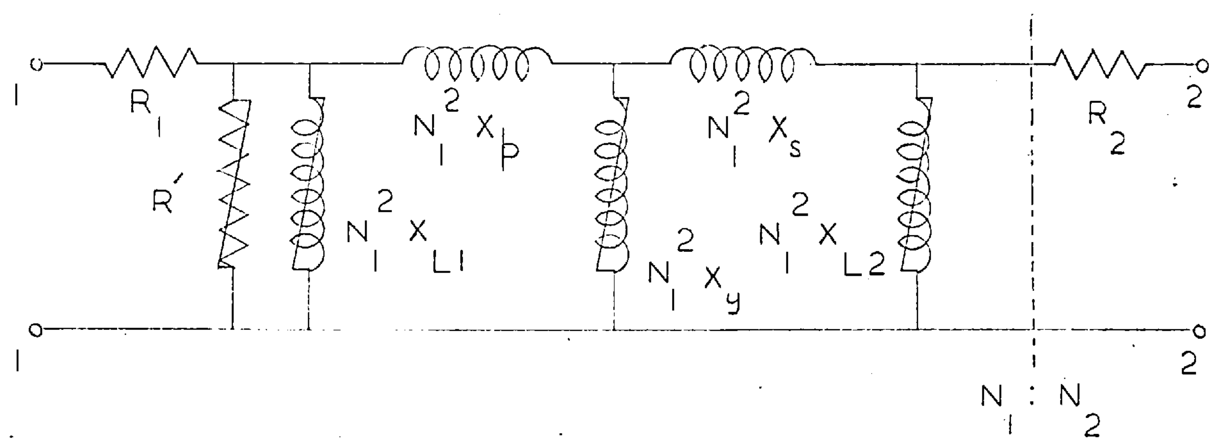

C. SIMPLIFIED EQUIVALENT CIRCUIT

FIG. 2.3 REPRESENTATION OF THE TRANSFORMER the ideal transformers respectively represent the number of turns on windings 1 and 2 of the actual transformer. R_1 and R_2 are the resistances of these two windings. By referring all the elements of the equivalent circuit of Fig. 2.3(b) to the primary side of ideal transformer 1, the number of ideal transformers is reduced to one. This transformer, having a turns-ratio of N_1/N_2, is placed as shown in Fig. 2.3(c).

If a detailed representation of iron loss is not required, all the loss can be assumed to be associated with any one reluctance in the magnetic circuit. This loss is then represented by a single resistance R' in the equivalent circuit of Fig. 2.3c. An equivalent circuit similar to that in Fig. 2.3b has been derived by Slemon.[24]

When the transformer is saturated, only the fundamental currents and voltages at the terminals of the transformer can be represented on the equivalent circuits derived above. The elements representing various iron paths become non-linear. The non-linear nature of these reactances is indicated symbolically as shown in Fig. 2.3c. The reactances X_p and X_s represent the air paths of the leakage fluxes. They are therefore linear.

2.8.2. Equivalent Tee and Pi circuits of the transformer.

When the magnetic circuit is unsaturated, the equivalent circuit of Fig. 2.3c is linear and can be replaced by equivalent Tee and Pi circuits. All the three circuits would be equivalent in so far as the impedances measured at terminal pairs 1-1 and 2-2 are concerned.

When the magnetic circuit is saturated, every operating condition can be described by an equivalent Tee or Pi circuit. Therefore, a range of operating conditions may be described by Tee and Pi circuits in which all the parameters are non-linear. These two circuits are shown in Figs. 2.4(a) and (b). The parameters of the Pi circuit are obtained by transformation of the Tee formed by the reactances X_p, X_s and X_y in Fig. 2.3c and are given by the equations[25]

$$X_1' = \frac{X_{L1}\left(X_y + X_p + \dfrac{X_y X_p}{X_s}\right)}{X_{L1} + X_y + X_p + \dfrac{X_y X_p}{X_s}} \cdot N_1^2 \qquad 2.13$$

$$X_3 = \left(X_p + X_s + \frac{X_p X_s}{X_y}\right) \cdot N_1^2 \qquad 2.14$$

$$X_2' = \frac{X_{L2}\left(X_y + X_s + \dfrac{X_y X_s}{X_p}\right) \cdot N_1^2}{X_{L2} + \left(X_s + \dfrac{X_y X_s}{X_p} + X_y\right)} \qquad 2.15$$

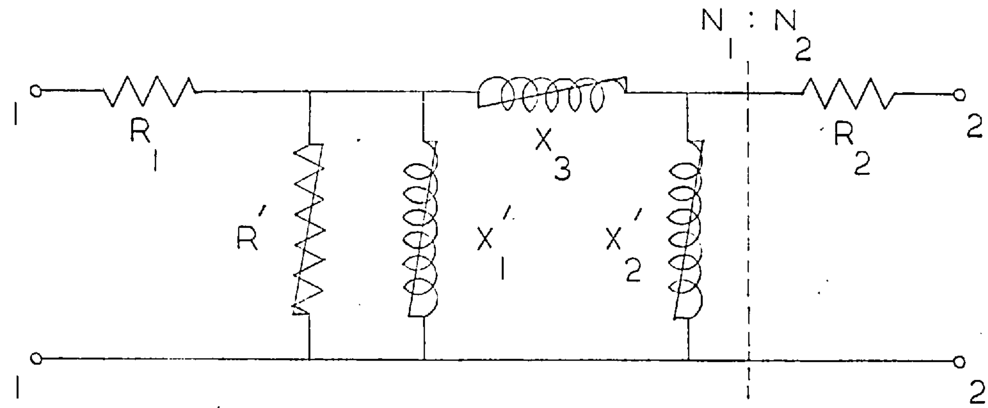

a. PI CIRCUIT

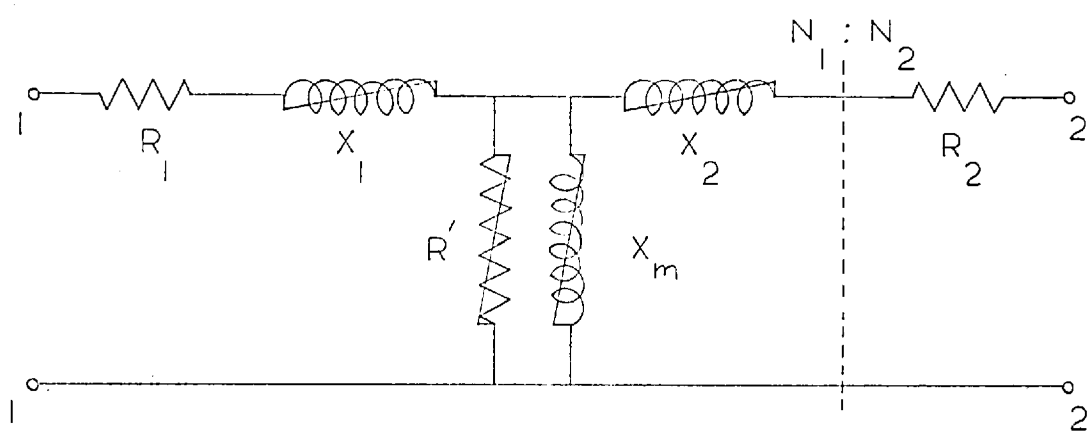

b. TEE CIRCUIT

FIG. 2.4 TEE AND PI CIRCUIT REPRESENTATIONS OF THE TRANSFORMER

The Tee circuit is the result of a further transformation of the Pi network, its parameters being[25]

$$X_m = \frac{X_1' \; X_2'}{X_1' + X_2' + X_3} \qquad 2.16$$

$$X_1 = \frac{X_1' \; X_3}{X_1' + X_2' + X_3} \qquad 2.17$$

$$X_2 = \frac{X_2' \; X_3}{X_1' + X_2' + X_3} \qquad 2.18$$

Especially when the transformer is unsaturated, X_y is much larger than X_p or X_s. The reactance X_3 of the Pi circuit is then essentially the sum of $N_1^2 \; X_p$ and $N_1^2 \; X_s$. The decrease in X_y on saturation of the yoke results in an increase in X_3.

It may be observed from the above equations that reactances X_1 and X_2 of the Tee circuit are not equal to $N_1^2 \; X_p$ and $N_1^2 \; X_s$ respectively. The division of reactance X_3 (Fig. 2.4a) into X_1 and X_2 is governed by the magnitudes of X_1' and X_2'. However, if the two limbs and the windings are identical, reactances X_{L1} and X_{L2} (Fig. 2.3b), as also reactances X_p and X_s, are equal. Reactances X_1' and X_2' are then equal. The equality of these reactances holds only when the iron is unsaturated. Since X_1' and X_2' are usually large as compared to X_3, reactances X_1 and X_2 are then approximately equal to $\frac{1}{2}X_3$. Further, since X_3 is very nearly the sum of $N_1^2 \; X_p$

and $N_1^2X_s$, reactances X_1 and X_2 become approximately equal to $N_1^2X_p$ (or $N_1^2X_s$).

When the transformer is supplying an inductive load connected to winding 2, limb L_1 operates at a higher flux density than L_2. On saturation of the magnetic circuit, reactance X_{L1} then becomes smaller than X_{L2}. The reactances of the Tee and Pi circuits obtained by transformation vary correspondingly.

The extent of approximation involved in representing the transformer by a Pi circuit in which X_3 is linear, or a Tee circuit in which X_1 and X_2 are linear, depends upon the saturation characteristics of various components of the magnetic circuit. If the yokes saturate appreciably as compared to the limbs, it becomes necessary to retain reactance $N_1^2X_y$ in the same position relative to $N_1^2X_p$ and $N_1^2X_s$ as in Fig. 2.3c. The Tee circuit is then a more appropriate representation than the Pi circuit. On the other hand, if saturation occurs mainly in the limbs, as in some cases,[26] the Pi circuit forms a better approximation to Fig. 2.3c than the Tee circuit.[27]

2.9. Equivalent circuits of a synchronous machine

2.9.1. Basis for the representation of a synchronous machine by an equivalent circuit.

The equivalent circuits developed in the following sections relate the fundamental components of flux and m.m.f. established by currents in the armature and field windings. These circuits are developed to represent the steady-state operation of a three-phase generator supplying a balanced load.

An equivalent circuit of an unsaturated machine can be developed by either reducing the machine to an equivalent transformer, or by regarding it as a special case of an induction motor. Both these points of view lead to similar equivalent circuits. The two points of view can be briefly explained as follows. Consider first the approach in which the machine is reduced to an equivalent transformer. In an ideal cylindrical-rotor machine, the air-gap is uniform. When such a machine is not saturated, the fundamental components of the armature-reaction and field m.m.f.s. establish a resultant flux which is sinusoidally distributed in the air-gap. The linkages of this flux with an armature phase vary sinusoidally in time. This variation could also be achieved with the machine at stand-still by exciting the field winding with a.c. (It is assumed that there are no damper circuits on the field system). The field winding has to be placed with its axis coincident with that of an armature phase. To achieve equality in the magnitudes of fluxes and m.m.f.s in the machine under the two modes of operation, the d.c. and peak a.c. excitations of the field have to be equal. In addition, the fundamental m.m.f. produced by the armature phase in line with the field has to be increased by 1.5 to allow for the influence of the other two phases in the rotating machine. The phase relationship of the alternating currents in the armature and field windings is dependent upon the power factor of operation of the rotating machine. Thus, these currents are in phase if the rotating machine operates at zero power factor lagging; the currents differ in phase by the angle $(90 - \delta)$ if the rotating machine operates at unity power factor. (δ is the load angle). This phase relationship is based on the positive directions of currents defined by dots and crosses in Fig. 2.5. The positive directions of the m.m.f.s. are given by the right-hand screw rule. A dynamic analogue of the machine at stand-still can be developed by the application of the methods discussed in the previous sections.

An equivalent circuit of the machine can also be derived by regarding the machine as a wound-rotor induction motor driven at synchronous speed. The equivalent circuit of the induction motor is first developed for the machine at stand-still (when it operates as a transformer). This equivalent circuit is then extended to represent normal operation of the machine by means of the "ideal induction machine" transformation.[22] The transformation of the rotor circuit quantities into corresponding quantities on the stator side involves the division of the rotor resistance and field voltage by slip. The slip of an induction motor driven at synchronous speed is zero. The referred rotor resistance then becomes infinite. However, the referred field voltage also becomes infinite. The excitation of a winding by an infinite voltage source in series with an infinite resistance could be regarded as excitation of the winding by a current source.[28] The d.c. excitation of the field winding could be therefore represented in the equivalent circuit by a current source. As indicated above, the phase relationship between the armature and equivalent field currents is governed by the power factor at which the rotating machine operates.

In a salient-pole machine the air-gap is not uniform. The magnitude of the fundamental flux established by the fundamental armature-reaction m.m.f., acting alone, therefore depends upon the spatial position of the axis of the m.m.f. The two-reaction theory[29] provides an approximate but adequate means of analysis of salient-pole machines. In this theory, the fundamental armature m.m.f. is resolved into components acting along the polar and the inter-polar axis (called the direct and quadrature axis respectively). Equivalent circuits relating the fundamental components of fluxes along the two axes to the respective m.m.f.s are derived by assuming the fluxes and m.m.f.s along the two axes to be mutually independent.

2.9.2. Equivalent circuits of a cylindrical-rotor machine operating at zero power factor.

When the machine operates at zero power factor, the fundamental components of the field and armature-reaction m.m.f.s act directly in opposition on a common magnetic system. The dynamic analogue of the machine is obtained by considering the lumped circuit representation of this system. The total flux in the magnetic system is once again divided into a mutual flux and leakage fluxes associated with the armature and field windings. The paths of these component fluxes are considered in the following sections.

A cross-section through an elementary two-pole cylindrical-rotor machine is shown in Fig. 2.5. A part of the rotor structure is shown unslotted. This corresponds to the usual practice followed in the construction of these machines. A single-layer arrangement of the windings has been shown for simplicity.

Fig. 2.5 shows some idealised paths of mutual flux at the instant that the current in phase A is at a maximum. The figure shows that the paths traverse different lengths of the stator and rotor cores. The total flux at various cross-sections in the cores is therefore different. The presence of slots on the stator and rotor causes the magnetic circuit to be radially unsymmetrical. Further, the stator and rotor teeth do not usually possess parallel sides. The areas of cross-section at various heights along a tooth are therefore different. These are some of the factors that cause the reluctances in various flux paths to differ. A lumped magnetic circuit of the system is derived by calculations based on an average length of the flux path in the cores and average areas of cross-section of the teeth and air-gap. For example, an equivalent reluctance of the air-gap is calculated by using Carter's coefficients; the area of cross-section of the stator teeth is frequently calculated by using Simpson's rule. Such details are not reproduced here.

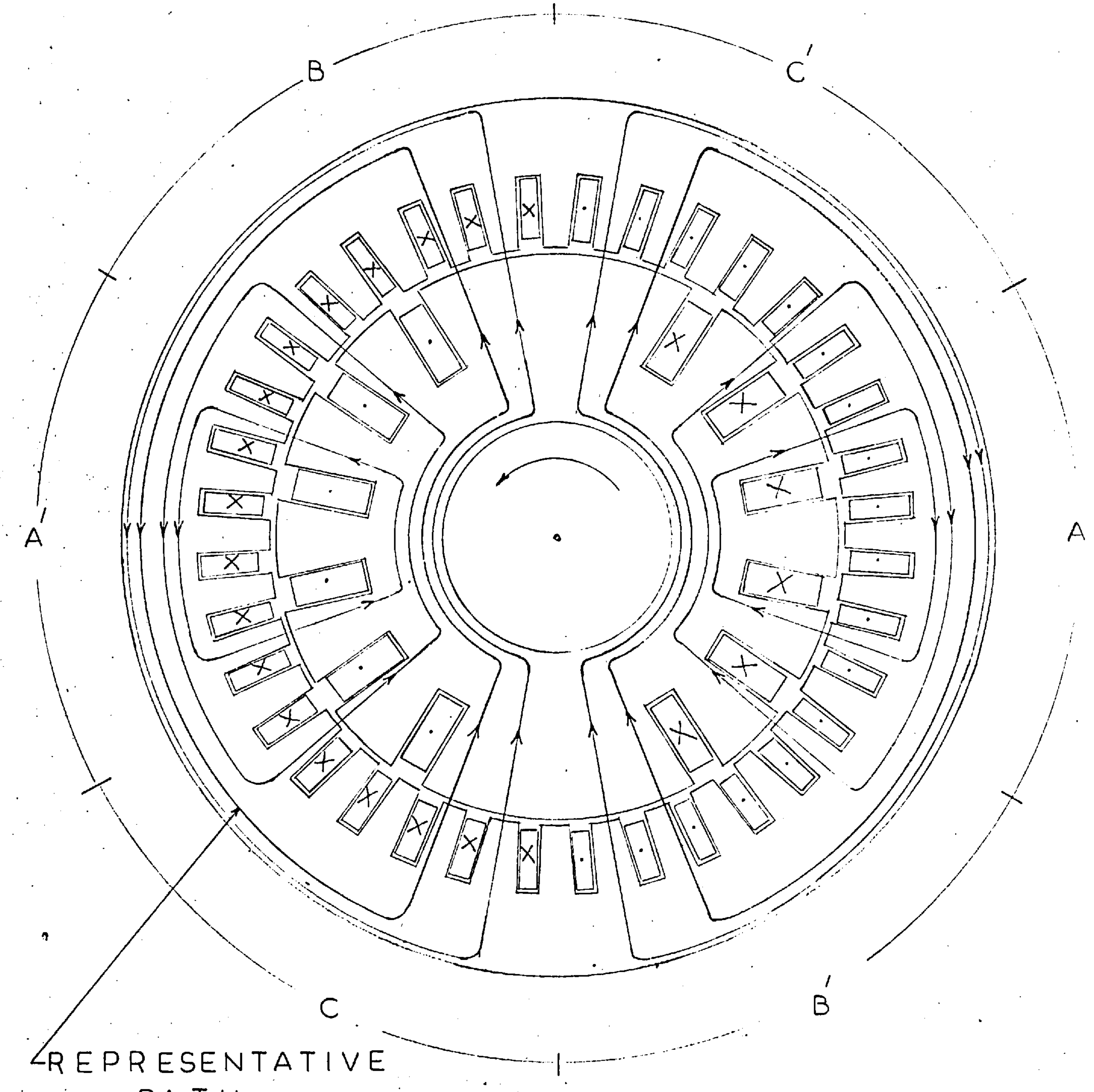

FIG. 2.5 SOME PATHS OF MUTUAL FLUX IN AN ELEMENTARY CYLINDRICAL-ROTOR MACHINE OPERATING AT ZERO POWER FACTOR

These details could be obtained by reference to any book on the design of synchronous machines.[30]

A representative path of mutual flux is shown in Fig. 2.5. This path is assumed to traverse a length of two-thirds the pole-pitch in the stator and rotor cores.[30]

The leakage flux associated with an armature phase can be divided into two main components. These components are the slot-leakage flux and overhang leakage flux. The overhang leakage flux largely exists outside the magnetic system. Hence it need not be considered during the development of the dynamic analogue. The slot leakage flux consists of component fluxes linking individual coil-sides to varying extents. The paths of these fluxes can be approximately represented as shown in Fig. 2.6a. The air path through the slots largely accounts for the reluctance in the path of the slot leakage fluxes. Therefore the reluctance of all the paths shown in the figure will be nearly equal and, to a large extent, independent of saturation of the armature core. These fluxes can be therefore replaced by an equivalent flux linking the coil-side entirely. The equivalent slot leakage fluxes of the three phases form belts around the conductors of a phase group as shown in Fig. 2.6b. At the instant shown, the current i_a in phase A is at a maximum while the currents in the

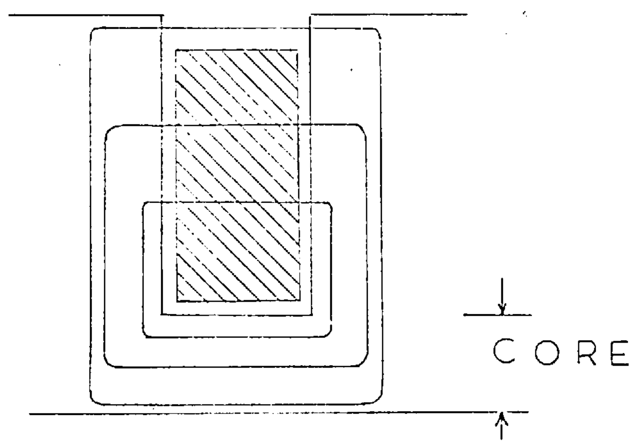

FIG. 2.6a IDEALISED PATHS OF SLOT LEAKAGE FLUX

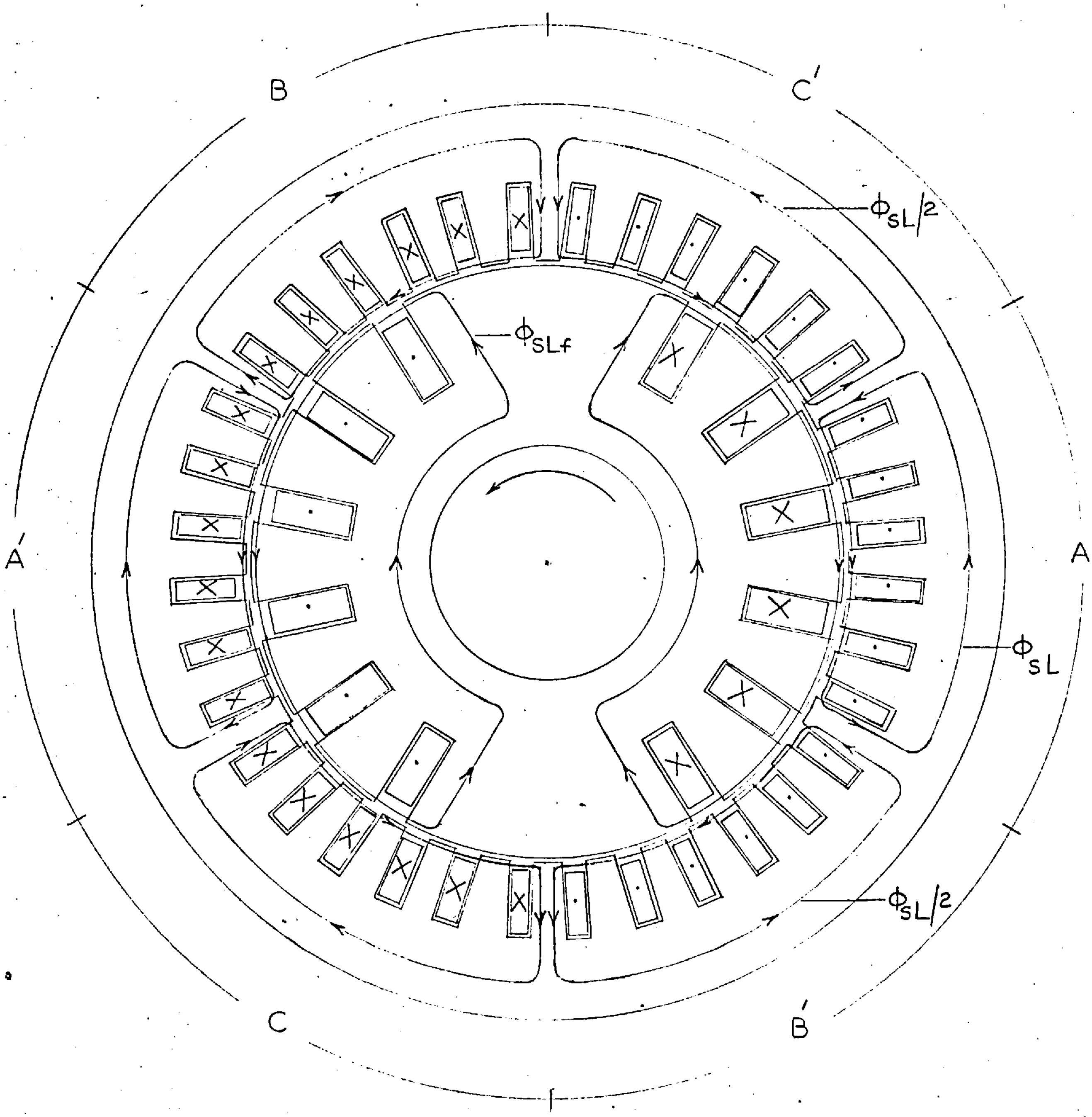

FIG. 2.6b REPRESENTATIVE PATHS OF THE EQUIVALENT SLOT LEAKAGE FLUXES IN THE CYLINDRICAL-ROTOR MACHINE

other two phases are $-i_a/2$. Since the paths of the slot leakage fluxes associated with the three phases are similar, it follows that the leakage fluxes associated with phases B and C would be equal to half the flux associated with phase A. As a result of this difference between the leakage fluxes, the total flux in the stator core varies from one phase belt to the next. However, this variation is generally small and can be neglected. In any case, the representation of this variation in a dynamic analogue can not be exact since the relative magnitudes of the leakage fluxes of the three phases vary from instant to instant. Also, such a refinement is not usually necessary as the ampere-turns required by the stator core form a small per cent of the total when the machine operates at the rated voltage.

In a practical machine, the armature winding is not sinusoidally distributed. In such a machine, the space-harmonic components of armature-reaction m.m.f. establish fluxes which are correspondingly distributed in the air-gap. A part of these fluxes also links the field winding and should be therefore classified as a mutual flux. However, since these fluxes are usually small, they are considered as forming the differential leakage flux of the armature.

A path of the equivalent slot leakage flux associated with the field winding is shown in Fig. 2.6b. This path is derived by making approximations similar to those employed in the preceding paragraphs. For a given operating power factor, the disposition of this path with respect to a representative path of mutual flux is invariant with time. Therefore the influence of rotor slot leakage flux on the saturation of the rotor core can be shown in a dynamic analogue.

Figs. 2.7a and b respectively show the lumped magnetic circuit and the dynamic analogue of the machine. S_{sL} in Fig. 2.7a is an equivalent reluctance representing the armature slot leakage flux paths. This reluctance has a value such that the flux associated with it is the slot leakage flux of phase A. The significance of the other symbols is explained in Figs. 2.7a and b. The iron loss in the machine is approximately represented by the resistance R' in Fig. 2.7b. This resistance mainly represents hysteresis and eddy current loss in the armature.

2.9.3. Influence of saturation on the dynamic analogue

If the distribution of resultant flux when the machine is saturated remains similar to that under unsaturated conditions, Fig. 2.7b will also be the fundamental-frequency dynamic analogue of the saturated

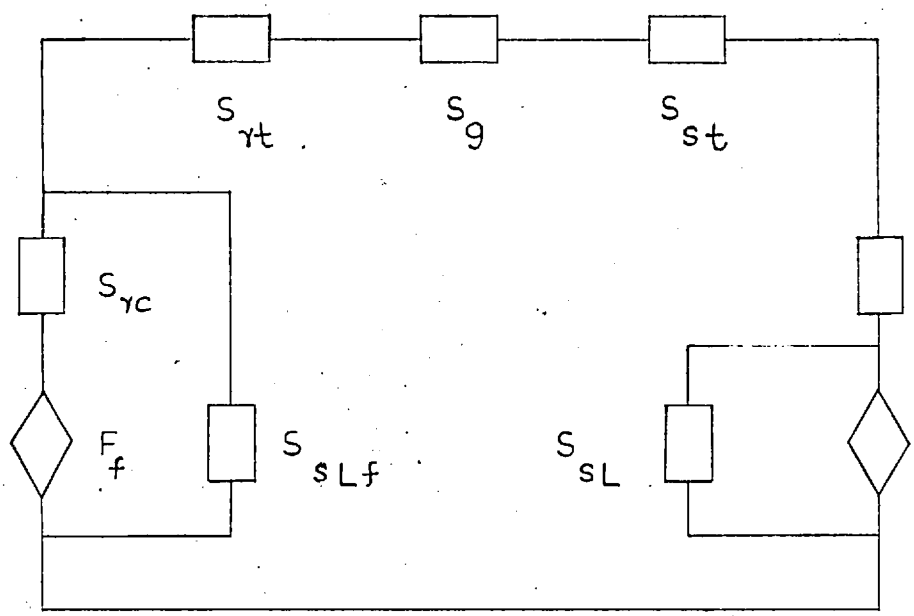

F_a, F_f FUNDAMENTAL COMPONENTS OF ARMATURE-REACTION AND FIELD M.M.F.S PER POLE

S_{sc}, S_{rc} RELUCTANCES OF STATOR AND ROTOR CORES

S_{st}, S_{rt} RELUCTANCES OF STATOR AND ROTOR TEETH

S_g RELUCTANCE OF AIR-GAP

S_{sL}, S_{sLf} RELUCTANCES OF EQUIVALENT ARMATURE AND FIELD LEAKAGE FLUX PATHS

FIG. 2.7 a MAGNETIC CIRCUIT OF THE MACHINE

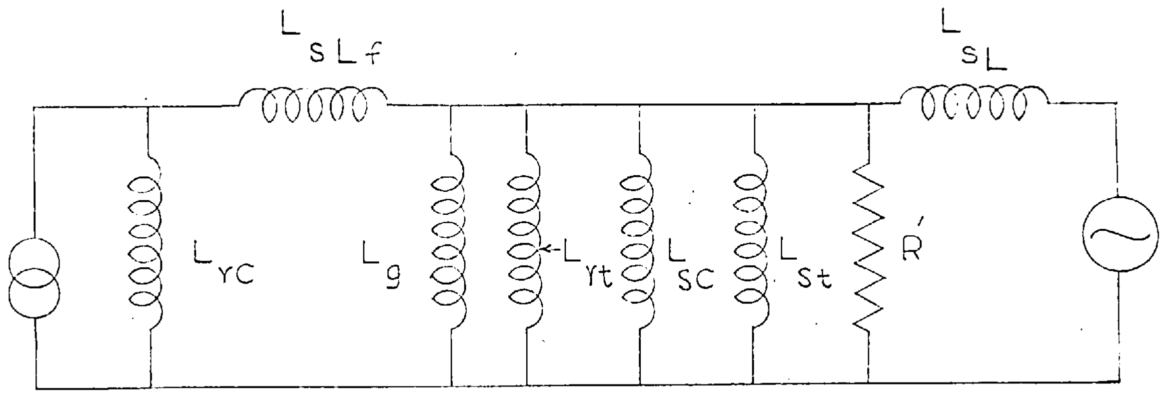

THE SUBSCRIPTS CORRESPOND TO THOSE IN FIG. 2.7 a

FIG. 2.7 b DYNAMIC ANALOGUE

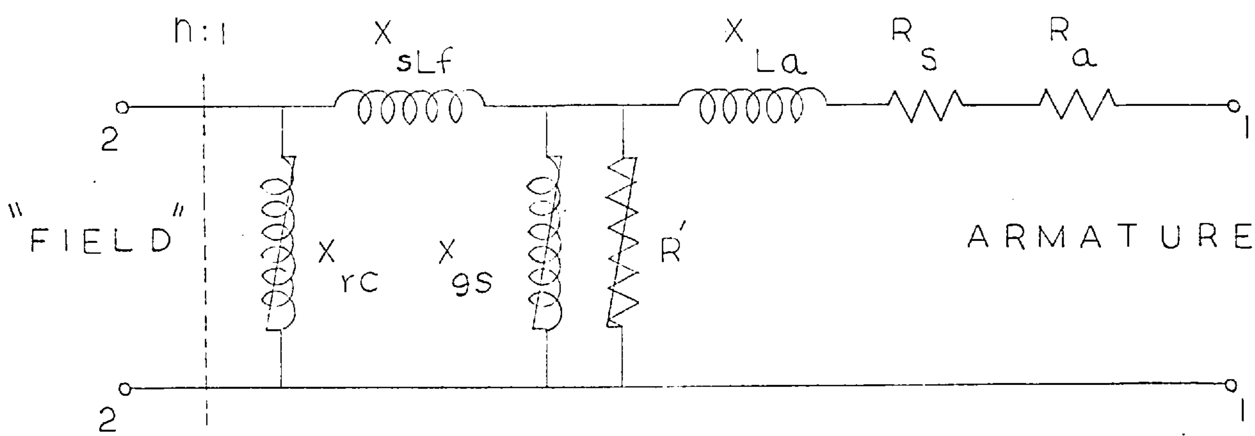

FIG. 2.8 EQUIVALENT CIRCUIT OF THE CYLINDRICAL-ROTOR MACHINE

machine. The inductances L_g, L_{sLf} and L_{sL} will remain constant. The other inductances representing various iron paths would be non-linear.

However, saturation influences the path of mutual flux through the stator and rotor teeth. When the teeth are highly saturated, the flux passing through the adjoining slots can not be ignored. These slots form paths magnetically in parallel with the teeth. A magnetic circuit composed of one slot and one tooth in parallel can be represented by an equivalent electric circuit consisting of two inductances in series. The two series inductances may be replaced by an inductance having an equivalent magnetisation characteristic. In the same way, the inductances L_{st} and L_{rt} in the dynamic analogue can be modified to include the flux passing down the slots.

Saturation of the teeth results in a flat-topped distribution of air-gap flux density. Consequently a larger flux per pole is required to generate a given fundamental voltage than when the distribution is sinusoidal. The increase in flux per pole results in increased saturation of the stator and rotor cores. For a given operating condition - for example, the machine on open-circuit-the reluctances representing the two cores can be approximately calculated allowing for the distribution of air-gap flux. When the armature and field windings are distributed sinusoidally, the resultant m.m.f. on load has the same distribution as the m.m.f. with the machine on open-circuit. Changes in the distribution of air-gap flux density due to saturation of the magnetic circuit are then similar under the two operating conditions of the machine. The same parameters of the dynamic analogue can then be employed to describe the operation of the machine both on load and on open-circuit.

When the windings are not distributed sinusoidally, the distribution of resultant m.m.f. with the machine on load is different from the distribution (of field m.m.f.) on no-load. The distribution of air-gap flux density is correspondingly different. If the change in the distribution is considerable, the reactances of the dynamic analogue do not have identical values (for the same fundamental voltage across their terminals) under the two operating conditions of the machine. In a cylindrical-rotor machine, the harmonic components of the field and armature m.m.f.s are usually small. The change in the distribution of resultant m.m.f. is therefore ignored for normal calculations.

2.9.4. Equivalent circuit of the machine

An equivalent circuit relating the current in an armature phase to the field current is obtained from the dynamic analogue of the machine by the inclusion of an ideal transformer. The turns-ratio of this transformer is determined by equating the fundamental components of the field and armature-reaction m.m.f.s per pole. The derivation of an equivalent circuit from a dynamic analogue is considered in greater detail in appendix A.

The peak values of the fundamental components of the armature-reaction and field m.m.f.s per pole are given by the following expressions. (Ref. 26, p. 227)

$$F_a = \frac{2.7\ I_a\ T_{ph}\ K_{w1}}{P} \qquad 2.19$$

$$F_f = \frac{4}{\pi}\,\frac{K_w\ N_f\ I_f}{P} \qquad 2.20$$

T_{ph} and N_f are respectively the turns per phase on the armature winding and the number of turns on the field winding. n, the turns-ratio, is obtained by calculating the value of $\frac{I_a}{I_f}$ from the above two expressions.

An equivalent circuit of the machine is shown in Fig. 2.8. R_a represents the armature resistance per phase. X_{gs} is the reactance corresponding to the parallel combination of inductances L_{st}, L_g, L_{sc} and L_{rt} in Fig. 2.7b. However, it should be pointed out that the reactances in Fig. 2.8 are not derived from the corresponding inductances in Fig. 2.7b by a simple multiplication of the latter by ω. The turns-ratios of the ideal transformers have to be taken into account in calculating the reactances. The method of calculation has been discussed in appendix A. An equivalent circuit similar to Fig. 28 has been derived by Slemon[22].

The overhang leakage reactance of an armature phase is connected in series with R_a. The reactance X_{La} in Fig. 2.8 is the sum of the slot leakage, overhang leakage and differential leakage reactances of an armature phase. The stray losses produced by the overhang leakage flux can be approximately accounted for by a resistance R_s connected as shown in Fig. 2.8.

2.9.5. Equivalent Tee and Pi circuits of the machine

If the field leakage flux is small, the influence of this flux on the saturation of the rotor core can be neglected. The reactance X_{rc} in Fig. 2.8 can then be assumed to function at the same voltage as X_{gs}. The machine is then represented by the Tee circuit of Fig. 2.9a.

When the circuit of Fig. 2.8 represents an unsaturated machine, it can be transformed into the circuit of Fig. 2.9b. This circuit may be described as a Pi circuit, if the resistances in the circuit are ignored. Since the

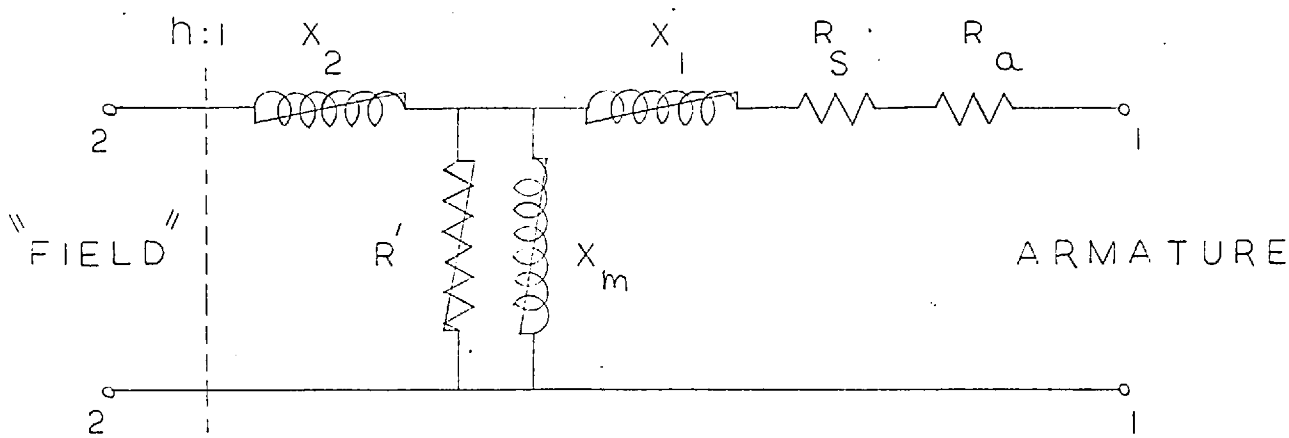

a. EQUIVALENT TEE CIRCUIT

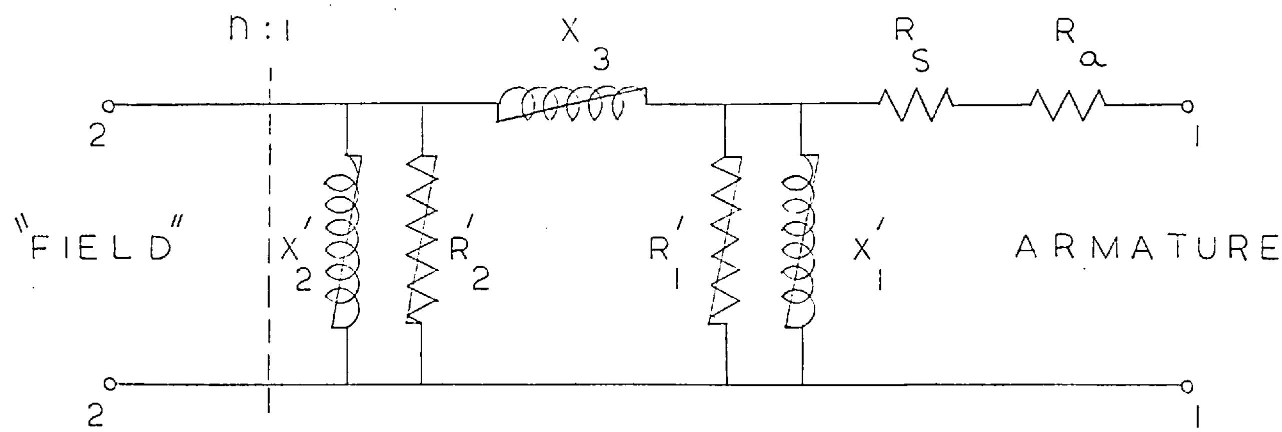

b. EQUIVALENT PI CIRCUIT

FIG. 2.9 TEE AND PI. CIRCUIT REPRESENTATIONS OF THE CYLINDRICAL-ROTOR MACHINE resistances can be usually ignored in comparison with the reactances, the following discussion is based on transformations of Fig. 2.8 performed by assuming the circuit to be wholly reactive.

When Fig. 2.8 describes an unsaturated machine, the Tee and Pi circuits derived by transformation will be equivalent. The Tee circuit with linear reactances X_1 and X_2, and the Pi circuit with a linear reactance X_3 will be only approximately equivalent to the circuit of Fig. 2.8, when the latter represents a saturated machine. The reactances of the Pi circuit are given by the following expressions.[25]

$$X_2' = \frac{X_{rc}\ (X_{gs} + X_{sLf} + \dfrac{X_{gs}\ X_{sLf}}{X_{La}})}{X_{rc} + (X_{gs} + X_{sLf} + \dfrac{X_{gs}\ X_{sLf}}{X_{La}})} \qquad 2.21$$

$$X_3 = X_{La} + X_{sLf} + \frac{X_{La}\ X_{sLf}}{X_{gs}} \qquad 2.22$$

and $$X_1' = X_{gs} + X_{La} + \frac{X_{gs}\ X_{La}}{X_{sLf}} \qquad 2.23$$

X_{gs} includes the linear reactance X_g of the air-gap. This reactance (X_g) largely determines the value of X_{gs} for operating conditions around the knee of the open-circuit characteristic of the machine. Even at higher operating voltages, reactance X_g exerts a linearising influence on X_{gs}. The percentage variations of X_3 are therefore smaller than in a transformer operated over a corresponding range of flux densities in the yoke. The following arguments can be employed to determine the influence of saturation on reactances X_1' and X_2'.

If the voltage across X_{rc} (Fig. 2.8) is held constant, the voltage across X_{gs} is higher on open-circuit than on load. The reactance X_{gs} is therefore smaller on open-circuit than on load. If X_{rc} is very small and if X_{sLf} is large as compared to X_{La}, the contribution of X_{gs} to reactance X_2' can be ignored. The reactance X_2' will then be a single-valued function of the voltage across its terminals. The variations of X_{gs} with load conditions will be then reflected in corresponding variations of reactance X_1'. However, if X_{La} is small, reactance X_1' can be assumed to be equal to X_{gs} (i.e. reactance X_1' will also be independent of the load conditions of the machine). The Pi circuit would then be a good approximation to Fig. 2.8.

On the other hand, if X_{La} is large as compared to X_{sLf} and if X_{rc} is also large, the Tee circuit becomes a more suitable approximation to Fig. 2.8. Thus, the Pi circuit is a better representation of a machine, having a large field leakage reactance, in which the field system is highly saturable, while the Tee circuit forms a better approximation when the machine has a large armature leakage reactance and comparatively little saturation of the field system. However, it is later seen that in the machines tested, the difference between the two circuits is not appreciable. This is due to the small magnitude of the contribution made by the field leakage flux to the saturation of the rotor core.

2.9.6. Equivalent circuit of a machine operating at power factors other than zero

If the magnetic circuit of the machine is radially symmetrical, the dynamic analogue and the equivalent circuit derived in the previous sections can be employed to describe the operation of the machine at power factors other than zero. The space displacement of the axis of the armature-reaction and field m.m.f.s. can be represented by a corresponding phase shift between the currents in the equivalent circuit. However, the magnetic circuit of a practical machine is not completely symmetrical owing to the presence of an unslotted part along the pole-axis. The length of the equivalent air-gap along the slotted part is larger than that along the unslotted part. The maximum flux density in the rotor teeth is a function of the spatial position of the resultant m.m.f. The reluctance in the path of the mutual flux is therefore different under open-circuit and load conditions of the machine. These effects are not considered for usual calculations. The calculations are performed assuming the equivalent circuit describing the machine on open-circuit to be valid under load conditions.

2.10. Equivalent circuit of a salient-pole machine

Unlike a cylindrical-rotor machine, the field winding in a salient-pole machine is concentrated round the poles. The m.m.f. established by the field current is distributed in a rectangular fashion over the pole-arc. Hence, to secure a nearly sinusoidal distribution of the air-gap flux density, the length of the air-gap has to be made non-uniform. The flux density distribution produced by the field m.m.f. F_f (acting alone) is not entirely sinusoidal in a practical machine.

Owing to the distributed nature of the armature-reaction m.m.f. and the non-uniform length of the air-gap, the air-gap flux density established by the m.m.f. (acting alone) is not distributed sinusoidally. Moreover, the flux density distribution is also dependent upon the spatial position of the axis of the m.m.f. As mentioned earlier, this factor is taken into account by resolving the fundamental armature-reaction m.m.f. into component m.m.f.s. F_{ad} and F_{aq} acting along the direct and quadrature axes respectively. Equivalent circuits for the direct-axis are derived in this section.

When the machine is not saturated, the harmonic components of air-gap flux do not influence the permeability of the magnetic paths of the fundamental flux. A dynamic analogue can be therefore derived to represent the paths of the fundamental flux ignoring the presence of the harmonic components. The m.m.f.s. included in this analogue are not, however, the m.m.f.s. F_f and F_{ad}. The m.m.f.s. in the analogue have to be defined in conjunction with an equivalent air-gap of uniform length. This definition is as follows.

The length of the equivalent air-gap can be taken to be equal to l_g, the effective air-gap at the polar axis. The equivalent direct-axis armature-reaction m.m.f. F'_{ad} can be now defined as a m.m.f. which produces the same fundamental flux density across the uniform air-gap as that existing in the machine. This definition ignores the reluctance of the iron parts of the magnetic circuit. The m.m.f.s. F_{ad} and F'_{ad} are related as follows. The peak air-gap flux density B_{gm} produced by F_{ad} is related to it by the expression

$$F_{ad} = \frac{B_{gm} \times l_g}{\mu_o} \qquad 2.24$$

The equivalent air-gap being also of length l_g, the m.m.f. F'_{ad} is given by the expression

$$F'_{ad} = B_{gf} \times l_g / \mu_o \qquad 2.25$$

B_{gf} is the peak fundamental flux density established by F_{ad}. The m.m.f.s. F_{ad} and F'_{ad} are therefore related as follows.

$$F_{ad}' = F_{ad} \times B_{gf}/B_{gm} \qquad 2.26$$

The ratio B_{gf}/B_{gm} can be calculated by using constants derived by Wieseman.[31] These constants have been determined by the method of flux plotting. The values given in the reference cover a range of salient-pole structures. These structures are defined by the ratios of the pole-arc to the pole-pitch and the maximum to minimum lengths of the air-gap. The actual and equivalent field m.m.f.s. can be related in a similar manner employing a set of constants given in reference 31.

2.10.1. Equivalent circuit of the direct-axis

The paths of mutual flux in the stator (armature) are similar to those in a cylindrical-rotor machine. The latter have been discussed in section 2.9.2. The influence of armature leakage flux on the saturation of the stator core is ignored for the reasons set out in that section. The path of mutual flux through the pole is adequately described by the representative path shown in Fig. 2.10. In addition to the mutual flux following this path, there is some amount of fringe flux at the pole-tips. For calculations, the presence of this flux is taken into account by modifying the reluctance of the air-gap.

Some paths of field leakage flux are shown in Fig. 2.11. This figure shows that a considerable part of the field leakage flux only links the winding partially. (See also the flux plot in reference 31). The total flux at various cross-sections along the height of the poles is therefore different, being a maximum in the yoke and the base of the pole and a minimum in the pole-shoe. The leakage flux paths contain a large air section. Therefore, for the usual levels of saturation of the poles, the influence of this saturation on the reluctance of the leakage flux paths and the distribution of leakage flux may be neglected. As a result, the actual field leakage flux can be approximately replaced by an equivalent flux linking the field winding entirely. This equivalent flux includes fluxes which exist at the ends of the poles and the pole shoes. The path of the equivalent flux is shown dotted in Fig. 2.11.

The flux at various sections along the height of the poles is then assumed to be the same. The pole system and the yoke are therefore represented by two reluctances

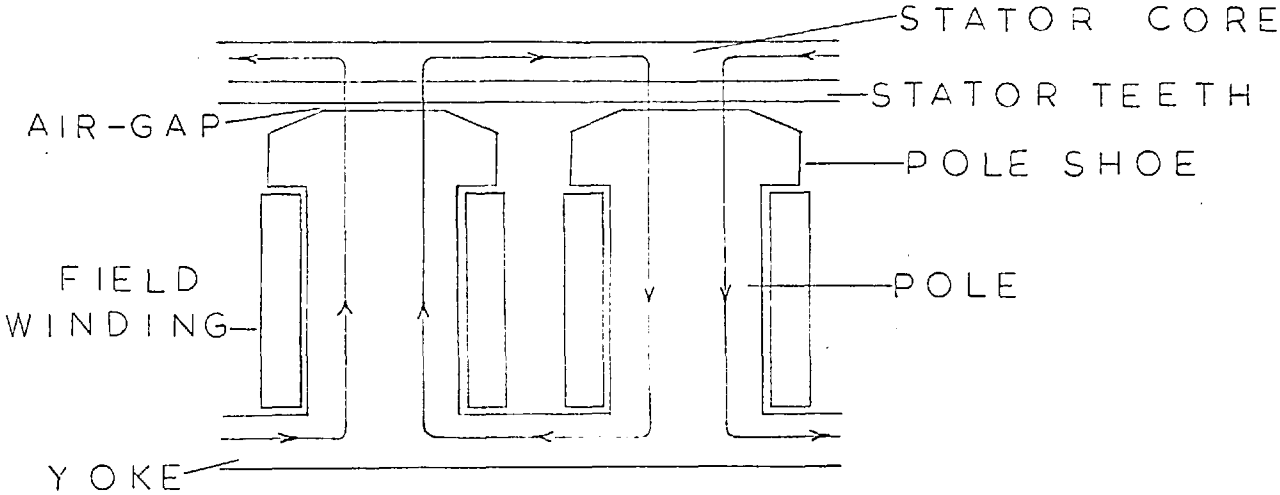

FIG. 2.10 A REPRESENTATIVE PATH OF MUTUAL FLUX ALONG THE DIRECT-AXIS OF A SALIENT-POLE MACHINE

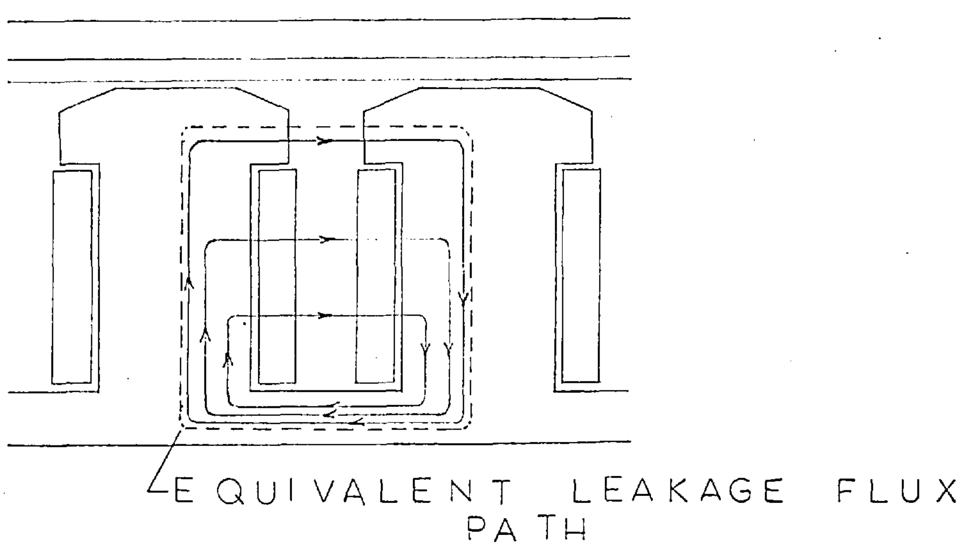

FIG. 2.11 SOME PATHS OF THE FIELD LEAKAGE FLUX

in series in the magnetic circuit. The magnetic circuit and the dynamic analogue based on the above considerations are shown in Figs. 2.12a and b. An equivalent circuit can be obtained from Fig. 2.12b by the inclusion of two ideal transformers. The final equivalent circuit of Fig. 2.12c, including only one ideal transformer, is derived by the considerations outlined in appendix A. The turns-ratio n of the ideal transformer in Fig. 2.12c is obtained by equating the expressions for the equivalent armature and field m.m.f.s. The conditions at terminals 1-1 of Fig. 2.12c correspond to the fundamental direct-axis phase voltage and current in the machine. The current at terminals 2-2 is the field current. The significance of various resistances in the equivalent circuit has been explained in section 2.9.4. The magnetic circuit of Fig. 2.12a has been employed by Saad Mikhail[15] to derive a relationship between the Potier and armature leakage reactances of a salient-pole machine.

On saturation of the magnetic system, the harmonic components of air-gap flux influence the reluctance of the paths of fundamental flux (i.e. flux associated with the fundamental air-gap flux density). For any one operating condition, the reactances of the equivalent circuit can be calculated allowing for the distribution

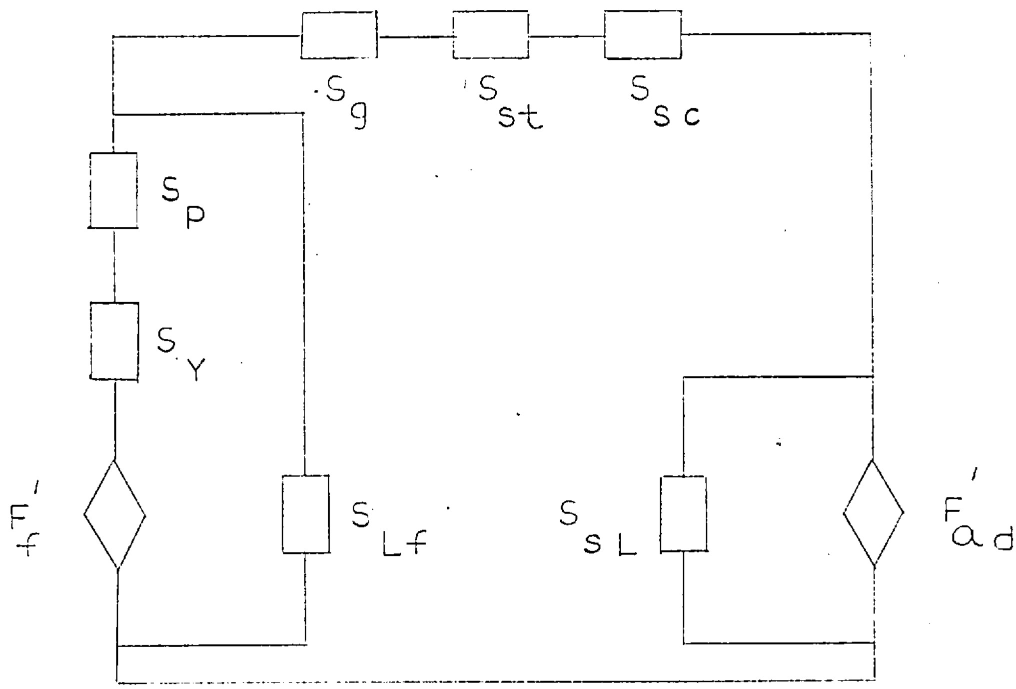

F'_f , F'_{ad} EQUIVALENT FIELD AND DIRECT-AXIS ARMATURE-REACTION M.M.F PER POLE

S_{Lf} RELUCTANCE OF THE AIR PATH OF THE EQUIVALENT FIELD LEAKAGE FLUX.

S_Y RELUCTANCE OF THE YOKE

S_P RELUCTANCE OF POLE AND POLE-SHOE

S_g RELUCTANCE BASED ON THE MINIMUM EFFECTIVE LENGTH OF AIR-GAP

FOR OTHER SUBSCRIPTS SEE FIG. 2.7a

FIG. 2.12a MAGNETIC CIRCUIT OF THE DIRECT-AXIS

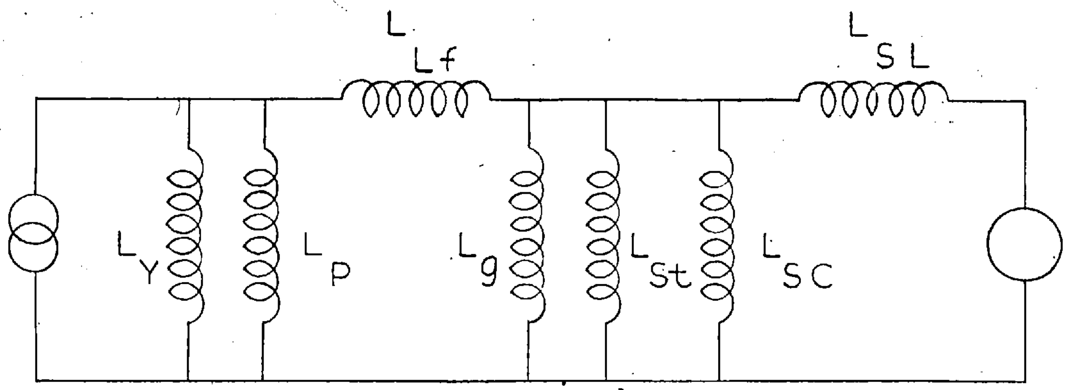

b. DYNAMIC ANALOGUE

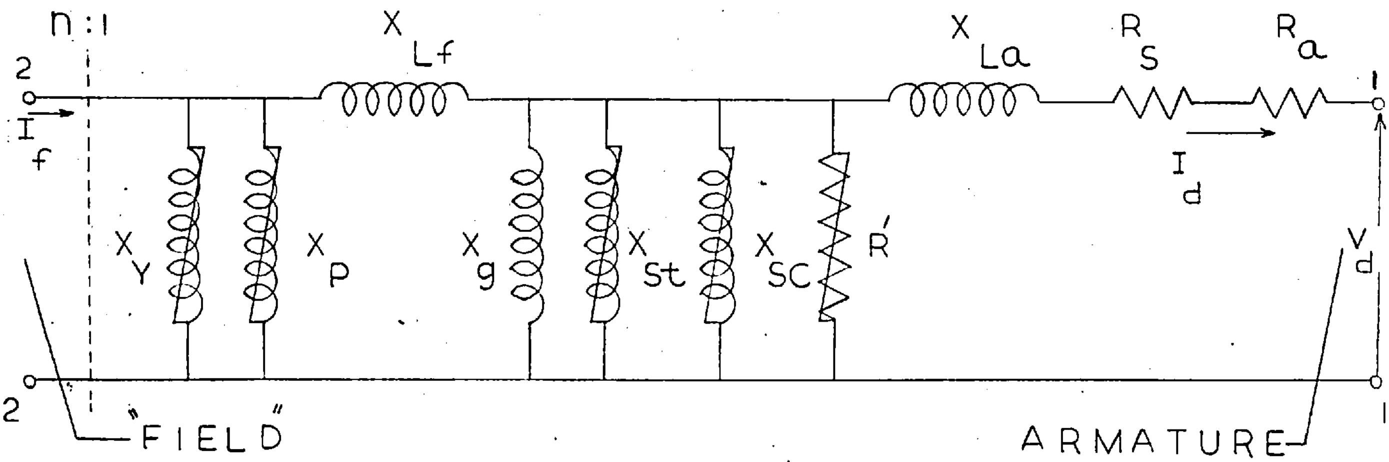

C. EQUIVALENT CIRCUIT

FIG. 2.12 REPRESENTATION OF THE DIRECT - AXIS OF A SALIENT - POLE MACHINE of the gap flux. The difference between the distributions of air-gap flux in the machine on open-circuit and when it is supplying a load is more pronounced than in a corresponding cylindrical-rotor machine. The changes in the distribution of air-gap flux are accompanied by changes in the waveform of the phase voltage. Some records of the phase voltage of a salient-pole machine on open-circuit and when the machine is supplying a zero power-factor load are included in chapter 5.

The changes in the distribution of gap flux influence the parameters of the equivalent circuit. For example, for the same fundamental flux the total flux per pole is larger when the machine is supplying a load than when it is on open-circuit. The increase in total flux results in additional saturation of the poles, yoke and the stator core. Therefore, for the same voltage across their terminals, reactances X_P, X_Y, and X_{sc} (Fig. 2.12c) have a smaller value when the machine is on load than when it is on open-circuit.

The equivalent circuit of Fig. 2.12c is more useful for representing the direct-axis of a machine having a large field leakage reactance. When such a machine operates under load conditions at which the field m.m.f. is much larger than the armature-reaction m.m.f. (e.g. at or above the rated terminal voltage), there is considerable saturation of the poles due to field leakage flux. At the same time, the distribution of the resultant air-gap flux is not significantly different from the distribution at the same generated voltage with the machine on open-circuit. An equivalent circuit with parameters calculated on the basis of the flux distribution on open-circuit can be then also employed to represent the machine on load. The condition referred to above would be obtained in a machine having a large number of poles and a small pole-pitch. The field leakage coefficient of such a machine is usually larger than that of a machine having a small number of poles and a large pole-pitch. For example, average coefficients of 1.4 and 1.2 are obtained for the two types of machines from the values given in reference 32.

The equivalent circuit of Fig. 2.12c can be transformed to the equivalent Tee and Pi circuits. Since Figs. 2.8 and 2.12c are similar, the remarks made in section 2.9.5 can also be applied to the transformation of Fig. 2.12c.

2.11. Equivalent circuit of the quadrature-axis

An equivalent circuit of the quadrature axis is derived by employing the methods described in the previous section. The only m.m.f. acting along the axis is F_{aq}. This m.m.f. acts on a magnetic circuit which includes a non-uniform air-gap. The resulting distribution of air-gap flux contains a substantial third harmonic.

An equivalent circuit is obtained by employing an equivalent reluctance of the air-gap. This reluctance is defined so as to relate the fundamental quadrature-axis flux and the m.m.f. F_{aq}, assuming the m.m.f. required by the unsaturated iron paths to be negligible. The equivalent reluctance can be calculated by using the constants given in reference 31.

The actual distribution of flux along the quadrature axis has been shown in reference 31. An idealised representation of the flux paths is shown in Fig. 2.13a. Most of the "mutual" flux follows a path through the pole-shoes and the upper part of the poles. The paths of this flux through the stator teeth and core are similar to the paths of the direct-axis flux. Usually the reluctance S_{gq} of the equivalent air-gap contributes mainly to the reluctance of the quadrature-axis flux paths. A magnetic circuit based on an approximate representation of the iron paths is therefore adequate. Such a magnetic circuit is shown in Fig. 2.13b. S_{st} and S_{sc} are reluctances of the stator teeth and core, and S is the reluctance of the mutual flux path through the pole-shoe and pole body. S_{sL} is an equivalent

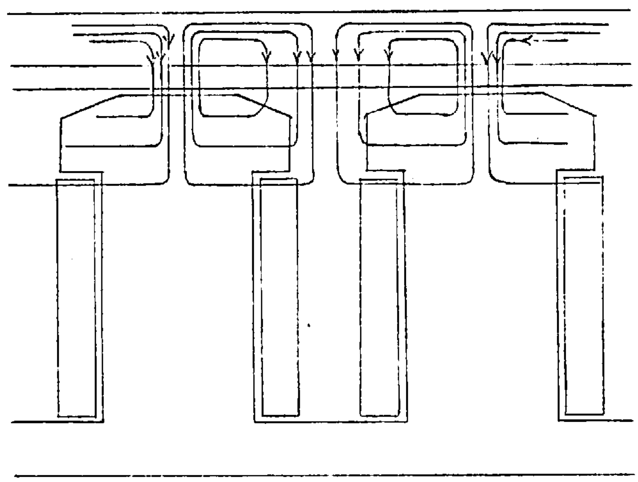

a. IDEALISED PATHS OF FLUX CROSSING THE AIR-GAP

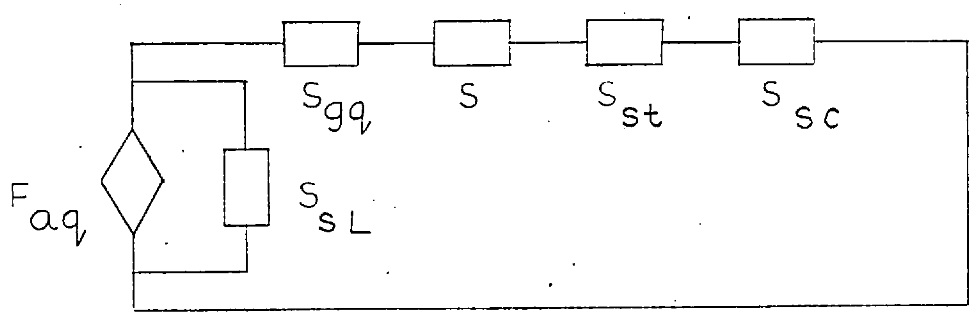

F_{aq} FUNDAMENTAL COMPONENT OF THE QUADRATURE-AXIS ARMATURE-REACTION M.M.F PER POLE

S_{gq} RELUCTANCE OF THE EQUIVALENT AIR-GAP

S RELUCTANCE OF THE FLUX PATH THROUGH THE FIELD SYSTEM

b. MAGNETIC CIRCUIT

FIG 2.13 MAGNETIC CIRCUIT OF THE QUADRATURE AXIS.

reluctance of the armature leakage flux paths. The equivalent circuit derived from Fig.2.13b will include one ideal transformer. This ideal transformer can be removed by referring the elements of the equivalent circuit to the primary side of the transformer. The resulting equivalent circuit is shown in Fig.2.13c. R_a and X_{La} are the armature resistance and armature leakage reactance per phase. X_{aq} is the quadrature-axis armature-reaction reactance. The voltage and current at the terminals of Fig. 2.13c are the quadrature-axis phase voltage V_q and current I_q. Reactances X_{aq} and X_{La} together form the quadrature-axis synchronous reactance X_q.

When the machine is saturated, the assumption that the direct and quadrature axes fluxes (and m.m.f.s.) exist independently of each other is not wholly correct. The interaction of the two axes has been examined in references 33 and 34. However, for ordinary calculations this interaction is ignored. In many cases the saturation of reactance X_q is not marked and it is sufficient to use the unsaturated value of X_q for calculations.

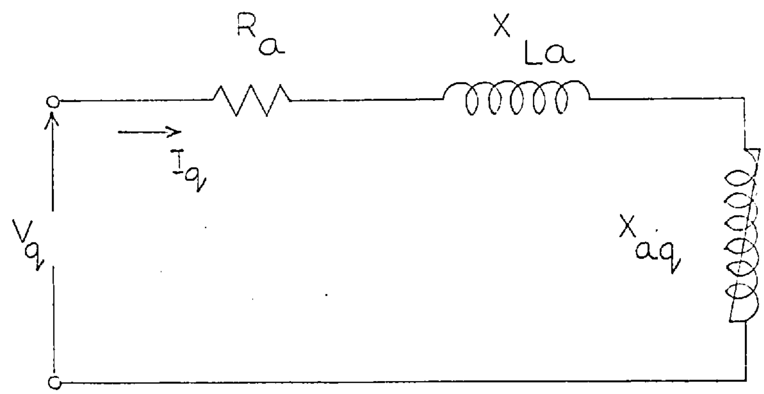

FIG. 2.13C EQUIVALENT CIRCUIT OF THE QUADRATURE AXIS OF A SALIENT-POLE MACHINE

CHAPTER 3

Determination of the parameters of the equivalent Tee and Pi circuits

3.1 Scope   Two methods of obtaining the parameters of a non-linear equivalent Tee circuit are explained. These methods are called the transfer-impedance and self-impedance methods. The methods of determination of the parameters of a Pi circuit are developed.

3.2 Determination of the parameters of the equivalent Tee circuit from tests

A Tee circuit of inductances is shown in Fig. 3.1a. When the reactance X_m of this circuit is saturable, it is possible to use its non-linear characteristics to determine the turns-ratio n explicitly. As an example may be mentioned the well-known Potier method of determining the leakage reactance of an alternator. Two alternative methods of deriving the Tee circuit are explained in this chapter. These methods are called the transfer-impedance and the self-impedance methods. The former is applicable when the voltages at both pairs of terminals of the circuit can be measured. The latter method is a modification which permits the determination of the turns-ratio when the voltage across one pair of terminals can not be measured. This situation arises when the circuit represents a synchronous machine. The voltage across the terminals of the equivalent circuit representing the field terminals is then not available.

Though the methods are explained by considering the determination of the parameters of a Tee circuit composed only of inductances, the methods can be employed, with small modifications, to determine the parameters of a Tee circuit of the type shown in Fig. 4.6. (P 99). Therefore the methods are called 'impedance' methods and not 'reactance' methods.

3.3.1 Transfer-impedance method

This method is based on open-circuit tests performed as per Figs. 3.1 (a) and (b). These tests yield the transfer-impedance characteristics drawn in Figs. 4.3 and 4.4 (P.94-5). These characteristics relate voltages V_2 and V_1' to currents I_1 and I_2' respectively.

Referring to Figs. 3.1(a) and (b),

$$X_m = \frac{nV_2}{I_1} = \frac{V_1'}{I_2'/n}$$

which gives $$\frac{X_m}{n} = \frac{V_2}{I_1} = \frac{V_1'}{I_2'} \qquad 3.1.$$

As saturation of the reactance X_m occurs when a definite number of ampere-turns are applied to it, if it saturates when the current I_1 is equal to I_a, it will only saturate when the current I_2' is equal to I_b, I_a and I_b being related by the equation $nI_a = I_b$.

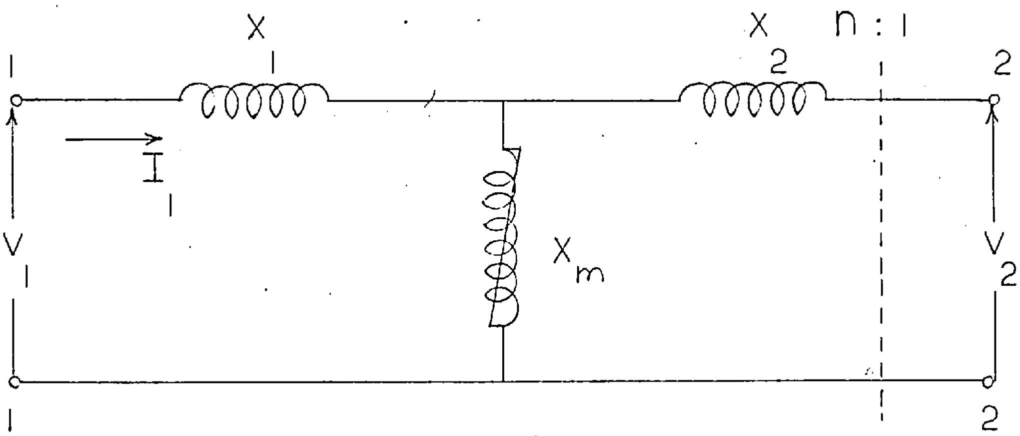

FIG. 3.1(a)

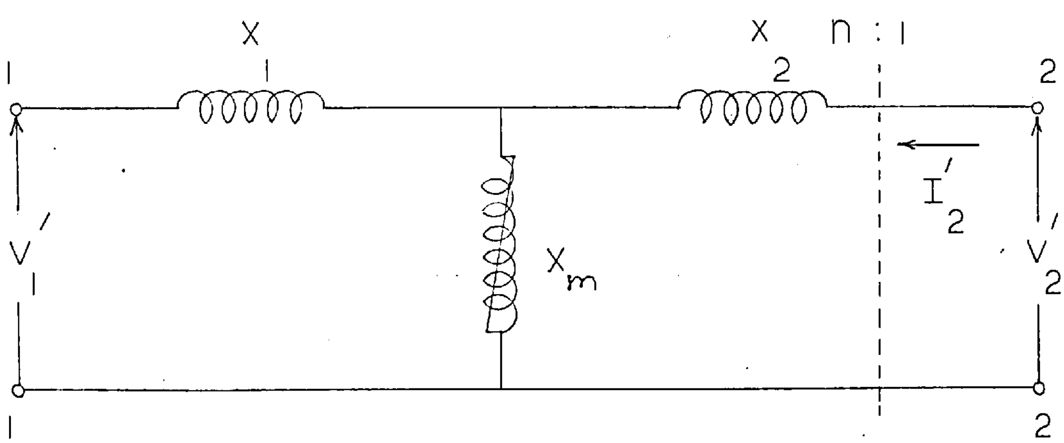

FIG. 3.1(b)

FIG. 3.1 OPEN-CIRCUIT TESTS ON THE TEE CIRCUIT

Further, as the ratio of the voltages V_1' and V_2 for the same current through X_m is equal to n, the voltage V_1' when a current I_b is passing through X_m will be n times as large as the voltage V_2 when I_a is passing through it. Thus, the voltages V_A and V_B and the currents I_A and I_B at the two points A and B on the characteristics of Fig. 4.4. will be in the ratio n, if the two points represent the same level of saturation of the reactance X_m. Conversely, if the points A and B are located upon the two characteristics, the ratio of their coordinates will be equal to n.

From eqn. 3.1, the ratios V_A/I_A and V_B/I_B are both equal to X_m/n. Since these ratios are the slopes of the lines drawn to the two points from the origin, the points A and B lie on the same straight line from the origin. The points A and B, and other similar pairs of points are, therefore, the points of intersection of the two characteristics with various straight lines drawn from the origin. It may be noted that the points of intersection are not defined in the unsaturated, linear parts of the two characteristics which are themselves coincident straight lines from the origin. This reiterates the impossibility of obtaining a singular value of n from tests on a linear circuit.

3.3.1.1. Magnitudes of the reactances of the network.

Once the turns-ratio has been found in the above manner, the reactances can be easily obtained by using the following formulae.

$$X_m = \frac{nV_2}{I_1} = \frac{V_1'}{I_2'/n} \qquad 3.2.$$

$$X_1 = \frac{(V_1 - nV_2)}{I_1} \qquad 3.3.$$

$$X_2 = \frac{(nV_2' - V_1')}{I_2'/n} \qquad 3.4.$$

The reactance X_m can be plotted as a function of the voltage nV_2 or V_1' across it.

3.3.2. Self-impedance method.

This method can be employed to obtain a solution of the network when one of the voltages is unknown, as in a synchronous machine. Assuming that the voltage V_2 in Fig. 3.1(a) cannot be measured, the reactances and the turns-ratio are determined in the following manner.

3.3.2.1. Value of the turns-ratio.

Consider two points (V_A, I_A) and (V_B, I_B) on the unsaturated and saturated parts of the characteristic showing V_1 as a function of I_1. Denoting the value of the reactance X_m when unsaturated by X_{uns}, the following equations can be written down.

$$V_A/I_A = (X_{uns} + X_1) \qquad 3.5.$$

$$V_B/I_B = (X_m + X_1) \qquad 3.6.$$

By subtraction, we obtain

$$(X_{uns} - X_m) = (\frac{V_A}{I_A} - \frac{V_B}{I_B}) \qquad 3.7.$$

Two similar points (V'_A , I'_A) and (V'_B , I'_B) on the graph of the voltage V'_1 against the current I'_2 will be related by the equations

$$\frac{V'_A}{I'_A} = \frac{X_{uns}}{n}$$

$$\frac{V'_B}{I'_B} = \frac{X'_m}{n} \qquad 3.8.$$

from which $$\frac{(X_{uns} - X'_m)}{n} = (\frac{V'_A}{I'_A} - \frac{V'_B}{I'_B}) \qquad 3.9.$$

X'_m will be equal to X_m if $I'_B/n = I_B$. If the quantities $(X_{uns} - X_m)$ and $\frac{(X_{uns} - X'_m)}{n}$ are plotted against I_B and I'_B respectively, as in Fig. 4.8*, n can be found by locating two points P and Q the coordinates of which are in the same ratio. The points P and Q cannot be directly obtained by a geometrical construction as in the last method and a trial-and-error method has to be used instead. The point P is fixed on one of the characteristics and the ratios of the absiccae and ordinates of the point P and points like Q are examined. The true point Q is obtained when the two ratios are equal.

Since the difference $(X_{uns} - X_m)$ is zero when the reactance X_m is unsaturated, this method fails, as expected, when applied to linear circuits.

*(P. 106)

3.3.2.2. Determination of the reactances:

The reactance X_m is calculated from eqn. 3.8 and can be plotted as a function of the voltage across it. The value of X_1 is given by eqn. 3.6.

In order to find the reactance X_2, an additional short-circuit test has to be performed as shown in Fig. 3.2. The ratio of the terminal currents is given by the equation

$$\frac{I_{2sc}}{n} = \frac{X_m}{X_2 + X_m} I_{1sc}$$

whence $$X_2 = X_m(I_{1sc} \cdot \frac{n}{I_{2sc}} - 1) \qquad 3.10$$

The reactance X_m will be equal to X_{uns} for the usual values of the short-circuit current.

3.3.3. Potier method.

The Potier method is an alternative method of obtaining the turns-ratio when one of the voltages is unknown. It is widely employed for the determination of the armature leakage reactance of synchronous machines.[8]

The reactance X_1 is found in this method from the characteristic relating V_1' to I_2' obtained from the no-load test of Fig. 3.1(b), and the zero power-factor characteristic relating the two quantities when a variable, purely reactive load is connected to the pair of terminals 1-1, the current through the load being kept

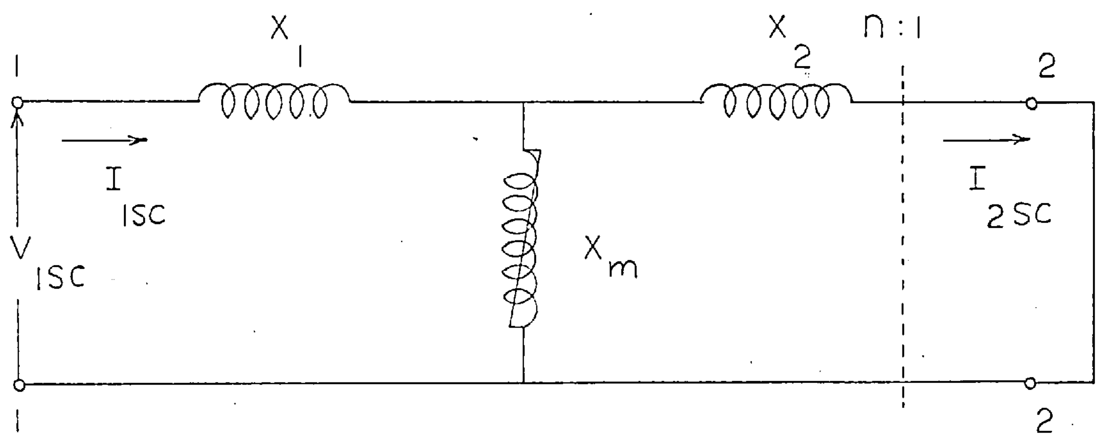

FIG. 3.2 SHORT — CIRCUIT TEST

constant. The two characteristics are shown in Figs. 4.9a and b. (P.112-13)

The reactance is determined from a triangle ABC* constructed by drawing the base CB equal to OO' (the current I_2' at short-circuit), and the line BA, parallel to the straight-line part of the open-circuit characteristic, to intersect the characteristic in A. The altitude AD of the triangle represents the voltage drop $I_L X_1$, and, since I_L is known, X_1 can be found.

The turns-ratio is the ratio of the current represented by the length CD and the current I_L.

The reactance X_m is determined from the open-circuit characteristic by using eqn. 3.8, and the reactance X_2 from the short-circuit test of Fig. 3.2 and eqn. 3.10.

Since the open-circuit and zero power-factor characteristics are parallel straight lines when the circuit is unsaturated, the above construction fails to yield a triangle with a definite altitude and, therefore, a definite value of n, or X_1, in that region of the characteristics.

*(Fig. 4.9a)

3.4. Solution of the Pi network.

3.4.1. Determination of the reactances from open-circuit tests.

If the turns-ratio of the ideal-transformer in Fig. 3.3. is known, the reactances of the Pi circuit can be found from the open-circuit tests shown in Figs. 3·3 and 3.4 by using the following formulae.

$$X_3/n = \frac{(V_2' - V_2)}{I_1} \quad \text{(Appendix B)} \qquad 3.11$$

$$X_1' = \frac{V_1}{I_1 - \frac{(V_1 - nV_2)}{X_3}} = \frac{V_1}{\frac{(nV_2' - V_1)}{X_3}} \qquad 3.12$$

$$X_2' = \frac{nV_2}{\frac{(V_1 - nV_2)}{X_3}} = \frac{nV_2'}{I_2'/n - \frac{(nV_2' - V_1)}{X_3}} \qquad 3.13$$

However, as shown in Appendix B, n cannot be explicitly determined from the terminal tests, whether the reactances X_1' and X_2' are saturable or not. The only method of obtaining a solution of the network is to assume a suitable value of n, for example, the ratio of the voltages V_1/V_2, and calculate the reactances from the above equations.

3.4.2. Determination of the reactances if one of the voltages is unknown

If the voltage across a pair of terminals (Voltages

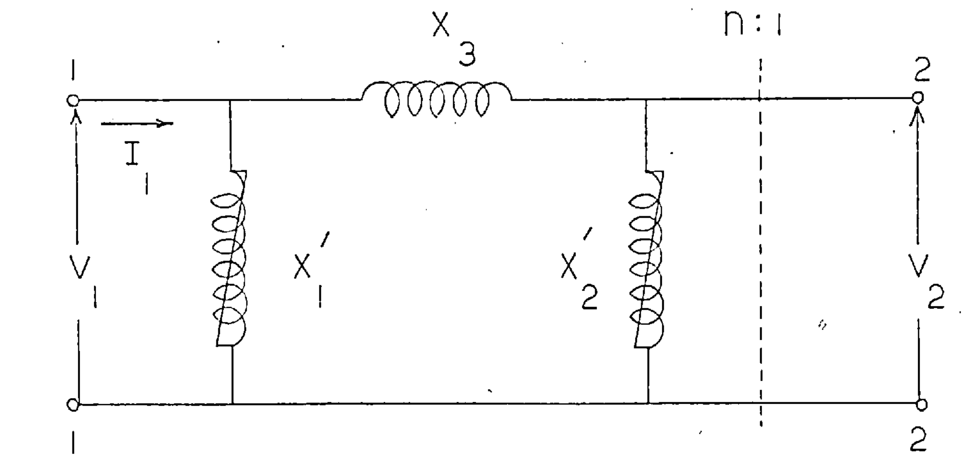

FIG. 3.3

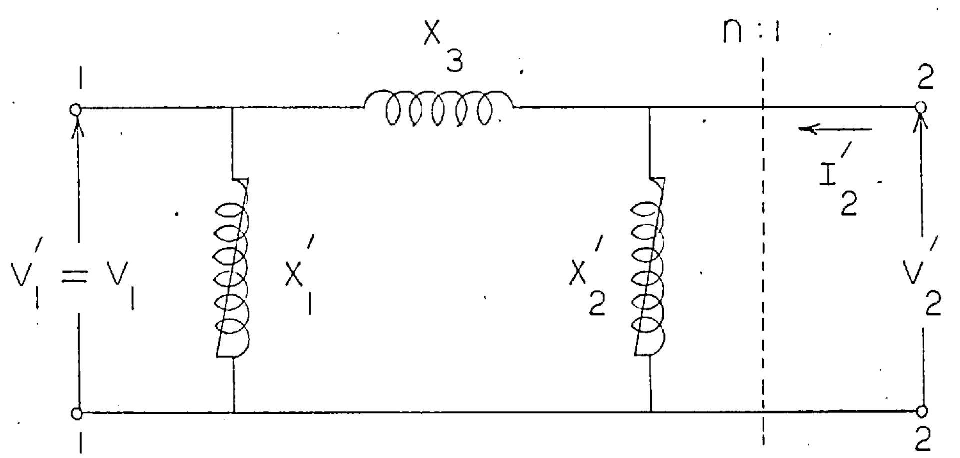

FIG. 3.4

FIGS. 3.3 AND 3.4 OPEN-CIRCUIT TESTS ON THE PI CIRCUIT

V_1 and V_1', for example) is unknown, the reactances cannot be obtained from the above equations and the following procedure has to be adopted instead.

The transfer impedance of the network is equal to

$$\frac{V_2}{I_1} = \frac{X_1' X_2'}{X_1' + X_2' + X_3} \cdot \frac{1}{n} \qquad 3.14$$

The ratio of the currents with the terminals 2-2 short-circuited (Fig. 3.5) is given by the expression

$$\frac{I_{2sc}}{I_{1sc}} = n \cdot \frac{X_1'}{X_1' + X_3}$$

from which $\quad X_3/X_1' = (n \cdot \frac{I_{1sc}}{I_{2sc}} - 1) \qquad 3.15$

Similarly, the ratio of the currents with the terminals 1-1 short-circuited is equal to

$$\frac{I_{1sc'}}{I_{2sc'}} = \frac{1}{n} \cdot \frac{X_2'}{X_2' + X_3}$$

from which $\quad \frac{X_3}{X_2'} = \frac{I_{2sc'}}{nI_{1sc'}} - 1 \qquad 3.16$

If all the above tests are performed at voltage levels which do not cause saturation of either X_1' or X'_2, the three reactances can be determined from the above equations for any assumed value of n.

The values of X_1' and X_2' when saturated can be determined from graphs of the voltages V_2 and V_2' against the currents I_1 and I_2' respectively. From a point just above the straight-line part of the characteristic

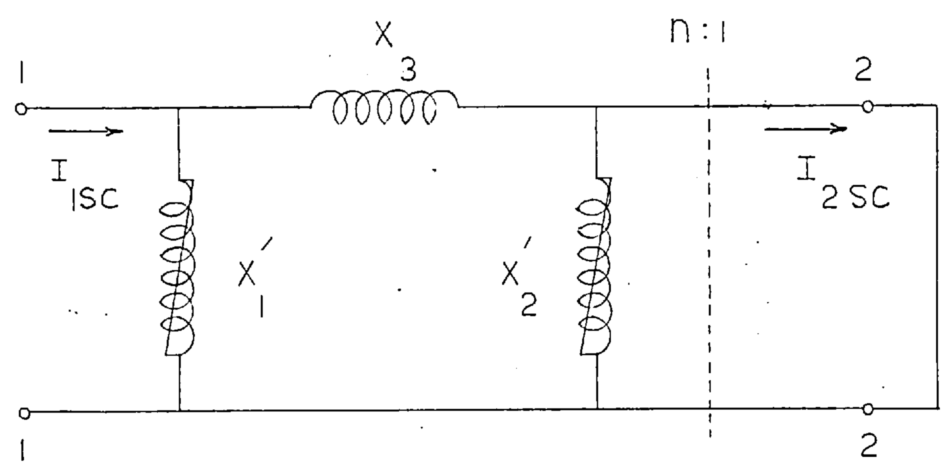

FIG. 3.5 SHORT-CIRCUIT TEST

relating V_2' to I_2' at which the voltage is V_{22}' , and at which the reactance X_1' may be assumed to be unsaturated, the current I_{22}' through X_2' and, hence, the value of the reactance X_2' at the voltage V_{22}' can be determined.

The value of the reactance X_1' at the voltage $(V_{22}' + I_{22}' \times X_3)$ is found from the graph of the voltage V_2 against the current I_1. **By locating** the point on the graph of the voltage V_2' against I_2' at which the voltage across X_1' is $(V_{22}' + I_{22}' \times X_3)$, the value of X_2' at a higher voltage is obtained. Through a repetition of this process, the reactances X_1' and X_2' are obtained as functions of the voltages across their terminals. The results can be alternatively presented in the form of characteristics relating the voltages across the reactances to the currents through them.

3.5. Solution of a circuit containing four reactances

As pointed out in the previous chapter, the equivalent circuit of Fig. 2.8 (P.48) can not be exactly reduced to the Tee and Pi circuits containing linear series elements. Consider the simpler circuit obtained by ignoring the resistances in Fig. 2.8. It is possible, in theory, to determine the reactances of this circuit from terminal tests. A possible method of determining the reactances would consist of synthesising various circuits from some of the terminal characteristics, using different assumed values of n and the ratio X_{sLf}/X_{La}. The circuits so obtained can be employed to 'predict' other terminal characteristics. The accuracy of the assumed values of X_{sLf}/X_{La} and n is indicated by the agreement between the predicted and test characteristics. An approximate circuit having terminal characteristics in good agreement with the test characteristics can sometimes be obtained by this means.

This method can be successfully used only if the reactances X_{sLf} and X_{La} significantly influence the terminal characteristics. These reactances are usually small in a circuit representing a synchronous machine. Therefore, large changes in the values of these reactances alter the terminal characteristics to a comparatively small extent. The method outlined above will therefore yield a number of circuits having characteristics in similar agreement with the test characteristics (i.e. a singular solution can not be obtained).

CHAPTER 4

Equivalent Circuits of a two-phase machine

4.1. Scope.

Tests on a two-phase induction motor at stand-still are described. The characteristics obtained from these tests are employed to determine the parameters of the equivalent Tee and Pi circuits of the machine. Equivalent circuits are also derived from characteristics obtained by tests on the machine as an alternator. The relationship between the characteristics obtained from the two types of tests is explained.

4.2. Choice of the test machine

The methods of determining the parameters of the Tee and Pi circuits outlined in the previous chapter could have been illustrated by tests on a two-winding transformer. An induction motor was employed as the test machine mainly because it could be operated both as a transformer and as an alternator. This facility is not readily available in an alternator of normal design. In such an alternator, the field inductance is usually large. In addition, damper circuits are often present on the field system of the machine. For both these reasons, an alternator of normal design can not be easily tested as a transformer.

The facility offered by the induction motor has made it possible to illustrate the similarity that exists between a transformer and an alternator even when the magnetic systems of both are saturated.

4.3. Specifications of the test apparatus

4.3.1. Test machine

A slip-ring induction motor of the following specifications was employed as the test machine.

Make	:	A.E.G., Berlin.
Rated voltage	:	100 volts
Horse-power	:	2
Rated speed	:	1350 r.p.m.
Number of poles	:	4
Number of phases	:	2

Single-layer windings with concentric coils were employed both on the stator and rotor of the machine. The windings on the stator and rotor were housed in 32 and 48 slots respectively. The lay-out of the windings is shown in Figs. 4.1a and b. The resistances of the stator and rotor phases were measured and found to be 0.49 and 0.3 ohm per phase respectively.

When operated as an alternator, the machine was driven by a 2 h.p., 200 volts, separately-excited d.c. motor.

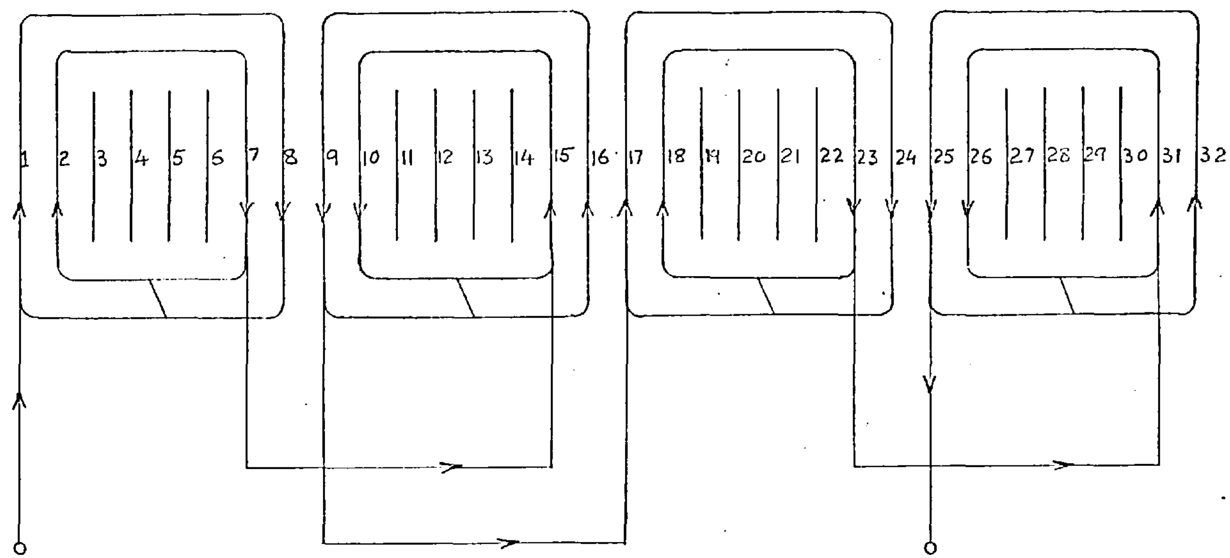

FIG. 4.1a ARRANGEMENT OF A PHASE ON THE INDUCTION MOTOR STATOR

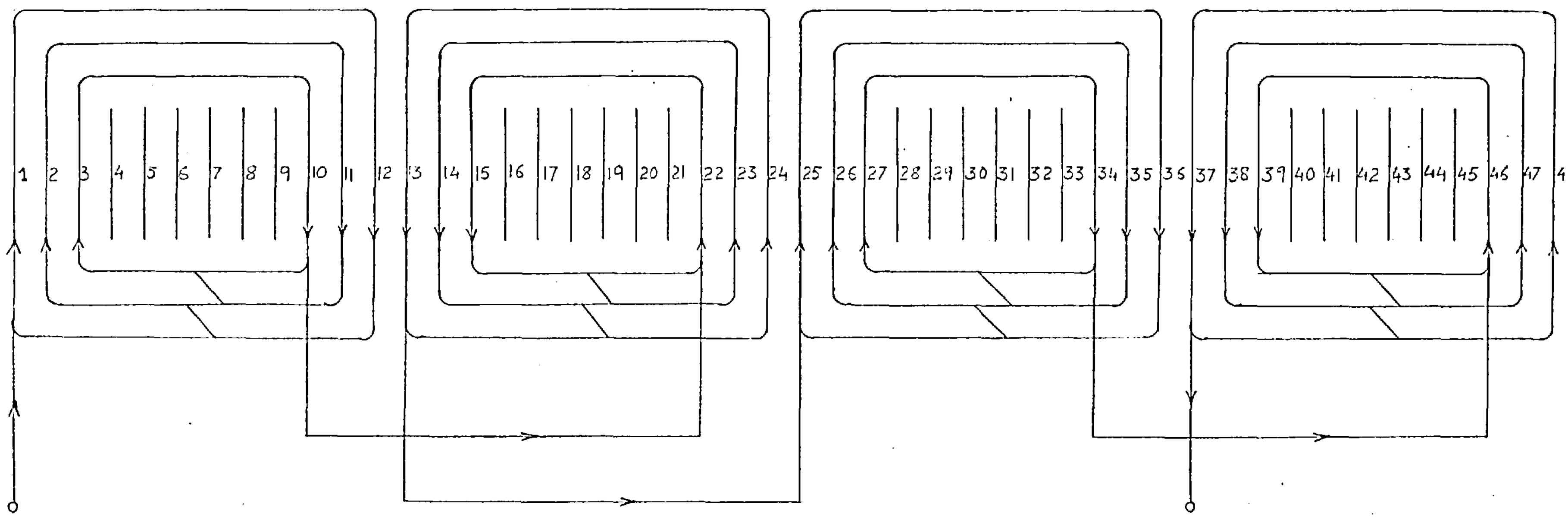

FIG. 4.1b ARRANGEMENT OF A PHASE ON THE INDUCTION MOTOR ROTOR

4.3.2. Voltage sources and measuring instruments.

The variable voltage supply required for tests on the machine at stand-still was obtained from a single-phase "Variac" auto-transformer of the following specifications.

Make	:	Claude-Lyons Ltd.
Type	:	50 - B
Input voltage	:	230 volts
Output voltage	:	0 - 270 volts
Maximum Current	:	20 amp

D.C. supplies for the driving motor and for excitation of the winding forming the field winding (during tests on the machine as an alternator) were obtained from 200 volts and 12 volts supplies in the laboratory.

Multi-range rectifier-type and moving-iron type voltmeters were employed for the measurement of voltages. The proportions of the fundamental and harmonic components of voltages and currents were measured by using a 'Radiometer' wave-analyser.[35] Alternating currents were measured with moving-iron type ammeters. Moving-coil instruments were employed for the measurement of direct currents.

4.3.3. Zero power factor load

Two out of a set of three similar air-cored reactors were employed as the zero power factor load. Each of the reactors consisted of two coils mounted on wooden boards capable of relative movement. These coils were each wound in three concentric sections which could be interconnected in various ways. The coils themselves could be connected in series or parallel, aiding or opposing. Thus, a very wide range of inductance could be obtained at the terminals of the reactors.

Each section of the coils had a resistance of 0.55 ohm , a specified self-inductance of 0.011 H, and a specified maximum mutual inductance of 0.0045 H.

4.4. Open-circuit characteristics of the machine at stand-still

Tests on the machine at stand-still were performed with the rotor placed in a position at which the axes of the stator and rotor phases were coincident. This position was located by exciting a stator phase and slowly turning the rotor till the voltage induced in a rotor phase was a maximum. The voltage induced in the other rotor phase was very nearly zero for this position of the rotor.

Open-circuit tests were performed as per Figs.

3.1a and b. (p.73). The characteristics obtained from these tests are shown in Figs. 4.2, 4.3 and 4.4. The reason for the use of both a rectifier and a moving-iron type voltmeter is explained below.

On saturation of the machine, the exciting current contained a third harmonic component. This component caused third harmonic voltage drops across the leakage reactances of the source and the winding excited. Consequently, both the voltage applied to this winding and the voltage induced in the open-circuited winding contained third harmonic components. These components were so disposed as to cause the waveforms of the two voltages to be peaked.

From the test results, discussed in the following sections, it is seen that the leakage reactances of a stator and a rotor phase respectively form approximately 14 and 5 per cent of the minimum magnetising reactance. Since the leakage reactances are small, their values determined from tests are subject to errors. Some of these errors could be avoided by a suitable choice of measuring instruments. The choice of the type of voltmeter may be mentioned as an example. The indication of a rectifier-type voltmeter is considerably influenced by the waveform of the measured voltage.[36] On the other hand, the indication of a moving-iron type voltmeter is

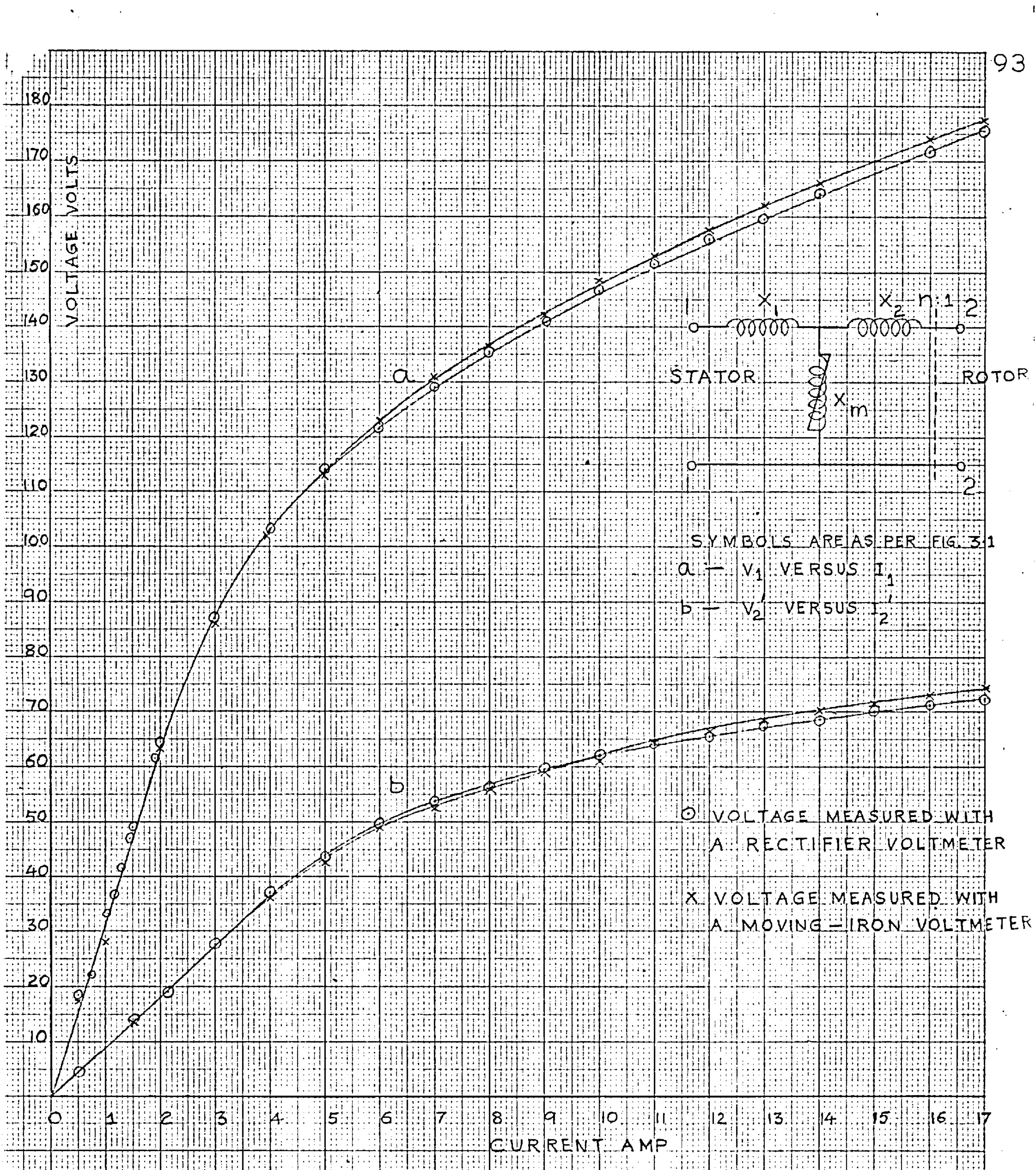

FIG 4.2 SELF-IMPEDANCE CHARACTERISTICS OF THE INDUCTION MOTOR AT STAND-STILL

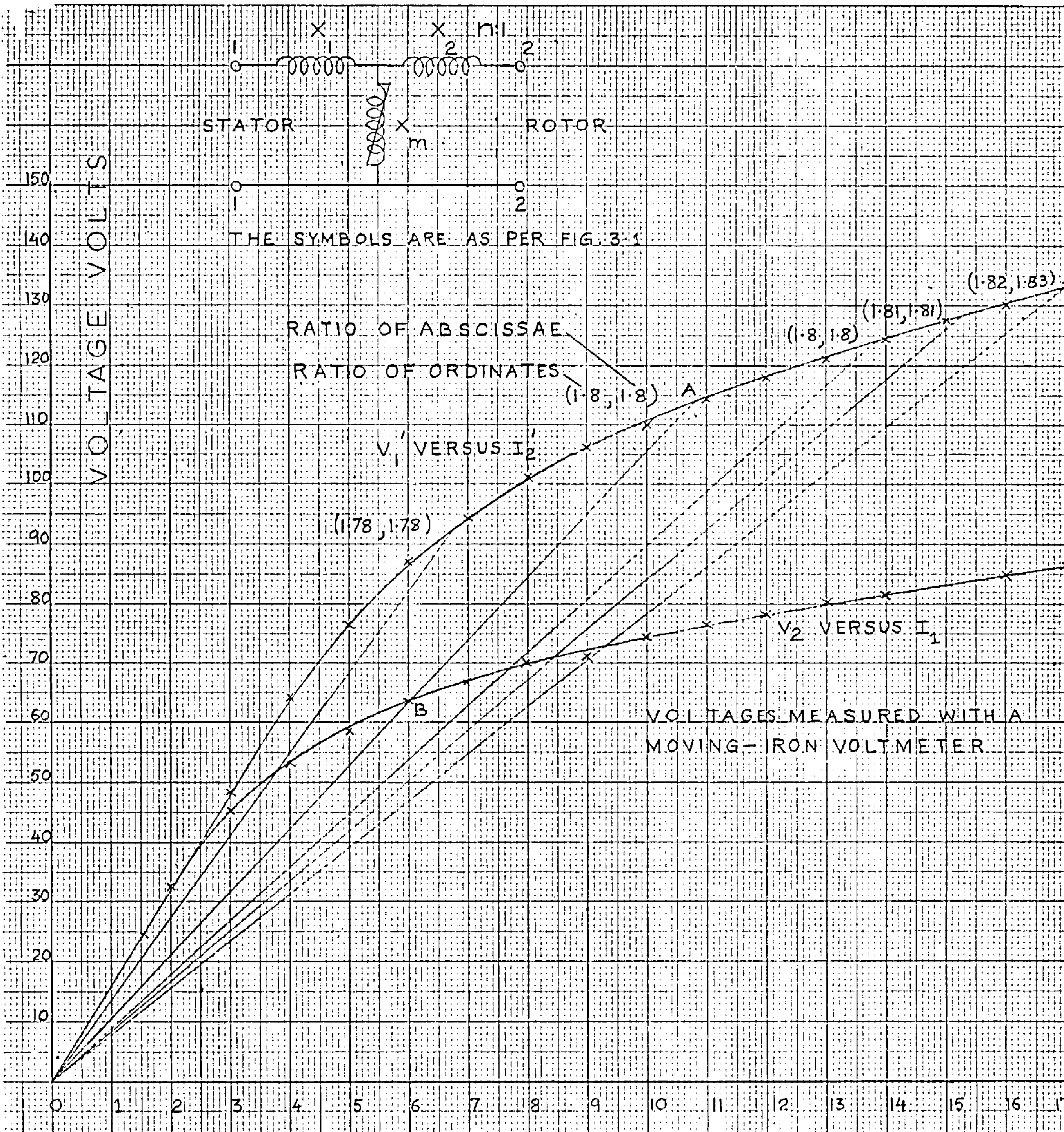

FIG. 4.3 TRANSFER-IMPEDANCE CHARACTERISTIC OF THE INDUCTION MOTOR AT STAND-STILL

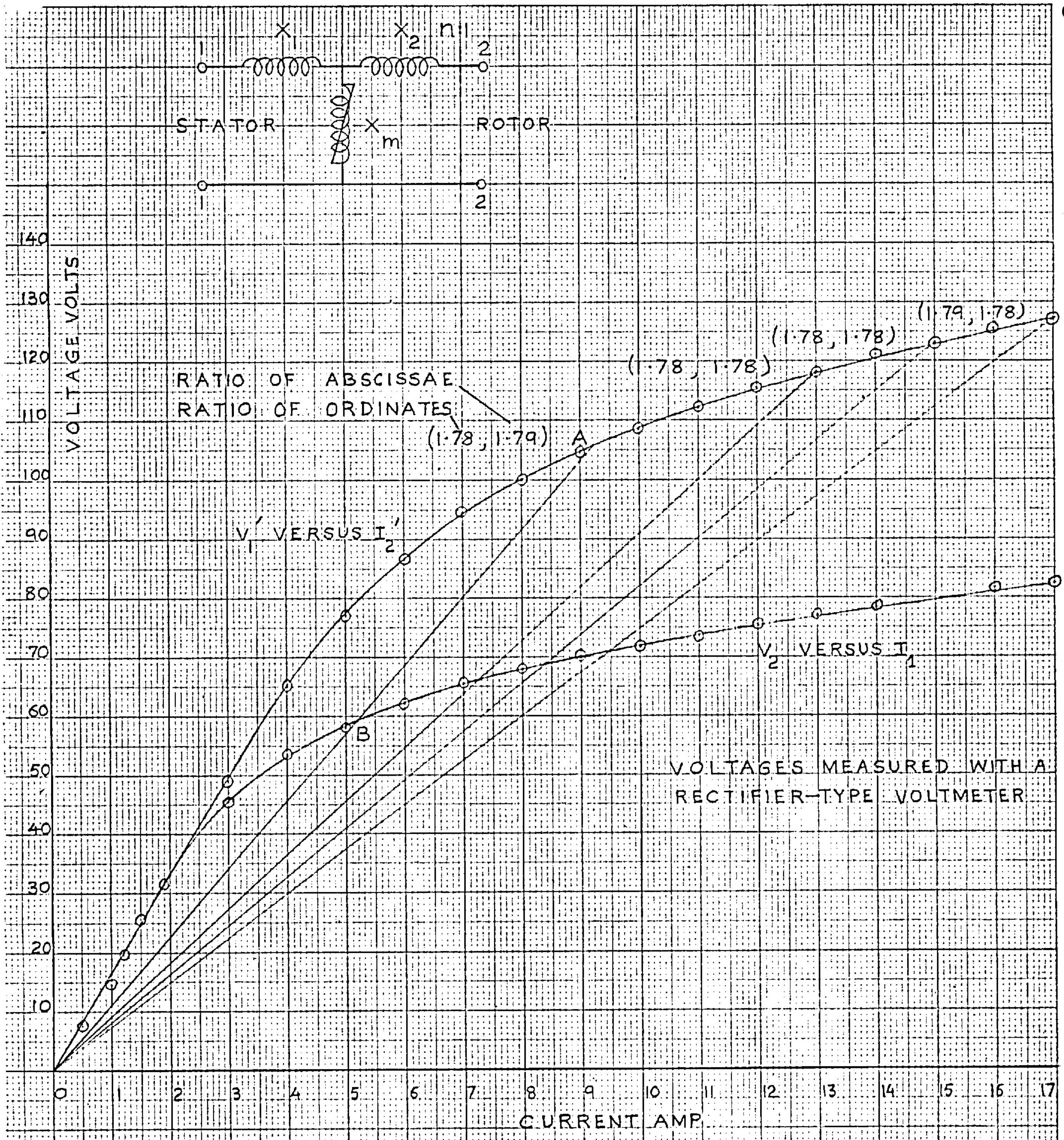

FIG 4.4 TRANSFER-IMPEDANCE CHARACTERISTICS OF THE INDUCTION MOTOR AT STAND-STILL

substantially independent of the waveform of the voltage.*
To assess the magnitude of the error caused by the use of a rectifier voltmeter, both types of voltmeters were employed to measure various voltages. From Fig.4.2 it can be seen that the maximum difference between the values of voltage V_1 indicated by the two voltmeters is approximately 1 per cent. The maximum difference between the indicated voltages in graph b, Fig. 4.2 is 2.5 per cent. The values of the induced voltages V_2 and V_1' indicated by the two voltmeters differ by a maximum of 5 per cent. Of the values quoted above, about 1 per cent may be ascribed to instrumental errors. The remaining difference mainly arises from the influence of harmonics on the indications of the rectifier voltmeter.

A resistance of 0.1 ohm was connected in series with the winding excited. The fundamental and harmonic components of the voltage drop across this resistance were measured. These measurements showed the fundamental and third harmonic components to be the principal components of the exciting current. The ratios of the third harmonic and fundamental components of the exciting currents were calculated from the measured voltages. These ratios were employed along with the indicated currents to obtain the corresponding fundamental components of the exciting currents. The fundamental components

* These remarks are made with specific reference to the waveforms obtained during the tests.

are plotted against the respective indicated currents in Fig. 4.5.

4.4.1. Errors involved in the neglect of iron loss and resistances of the windings

The methods of determination of the parameters of the Tee and Pi circuits discussed in the preceding chapter refer to purely inductive circuits. An equivalent circuit of the test machine includes resistances representing copper and iron losses in the machine. These resistances are placed in the equivalent circuit as shown in Fig. 4.6. Some observations on the errors involved in calculating the parameters of the Tee circuit ignoring the resistances are made in the following paragraphs.

The transfer-impedance characteristics drawn in Figs. 4.3 and 4.4.are the characteristics of the impedance Z_m/n. Z_m is the impedance formed by the parallel combination of R' and X_m. Figs. 4.3 and 4.4 show straight lines drawn from the origin to intersect the two graphs. Corresponding points of intersection, such as A and B in Fig. 4.3, represent operating conditions at which Z_m/n has the same value.

A comparison was made of the ratios of the third harmonic and fundamental components of the induced

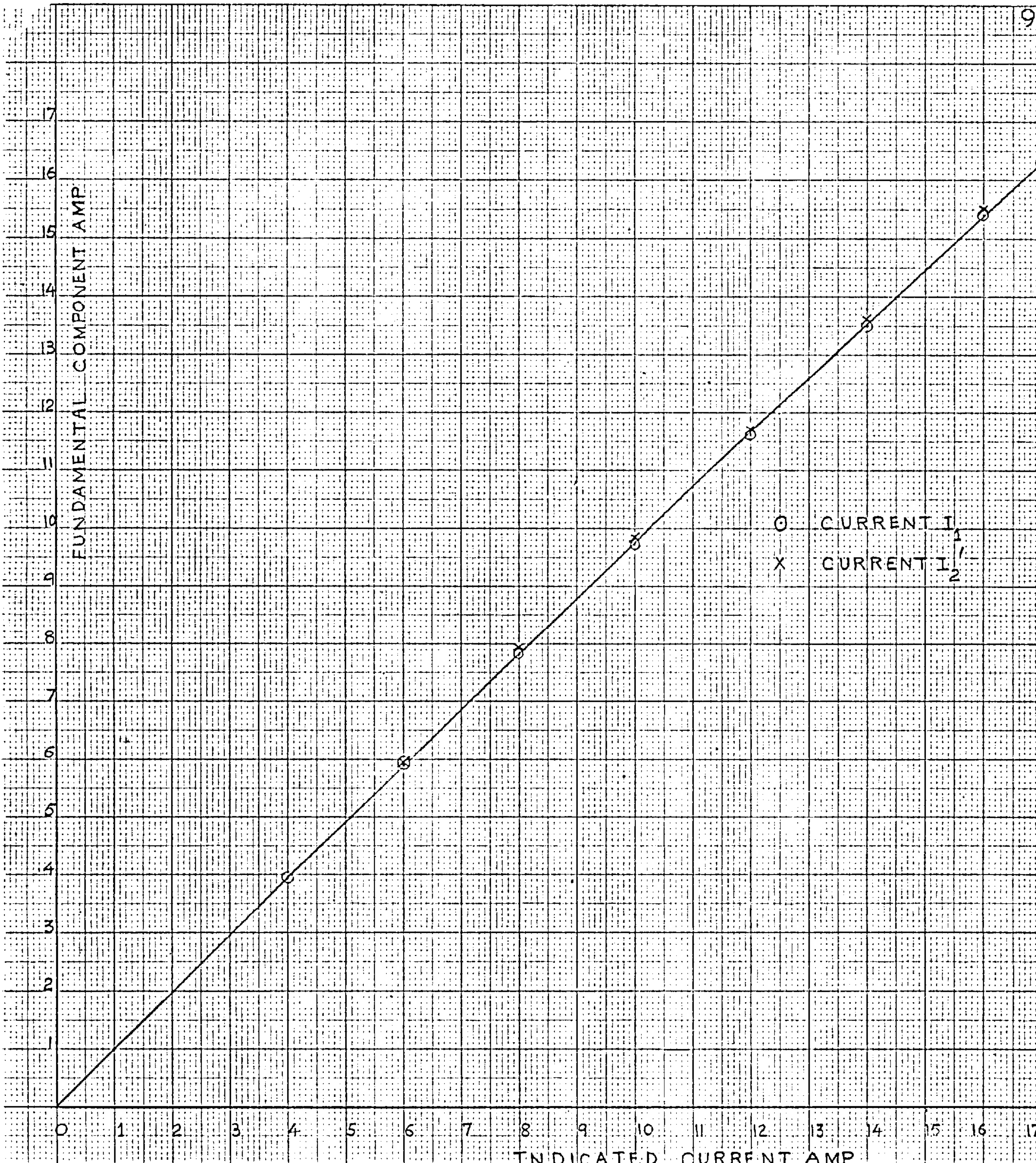

FIG. 4.5 FUNDAMENTAL COMPONENTS OF THE EXCITING CURRENTS

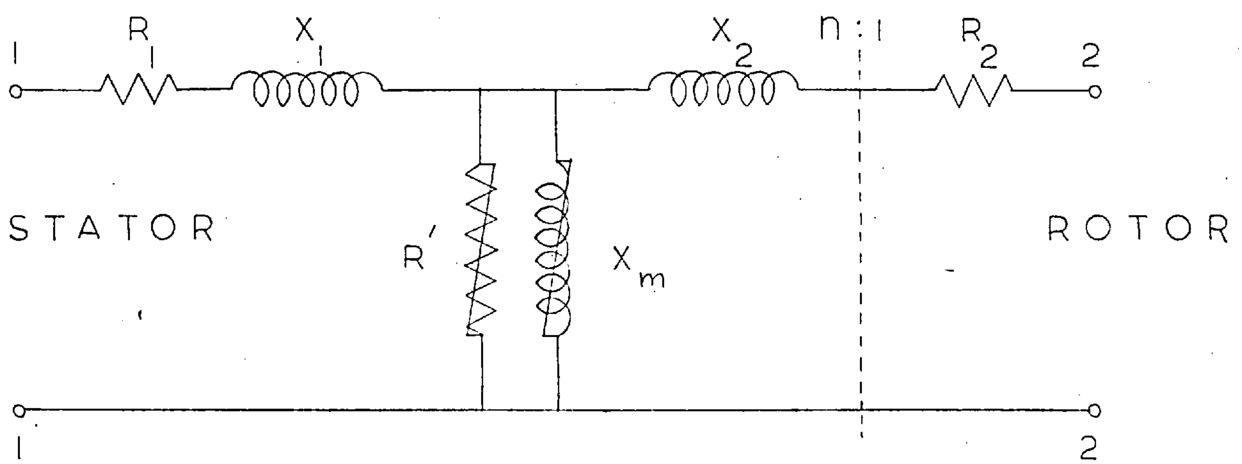

FIG. 4.6 EQUIVALENT TEE CIRCUIT, INCLUDING LOSSES, OF THE INDUCTION MOTOR AT STAND-STILL

voltages at various pairs of corresponding points in Fig. 4.3. This comparison showed the ratios associated with V_1' to be approximately 2 per cent larger than those associated with V_2. This difference between the two ratios is small and can be ignored. Hence the waveforms of the induced voltages at corresponding points on the two graphs may be assumed to be similar. The equality of the values of impedance Z_m/n at these points then implies the equality of voltages V_1' and nV_2. Therefore, the ratio of voltages V_1' and V_2, or currents I_2' and I_1, at corresponding points is equal to n. The presence or absence of R' hence does not influence the turns-ratio.

An approximate indication of the error caused by evaluating X_m ignoring the presence of R' (Fig. 4.6) is obtained as follows. If the small phase difference between V_1 and V_2 is ignored, the component of I_1 in phase with V_1 may be assumed to be the current through R'. Then the quadrature component of I_1 represents the current through X_m. The phase-angle between V_1 and I_1 was measured and found to be of the order of 80°. The in-phase and quadrature components of I_1 are therefore equal to 0.173 I_1 and 0.985 I_1 respectively. Hence, the value of X_m obtained by dividing nV_2 by I_1 is 1.5 per cent smaller than that obtained by dividing nV_2 by 0.985 I_1. Since the error involved is small, X_m

has been calculated ignoring the influence of R'.

The reactance X_1 was calculated from a set of measured values of V_1, V_2 and I_1 taking into account the phase relationship between V_1 and I_1. The voltage drop across the winding resistance R_1 was also taken into account. The calculated value of X_1 was found to be within 4 per cent of the value obtained by dividing the arithmetic difference between V_1 and nV_2 by I_1.

An average value of reactance X_2 = 0.45 ohm was obtained from calculations in which the resistances R_2 and R' were ignored. This value is 0.05 ohm larger than the reactance calculated taking the resistances into account.

The above results indicate that the errors involved in ignoring the resistances in the equivalent Tee circuit are small. This conclusion would also apply to other methods of determination of the parameters of the Tee circuit. In addition, the results also show that the parameters of the Pi circuit may be determined ignoring the resistances in the equivalent circuit.

4.4.2. Parameters of the equivalent Tee circuit determined by the transfer-impedance method

The average values of n obtained from Figs. 4.3 and 4.4 are 1.81 and 1.78 respectively. The variations in the values of n over the range of the test characteristics amount to 2 per cent of the average values. The difference between the two average values of n and the variations in its values could arise from instrumental and graphical errors of the order of 1 per cent.

Equation 3.2 was employed to calculate the values of X_m. The calculated values are plotted in graphs a, b and c, Fig. 4.7a as functions of the measured values of I_1. Graph a shows the values of X_m calculated by using the voltages indicated by the moving-iron voltmeter and the fundamental component of I_1. Graph b shows the values that were obtained by employing the voltages indicated by the rectifier voltmeter and the indicated current I_1. The values of X_m determined by using the voltages indicated by the rectifier voltmeter and the fundamental component of I_1 are plotted in graph c.

An average difference of 5 per cent between the reactances in graphs a and c represents the error caused by the use of the rectifier voltmeter. The error resulting from the use of the indicated current instead of its fundamental component is represented by the vertical intercepts between graphs b and c.

The reactance X_1 was calculated from operating points situated in the saturated regions of the test characteristics by employing equation 3.3. The calculated

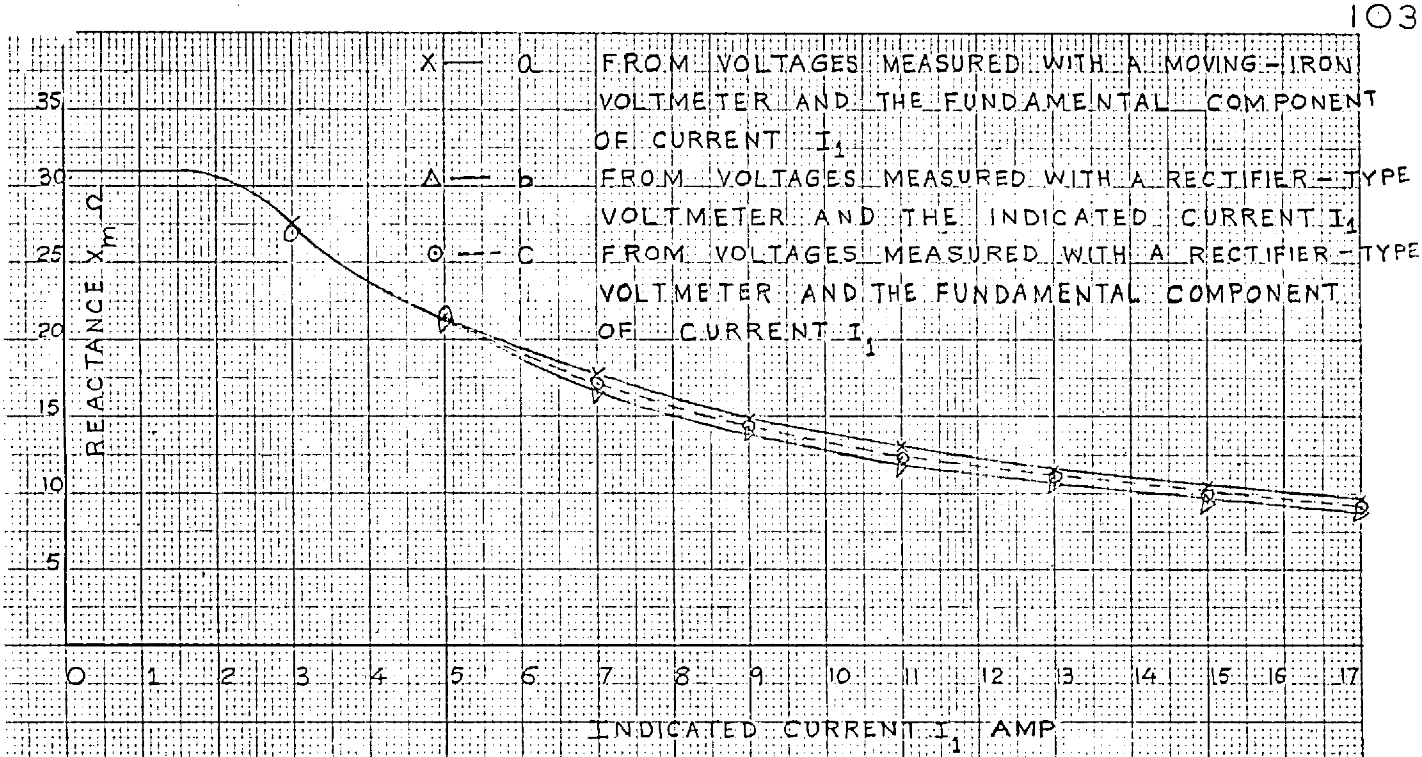

FIG. 4.7a REACTANCE X_m

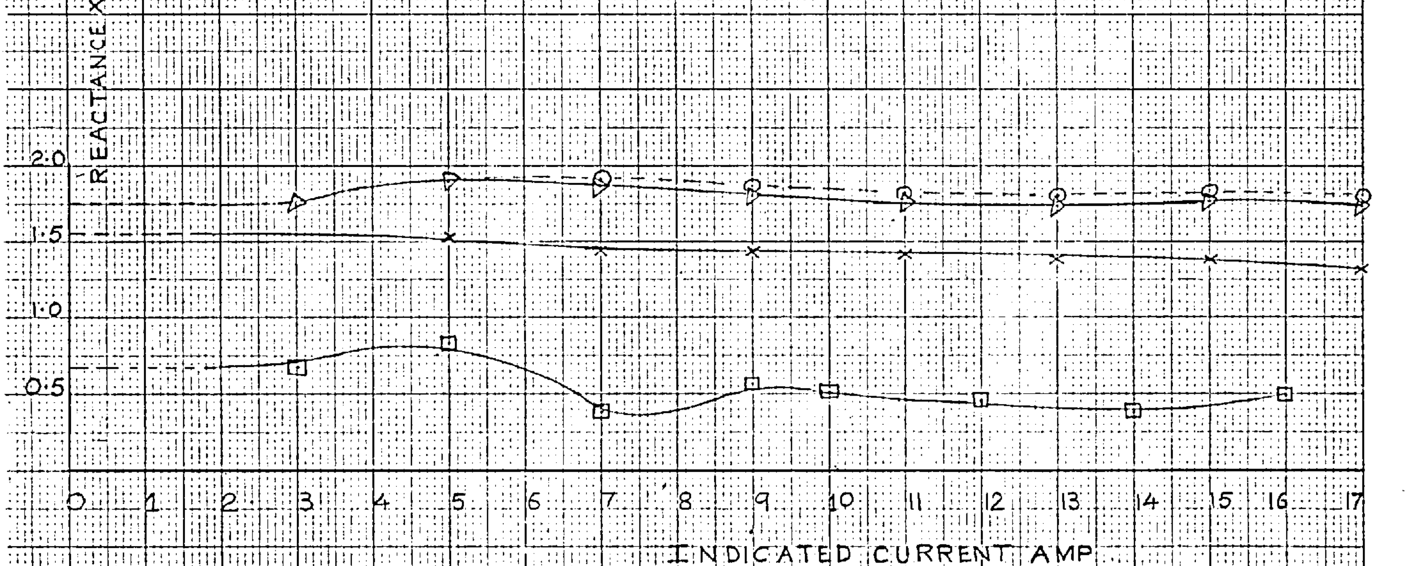

x — a
Δ — b REACTANCE X_1 VERSUS I_1. THE SIGNIFICANCE OF
⊙--- c THE SYMBOLS IS AS EXPLAINED ABOVE

□ — d REACTANCE X_2 VERSUS I_2'

FIG. 4.7b REACTANCES X_1 AND X_2

values are plotted as functions of the indicated current I_1 in graphs a, b and c, Fig. 4.7b. The graphs are denoted by symbols corresponding to those employed in Fig. 4.7a. The significance of these symbols has been explained above. The slope of the unsaturated part of graph a, Fig. 4.2 represents the reactance $(X_{uns} + X_1)$ while the slope of the unsaturated part of the transfer-impedance characteristics represents the reactance X_{uns}/n. The reactance X_1 could be calculated as the difference between $(X_{uns} + X_1)$ and $n \times X_{uns}/n$. However, the reactance obtained by this calculation is considerably influenced by small errors in the measurement of the two slopes. It may be observed from Fig. 4.2 that the possible error in the value of reactance $(X_{uns} + X_1)$ is of the order of an ohm. Hence, assuming that $X_{uns/n}$ is exactly determined, the value of X_1 could be in error by an ohm. Graphs a, b and c, Fig. 4.7b are partly drawn dotted to indicate this uncertain nature of the reactance. The values indicated by the dotted lines are nominal values of the reactance.

The average values of X_1 obtained from graphs a and c differ by approximately 20 per cent. This difference is partly caused by the influence of harmonics on the voltages indicated by the rectifier voltmeter. A part of this difference (about 10 per cent) could be the result of errors in the measurement of voltages. The difference between graphs a and c illustrates the need for a proper choice of the measuring instruments.

Graph d, Fig. 4.7b shows the values of X_2 calculated by using equation 3.4. The fundamental components of V_2', V_1' and I_2' were employed in these calculations. The variations in graph d occur on account of the small magnitude of X_2. These variations could be caused by experimental and graphical errors of the order of 1 per cent. An approximate value of 0.45 ohm can be employed for this reactance.

4.4.3. Parameters of the equivalent Tee circuit calculated by the self-impedance method

This method has been employed to determine an average value of the turns-ratio from the test characteristics drawn in Figs. 4.2 and 4.3. The voltages V_2 and V_2' are assumed to be unknown.

Fig. 4.8 shows the reactances $(X_{uns} - X_m)$ and $(X_{uns} - X_m)/n$ plotted as functions of I_1 and I_2' respectively. The method of determining n by locating corresponding points on the two characteristics is illustrated by points P and Q. An average turns-ratio of 1.8 is obtained from characteristics a and b in Fig. 4.8.

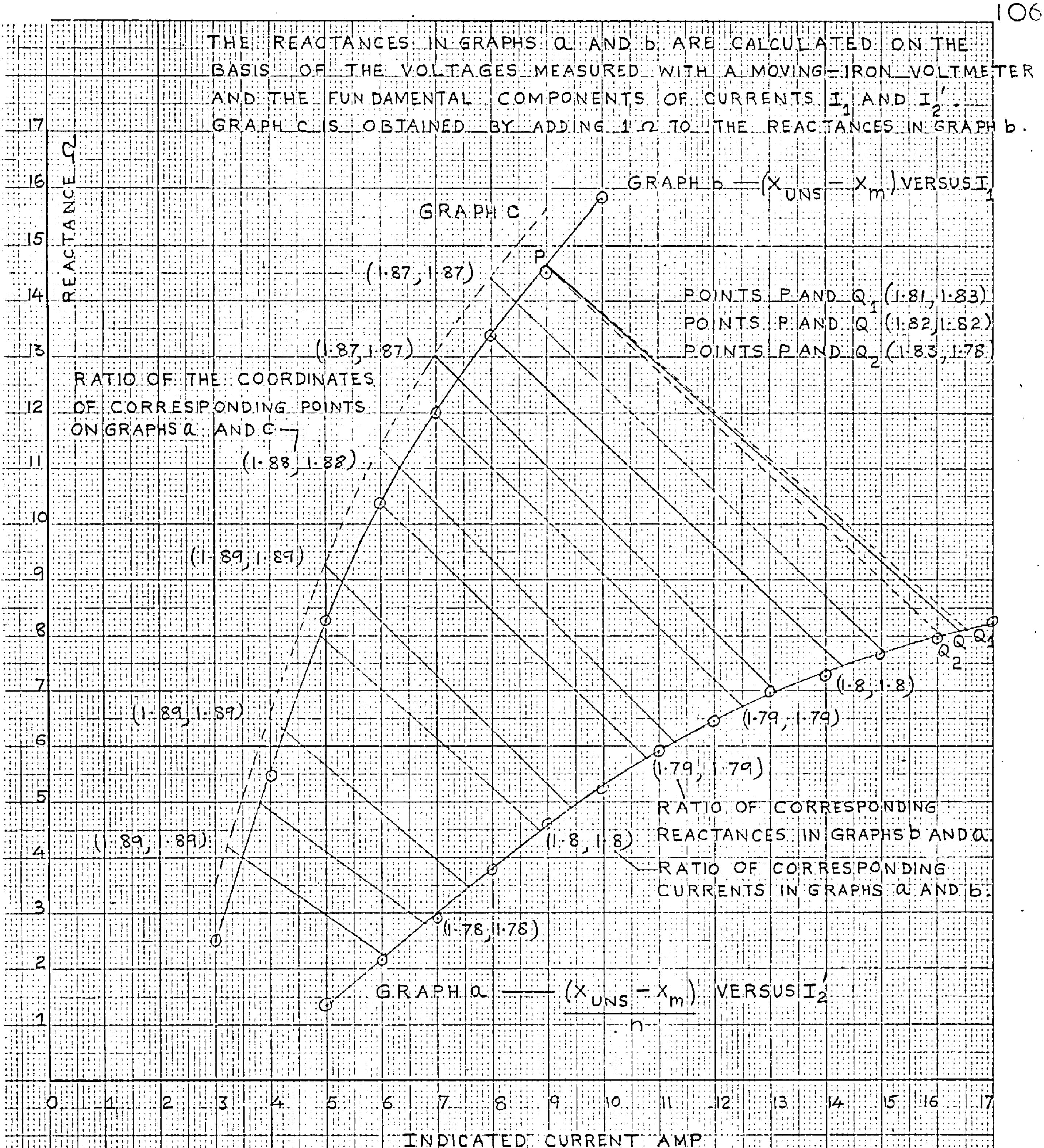

FIG 48 DETERMINATION OF n BY THE SELF-IMPEDANCE METHOD

As stated earlier, the possible error in the measurement of the slope of the linear part of graph a, Fig. 4.2 is of the order of an ohm. To obtain an indication of the influence of such an error on the turns-ratio determined by this method, an additional characteristic c has been drawn in Fig. 4.8. This characteristic is displaced from b by an ohm. An average turns-ratio of 1.89 is obtained from graphs a and c.

Reactance X_m is directly proportional to n. Therefore, the values of X_m corresponding to the values of n quoted above are determined by multiplying the reactances obtained from graph a, Fig. 4.7a by the factors $1.8/_{1.81}$ and $\frac{1.89}{1.81}$. Both the values of n (1.8 and 1.89) have been used to calculate X_1. Graph **a**, Fig. 4.8a shows the values of X_1 corresponding to a turns-ratio of 1.8. The average reactance from this graph is within 5 per cent of the reactance obtained from graph a, Fig. 4.7b. The values of X_1 corresponding to a turns-ratio of 1.89 are plotted in graph **b**, Fig. 4.8a. The average reactance determined from graph **b** is approximately 40 per cent lower than that obtained from graph a, Fig. 4.7b. In addition, the reactance in graph b, Fig. 4.8a varies to a greater extent than the reactances in graph a, Fig. 4.7b and graph **a**, Fig. 4.8a.

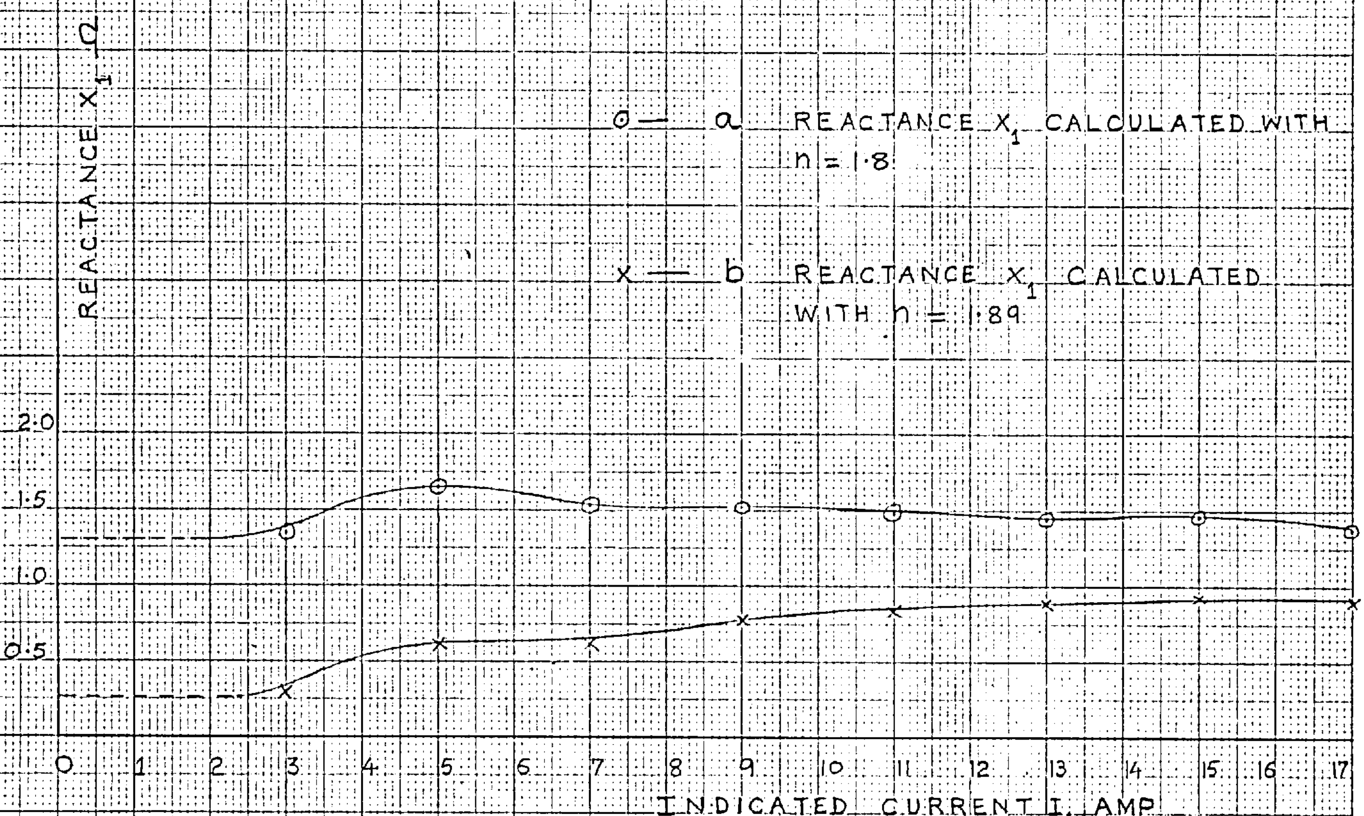

FIG 4.8a REACTANCE X_1 DETERMINED BY THE SELF-IMPEDANCE METHOD

Better approximations to n and X_1 can be determined if it is known (as in the present case) that X_1 is nearly constant at all operating points on the test characteristics. The following procedure is employed to determine better values of n and X_1.

The symbols X_{11} and X_{12} denote the values of X_1 corresponding to turns-ratios of n_1 and n_2. Manipulation of equation 3.3 leads to the following expression relating X_{11} and X_{12}.

$$X_{12} = X_{11} - \frac{(n_2 - n_1)}{n_1} \cdot \frac{n_1 V_2}{I_1} \qquad 4.1$$

The reactances X_{11} and X_{12} can be evaluated from the currents and voltages at various operating points on the test characteristics. The values of X_{11} and X_{12} will be related in each case by an expression similar to equation 4.1. If n_2 were to be the "correct" value of the turns-ratio, the values of X_{12} in all such expressions would be equal. Therefore, when n_2 is not known, its value can be determined by equating two expressions similar to equation 4.1. The reactance X_{12} can be then obtained by substituting the value of n_2 in one of the expressions.

The procedure outlined above was used to calculate better approximations to n and X_1. A turns-ratio of 1.89, determined from graphs a and c in Fig. 4.8, was employed as n_1. Values of the reactance X_{11} were obtained from graph b, Fig. 4.8a. A value of $n_2 = 1.84$ was obtained by equating the values of X_{11} at 5.0 and 13.0 amp. The corresponding value of reactance X_{12} is 1.2 ohms. It may be noted that n_2 is closer than n_1 to the turns-ratio of 1.81 determined by the transfer-impedance method. Also, the reactance X_{12} is in better agreement with the average reactance obtained from graph a, Fig. 4.7b than either of the two values of X_{11}. Similar calculations were performed using other pairs of points on graph b, Fig. 4.8a. These calculations yielded different values of n_2 and X_{12}. However, all these values were better approximations to n and X_1 than the original values employed in the calculations. This procedure will yield incorrect results when the reactance X_1 is not constant over a range of operating points on the characteristics.

4.5. Potier-type tests on the machine

Potier-type tests were performed on the machine at stand-still. A rotor phase was employed as the primary winding of a transformer. The stator phase located with its axis coincident with that of the rotor phase formed the secondary winding. One of the reactors described in section 4.3.3 was employed as the load. A zero power factor characteristic, relating the voltage at the terminals of the secondary winding to the primary current, was obtained by varying the primary voltage and load reactance, keeping the load current constant. A Potier test was also performed on the machine by operating it as a two-phase alternator. A rotor phase was employed as the field winding. A load current of 4.5 amp was employed for both types of tests. The terminal voltages were measured with a moving-iron voltmeter.

Figs. 4.9a and b show the characteristics obtained from tests on the machine at stand-still. The reactances calculated from the altitudes of various Potier triangles are plotted in graph a, Fig. 4.10 against the open-circuit voltages denoted by the vertices of the triangles. An indication of the possible error in the Potier reactance is provided by a comparison of the values of the reactance obtained from triangles PQR and P'Q'R in Fig. 4.9b. The difference QQ' corresponds to an error of 1.2 per cent in the measurement of primary current at the point R. The difference between the reactances determined from the two triangles is 0.2 ohm . The possible error in the Potier reactance evaluated from triangles located in the partially saturated regions of the test characteristics (below 90 volts on the open-circuit characteristic) is larger.

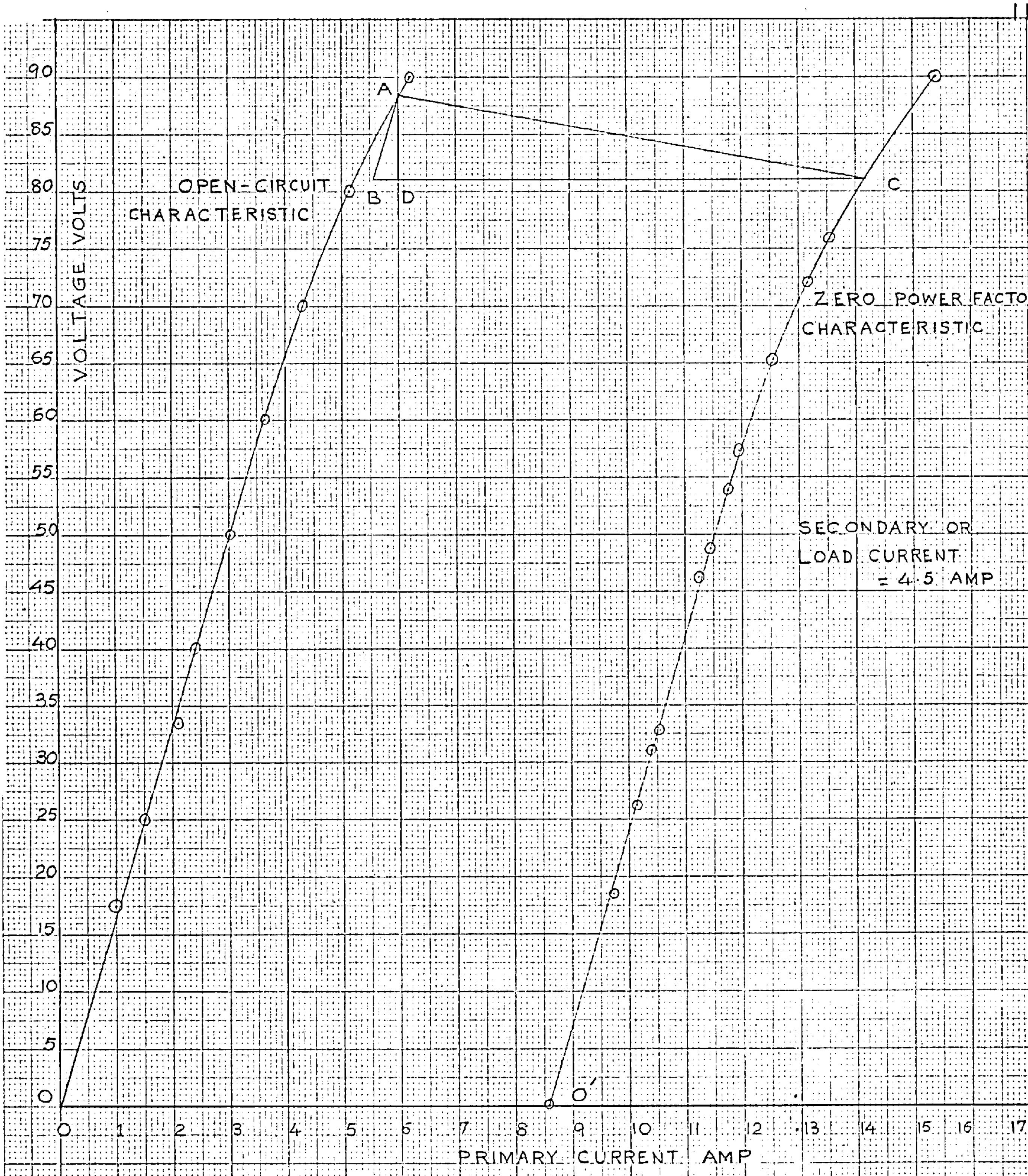

FIG. 49a CHARACTERISTICS OBTAINED BY POTIER-TYPE TESTS ON THE INDUCTION MOTOR AT STAND-STILL

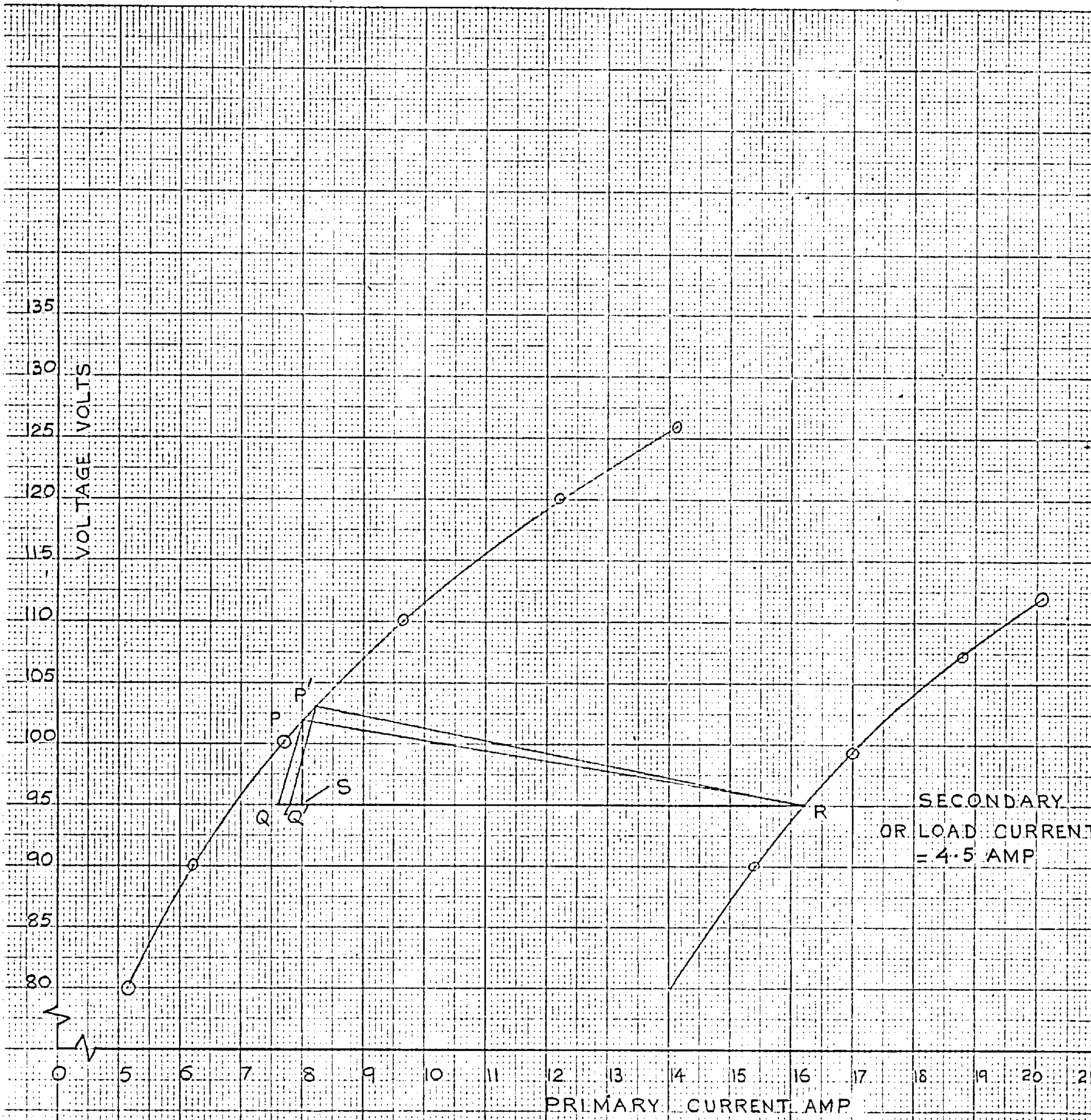

FIG 49 b CHARACTERISTICS OBTAINED BY POTIER-TYPE TESTS ON THE INDUCTION MOTOR AT STAND-STILL

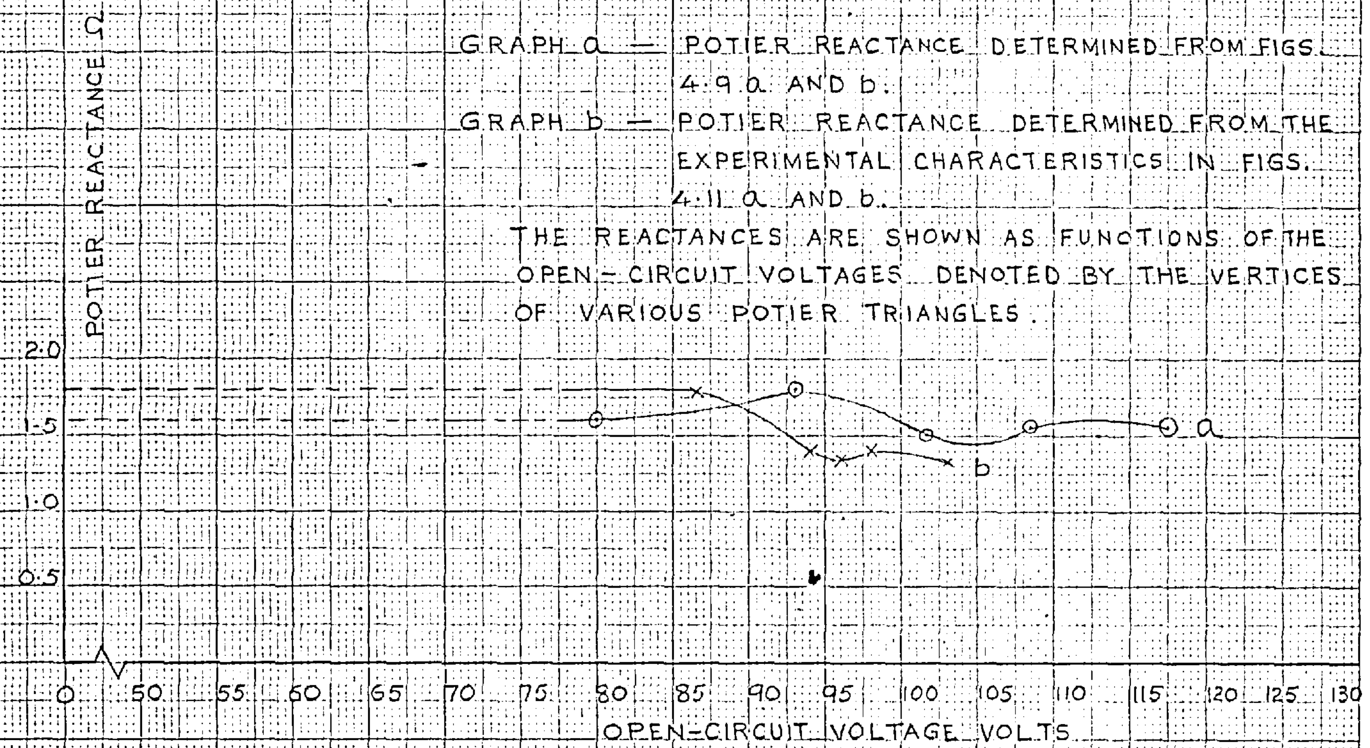

FIG. 4.10 POTIER REACTANCE OF A STATOR PHASE OF THE INDUCTION MOTOR

An explicit value of Potier reactance can not be determined from the linear regions of the test characteristics. Hence, a value of the reactance equal to the first explicitly determined value has been adopted in this region. Graph a, Fig. 4.10 is then produced back to the ordinate-axis as shown by the dotted line.

The equivalent primary current is represented by the length SR in triangle PQR (Fig.4.9b). The turns-ratio is equal to the ratio of this equivalent current and the load current. An average turns-ratio of 1.82 is obtained from various Potier triangles. This ratio is in good agreement with the average value of 1.81 determined by the transfer-impedance method. An average Potier reactance of 1.55 ohms is obtained from graph a, Fig.4.10. This reactance compares with an average reactance of 1.4 ohms determined by the transfer-impedance method.

4.5.1. Results of Potier tests on the machine operating as an alternator

Figs. 4.11 a and b show the characteristics obtained from tests on the machine as an alternator. The linear part of the zero power factor characteristic drawn dotted was obtained from a preliminary test. The slope of this line is slightly smaller than the slope of the open-circuit characteristic, and, consequently, Potier triangles like ABC in Fig. 4.11a can be fitted between the two characteristics. The Potier reactance calculated from this triangle is much larger than that calculated from the altitude of triangle A'B'C' (Fig. 4.11b). (The base B'C' is equal to BC).

An examination of the wave-form of the short-circuit current in an armature phase showed the current to be distorted. The harmonic components of this current were measured using the Wave-analyser. These measurements showed the third and fifth harmonic components of current to be 0.14 and 0.135 of the fundamental component respectively. In addition, it was observed that the terminal voltage when the machine was loaded was initially distorted. For example, at an indicated terminal voltage of 25 volts, the third and fifth harmonic components of voltage were respectively 18 and 22 per cent of the fundamental component. Both the current and the voltage became increasingly sinusoidal as the load inductance increased. Thus, at a terminal voltage of 45 volts, the third and fifth harmonic components of voltage formed 6 and 8 per cent of the fundamental component respectively. The load current was practically sinusoidal for terminal voltages above 25 volts.

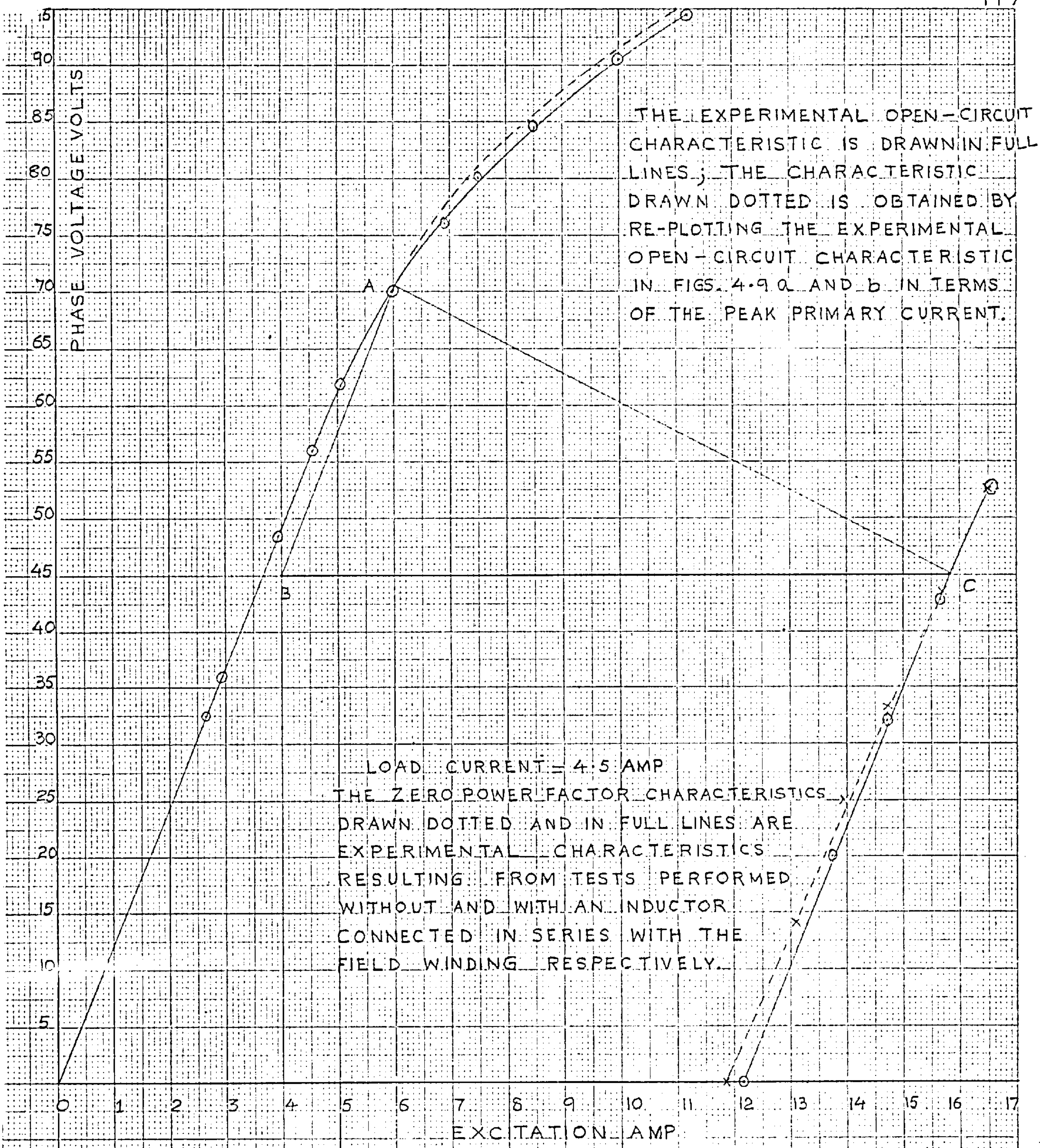

FIG. 4.11a CHARACTERISTICS OF THE INDUCTION MOTOR TESTED AS AN ALTERNATOR

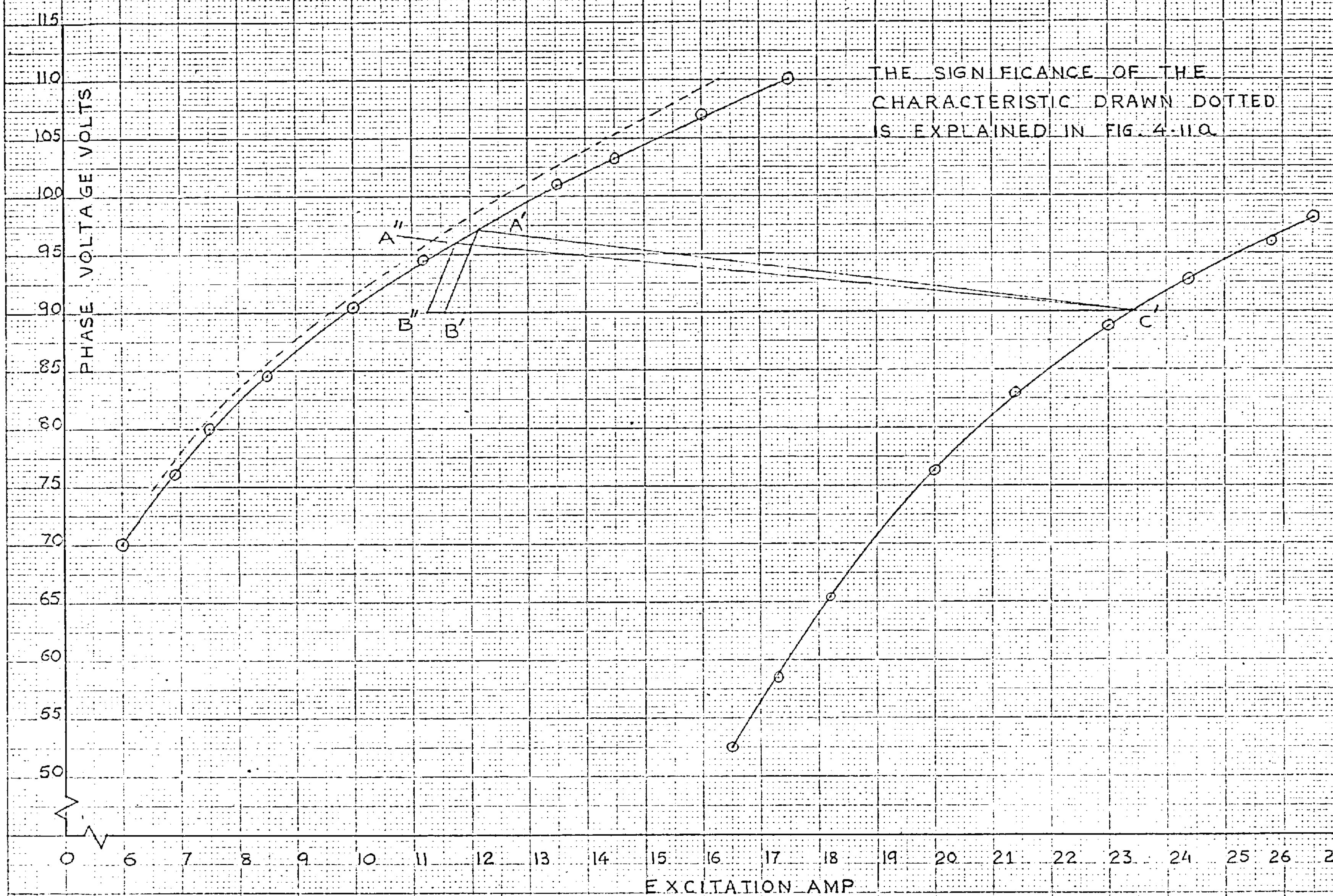

FIG. 4.11 b CHARACTERISTICS OF THE INDUCTION MOTOR TESTED AS AN ALTERNATOR

The presence of harmonics in the short-circuit current caused the moving-iron type ammeter to indicate a current 1.02 times larger than the fundamental current. The zero power-factor characteristic was obtained by keeping the indicated armature current constant. Therefore, the component of armature-reaction m.m.f. due to the fundamental current was smaller at short-circuit than at other points on the characteristic (at which the load current was practically sinusoidal) by a factor of 1.02. The field current was correspondingly smaller than that required to circulate a fundamental-frequency short-circuit current of 4.5 amp. The use of a smaller field current at short-circuit as the base of the Potier triangles leads to triangles such as ABC in Fig. 4.11a.

The presence of harmonics caused the voltmeter to indicate a voltage larger than the fundamental terminal voltage. The slope of the linear part of the zero power factor characteristic obtained by plotting the indicated voltages is therefore larger than the actual slope. This increase in slope partly compensates for the reduced field current at short-circuit. No such compensation however occurs for terminal voltages above 45 volts. At such voltages the difference between the indicated terminal voltage and the fundamental voltage is negligible.

An examination of the field current with the armature short-circuited showed that the current contained a harmonic component. To suppress this component, an inductor was connected in series with the field winding. It was observed that on suppression of the harmonic component of field current, the armature short-circuit current became nearly sinusoidal. This observation could be explained as follows. The third harmonic component of the field m.m.f. at short-circuit induced a third harmonic voltage E_3 in the armature phases. This voltage caused a third harmonic current I_3 to flow through the short-circuited armature phases. The current I_3 establishedam.m.f., the fundamental component F_3 of which revolved at three times the synchronous speed in a direction opposite to the direction of rotation of the rotor. (Ref. 8, p. 218). A fourth harmonic voltage was consequently induced in the field winding. A current I_4 was established in the closed path formed by the field winding and a potential-divider arrangement of resistors connected across the winding for the control of field excitation. This current I_4 set up a pulsating m.m.f, the space fundamental of which could be resolved into two equal m.m.f.s (Ref. 8, p. 201) rotating at four times the synchronous speed in opposite directions.

These m.m.f.s. revolved at three and five times the synchronous speed with respect to the stator. The component revolving at three times the synchronous speed reacted with the m.m.f. F_3 while the other component caused a fifth harmonic current to flow in the stator phases.

Since the 'forward' and 'backward' rotating components of the m.m.f. established by current I_4 were equal, each of the components could be associated with a current $I_4/2$. Fig. 4.12a shows an equivalent circuit relating the third-harmonic current I_3 and the current $I_4/2$. This circuit is derived by regarding the two currents as currents in the stator and rotor windings of an induction motor having balanced two-phase windings on the stator and rotor. This machine is connected to a third-harmonic source E_3 and is driven at a slip of 4/3. The reactances X_1'' and X_m'' in Fig. 4.12a are the leakage and magnetising reactances, at fundamental frequency, measured at the terminals of a stator phase. These reactances are approximately equal to the reactances X_1 and X_m determined by tests on the actual machine at stand-still. X_2'' is the referred leakage reactance of a rotor phase measured at fundamental frequency. This reactance is also nearly equal to X_2. R_t is the total resistance in the path of current I_4. The turns-ratio

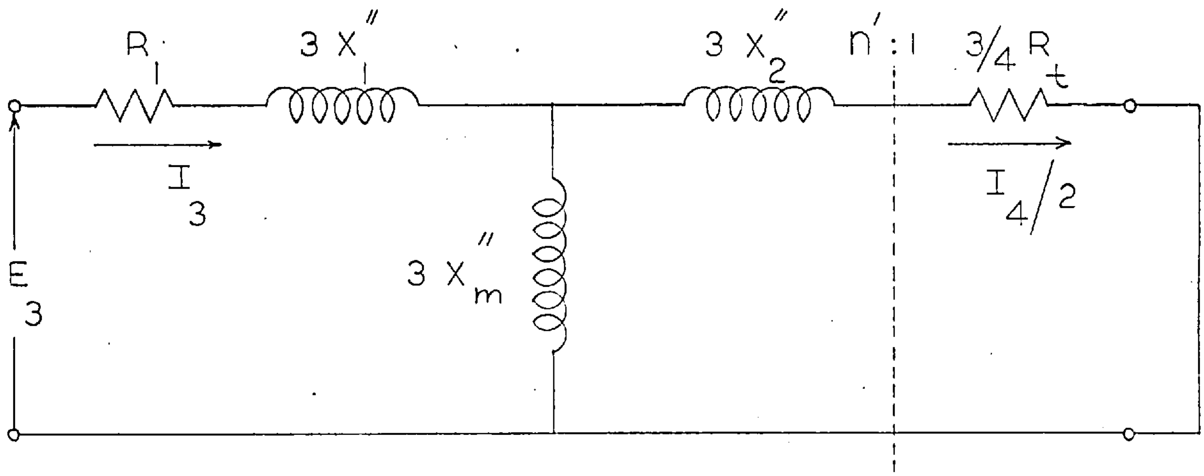

FIG. 4.12 a

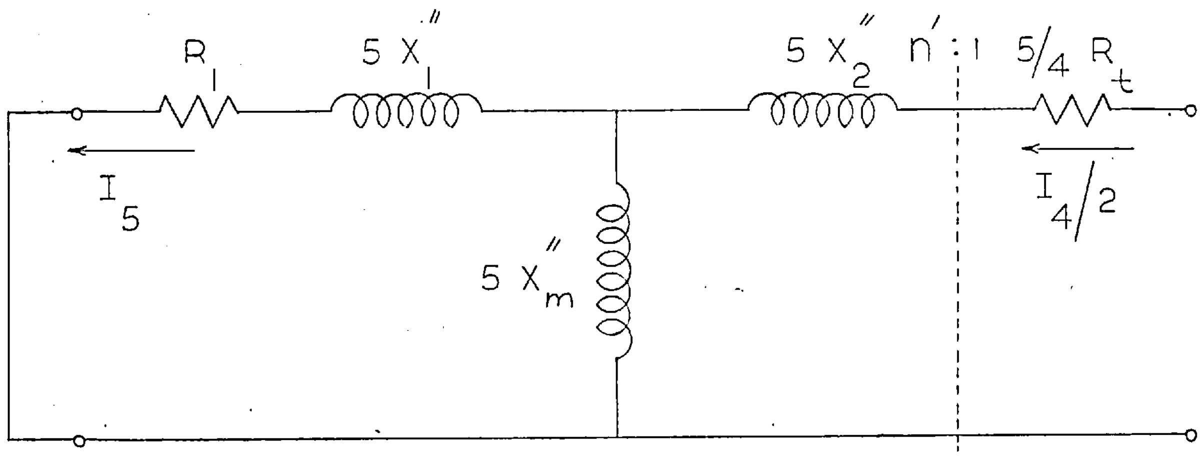

FIG. 4.12 b

FIG. 4.12 EQUIVALENT CIRCUITS RELATING TO THE HARMONIC COMPONENTS OF THE ARMATURE SHORT-CIRCUIT CURRENT n' is nearly equal to ratio n obtained from Fig. 4.3. An equivalent circuit relating the fifth harmonic current I_5 induced in a stator phase to the component $I_4/2$ is shown in Fig. 4.12b.

The insertion of an inductor in series with the field winding is represented by an increase in reactance X_2'' in Figs. 4.12a and b. For the same driving voltage E_3, the currents I_3, I_5 and $I_4/2$ are consequently reduced. As far as the harmonic components of load current are concerned, an increase in the load inductance is represented by an increase in X_1'' in Figs. 4.12a and b. A simplified analysis shows that currents I_3 and I_5 decrease even though the voltage E_3 increases with increasing field current. The connection of an inductor in series with the field winding leads to further suppression of the harmonic components of load current.

An approximate indication of the relative magnitudes of I_3 and I_5 can be obtained if it is assumed that reactances $3X_m''$ and $5X_m''$ in Figs. 4.12a and b can be ignored in comparison with the impedances connected in parallel. The currents I_3, $I_4/2n'$ and I_5 then become equal. The measured third and fifth harmonic components of the short-circuit current in a stator phase respectively form 14 and 13.5 per cent of the fundamental component. The agreement between the two values shows that the above approximation is reasonable. In the foregoing explanation no mention has been made of the third and fifth harmonic components of short-circuit current caused by the fifth harmonic voltage induced in a stator phase by the field m.m.f. This voltage is small in comparison to the third harmonic voltage E_3 and hence its effect has been ignored.

In the alternators employed in practice, the three phases are usually connected in star. By performing the short-circuit test by connecting together the three line terminals of the machine, the third harmonic component of short-circuit current is suppressed. The fifth harmonic component is small. Therefore the short-circuit current is nearly sinusoidal in such machines. In addition, the voltage across a phase is deduced from the measured line-to-line voltage. By this means the influence of the third harmonic component present in the phase voltage is eliminated. Hence, the effects discussed above are not present during tests on a normal three-phase machine.

4.5.2. Leakage reactance of a stator phase obtained from tests on the machine as an alternator

The linear part of the zero power factor characteristic drawn solid in Fig.4.11a was obtained by performing the Potier test with an inductor connected in series with the field winding. Checks made at some points on the characteristic showed that the presence or absence of the inductor did not significantly alter the remaining part of the characteristic.

The slopes of the linear parts of the open-circuit and modified zero power factor characteristics are nearly equal. The effect of an increase of 0.3 amp in the base of the Potier triangles may be assessed by comparing the reactances obtained from triangles A'B'C' and A"B"C' in Fig.4.11b. The reactances obtained from these two triangles differ by 0.3 ohm. Hence the effect examined in the previous section does not materially alter the reactance obtained from triangles such as A'B'C'. Changes in the length of the base, however, significantly alter the reactance evaluated from triangles such as ABC, Fig. 4.11a.

Graph b, Fig. 4.10 shows the Potier reactance determined from Figs. 4.11a and b. Considering the inherent inaccuracy of the method, the agreement between the reactances shown in graphs a and b is satisfactory. An average turns-ratio of 2.58 is obtained from Figs. 4.11a and b. This ratio is very nearly the expected value of $\sqrt{2}$ times the average turns-ratio of 1.81 determined from Fig. 4.3. The turns-ratios are related by the factor $\sqrt{2}$ owing to the fact that in one case the turns-ratio is the ratio of the r.m.s. values of the equivalent alternating current in the rotor and the load current, while in the other case it is the ratio of the equivalent direct-current in the rotor and the r.m.s. load current.

Efforts made to determine the leakage reactance of a rotor phase by the Potier method were not successful owing to the small magnitude of the reactance.

4.5.3. Relation between the characteristics obtained from tests on the machine as a transformer and as an alternator

The test characteristics of Figs. 4.9a and b can be related to those in Figs. 4.11a and b by the following considerations. The relation between the open-circuit characteristics in the two sets of figures is considered first. For brevity, the operations of the machine as a transformer and as an alternator are respectively called mode A and mode B operation of the machine. The effect of hysteresis is not taken into account in the following explanation.

Consider operating points on the two sets of open-circuit characteristics such that the d.c. and peak a.c. excitations at these points are equal. (These points are referred to as "corresponding" points in the ensuing discussion). The distribution of air-gap flux density at the instant that the current in mode A operation is a maximum would be the same as the distribution due to the field m.m.f. This similarity between the two distributions holds irrespective of the extent of saturation of the magnetic circuit. A set of open-circuit characteristics is drawn dotted in Figs. 4.11a and b. These characteristics are obtained by re-plotting the open-circuit characteristics in Figs. 4.9 and b in terms of the peak a.c. excitations. These peak excitations have been approximately calculated by the addition of the peak fundamental and third harmonic components of the exciting current. Any phase displacement between the two components caused by hysteresis has been neglected. The factors causing the difference between the dotted and experimental characteristics are explained below.

At corresponding points on the open-circuit characteristics in Figs.4.9 and 4.11, the voltage induced in a stator phase by the fundamental component of air-gap flux is the same for both modes of operation of the machine when it is unsaturated. However, additional fundamental-frequency voltages are induced in mode A operation by the fluxes distributed harmonically. These fluxes induce harmonic voltages in a stator phase in mode B operation of the machine. Therefore, to obtain the same fundamental voltage, the field excitation has to be increased to a value larger than the peak a.c. excitation. The proportion of the additional fundamental-frequency voltage induced in mode A operation by the harmonically-distributed fluxes can be calculated by the following expression.

$$\frac{E_{fn}}{E_{f1}} = \frac{1}{n} \times \frac{B_{mn}}{B_{m1}} \times \frac{K_{wn}}{K_{w1}} \qquad 4.2$$

E_{fn} is the voltage induced by the nth harmonic component of air-gap flux. B_{mn} is the peak value of the corresponding flux density. K_{wn} is the nth harmonic winding factor of a stator phase.

For operating voltages at which the magnetic circuit is unsaturated, the ratio B_{mn}/B_{m1} is equal to the ratio of the corresponding components of the m.m.f. established by a rotor phase. The distribution of this m.m.f. is approximately described by the following equation.

$$F = \frac{4}{\pi} \frac{N_f}{P} i \left[0.902 \sin \theta + 0.103 \sin 3\theta \right] \qquad 4.3$$

N_f is the number of turns on a rotor phase. i is the instantaneous current in the phase and θ is the angle in electrical degrees measured from the inter-polar axis. The coefficients in the above expression are respectively equal to K'_{w1} and $K'_{w3}/3$, where K'_{wn} is the nth harmonic winding factor of a rotor phase. The winding factors of a stator and a rotor phase for the fundamental and third harmonic components are equal.

The ratio F_{f3}/E_{f1} calculated from equations 4.2 and 4.3 is 0.013. In order to secure an increase of 1.3 per cent in the fundamental terminal voltage, the field current has to be increased correspondingly when the main magnetic circuit is unsaturated. The slopes of the linear parts of the two open-circuit characteristics in Fig. 4.11a should then differ by a corresponding amount. However, since this difference is small, it is obscured by experimental and graphical errors.

On saturation of the magnetic circuit, two additional factors contribute to the difference between the dotted and experimental characteristics. These factors are the changes in the distribution of air-gap flux and the presence of a third harmonic (time) component in the induced voltage in mode A operation of the machine. As stated in section 4.4, this component arises due to harmonic voltage drops across the leakage reactances of the source and the winding excited. The two effects mentioned above can be considered separately as shown below.

The influence of changes in the distribution of air-gap flux is considered in the present paragraph. The induced voltage is assumed to vary sinusoidally in time. Consider again two corresponding points on the open-circuit characteristics in Figs. 4.9a and b, and Figs. 4.11a and b. On account of saturation, the distribution of air-gap flux in mode B operation, and in mode A operation at the instant that the exciting current is a maximum, is more flat-topped than the corresponding m.m.f. distribution described by equation 4.3. The ratio E_{f3}/E_{f1} therefore increases. As a result, the additional field m.m.f. required to generate the voltage E_{f3} is larger than that required in the absence of saturation.

The presence of a peaking third-harmonic component in the induced voltage in mode A operation indicates that the time-variation of the flux linking a stator phase can be represented by a flat-topped wave. The influence of this variation of flux linkages is more clearly seen by assuming the air-gap flux to be sinusoidally distributed in space. Consider corresponding operating points on the two sets of open-circuit characteristics. At the instant that the a.c. excitation is at its peak value, the flux distributions in both modes of operation of the machine are similar. The flux linkages with a stator phase vary sinusoidally in time in mode B operation of the machine as shown in graph b, Fig. 4.13. The variation of flux linkages in mode A operation is represented by a flat-topped wave having the same peak value as in graph b. (graph a, Fig. 4.13). The dotted graph c in Fig. 4.13 shows the fundamental component of graph a. The voltage induced by this component is larger than that induced by a change of flux linkages as per graph b. This effect adds to the effect of a change in

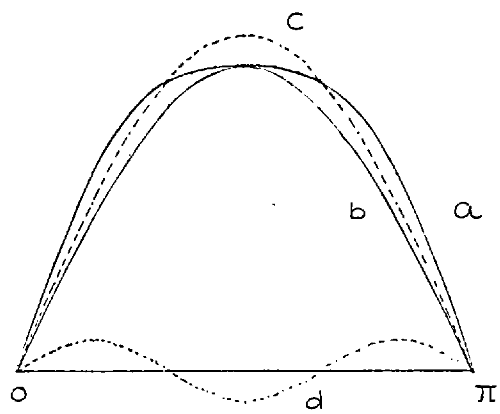

a — VARIATION OF FLUX LINKAGES WITH A STATOR PHASE IN MODE A OPERATION OF THE MACHINE

b — VARIATION OF FLUX LINKAGES WITH A STATOR PHASE IN MODE B OPERATION OF THE MACHINE

c AND d — FUNDAMENTAL AND THIRD HARMONIC COMPONENTS OF a

FIG. 4.13 VARIATION OF FLUX LINKAGES WITH A STATOR PHASE OF THE MACHINE the distribution of air-gap flux caused by saturation.

It may also be pointed out that the additional field excitation required to secure a specified increase in fundamental voltage increases with saturation of the magnetic circuit. This may be seen by an examination of the open-circuit characteristics in Figs. 4.11a and b. For example, the increase in field current corresponding to an increase in the voltage from 50 to 51 volts is 0.1 amp , while that corresponding to an increase in the voltage from 105 to 106.5 volts is 0.7 amp. All these factors cause the dotted and experimental open-circuit characteristics to diverge as shown in Figs. 4.11a and b.

The zero power factor characteristics in Figs. 4.9a and b can be related to the characteristics in Figs. 4.11a and b in a similar manner. The same load current was employed for both types of tests. Therefore, the same m.m.f. was established by a stator phase in both types of tests. As in the previous case, the relation between the two modes of operation of the machine can be established by considering corresponding operating points on the two sets of zero power factor characteristics. The flux distributions at the instant that the current in a stator phase is maximum are similar in both types of tests. The difference between the two sets of characteristics, arising out of the non-sinusoidal distribution of the rotor winding and saturation, can be explained as in the preceding paragraphs. The fact that the turns-ratio determined from Figs. 4.11a and b is nearly $\sqrt{2}$ times that determined from Figs. 4.9a and b indicates that the two sets of zero power factor characteristics are related in the same manner as the open-circuit characteristics. This conclusion is reinforced by the similar values of Potier reactance determined from the two sets of characteristics.(graphs a and b, Fig. 4.10)

4.6. Equivalent Pi circuit of the test machine

Fig. 4.14 shows the values of X_3/n calculated by using equation 3.11 (p. 80). The quantities V_2', V_2 and I_1 (see Figs. 3.3 and 3.4, p 81) were obtained from the test characteristics of Figs. 4.2 and 4.3. The fundamental component of I_1 was employed for calculating X_3/n. The variations of approximately 10 per cent (from a mean value of 1.0 ohm) in Fig. 4.14 could be caused by errors of the order of 1 per cent in the voltages V_2' and V_2. The influence of such errors is more pronounced on the values of X_3/n calculated from voltages and currents at operating points located in the partially-saturated and unsaturated regions of the

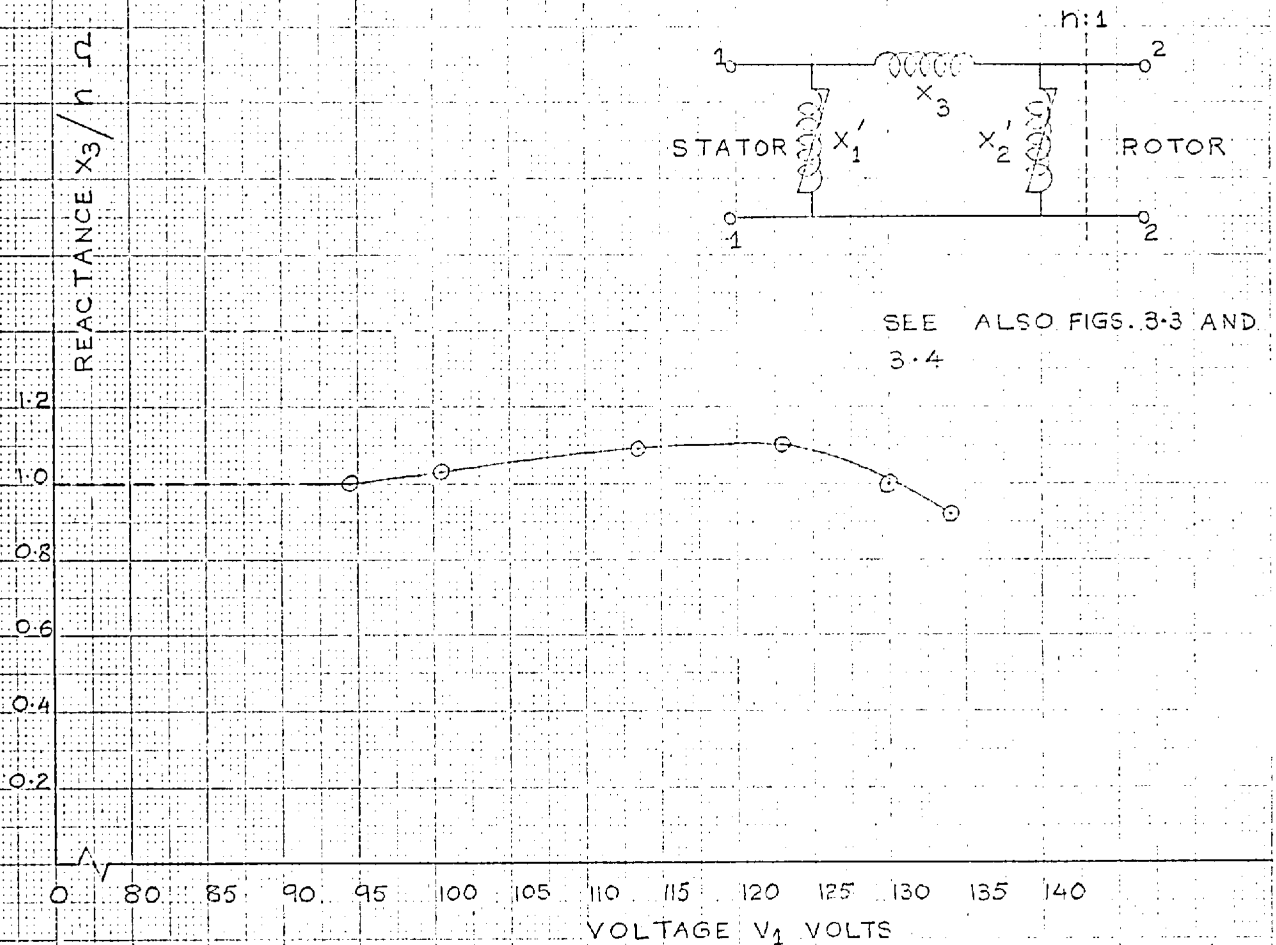

FIG. 4.14 REACTANCE X_3/n OF THE EQUIVALENT PI CIRCUIT OF THE MACHINE AT STAND-STILL

test characteristics. Hence the values of X_3/n obtained from these points are not shown in Fig. 4.14. The graph is produced back to the ordinate-axis by a dotted line.

Further calculations were performed by employing a reactance X_3/n of 1.0 ohm . To obtain a comparison of the equivalent Tee and Pi circuits, a turns-ratio of 1.81 was employed to evaluate the reactances of the Pi circuit. This ratio is equal to the average ratio obtained from Fig. 4.3. The reactance X_3 is then 1.81 ohms. Equations 3.12 and 3.13 were used for calculating X_1' and X_2'. The results of these calculations are shown in Fig. 4.15. These results are presented in the form of characteristics relating the voltages and currents associated with each of the two reactances. This manner of presentation facilitates calculation of the terminal properties of the network. Since the values of X_3/n in Fig. 4.14 vary by 10 per cent, the characteristics of X_1' and X_2' could be in error by a similar amount.

Points marked by crosses in Fig. 4.15 were obtained by transformation of the equivalent Tee circuit. Average values of 1.4 and 0.45 ohms were employed for reactances X_1 and X_2. The values of X_m were obtained from graph a, Fig. 4.7a. The values of X_3 obtained by transformation vary between 1.87 and 1.91 ohms. The characteristics of X_1' and X_2' derived by transformation are in reasonable

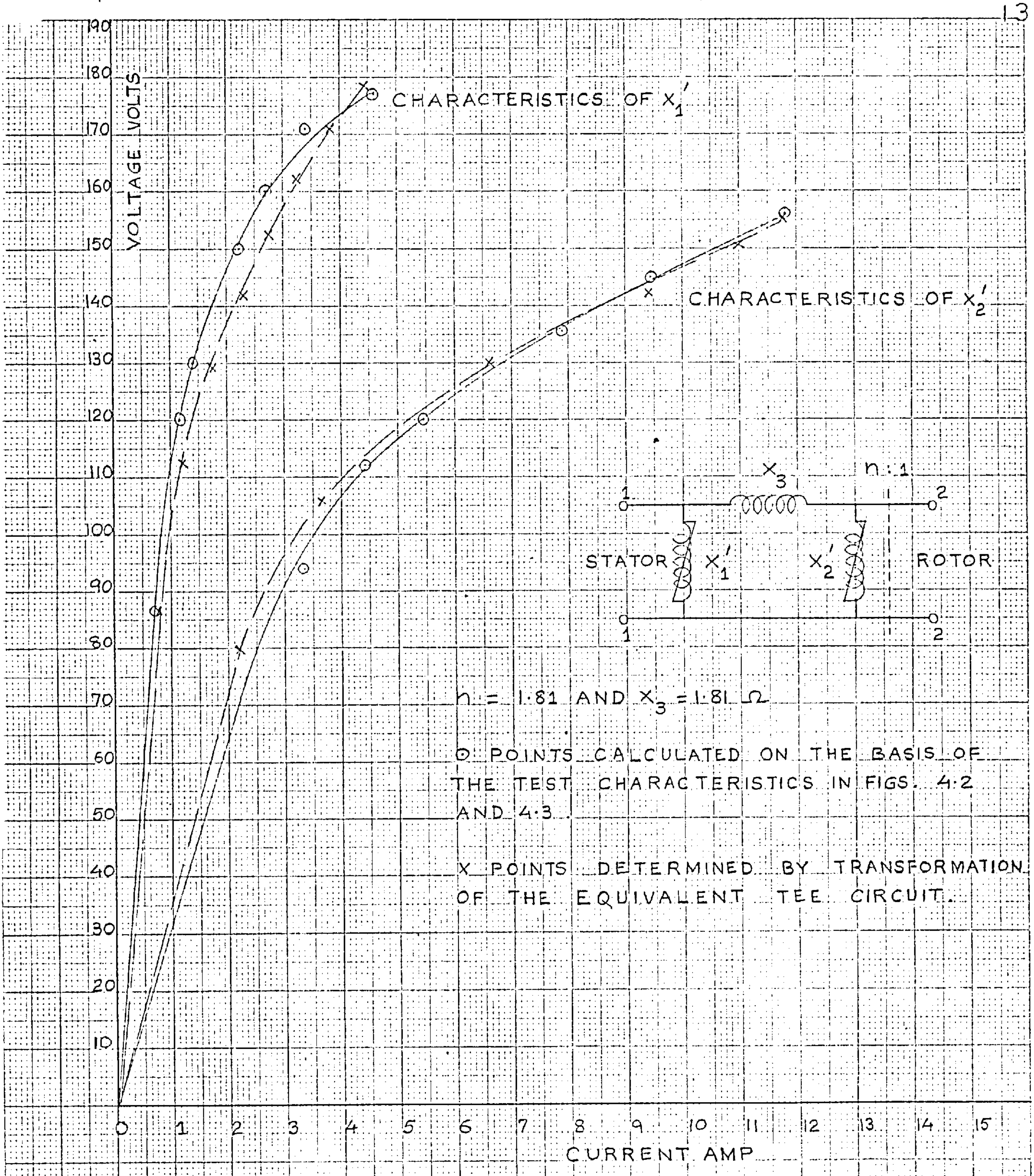

FIG. 4.15 CHARACTERISTICS OF THE NON-LINEAR REACTANCES OF THE PI CIRCUIT REPRESENTING THE MACHINE AT STAND-STILL

agreement with the characteristics obtained by direct calculations. This agreement suggests that the machine can be represented by either the Tee or the Pi circuit to the same degree of accuracy.

4.6.1. Equivalent Pi circuit based on characteristics of the machine as an alternator

The parameters of the equivalent Pi circuit were determined from the characteristics drawn in Figs. 4.11a and b by employing the method outlined in section 3.4.2 of chapter 3. The reactances were calculated using a turns-ratio of 2.6. This ratio is nearly $\sqrt{2}$ times the turns-ratio of 1.81 employed above for evaluating the parameters of the Pi circuit from the characteristics of Figs. 4.2 and 4.3.

Two of the three terminal measurements specified in equations 3.14 to 3.16 are obtained from Fig. 4.11a. These two measurements are the slope of the unsaturated part of the open-circuit characteristic, and the ratio of the field and armature currents with the armature short-circuited. The third measurement was obtained by operating the machine as an alternator with a stator phase as the field winding. The ratio of the short-circuit current in a rotor phase and the corresponding field current furnished the third measurement. The influence of harmonics in the short-circuit current was minimised by the connection of an inductor in series with the field winding. The field excitation required to circulate a short-circuit current of 7.0 amp was found to be 5.6 amp .

In order to utilise the measurements made with a stator phase used as the field winding, it is necessary to specify a turns-ratio n_2. n_2 is the ratio of the short-circuit current in a rotor phase and its equivalent field current in a stator phase. As stated in Chapter 2, the turns-ratio is obtained by equating the fundamental components of the m.m.f.s produced by currents in the two windings. It may be also recalled that to establish the same peak fundamental m.m.f. with d.c. excitation of a winding as with a given a.c. excitation, the d.c. excitation has to be equal to $\sqrt{2}$ times the r.m.s. a.c. excitation. (Assuming that the magnetic circuit is unsaturated). These factors can be used to relate n_2 to the ratio n_1 (2.6) of the equivalent field current and the armature short-circuit current when a rotor phase is employed as the field winding. The relationship of n_2 and n_1 is as follows.

$$n_1 = \frac{\text{Equivalent field current in a rotor phase}}{\text{Short-circuit current in a stator phase}}$$

$$= \frac{\sqrt{2} \text{ x Alternating current in a rotor phase}}{\frac{\text{Equivalent direct current in a stator phase}}{\sqrt{2}}}$$

$$= 2 \times n_2$$

$$\text{or } n_2 = \tfrac{1}{2}\, n_1 \qquad 4.4.$$

The calculated value of reactance X_3 is 2.33 ohms. The corresponding characteristics of X_1' and X_2' were calculated using the test characteristics of Figs. 4.11a and b. A modified form of the method suggested in section 3.4.2. was employed for determining the characteristics of X_1' and X_2'. In this modified form, an operating point lying just above the straight-line part of the zero power factor characteristic was chosen. At this point, the reactance X_1' could be assumed to be unsaturated. Based on this operating point, the current through X_2' and the voltage V_{22} across the reactance were calculated. Next an operating point at which the voltage across X_2' is V_{22} was located on the open-circuit characteristic by employing a trial-and-error procedure. The current through X_1' at a voltage V_{11} across it was then known. Further, knowing the field current at a voltage V_{11} on the zero power factor characteristic, the current through X_2' could be calculated at a voltage across X_2' higher than V_{22}. This procedure was repeated to determine the characteristics of X_1' and X_2'. The characteristics of X_1' and X_2' determined in this manner are shown in graphs a and a', Fig.4.16.

The difference between the value of X_3 = 2.33 ohms and the value of X_3 = 1.81 ohms quoted in the previous section is mainly caused by small errors in the measurement of various short-circuit currents. For example, if the d.c. excitation of a stator phase required to circulate a short-circuit current of 7.0 amp in a rotor phase is taken as 5.7 amp. (instead of 5.6 amp), the calculated reactance X_3 becomes 2.9 ohms. The unsaturated values of X_1' and X_2' alter correspondingly. The saturated values of these reactances are based on the value of X_3 and the unsaturated value of X_1'. Hence, the saturated values are also influenced by errors in the measurement of the short-circuit currents. To illustrate this statement, characteristics of X_1' and X_2' corresponding to X_3 = 2.9 ohms are also shown in Fig.4.16. Points on these characteristics, drawn dotted, are marked by triangles. Comparing corresponding characteristics, it may be observed that the increase in X_3 results in an increase of approximately 25 per cent in the current through X_1'. The decrease in the current through X_2' is of a similar magnitude. However, this change in the characteristics of X_1' and X_2' does not

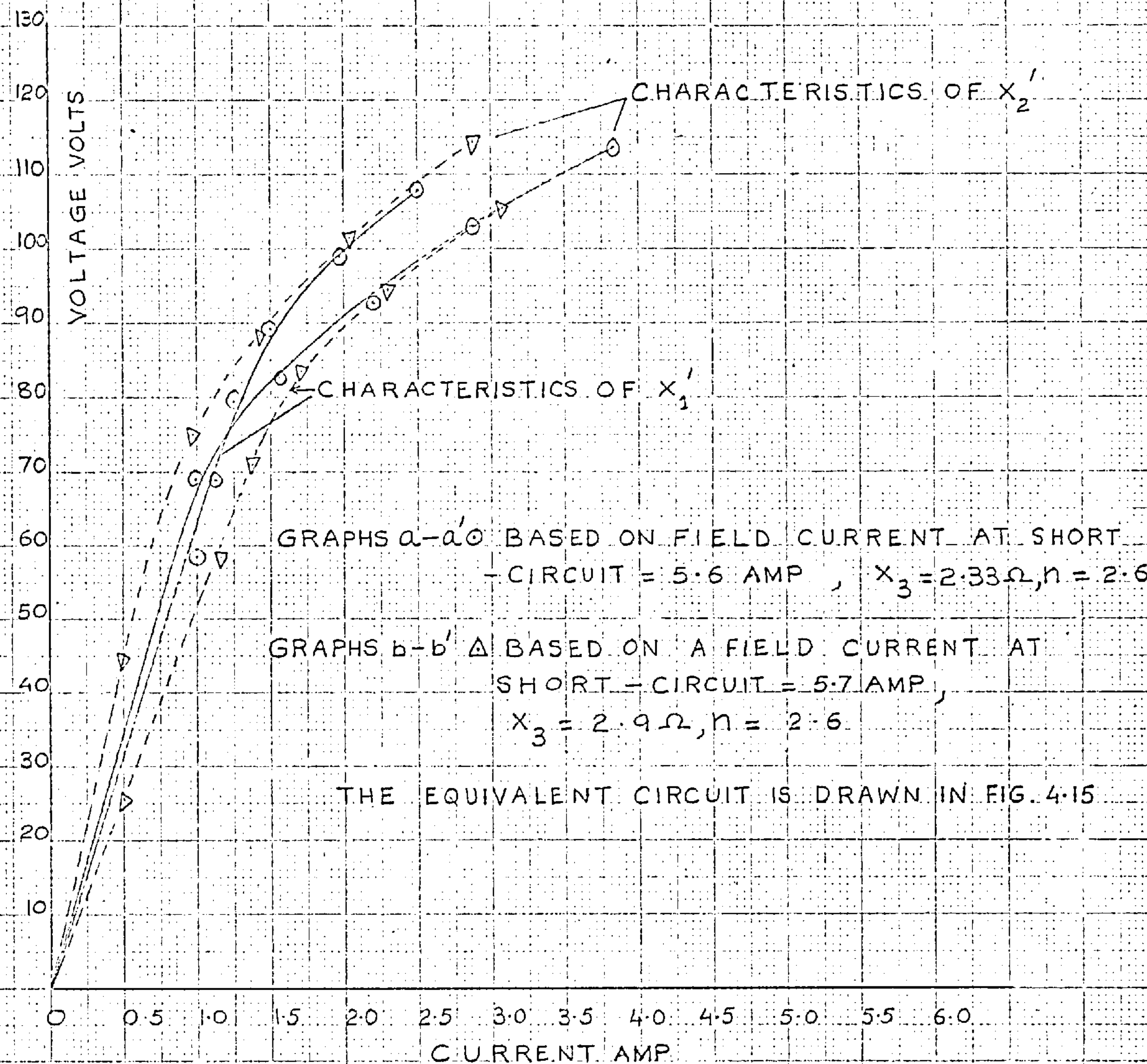

FIG. 4.16 CHARACTERISTICS OF THE NON-LINEAR REACTANCES OF THE PI CIRCUIT REPRESENTING THE MACHINE OPERATING AS AN ALTERNATOR

significantly alter the total current required by the two together. Hence, the parameters of the Pi circuit determined in the above manner could be employed to calculate the field excitation under different load conditions. The calculated excitation would be reasonably accurate.

The problems associated with the experimental determination of the parameters of the equivalent Pi circuit are discussed in more detail in the following chapter.

CHAPTER 5

Equivalent Circuits of the micro-machine

5.1. Scope. Tests on a model synchronous machine called the micro-machine are described. These tests were performed on the machine employing, in turn, field systems of salient-pole and cylindrical-rotor type construction with the same stator. The parameters of the equivalent Tee and Pi circuits of the machine are determined from the characteristics obtained from tests. It is shown that the referred field leakage reactance in the equivalent Tee circuit, and the parameters of the equivalent Pi circuit can be only approximately determined from terminal measurements. The results indicate that the equivalent Tee and Pi circuits constitute equally satisfactory representations of the micro-machine with a cylindrical-rotor. The error involved in using the Potier reactance for calculating the zero power factor characteristics of the micro-machine with a salient-pole rotor is seen to be small. Since the parameters of the equivalent Pi circuit can be only approximately determined from terminal measurements, the results indicate that the use of Potier reactance is both adequate and justified for the machine examined.

5.2. The micro-machine and other test apparatus

Tests were performed to assess the extent of additional saturation (due to field leakage flux) of the magnetic system of a salient-pole machine and the influence of this saturation on the Potier reactance of the machine. The micro-machine[37] was employed as the test machine. A constructional feature of this machine is that different rotors can be employed with the same stator. This feature makes it possible to obtain a direct comparison of saturation effects in a cylindrical-rotor and a salient-pole machine. Tests were performed on the machine employing one cylindrical-rotor and two salient-pole field systems. The specifications of the machine are as follows:

Make	:	Alsthom, France.
kVA Output	:	0.6 - 4.5
Rated Voltage	:	220 volts
Number of phases	:	3
Speed	:	1500 r.p.m.
Stator number	:	334819
Salient-pole rotor A number	:	334818
Salient-pole rotor B number	:	334819
Cylindrical rotor number	:	334827

Air-gap with salient-pole rotor A: 0.8 mm.

Air-gap with salient-pole rotor B: 0.31 mm.

Air-gap with cylindrical rotor : 0.3 mm.

The stator has 54 slots and is wound with two double-layer windings connected in series. The windings are similar fractional-slot windings consisting of coils having a pitch of 1-13. Each slot contains 14 conductors. The resistance of an armature phase, consisting of 126 turns in series, is 0.15 ohm . The phases are connected in star.

The field windings in the salient-pole rotors are located in deep slots as shown in Fig. 5.1(a). The field winding of the cylindrical-rotor machine is of the concentric type. The winding is housed in 24 slots arranged as shown in Fig. 5.1(b).

A ganged unit of three single-phase "Variac" auto-transformers was employed as the source of variable voltage a.c. supply. The specifications of the three components have been given in section 4.3.2. of Chapter 4. The d.c. supplies were derived from the 200-volts supply in the laboratory.

Measurements of voltages and currents were made with multi-range moving-iron instruments specified to be accurate to within 1.5 per cent of the maximum value of the range as per BS 89. The instruments were checked against precision multi-range meters with a specified accuracy of half per cent of the full scale readings.

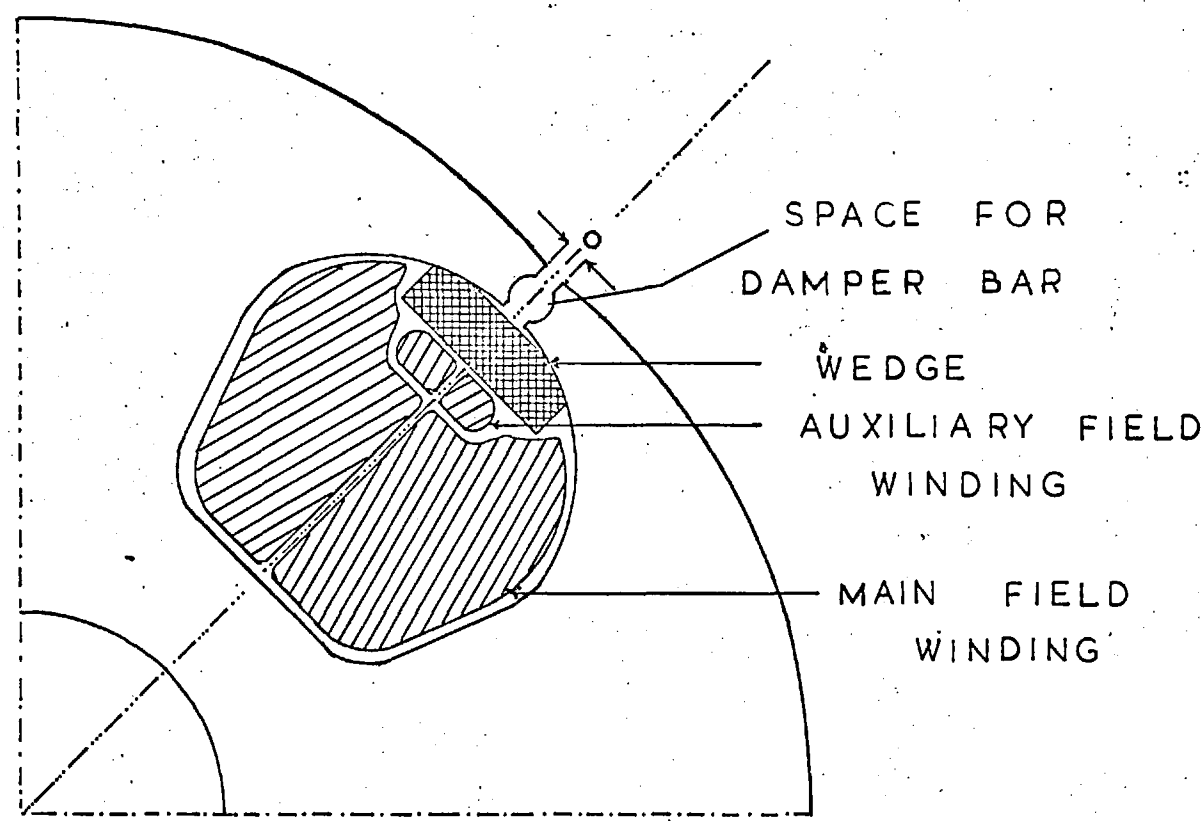

o — SLOT OPENING
15 mm. IN MACHINE A
5 mm. IN MACHINE B

FIG. 5.1a ARRANGEMENT OF THE FIELD WINDING IN THE SALIENT - POLE ROTOR OF THE MICRO-MACHINE

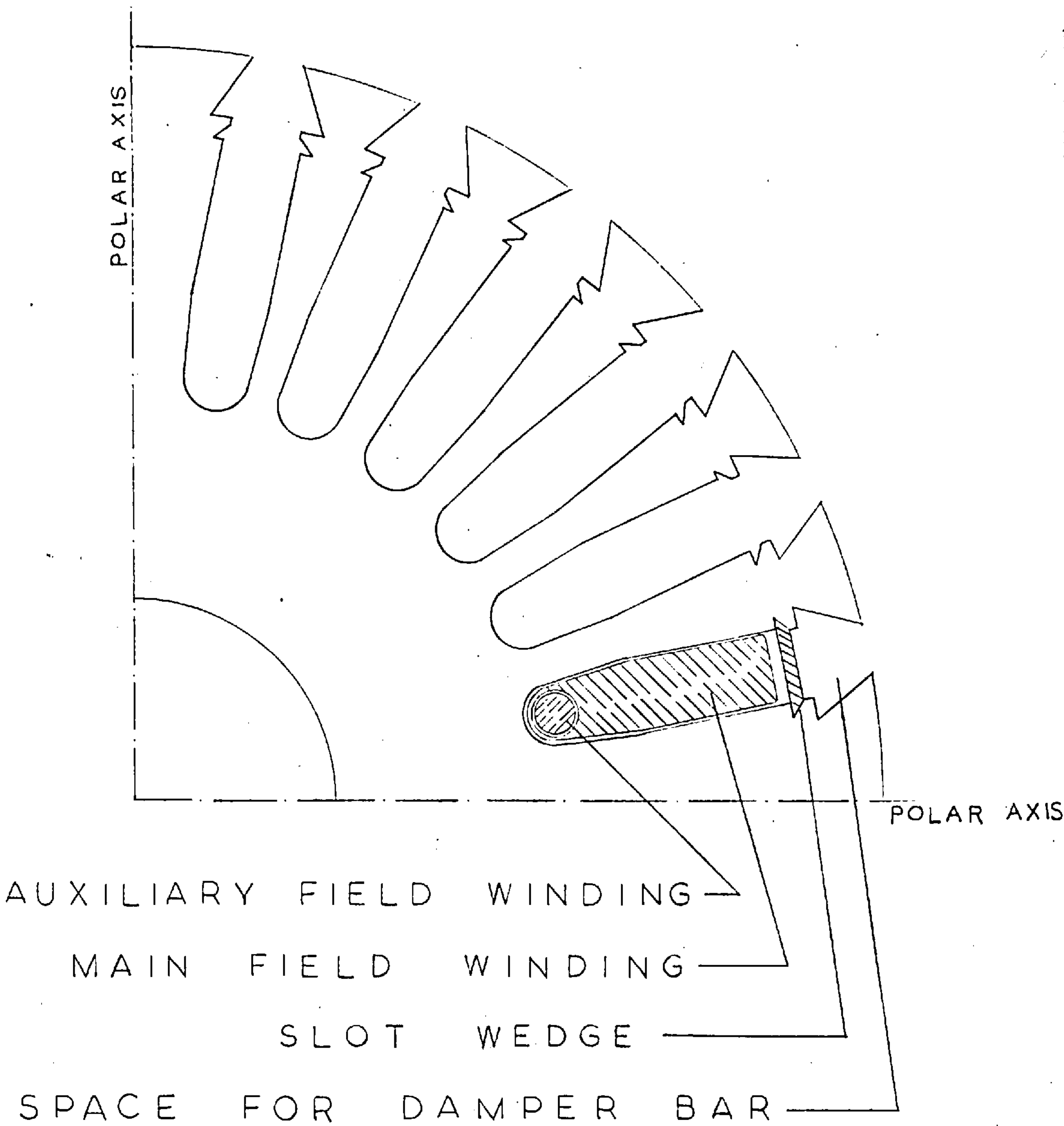

FIG. 5.1b A QUADRANT OF THE CYLINDRICAL ROTOR SHOWING DISPOSITION OF THE SLOTS

For convenience, the characteristics of the machine with salient-pole rotors A and B and the cylindrical-rotor are referred to hereafter as the characteristics of machines A, B and C respectively.

5.3. Characteristics of the machines.

The zero power factor characteristics of the machines were determined for a range of load currents by testing the machines as alternators. The inductors described in section 4.3.3. were employed as the load. The characteristics were checked by testing the machines as over-excited synchronous motors.[38] Good agreement has been obtained between the two sets of characteristics.

The test characteristics of machine A are shown in Figs. 5.2(a) and (b). Those of machine B are drawn in Figs. 5.3(a) and (b). Figs. 5.4(a) and (b) show the characteristics of machine C. Approximate calculations based on the measured losses in machine B and on information supplied by the manufacturers regarding the losses in the other two machines have shown that the influence of losses on the test characteristics of the machines is negligible. Similar calculations have also indicated that the influence of the resistance of the load on the characteristics can be ignored.

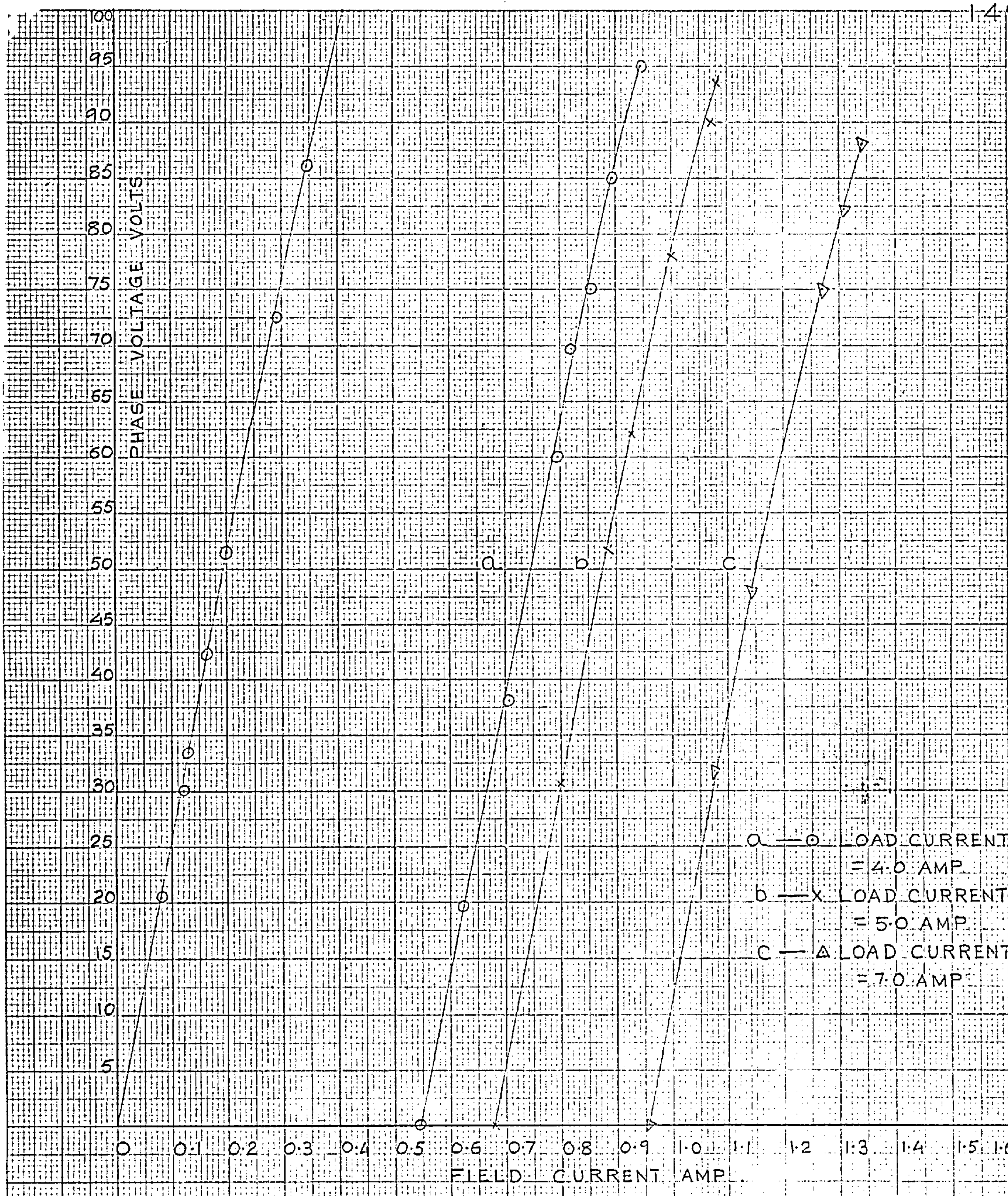

FIG 5.2 a OPEN-CIRCUIT AND ZERO POWER-FACTOR CHARACTERISTICS OF MACHINE A

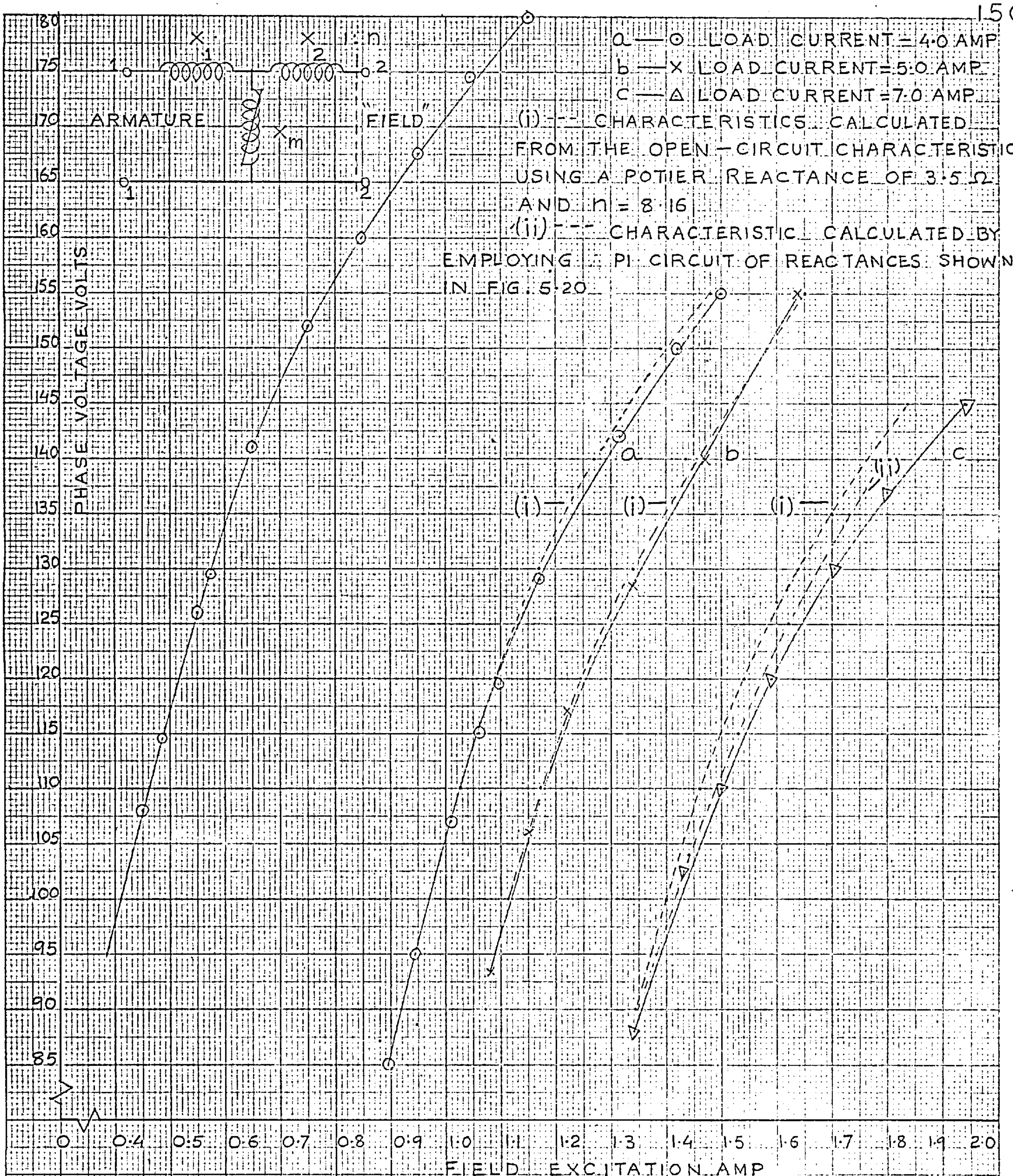

FIG 5.2 b OPEN-CIRCUIT AND ZERO POWER-FACTOR CHARACTERISTICS OF MACHINE A

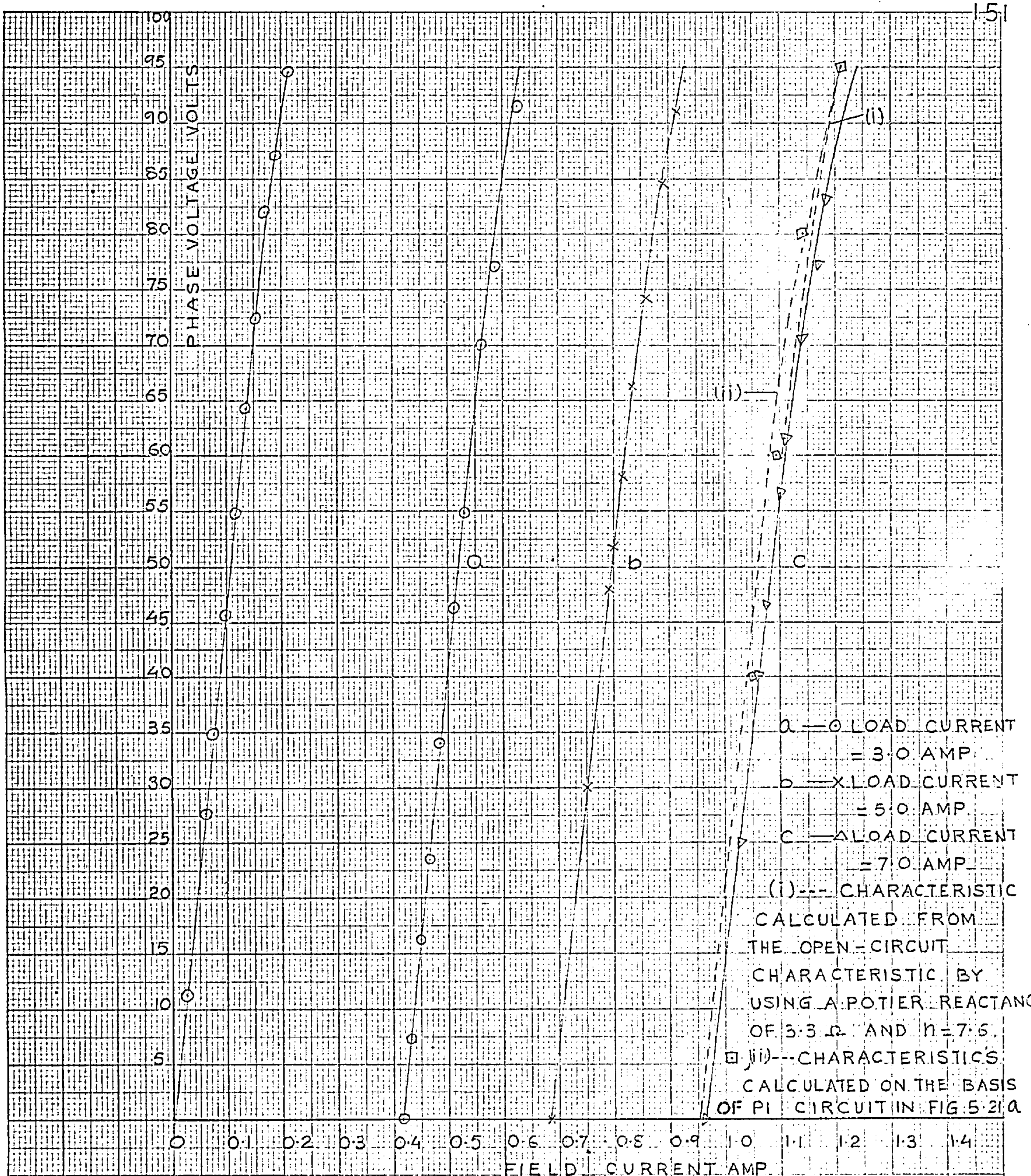

FIG 5.3 a OPEN-CIRCUIT AND ZERO POWER-FACTOR CHARACTERISTICS OF MACHINE B

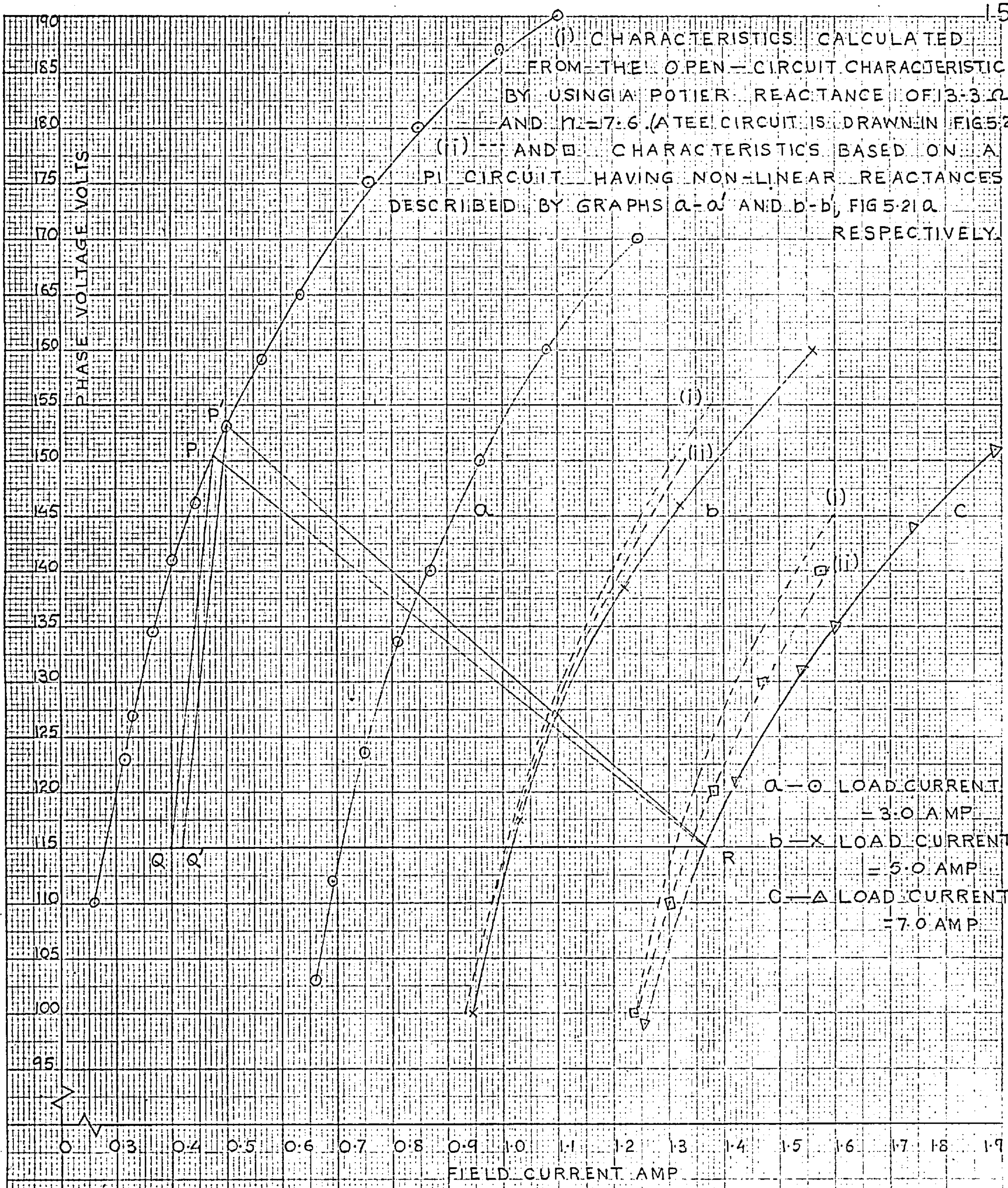

FIG 5.3b OPEN-CIRCUIT AND ZERO POWER-FACTOR CHARACTERISTICS OF MACHINE B

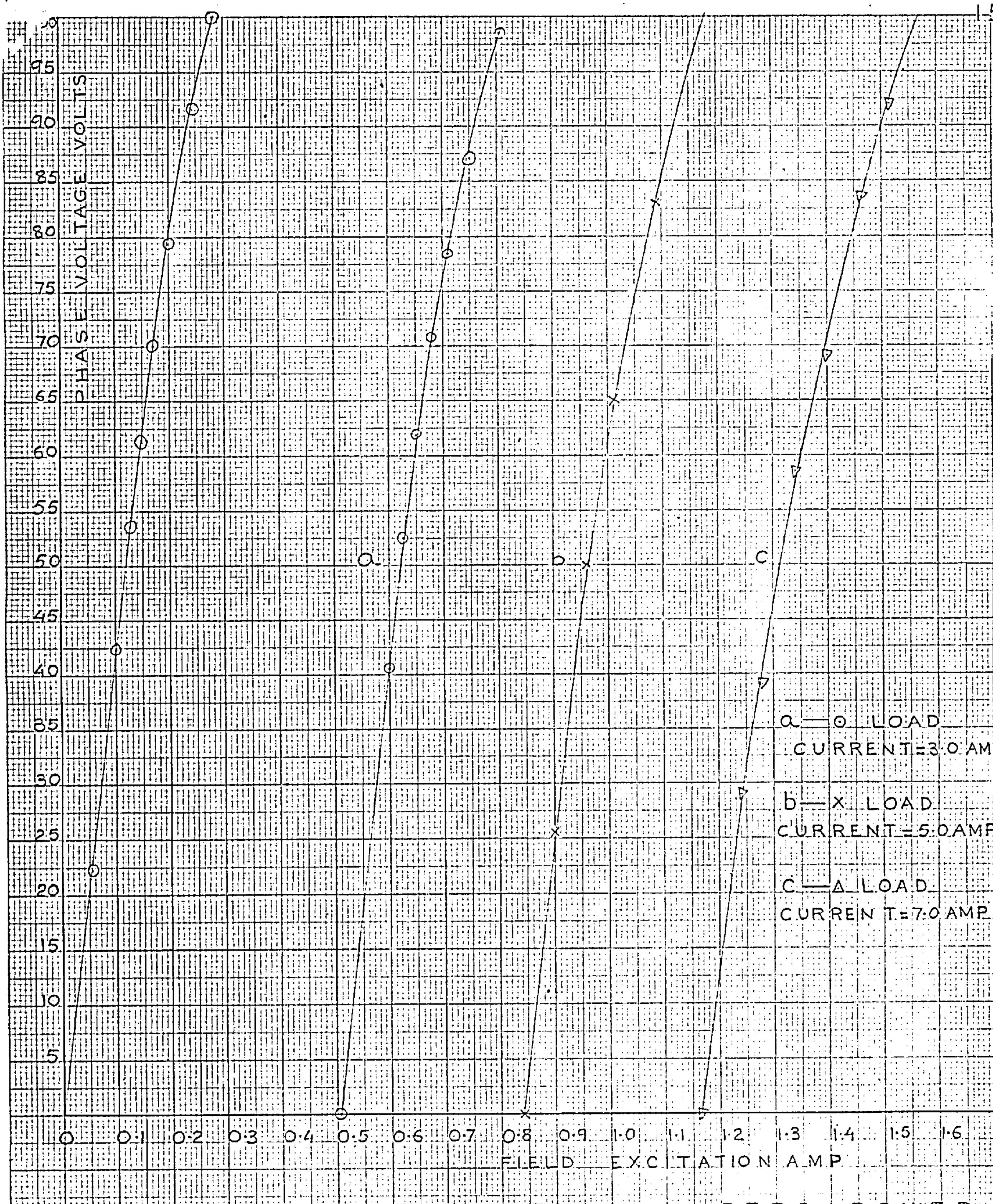

FIG 54a OPEN-CIRCUIT AND ZERO POWER-FACTOR CHARACTERISTICS OF MACHINE C

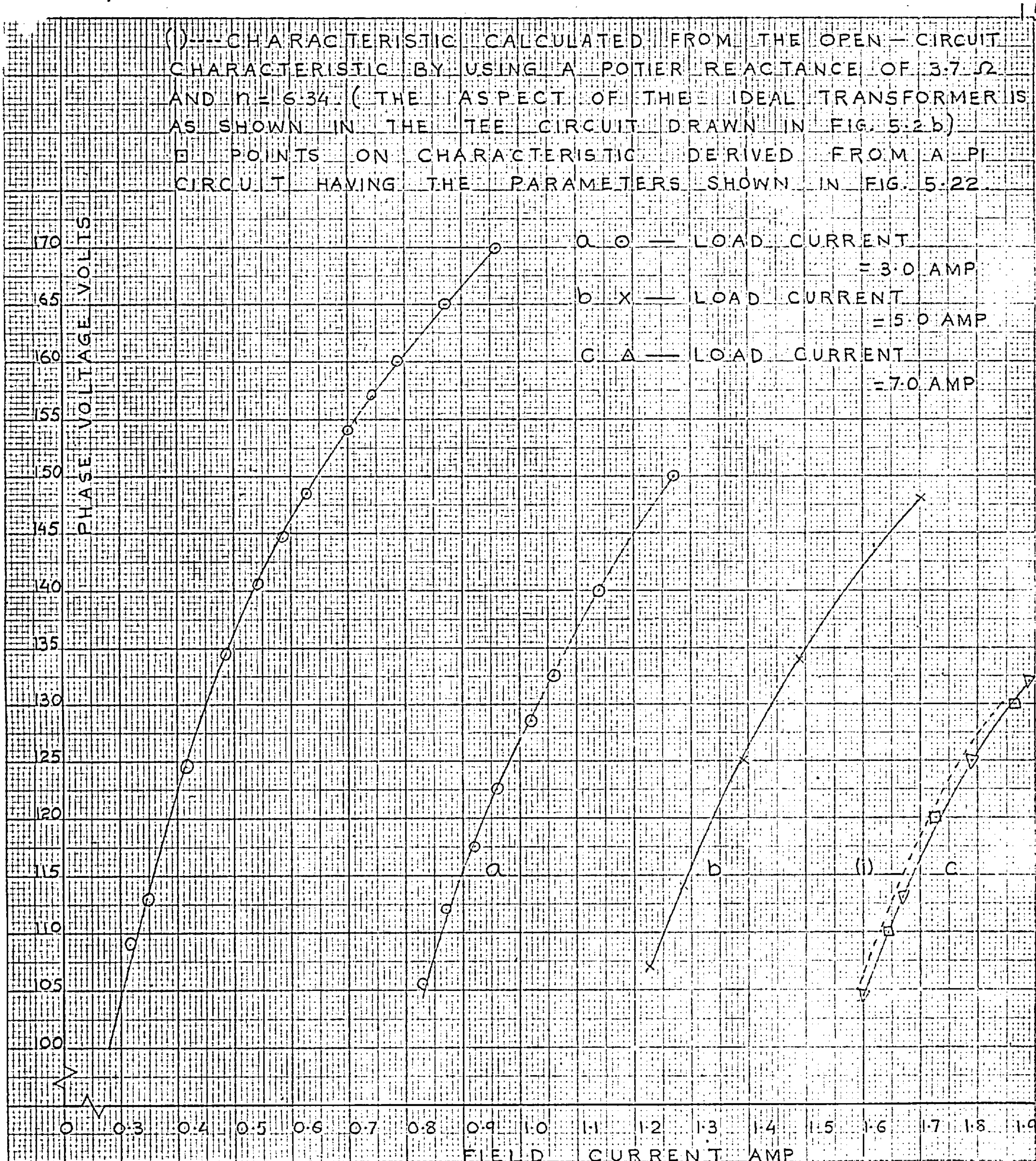

FIG 5.4 b OPEN-CIRCUIT AND ZERO POWER-FACTOR CHARACTERISTICS OF MACHINE C

5.4.1. Potier reactance of the salient-pole machines.

Graphs a, b and c in Figs. 5.5 and 5.6 show the Potier reactance of machines A and B respectively. The reactance is plotted against the open-circuit voltage denoted by the vertex of the Potier triangle. The graphs are denoted by symbols corresponding to those employed in Figs. 5.2a and b and 5.3a and b. The values of turns-ratio marked are the ratios of the load current and the equivalent field current. These values are average values obtained from the test characteristics. An indication of the limits of possible error in the determination of the reactance is provided by comparing triangles PQR and P'Q'R in Fig. 5.3(b). The length QQ' corresponds to a total error of 1.5 per cent in the measurement of field excitation at short-circuit and at the point R. The resulting difference in Potier reactance is 0.3 ohm. The influence of these errors is larger on the values obtained from the partially saturated regions of the test characteristics (below 140 volts on the open-circuit characteristic in Fig.5.3(b)). Hence, values of Potier reactance in this region are not shown in Figs. 5.5. and 5.6. The significance of graphs marked 'd' in the two figures is explained in a later section.

GRAPHS a, b AND C — POTIER REACTANCES DERIVED FROM THE OPEN-CIRCUIT CHARACTERISTIC AND CORRESPONDING ZERO POWER FACTOR CHARACTERISTICS IN FIGS. 5·2 AND 5·3. THE REACTANCES IN FIGS. 5·5 AND 5·6 ARE PLOTTED AS FUNCTIONS OF THE OPEN-CIRCUIT VOLTAGES DENOTED BY THE VERTICES OF THE POTIER TRIANGLES.

GRAPHS d — REACTANCE X_1 OF THE TEE CIRCUIT DETERMINED BY THE SELF-IMPEDANCE METHOD. THE REACTANCE IS SHOWN AS FUNCTION OF THE VOLTAGE ON THE EXPERIMENTAL CHARACTERISTICS IN FIGS. 5·11 AND 5·12.

THE VALUES OF n SHOWN ARE AVERAGE VALUES.

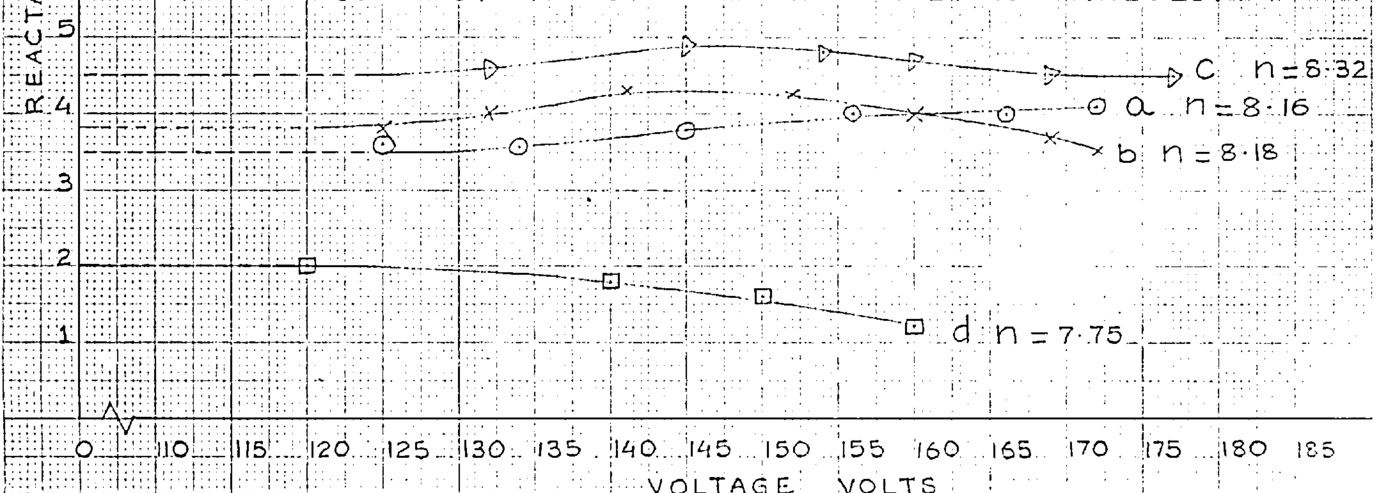

FIG. 5·5 POTIER REACTANCE OF MACHINE A

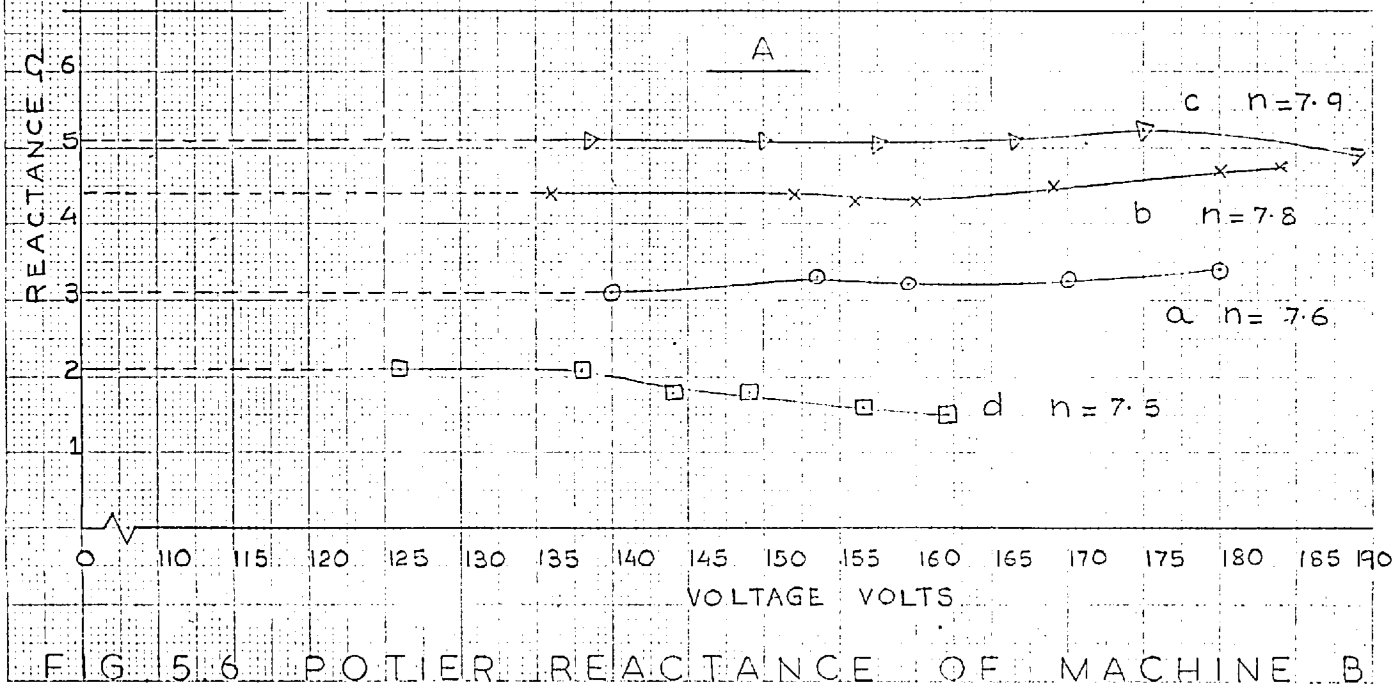

FIG. 5·6 POTIER REACTANCE OF MACHINE B

The significance of the variations of Potier reactance and the difference between the average values obtained from various graphs can be judged by expressing the changes in Potier reactance as corresponding changes in the field currents on load. This has been done by calculating the zero power factor characteristics from the open-circuit characteristics, employing the minimum values of Potier reactance and the corresponding turns-ratio.

The minimum Potier reactance and turns-ratio of machine A are 3.5 ohms and 8.16. The corresponding values for machine B are 3.3 ohms and 7.6. It is seen in the following section that the minimum values of Potier reactance of machines A and B are in reasonable agreement with the minimum Potier reactance of machine C.

The calculated characteristics are drawn dotted and marked (i) in Figs. 5.2b and 5.3b. The calculated characteristics do not differ significantly from the part of the test characteristics shown in Figs. 5.2a and 5.3a. As an illustration of this fact, the calculated characteristic (i) associated with graph c, Fig. 5.3a is shown in the figure. For operating voltages below 60 volts, characteristic (i) is practically coincident with the test characteristic. This coincidence would be expected in view of the fact that the magnetic circuit is unsaturated in this region of the test characteristics. The significance of the other characteristics drawn in Figs. 5.2b, 5.3a and 5.3b is explained in a later section.

From Fig.5.2b it can be seen that the variations of Potier reactance in graphs a and b, Fig. 5.5 correspond to very small changes in field current. The more pronounced difference between corresponding field currents in the calculated characteristic and experimental characteristic c in Figs. 5.2b and 5.3b indicates the presence of additional saturation in the machines when they are on load. The two factors that lead to this additional saturation on load are increase in the field leakage flux and changes in the distribution of air-gap flux density. Increase in the field leakage flux results in increased saturation of the poles; changes in the distribution of air-gap flux density lead to increased saturation of the poles, yoke and stator core.

The effects being considered are small. Therefore, a consistent quantitative indication of the influence of the two factors mentioned above can not be easily obtained. Only a general discussion of the influence of these factors is included in the following paragraphs.

The changes in the distribution of air-gap flux density are reflected in the waveform of the phase voltage. Fig.5.7(a) shows a record of the phase voltage of machine A operating on open-circuit. Fig. 5.7(b) shows the voltage when the machine, operating as a synchronous motor, draws a zero power factor current of 5.0 amp.. Figs. 5.8(a) and (b) are similar records of the phase voltage of machine B. All four records refer to an operating condition denoted by a line-to-line voltage of 220 volts.

The fundamental and harmonic components of the phase voltages were measured with the wave-analyser. These measurements showed the fifth and higher harmonic components to be small. Hence the distribution of air-gap flux density may be approximately represented by the expression

$$B = B_{m1} \sin \theta \pm A\, B_{m1} \sin 3\theta \qquad (5.1)$$

The positive and negative signs correspond to flat-topped and peaked distributions of air-gap flux density respectively. B_{m1} is the peak value of the fundamental air-gap flux density. A is the ratio of the third harmonic and fundamental components of flux density. θ is the electrical angle measured from the inter-polar axis.

The average flux density over a pole pitch becomes

$$\overline{B} = \frac{2}{\pi} B_{m1} \left(1 \pm \frac{A}{3}\right) \qquad (5.2)$$

Saturation of the magnetic circuit tends to make

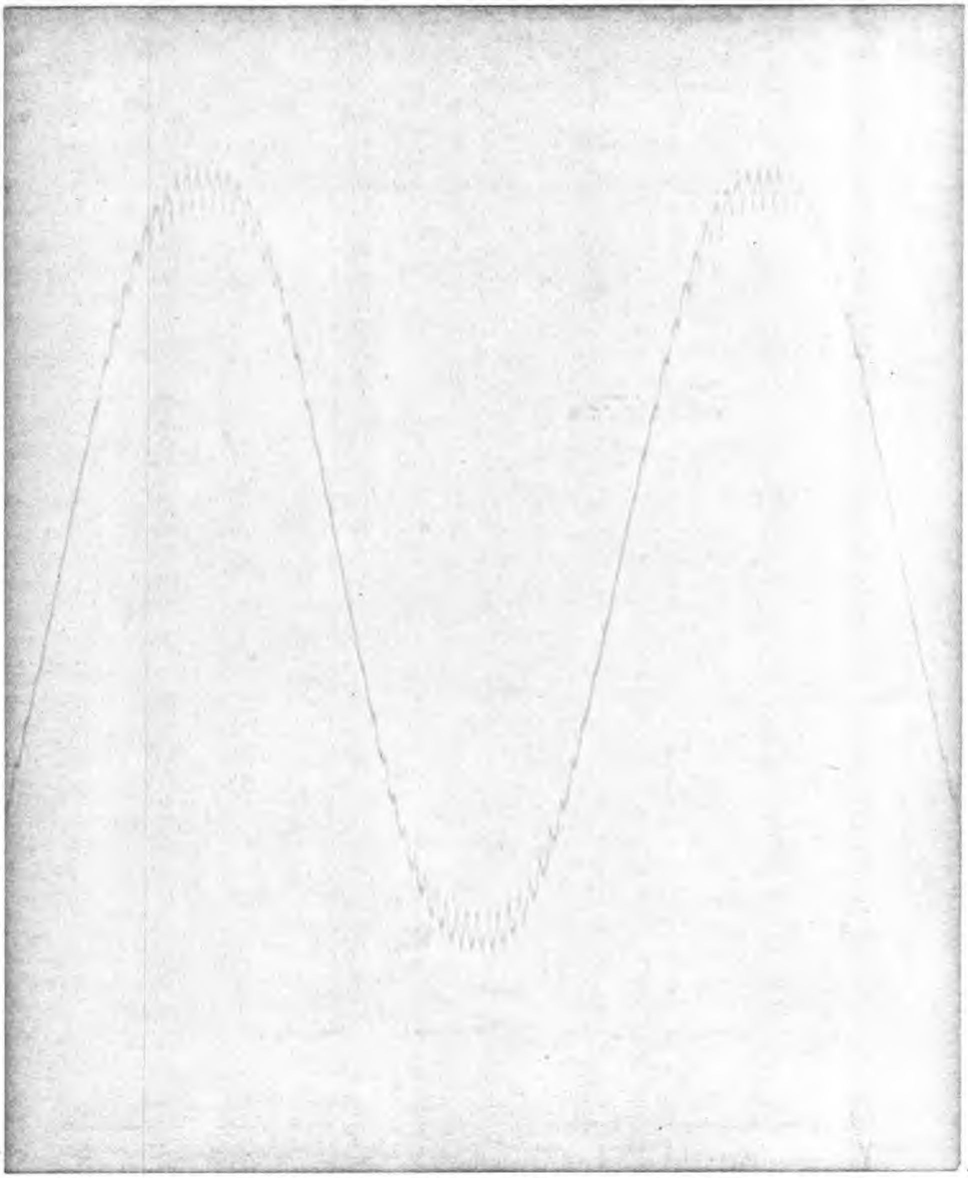

OPERATING LINE VOLTAGE = 220 V.

FIG. 5.7 a PHASE VOLTAGE OF MACHINE A ON OPEN-CIRCUIT

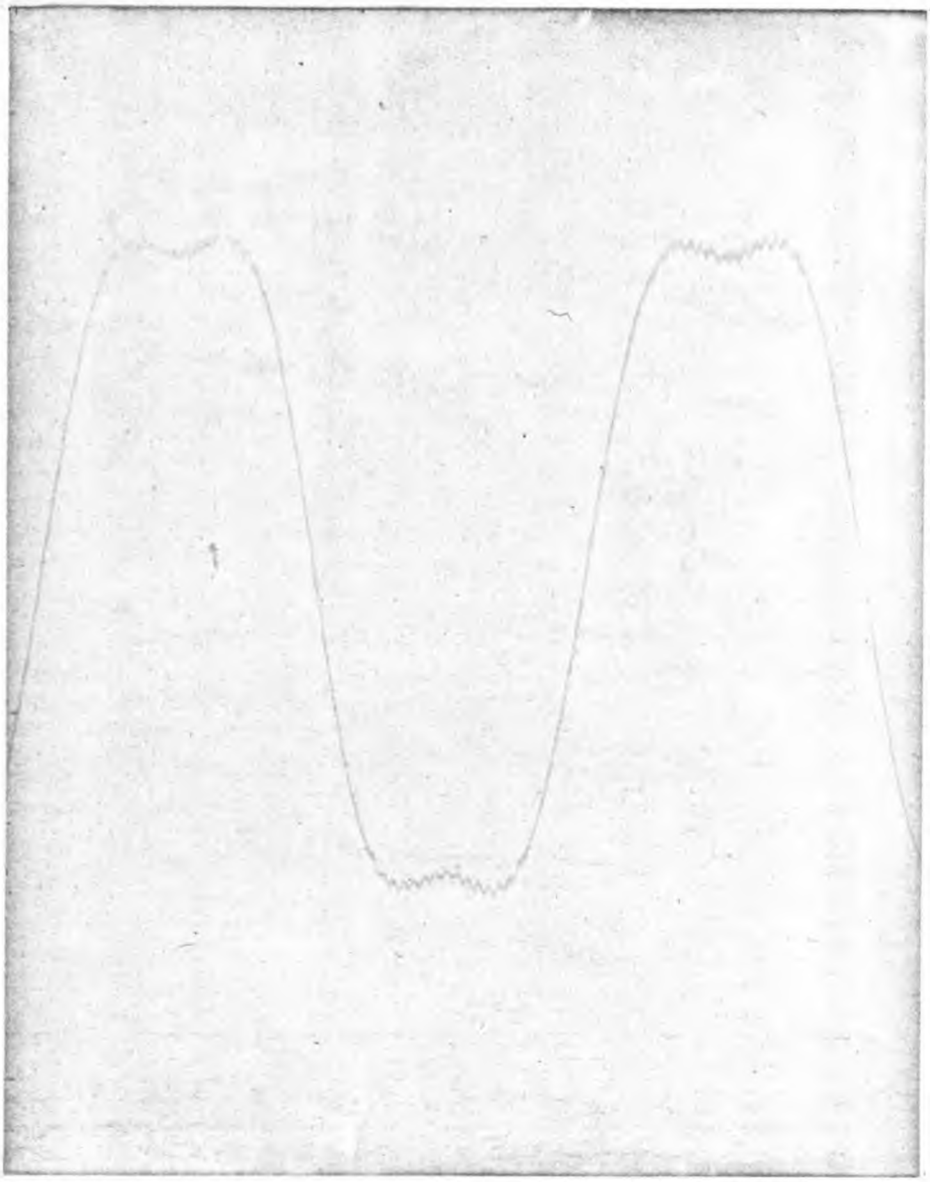

OPERATING LINE-TO-LINE VOLTAGE
= 220 VOLTS

LOAD CURRENT = 5 AMP

FIG. 5.7b PHASE VOLTAGE OF MACHINE A OPERATING AT ZERO POWER FACTOR

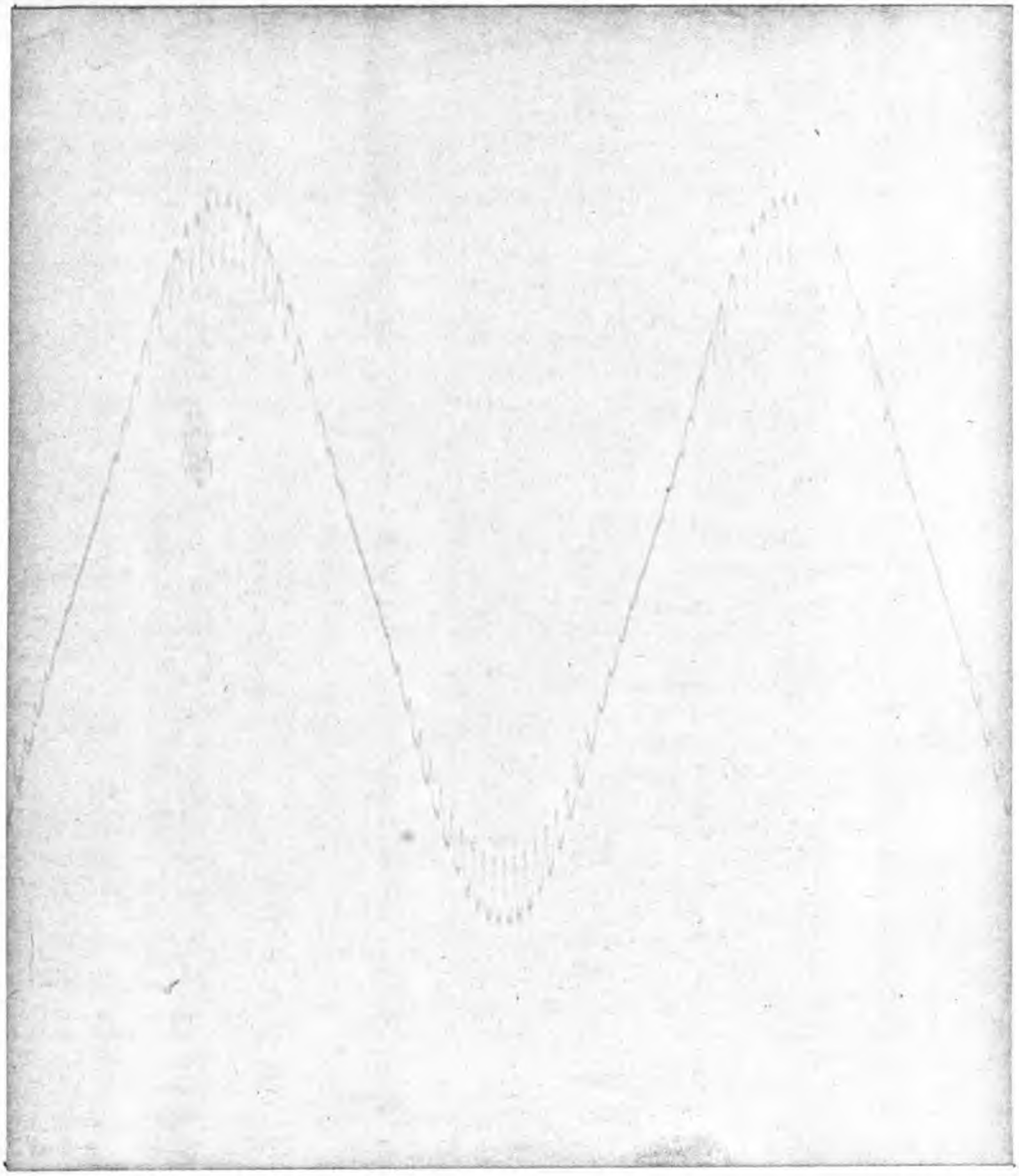

OPERATING LINE-TO-LINE VOLTAGE

= 220 VOLTS

FIG. 5.8 a PHASE VOLTAGE OF MACHINE B OPERATING ON OPEN-CIRCUIT

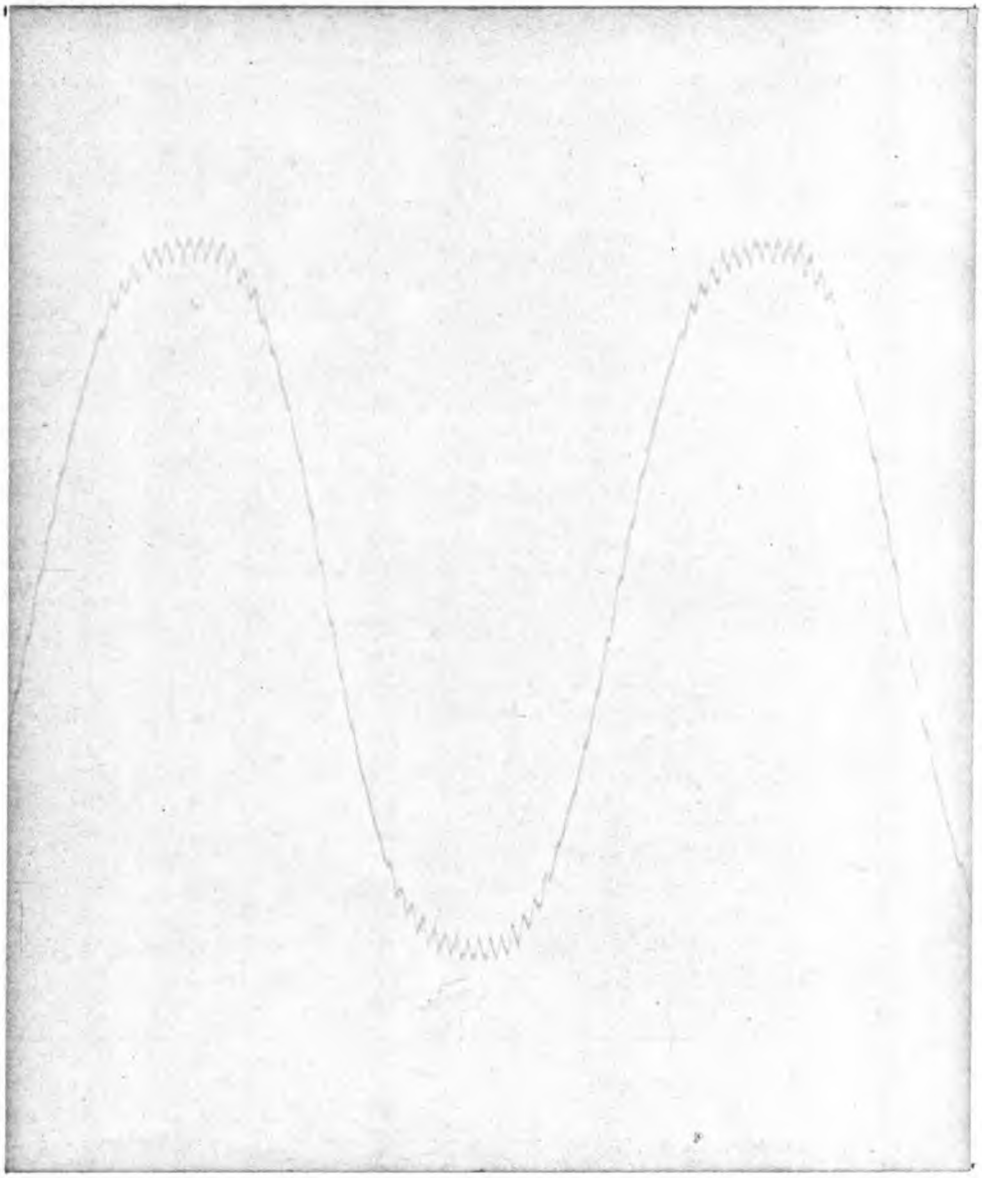

OPERATING LINE-TO-LINE VOLTAGE

= 220 VOLTS

LOAD CURRENT= 5 AMP

FIG. 5.8 b PHASE VOLTAGE OF MACHINE B OPERATING AT ZERO POWER FACTOR the distribution of flux-density flat-topped. Therefore, if the poles are so shaped as to produce a peaked distribution of air-gap flux density when the magnetic circuit is unsaturated, the proportion of the third harmonic component of open-circuit phase voltage will at first diminish on saturation of the magnetic circuit. On the other hand, with poles so shaped as to produce a flat-topped distribution of flux density when the magnetic circuit is unsaturated, the proportion of the third harmonic phase voltage will increase on saturation. Such a check together with the visual indication provided by the waveforms of the open-circuit phase voltages showed the distributions of flux-density to be flat-topped in machine A and peaked in machine B. The distributions of air-gap flux density in both the machines when they are supplying load are clearly flat-topped.

Equation 5.1 describes the distribution of flux density at the armature surface. Nevertheless the average flux density $\overline{B}$ can be used as a measure of the total flux in the poles of a salient-pole machine operating on open-circuit. However, a part of the air-gap flux established by the fundamental armature m.m.f. does not link the field winding. Hence, the flux density $\overline{B}$ does not provide an exact indication of the flux in the poles of the machine operating on load. The ratios of pole-arc to pole-pitch of machines A and B are 0.91 and 0.97 respectively. These ratios are larger than those usually employed in practical salient-pole machines. An approximate flux plot showed that except for the flux contained within 5 electrical degrees of the inter-polar axis, all the flux established by the direct-axis armature m.m.f. (acting alone) of machine A links the field winding. The flux not linking the field winding of machine B would be of a similar order of magnitude. Therefore, the error involved in using $\overline{B}$ (equation 5.2) as a measure of the total flux in the pole systems of machines A and B is small.

The generated fundamental voltage is proportional to B_{m1}. Therefore, the ratio $\overline{B}/B_{m1}$ can be used to compare the total flux per pole under two operating conditions of the machines at which the generated fundamental voltages are equal. The quotient of the values of this ratio under the two operating conditions is an indication of the change in the total flux per pole. This quotient is denoted by K'.

Values of the ratio A in equation 5.1 were calculated from the measured fundamental and third harmonic components of phase voltage by using the following expression.

$$\frac{E_3}{E_1} = \frac{K_{w3}}{K_{w1}} \times \frac{B_{m3}}{B_{m1}} = \frac{K_{w3}}{K_{w1}} \times A$$

The minimum values of Potier reactance of machines A and B were used for calculating the fundamental generated voltage corresponding to a given voltage on the zero power factor characteristics. Based on the values of A, values of the ratio K' were calculated. K' is the ratio of the total flux per pole required to generate a given fundamental voltage on load and on open-circuit. The calculated values of K' are given in table 5.1 (p.167). The distribution of air-gap flux density alters considerably as the terminal voltage of the machines on load increases from zero. However, since the iron is unsaturated in this region of the operating characteristics, these changes in the distribution of air-gap flux density do not influence the test characteristics or the Potier reactance. Hence only the values of K' referring to operating points located in the saturated regions of the test characteristics are included in Table 5.1.

The fact that the values of K' in Table 5.1 are greater than unity indicates that a larger flux per pole is required to generate a given fundamental voltage when the machines are supplying load than when they are on open-circuit. The increase in the total flux per pole becomes more pronounced as the load current is increased.

Table 5.1

Values of ratio K' in machines A and B

Generated Phase Voltage volts.	Machine B Load current in amp			Machine A Load current in amp	
	3.0	5.0	7.0	5.0	7.0
93.5	1.08	1.15	1.21	1.10	1.14
107.5	1.08	1.13	1.18	1.08	1.12
145.0	1.03	1.065	1.10	1.05	1.075
155.0	1.02	1.05	1.07	1.045	1.07
170.5	1.02	1.03	1.05	1.04	1.03

The reduction in ratio K' with increasing generated voltage indicates that the distribution of air-gap flux density in the machines on load gradually approaches the distribution that exists when they are on open-circuit. The additional field current required to secure a specified increase in the fundamental generated voltage progressively increases with saturation of the magnetic circuit. Therefore, the above decrease in K' does not signify a correspondingly smaller difference between the field currents required to generate a given fundamental voltage under the two operating conditions of the machines. Thus, in spite of the decrease in K', the experimental and calculated zero power factor characteristics could progressively diverge as shown in graph c, Fig. 5.2b or graphs b and c, Fig. 5.3b.

From equation 5.1, the flux density at the polar axis is $B_{m1}\ (1 \mp A)$. This flux density is a measure of the saturation of the stator teeth located at a given instant along the polar-axis. The symbol A' denotes the ratio of the flux densities at the polar axis under two operating conditions of the machines at which B_{m1} has the same value (i.e. same fundamental generated voltage). Values of A' have been plotted in Fig. 5.9 as a function of the fundamental generated voltage of machine B. The values shown relate the flux densities at the polar

A′ IS THE RATIO OF THE AIR-GAP FLUX DENSITIES AT THE POLAR AXIS UNDER TWO OPERATING CONDITIONS AT WHICH THE FUNDAMENTAL GENERATED VOLTAGES ARE THE SAME. THE VALUES SHOWN ARE THE RATIOS OF THE FLUX DENSITIES IN MACHINE B WHEN THE MACHINE IS ON OPEN-CIRCUIT AND WHEN IT SUPPLIES A ZERO POWER FACTOR LOAD CURRENT OF 7 AMP.

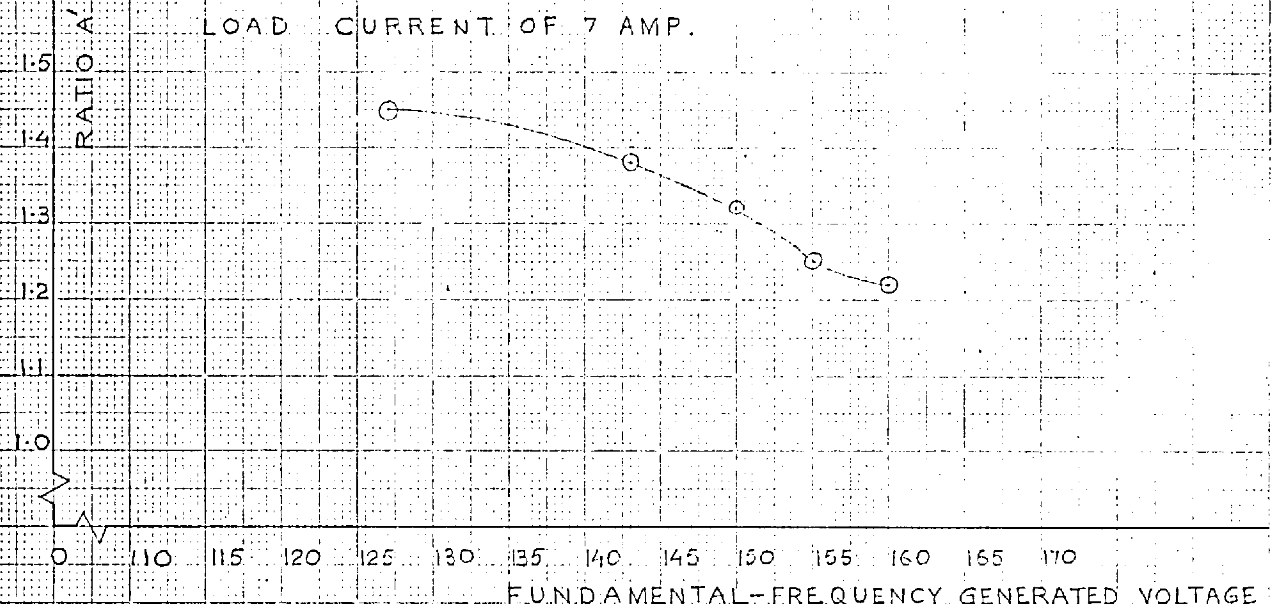

FIG. 5.9 RATIO A′ OF MACHINE B

axis of machine B operating on open-circuit to the flux densities when it is supplying a load current of 7.0 amp. Values of A' for fundamental generated voltages at which the machine is unsaturated are not shown in Fig. 5.9. The figure shows that the operating flux density when the machine is on open-circuit is on an average 1.3 times as large as the corresponding flux density when the machine is supplying load. The reduced flux density on load signifies reduced saturation of the stator teeth located along the polar-axis. The m.m.f. required by these teeth would be correspondingly smaller.

If the increase in m.m.f. due to increased saturation of the poles, yoke, and the stator core were less than the decrease due to reduced saturation of the teeth, the experimental zero power factor characteristics would lie to the left of calculated characteristics (i). The actual disposition of the experimental and calculated characteristics in Fig. 5.3(b) thus indicates that the increase in field m.m.f. predominates.

A part of the increased saturation of the poles occurs on account of the increase in field leakage flux on load. An approximate indication of this increase is obtained by ignoring the changes in field m.m.f. corresponding to the changes in the distribution of air-gap flux density discussed above. The increase in field leakage flux is then equal to the leakage flux associated with the component of field m.m.f. equivalent to the armature-reaction m.m.f. This flux is represented by the voltage drop across the referred field leakage reactance caused by the load current. The referred field leakage reactances of the machines have been approximately calculated from measured transient reactances in section 5.6.1. The values obtained are 2.4 ohms and 3.37 ohms for machines A and B respectively. The voltage drop across the referred reactance of machine B due to a load current of 7.0 amp is 23 volts. This voltage drop forms about 12 per cent of the maximum voltage on the open-circuit characteristic (Fig.5.3 (b)). The increase in field leakage flux on load thus forms 12 per cent of the main flux. This increase compares with an increase of 7 per cent in the main flux due to changes in the distribution of air-gap flux density.

The influence of saturation due to field leakage flux on the test characteristics is similar to the influence of changes in the distribution of air-gap flux density discussed above. Saturation due to field leakage flux is taken into account by representing the machines by the equivalent circuit of Fig. 2.8, or, more approximately, by the Pi circuit.

Comparison of the intercepts between characteristics (i) and experimental characteristics b and c shows that additional saturation on load is less pronounced in machine A. The smaller referred field leakage reactance of the machine indicates that, for the same load current, additional saturation on load due to field leakage flux is smaller in machine A. Further, a comparison of the values of K' in Table 5.1 shows that changes in the distribution of air-gap flux density are also slightly smaller in machine A. In addition, it is possible that the magnetisation characteristics of the two rotors are slightly different, so that the increase in flux corresponds to different increments in field m.m.f. in the two machines.

5.4.2. Potier reactance of machine C.

Graphs a, b and c in Fig. 5.10 show the Potier reactance of machine C determined from the test characteristics of Figs. 5.4(a) and (b). Unlike the graphs in Figs. 5.5 and 5.6, all three graphs in Fig.5.10 yield similar values of Potier reactance for voltages above 140 volts.

The characteristic drawn dotted in Fig.5.4(b) is calculated from the open-circuit characteristic by employing the minimum Potier reactance of 3.7 ohms and

THE POTIER REACTANCES ARE DERIVED FROM THE TEST CHARACTERISTICS IN FIGS. 5·4 a AND b. THE LETTERS EMPLOYED TO DENOTE THE GRAPHS DRAWN BELOW CORRESPOND TO THOSE IN FIGS. 5·4 a AND b. THE REACTANCES ARE SHOWN AS FUNCTIONS OF THE OPEN-CIRCUIT VOLTAGES DENOTED BY THE VERTICES OF THE POTIER TRIANGLES.

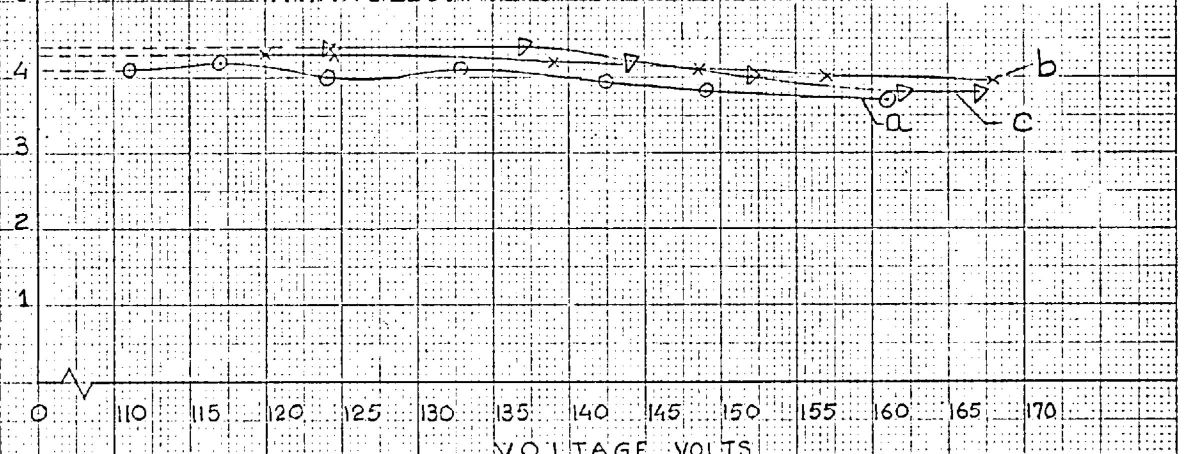

FIG 5.10 POTIER REACTANCE OF MACHINE C

the corresponding turns-ratio of 6.34. Comparison of this characteristic and experimental characteristic c shows that the variations of Potier reactance in graph c, Fig. 5.10 correspond to a maximum increase of 1 per cent in the field current required on load. The small magnitude of this increase leads to the conclusion that additional saturation due to field leakage flux and changes in the distribution of air-gap flux density is very small in the machine.

The minimum Potier reactance of 3.7 ohms of machine C compares with a reactance of 3.5 ohms of machine A. The agreement of these two values with the minimum Potier reactance (3.3 ohms) of machine B can be regarded as satisfactory considering that the possible error in Potier reactance is 0.3 ohm. An additional factor that causes some difference in the minimum values of Potier reactance is the dependence of the differential leakage component of armature reactance on the rotor employed.

A check on the test results is provided by the value of leakage reactance of machine C supplied by the manufacturer. This value of 3.5 ohms is in good agreement with the minimum Potier reactance determined from tests. Similar values of leakage reactances of machines A and B have not been supplied by the manufacturer.

5.5. Self-impedance characteristics of the machines.

The self-impedance characteristics of the machines were determined by driving the rotor at synchronous speed and exciting the stator from a three-phase supply. The rotor was maintained in the same position relative to the fundamental armature m.m.f. as when the machine was synchronised. The control of the position of the rotor was achieved by altering the armature current of the d.c. motor. The above precaution was taken to ensure that the fundamental armature m.m.f. acted along the direct-axis.

The three line currents were not balanced. The maximum difference between the currents was 2 per cent. This difference primarily arose due to unequal magnitudes of the phase voltages supplied by the "Variac" auto-transformer. A part of this difference can also be attributed to lack of perfect symmetry of the three phases of the machine. Average values of currents and voltages have been employed for drawing the characteristics shown in Figs. 5.11, 5.12 and 5.13.

The direct-axis synchronous reactance X_d is the sum of reactances X_m and X_1 of the Tee circuit drawn in Fig.5.11. The unsaturated value of this reactance can be calculated by dividing the open-circuit voltage generated by a given field current by the short-circuit

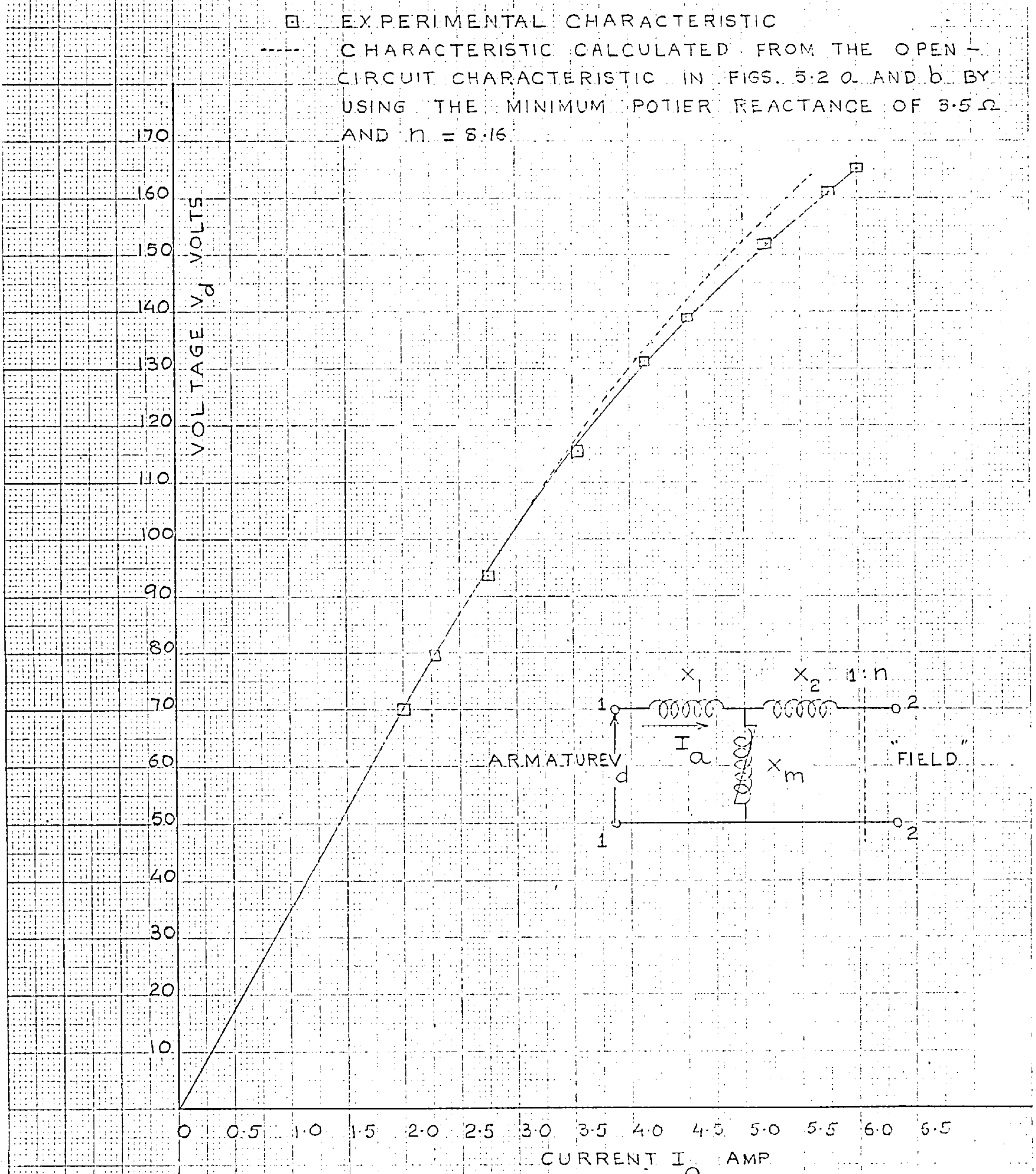

FIG. 5.11 SELF-IMPEDANCE CHARACTERISTI[C] OF MACHINE A

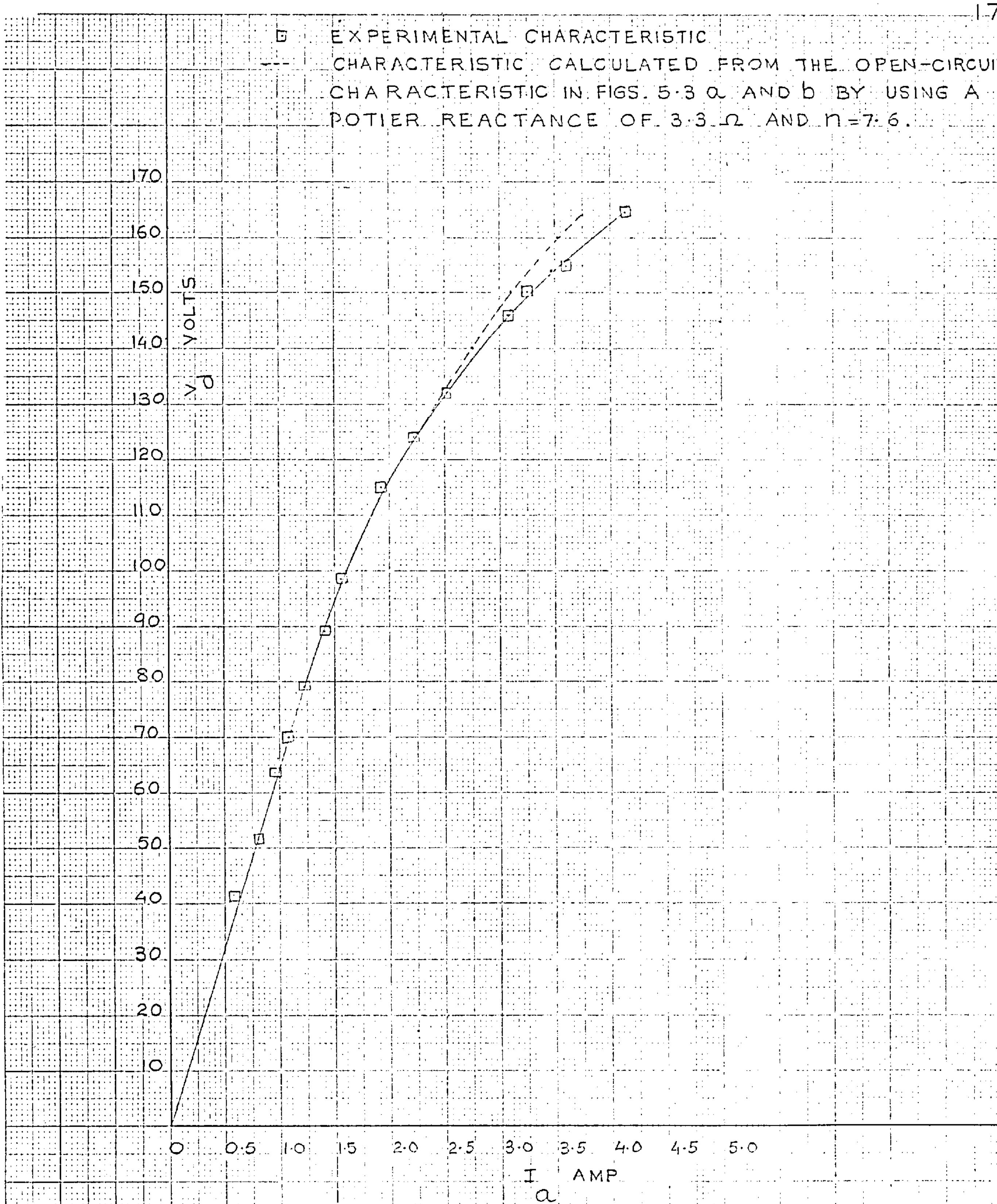

FIG. 5.12 SELF-IMPEDANCE CHARACTERISTIC OF MACHINE B

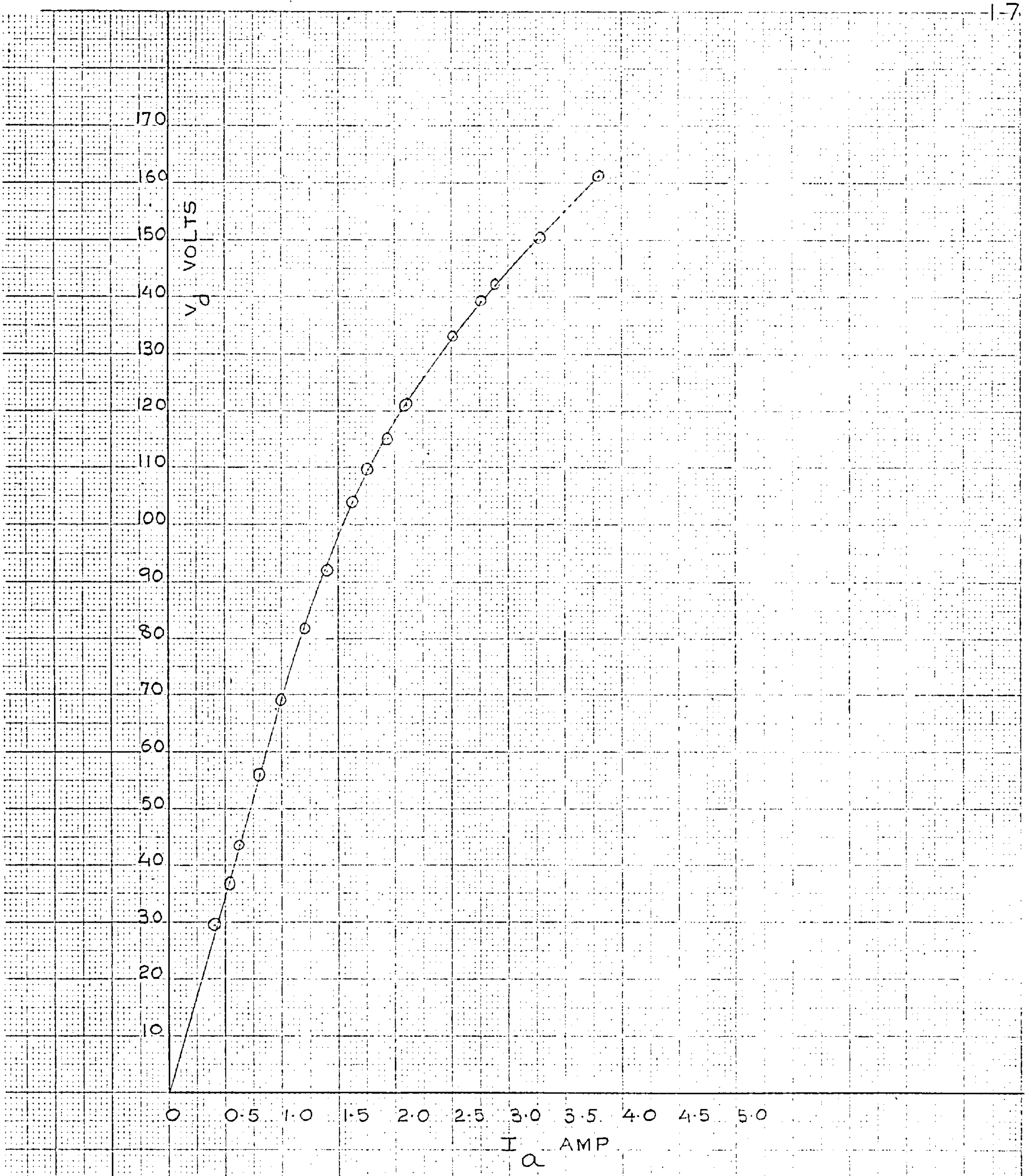

FIG. 5.13 SELF-IMPEDANCE CHARACTERISTIC OF MACHINE C

armature current circulated by the same field current. (Ref. 8, p. 434). This calculated reactance is more reliable than the reactance obtained from the slope of the linear part of the self-impedance characteristics.

A modification of the self-impedance method suggested in chapter 3 simplifies the determination of the turns-ratio by this method. Referring to Fig. 4.8 (p.106), the coordinates of corresponding points P and Q are related as follows.

$$\frac{(X_{uns} - X_m)}{\frac{(X_{uns} - X_m)}{n}} = \frac{I_2'}{I_1}$$

$$\text{or } (X_{uns} - X_m)\, I_1 = \frac{(X_{uns} - X_m)}{n} I_2'$$

Since $I_2' = nI_1$, it follows that the products of the coordinates of points P and Q are equal. Similar products of the coordinates are plotted against the respective currents in Fig. 5.14. The turns-ratio is obtained from Fig. 5.14 by calculating the ratio of the currents at corresponding points, like A and B, on the two graphs. Both these points have the same ordinate.

The graphs drawn in Fig. 5.14 refer to machine A. The values shown in these graphs have been calculated from the open-circuit characteristics in Figs.5.2(a) and (b) and the self-impedance characteristics in Fig. 5.11. The symbols I_a and I_f respectively denote the armature current in the self-impedance test and the field current in the open-circuit test. For convenience, the values of $n(X_{uns} - X_m) I_f$ shown in Fig. 5.14 are plotted against $5I_f$ and not against I_f. However, the values of turns-ratio marked on the figure are the ratios of the armature and equivalent field currents. Figs. 5.15 and 5.16 show similar sets of graphs for machines B and C.

5.5.1. Reactance X_l of machines A and B

To facilitate reference to the reactance in the text, the symbol X_l has been used in the following paragraphs to denote the armature leakage reactance determined by the self-impedance method. As originally defined in chapter 3, this symbol would also denote the Potier reactance and the "true" armature leakage reactance.

Average values of turns-ratio obtained from Figs. 5.14 and 5.15 are respectively equal to 7.75 and 7.5. The calculated values of reactance X_l of machines A and B are plotted in graphs d, Figs. 5.5 and 5.6. These values are plotted as functions of the voltages shown on the self-impedance characteristics of the two machines. Some of the reasons for the difference between the minimum Potier reactances of the two machines and the

GRAPH a' — $n(X_{UNS} - X_m) I_f$ CALCULATED FROM THE OPEN-CIRCUIT CHARACTERISTIC IN FIGS. 5·2 a AND b. THE PRODUCT IS PLOTTED AGAINST CURRENT $5I_f$.

GRAPH a — $(X_{UNS} - X_m) I_a$ CALCULATED FROM THE TEST CHARACTERISTIC IN FIG 5·11. THE PRODUCT IS PLOTTED AGAINST CURRENT I_a.

THE VALUES OF n MARKED BELOW ARE THE RATIOS OF CURRENTS I_a AND I_f GIVEN BY CORRESPONDING POINTS LIKE A AND B.

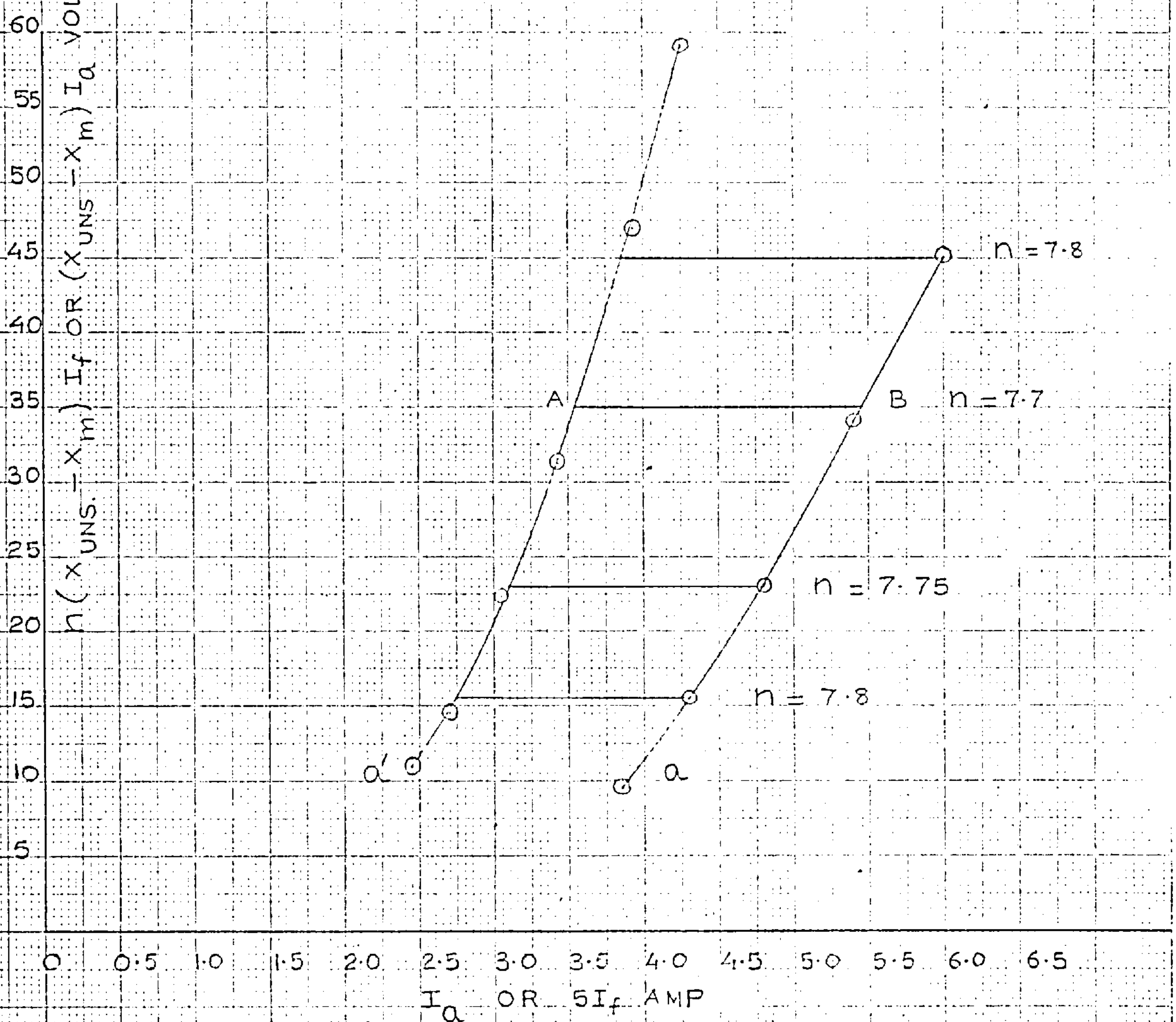

FIG. 5.14 DETERMINATION OF THE TURNS-RATIO n OF THE IDEAL TRANSFORMER IN THE EQUIVALENT TEE CIRCUIT OF MACHINE A

GRAPH a' — $n(x_{UNS} - x_m) I_f$ DETERMINED FROM THE OPEN-CIRCUIT CHARACTERISTIC IN FIGS. 5·3 a AND b. THE PRODUCT IS PLOTTED AGAINST $5 I_f$.
GRAPH a — THE PRODUCT $(x_{UNS} - x_m) I_a$ DETERMINED FROM THE TEST CHARACTERISTIC IN FIG. 5·12. THE PRODUCT IS PLOTTED AGAINST THE CURRENT I_a.
THE VALUES OF n SHOWN BELOW ARE THE RATIOS OF CURRENTS I_a AND I_f GIVEN BY CORRESPONDING POINTS SUCH AS A AND B.

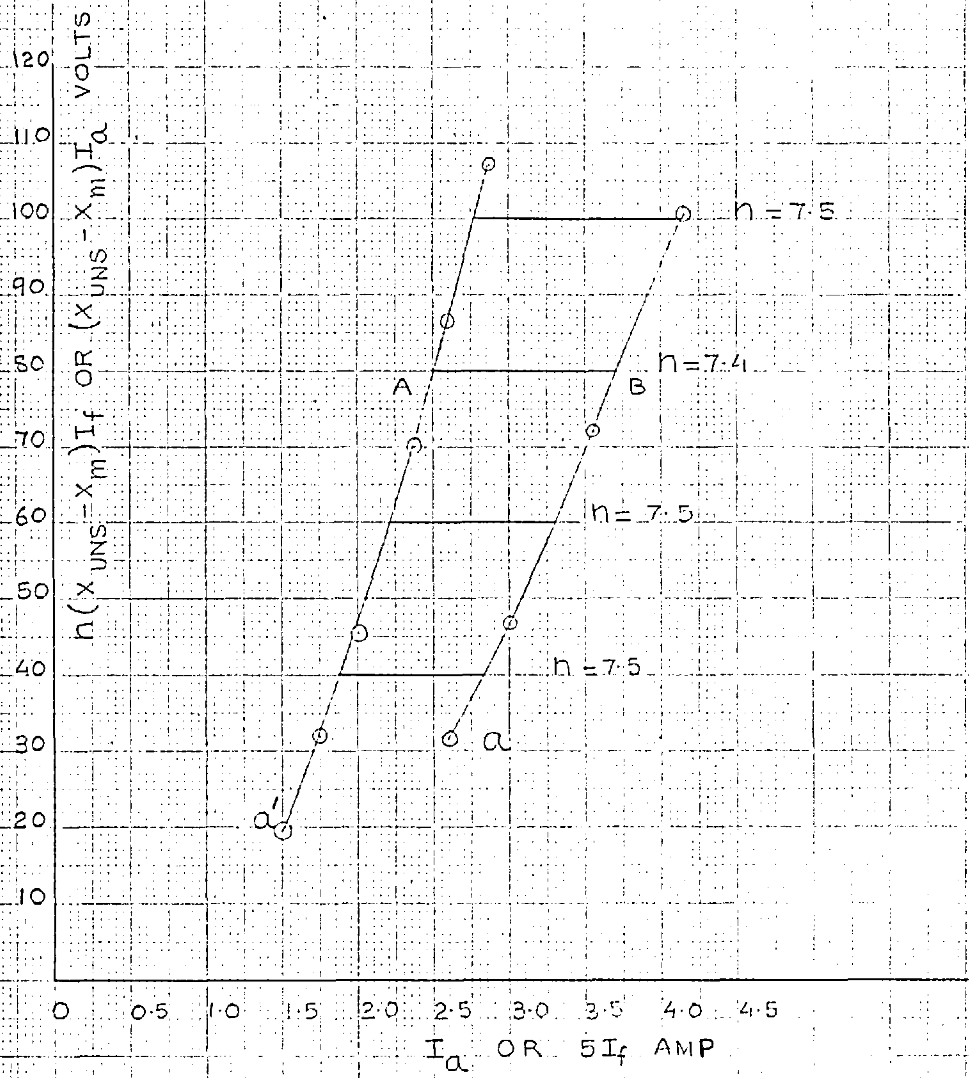

FIG. 5.15 DETERMINATION OF THE TURNS-RATIO n OF THE IDEAL TRANSFORMER IN THE EQUIVALENT TEE CIRCUIT OF MACHINE B

GRAPHS a' AND b' — THE PRODUCT $n(x_{UNS} - x_m) I_f$ DETERMINED FROM THE OPEN-CIRCUIT CHARACTERISTIC IN FIGS. 5·4 a AND b. THE PRODUCTS ARE PLOTTED AGAINST CURRENT $5I_f$.

GRAPHS a AND b — THE PRODUCT $(x_{UNS} - x_m) I_a$ DERIVED FROM THE CHARACTERISTIC IN FIG. 5·13. THE PRODUCT IS SHOWN AS FUNCTION OF I_a.

GRAPHS a AND a' ARE CALCULATED BY USING $nx_{UNS} = 412{\cdot}5\,\Omega$ AND $x_d = 68{\cdot}75\,\Omega$, WHILE THE CORRESPONDING VALUES FOR b AND b' ARE $422{\cdot}5\,\Omega$ AND $71\,\Omega$.

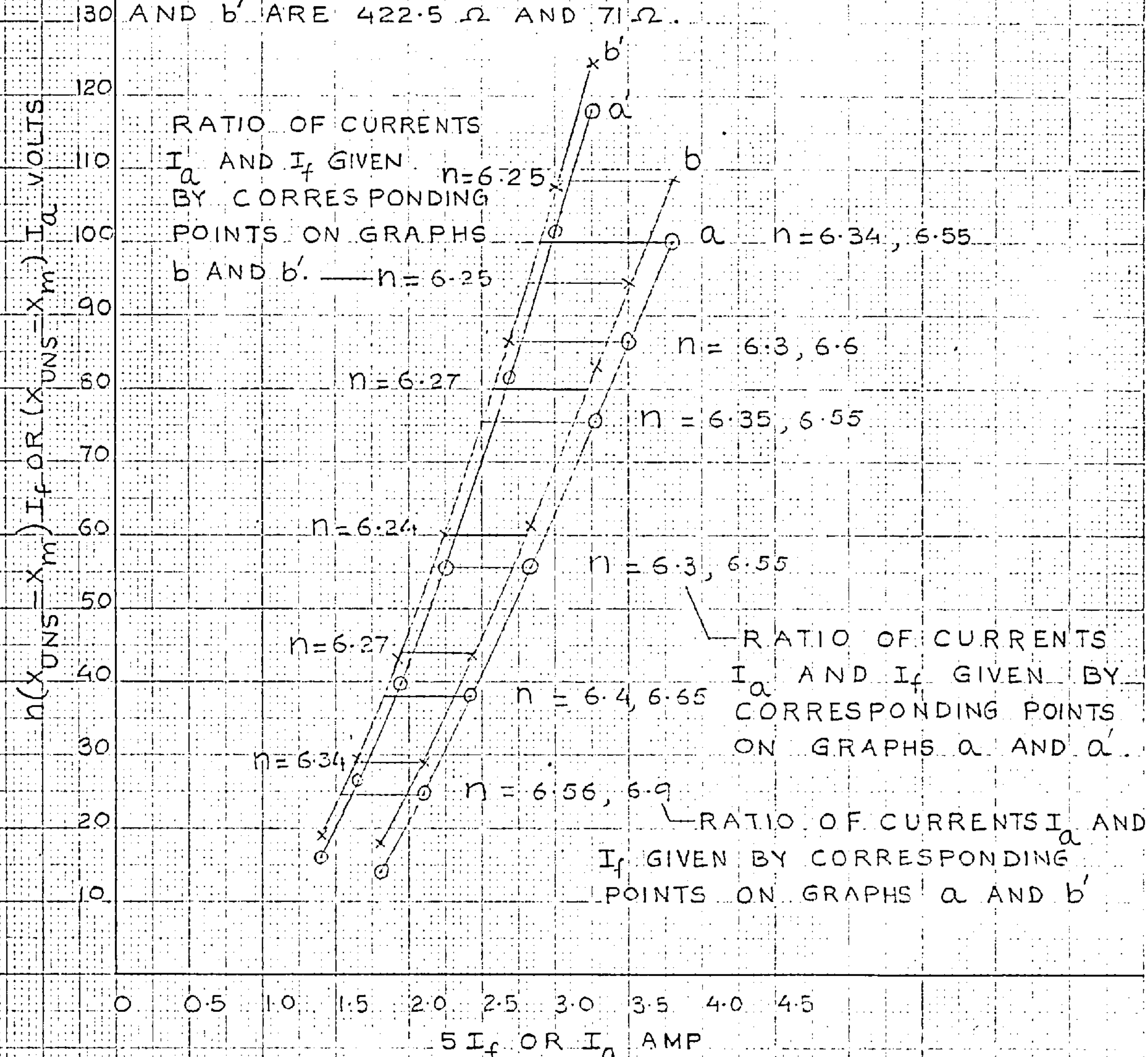

FIG 5.16 DETERMINATION OF THE TURNS-RATIO OF THE IDEAL TRANSFORMER IN THE EQUIVALENT TEE CIRCUIT OF MACHINE C

values of reactance X_1 are stated in the following paragraphs.

A part of the difference between the minimum Potier reactance and X_1 is due to experimental errors. Comments on the accuracy of the self-impedance method are included in the following section. It is possible that during the self-impedance test the axis of the fundamental armature-reaction m.m.f. was displaced from the polar-axis of the machine. However, in view of the care taken to properly locate the axis of the armature-reaction m.m.f., any displacement in the axis would be only of the order of 4 degrees.

Due to the non-uniform length of the air-gap, a peaked distribution of air-gap flux density is established during the self-impedance test. Figs. 5.17(a) and (b) show the corresponding waveforms of the phase voltages of machines A and B. These waveforms refer to an operating condition defined by a line-to-line voltage of 220 volts. These waveforms may be compared with the waveforms of the phase voltages of the two machines on open-circuit. The latter waveforms are shown in Figs. 5.7(a) and 5.8(a).

The distributions of air-gap flux density at corresponding operating points on the open-circuit and self-impedance characteristics of the two machines can

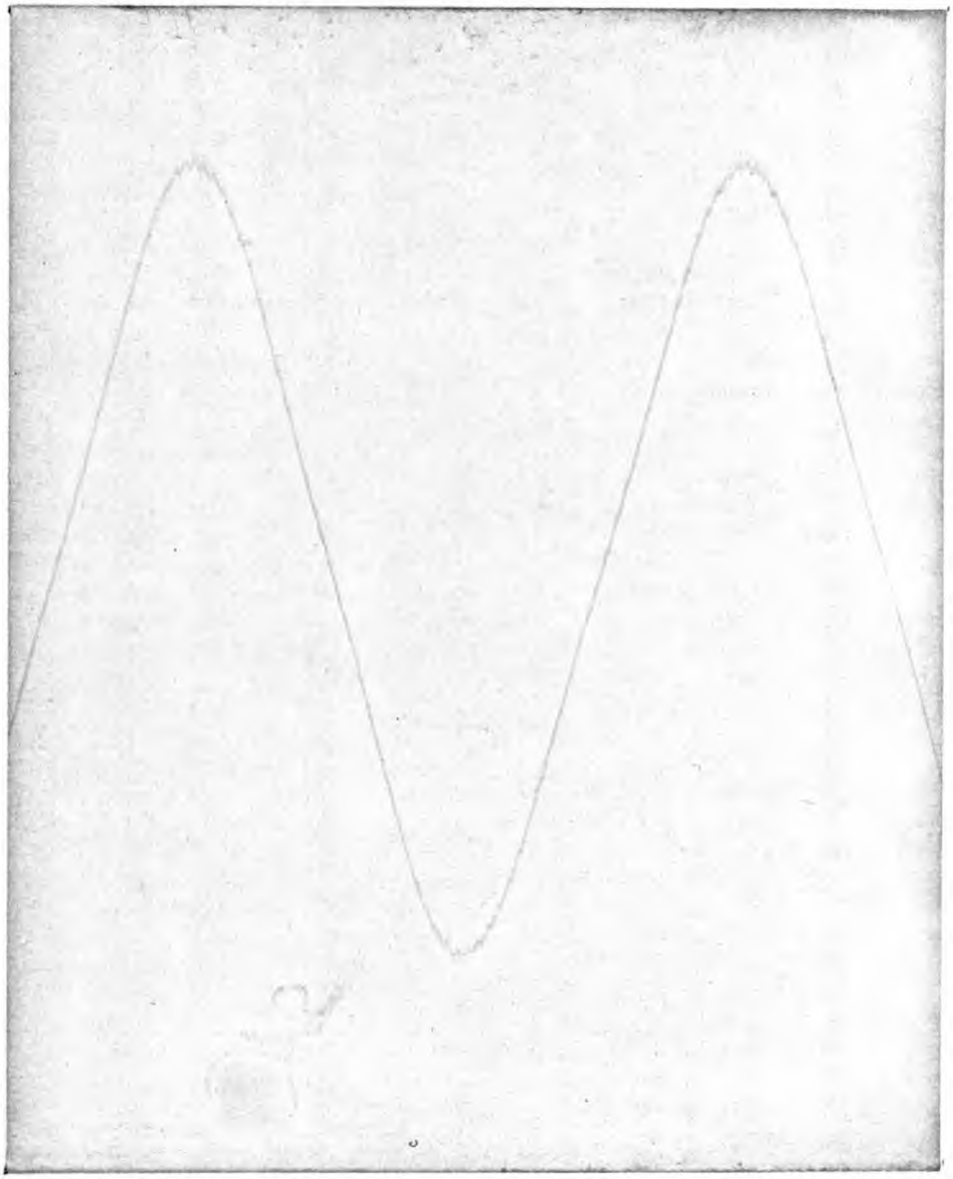

OPERATING LINE-TO-LINE
VOLTAGE = 220 VOLTS

FIG. 5.17 a PHASE VOLTAGE OF MACHINE A DURING THE SELF-IMPEDANCE TEST

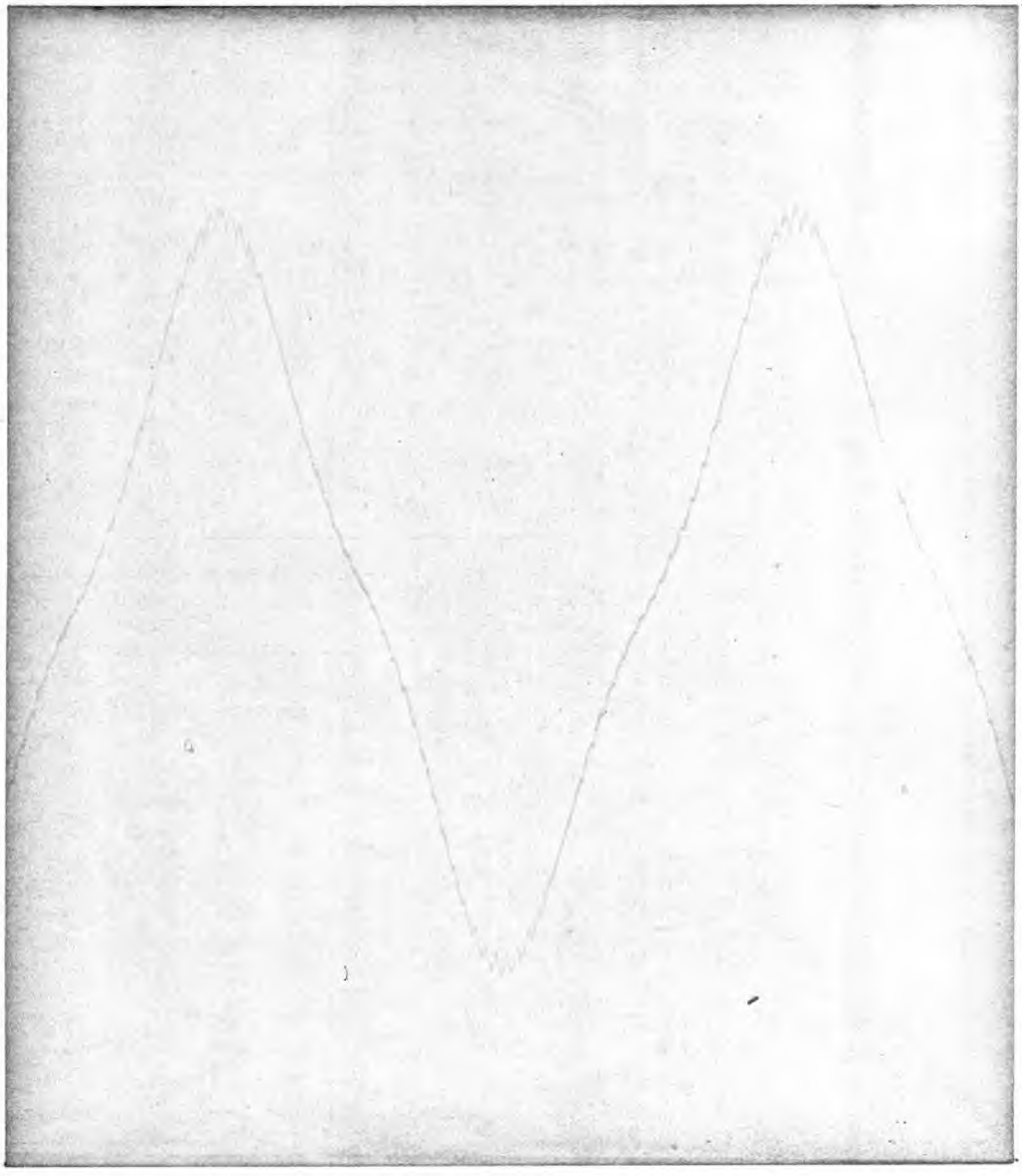

OPERATING LINE-TO-LINE VOLTAGE
= 220 VOLTS

FIG.5.17b PHASE VOLTAGE OF MACHINE B DURING THE SELF-IMPEDANCE TEST be compared in the following manner. (The "corresponding" points are points on the two characteristics at which the fundamental generated voltages are equal). Owing to a peaked distribution of air-gap flux density, the flux density at the polar axis is higher during self-impedance tests on the machines. Therefore, for the same fundamental flux, the teeth located along the polar-axis operate at a higher flux density during the self-impedance tests than during open-circuit tests on the machines. Consequently if these teeth are saturated, a larger m.m.f. is required to establish the same fundamental flux during self-impedance tests on the machines. On the other hand, the average flux density over a pole-pitch is smaller when the distribution of flux density is peaked than when the distribution is flat-topped. The total flux per pole during self-impedance tests on the machines is then smaller than the flux at corresponding operating points on the open-circuit characteristics. The poles, yoke and stator core are therefore saturated to a lesser extent during the self-impedance tests. However, the m.m.f. required to generate a given fundamental voltage during the self-impedance test is larger than that required to generate the same voltage on open-circuit. This fact can be seen by a comparison of the experimental self-impedance characteristics with the characteristics drawn dotted in Figs. 5.11 and 5.12. The latter have been calculated from the open-circuit characteristics by using the minimum values of Potier reactance and the corresponding turns-ratio. The maximum difference between corresponding currents in the experimental and calculated characteristics is 6.5 per cent in machine A and 9.6 per cent in machine B. As stated before, the currents in the three phases differed by about 2 per cent during the self-impedance tests on the machines. The three line voltages were also not exactly equal. Both these factors could cause the experimental characteristics to be in error by about half the percentage values quoted above.

5.5.2. Reactance X_1 of machine C.

Two sets of graphs a, a' and b, b' are drawn in Fig. 5.16 to assess the influence of errors in the measurement of the field current at short-circuit and the slope nX_{uns} of the open-circuit characteristics. Both these factors influence the unsaturated value of X_d. Graphs a and a' are obtained from calculations based on a slope of 412.5 ohms and the corresponding value of X_d = 68.75 ohms. Graphs b and b' are calculated by using a slope of 422.5 ohms and a reactance X_d of 71 ohms. The difference in slopes corresponds to an error of 2.5 per cent in the measurement of open-circuit voltages. The difference between the two values of X_d corresponds to an error of 3 per cent in the measurement of the field current at short-circuit.

The average values of n from graphs a-a', b-b' and a-b' are 6.35, 6.25 and 6.6 respectively. The corresponding values of reactance X_l are shown in graphs a, b and c, Fig. 5.18. Values of X_l below 130 volts on the self-impedance characteristics are subject to larger errors. Hence these values are not shown in Fig. 5.18. As would be expected, the accuracy of the method is very poor for voltages below 145 volts on the self-impedance characteristic. The corresponding voltages on the open-circuit characteristic are below 135 volts. However, consistent values of reactance X_l are obtained from the region above 145 volts. A comparison of graphs b and c in Fig. 5.18 shows the possible error in these values of X_l to be about 13 per cent. This figure compares with a possible error of 7 per cent in the determination of Potier reactance.

Unlike the reactances of the two salient-pole machines, the agreement between Potier reactance and reactance X_l is reasonably good for machine C. This agreement again indicates that additional saturation of the cylindrical-rotor machine due to field leakage flux x — GRAPH a — REACTANCE X_1 CALCULATED BY EMPLOYING A TURNS-RATIO $n = 6{\cdot}35$.

⊙ — GRAPH b — REACTANCE X_1 CALCULATED BY EMPLOYING A TURNS-RATIO $n = 6{\cdot}25$.

⊡ — GRAPH C — REACTANCE X_1 CALCULATED BY EMPLOYING A TURNS-RATIO $n = 6{\cdot}6$. THE VALUE OF $6{\cdot}25\ \Omega$ IS BASED ON THE REACTANCES $nX_{UNS} = 412{\cdot}5\ \Omega$ AND X_d (UNS) $= 68{\cdot}75\ \Omega$. THE CORRESPONDING VALUE WITH $nX_{UNS} = 422{\cdot}5\ \Omega$ AND X_d (UNS) $= 71\ \Omega$ IS $7\ \Omega$.

THE REACTANCES ARE PLOTTED AS FUNCTIONS OF THE VOLTAGES GIVEN BY FIG. 5.13.

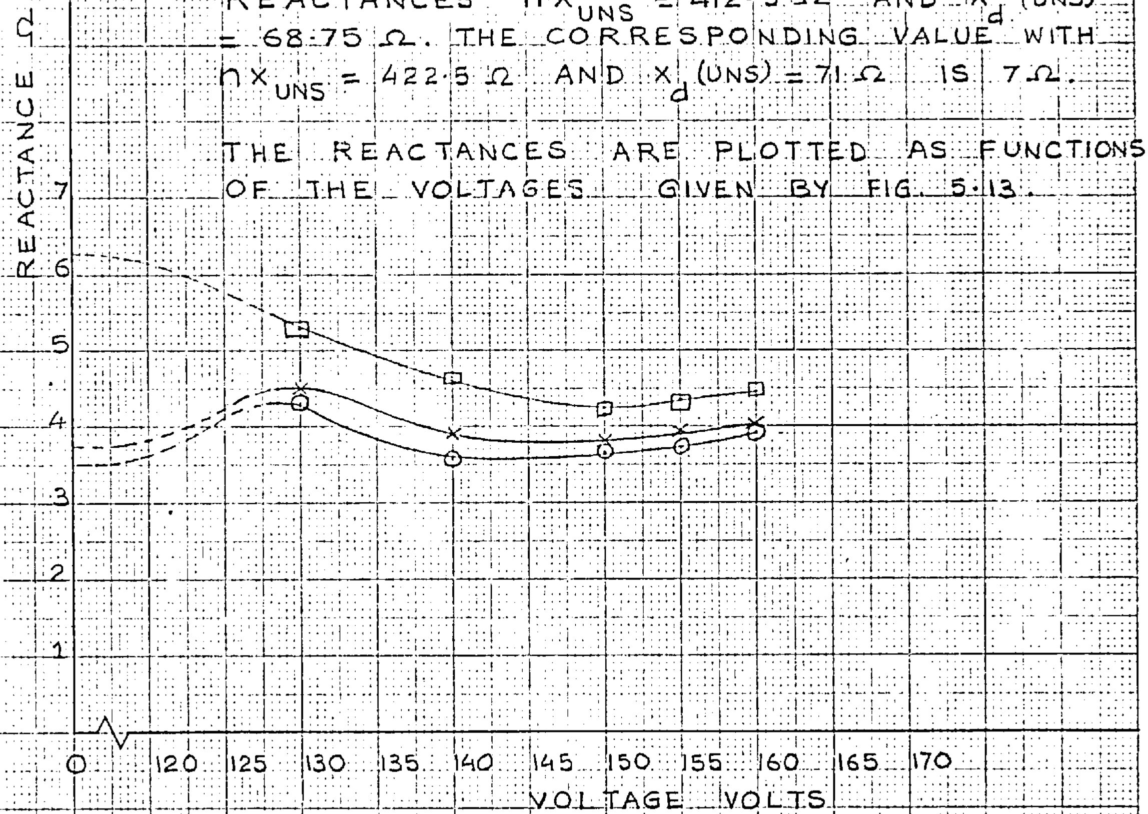

FIG. 5.18 REACTANCE X_1 OF MACHINE C

and changes in the distribution of air-gap flux density is small.

It may be pointed out that only one point on the self-impedance characteristic has to be determined to obtain a value of the reactance X_1. For accuracy this point must be located in the highly saturated region of the characteristic.

5.6. Equivalent Pi circuit of the machines

5.6.1. Evaluation of the parameters of the equivalent circuit.

The terminals 2-2 of the equivalent circuit drawn in Fig. 5.20*form the "field" terminals. The formulae derived in section 3.4.2. are based on the equivalent circuit of Fig. 3.4. (p. 81). Since n is defined as the ratio of equivalent armature and field currents, the aspect of the ideal transformer has been changed as is shown by a comparison of the two figures. This change is taken into account by replacing n by 1/n in eqns. 3.14, 3.15 and 3.16.

The reactances of the Pi circuit can be calculated by using the three equations referred to above. The ratio of the armature and field currents with the armature short-circuited, and the open-circuit transfer-impedance are obtained from the test characteristics in Figs. 5.2(a)

* P. 210

to 5.4 (a). The ratio of the armature and field currents with the field terminals short-circuited constitutes the third condition.

At first sight it appears possible to measure this ratio by performing a locked rotor test.[39] This test could not be performed due to the presence of damper windings on the rotors. As an alternative, the transient reactances of the three machines were obtained from sudden three-phase short-circuit tests.[39] The transient reactance is the reactance measured at the armature terminals with the field winding short-circuited. The unsaturated values of this reactance for the three machines are as follows.

Transient reactance of machine A : 7.6 ohms.

Transient reactance of machine B : 9.7 ohms.

Transient reactance of machine C : 6.0 ohms.

However, the use of transient reactance or other measurements made with the field winding short-circuited is not strictly valid for the reasons stated below. When the machines are unsaturated, their Tee and Pi circuit representations are equivalent to each other. The following remarks are therefore based on the Tee circuit representation of the machines. The parameters of the equivalent Pi circuits of the machines are determined by transformation of the respective Tee circuits.

Only the field leakage flux that exists in the iron and causes additional saturation is represented in the dynamic analogues from which the equivalent circuits of the machines are derived. However the field leakage flux which partly determines the field current during the locked-rotor test includes the overhang leakage flux existing entirely in air. This field leakage flux also partly determines the difference between the field currents during the transient and steady-state phases of the sudden three-phase short-circuit test. Ignoring for the present the influence of other factors, the referred field leakage reactance determined by either of the two tests would then be larger than the reactance corresponding to the leakage flux causing additional saturation of the rotor iron. In the case of a salient-pole machine, the length of the overhang of the field winding is small, and the overhang leakage flux forms only a small part of the total field leakage flux. The length of the overhang is comparatively large in the case of a cylindrical-rotor machine. In this type of machine, particularly in one having two poles, the overhang leakage flux could form a substantial part of the total field leakage flux. When the equivalent circuit of Fig. 2.12c (p 64) is linear, little error is involved in replacing it by the Tee circuit of Fig. 5.11. In Fig. 5.11, X_2 represents the referred field leakage reactance. Reactance X_3 of the Pi circuit, derived by transformation of Fig. 5.11, includes both the reactances X_1 and X_2. Consequently, the percentage difference between the values of X_2 evaluated by including the contribution of the field overhang leakage flux and excluding it is larger than that between the two corresponding values of X_3.

Thus, for the salient-pole machines, the influence of the field overhang leakage reactance on the parameters of the Pi circuit would be small. In the absence of other effects, these parameters could then be determined by the locked rotor test (performed with the damper winding removed) or by the sudden three-phase short-circuit test. However, allowance has also to be made for the effects of the different distributions of the armature and field windings and the non-uniform length of the air-gap. These factors cause the measured transient reactance to be larger than the reactance corresponding to the "actual" field leakage flux. Kilgore[40] has derived an expression for the transient reactance of a salient-pole machine. This expression involves the reactance X_{uns} and constants describing the distributions of air-gap flux density established by the field m.m.f. and the fundamental armature m.m.f., each acting alone. A similar method is employed below to determine the "actual" referred field leakage reactance X_2 of machine A. This method is based on constants evaluated by approximately representing the distributions of air-gap flux density by their fundamental and third harmonic components. These components of flux density are calculated from the measured fundamental and third harmonic components of phase voltage. The calculated constants describing the flux distribution in machine A are as follows. The symbols employed are adopted from reference 31.

Ratio of the peak fundamental and actual flux densities due to field m.m.f. $= A_1$	1.06
Ratio of the total flux to the fundamental flux per pole established by field m.m.f. $= K_\phi$	1.02
Ratio of the peak fundamental and actual flux densities due to fundamental direct-axis armature-reaction m.m.f. $= A_{d1}$	0.877
Ratio of the total flux to the fundamental flux per pole set up by the fundamental direct-axis armature-reaction m.m.f. $= K_1$	0.953

During the transient phase of the sudden short-circuit test the field and armature windings carry, in general, both fundamental-frequency alternating currents and direct currents. The a.c. in the armature corresponds to the d.c. in the field; the d.c. in the armature leads to a.c. in the field winding. There are additional components of current in the two windings due to such factors as the harmonic components of armature m.m.f. These components of current are usually very small. They are neglected in the present analysis. Only the fundamental component of the armature-reaction m.m.f. is considered in this analysis.

If the sudden short-circuit test is conducted with the test conditions so adjusted as to cause no saturation of the magnetic system, each of the components of current in the armature and field windings can be considered to act separately. The total flux linking either winding can be determined by superposing the fluxes due to individual components of current.

The interaction of the fluxes due to fundamental-frequency alternating current in the armature and the corresponding direct current in the field winding can be then reproduced by a locked rotor test performed with the damper winding removed. In practice, this locked rotor test is conducted by exciting two armature phases, connected in series, from a single-phase supply. The short-circuited field winding is located with its axis coincident with the axis of the resultant armature m.m.f.[39] The disposition of the two armature windings with respect to the direct-axis and their connection in series, ensures that no voltage is induced in the windings by the third harmonic component of air-gap flux. The voltage across one phase corresponds mainly to the fundamental air-gap flux.

In the case of the normal operation of the machine, voltage measurements are made between lines to exclude the contribution of the third harmonic voltage. The phase voltage is deduced from the measured line-to-line voltage. This remark also applies to the measurement of voltage in the sudden three-phase short-circuit test.

For calculations, both the practical locked rotor test and the sudden three-phase short-circuit test can be visualised in terms of a hypothetical locked rotor test performed by employing one armature phase. In this test, an armature phase is located with its axis coincident with the direct-axis. This phase is excited with a.c. The fundamental component of the alternating m.m.f. set up by current I_a in the phase is increased by 1.5 times to allow for the contribution of the other two phases in the actual machine. Thus, the m.m.f. acting along the direct-axis is equal to the fundamental armature-reaction m.m.f. F_a set up by all three phases of the actual machine. The flux produced by this m.m.f. links the armature and the short-circuited field winding.

As mentioned above, the practical locked rotor test and the sudden short-circuit test are so conducted as to exclude the influence of the third harmonic component of flux. Therefore only the voltage induced in an armature phase by the fundamental component of flux must be considered in the hypothetical test. However, the flux linking the field winding is the total flux in all three tests.

The magnetic circuit of the machine is assumed to be unsaturated. Therefore, the individual fluxes due to the armature-reaction and field m.m.f.s are superposed to determine the resultant mutual flux.

The calculations in the following sections are based on the assumption that the resistances of the armature and field windings are negligible. Iron losses are also neglected, and it is assumed that in the case of the sudden three-phase short-circuit test, the field winding is normally connected across a d.c. source of negligible internal impedance.

As the field winding is short-circuited, the total flux linking it must be zero. The total mutual flux per pole set up by the fundamental armature-reaction m.m.f. F_a is given by the expression,

$$\varnothing_a = \frac{\mu_0 F_a}{l_g} \times A_{d1} \times \frac{2}{\pi} \times a \times K_1$$

$$= \frac{F_a}{S_g} \times 0.877 \times 0.953 \qquad (5.3)$$

The symbol a represents the area of cross-section at the air-gap. S_g is a reluctance based on the effective minimum length, l_g, of the air-gap. The reluctance of iron paths is neglected.

The mutual flux per pole due to a current $i_f = I_f'$ $\sin \omega t$ in the field winding has the following time-maximum value.

$$\varnothing_f' = \frac{1}{S_g} \times \frac{N_f \; I_f'}{P} \times A_1 \times K_\varnothing$$

$$= \frac{1}{S_g} \times \frac{N_f \; I_f'}{P} \times 1.06 \times 1.02 \qquad (5.4)$$

N_f is the total number of turns on the field winding.

The peak value of the leakage flux per pole linking the field winding alone is represented by $\varnothing_{Lf}'$. Equating the fluxes linking the field winding, we have

$$\frac{F_a}{S_g} \times 0.877 \times 0.953$$
$$= \frac{1}{S_g} \times \frac{1}{P} \times N_f \; I_f' \times 1.06 \times 1.02 + \phi_{Lf}' \qquad (5.5)$$

or
$$1.06 \times \frac{1}{S_g} \times \frac{1}{P} \times N_f \; I_f'$$
$$= \frac{1}{S_g} \times F_a \times 0.877 \times \frac{0.953}{1.02} - \frac{\phi_{Lf}'}{1.02} \qquad (5.6)$$

The fundamental component of the resultant air-gap flux has the following value.

$$\phi_g = \frac{1}{S_g} \times F_a \times 0.877 - \frac{1}{S_g} \times \frac{1}{P} \times N_f \; I_f' \times 1.06 \qquad (5.7)$$

Substituting for the second term from equation 5.6, we obtain,

$$\phi_g = (\frac{1}{S_g} \times F_a \times 0.877) \times 0.065 + 0.98 \; \phi_{Lf}' \qquad (5.8)$$

The measured transient reactance corresponds to the linkages with the armature phase set up by flux ϕ_g and the armature leakage flux. The linkages due to ϕ_g yield a reactance denoted by X. This reactance is the parallel combination of reactances X_{uns} and x_2 of a Tee circuit similar to that in Fig. 5.11. The small letter is used to indicate that x_2 is not the "actual" referred field leakage reactance.

The reactance X is the difference of the transient and armature leakage reactances. Employing the minimum Potier reactance of 3.5 ohms as the armature leakage reactance, X becomes 4.1 ohms. The term enclosed within brackets in equation 5.8 represents the fundamental flux per pole established by F_a. If equation 5.8 is multiplied through out by the term $2\pi f\ T_{ph}\ K_{w1}/\sqrt{2}\ I_a$, the following equation is obtained.

$$X = 0.065\ X_{uns.} + \frac{0.98 \times 2\pi f\ T_{ph}\ K_{w1}}{\sqrt{2}\ I_a}\ \phi'_{Lf} \qquad (5.9)$$

Employing a turns-ratio of 8.16, a value of X_{uns} = 31.5 ohms is obtained from the open-circuit characteristic of Fig. 5.2a. Equation 5.9 then yields

$$\frac{2\pi f\ T_{ph}\ K_{w1}}{\sqrt{2}\ I_a}\ \phi'_{Lf} = 2.1 \text{ ohms.} \qquad (5.10)$$

By following the procedure outlined in appendix A, an expression for the "actual" referred field leakage reactance X_2 can be derived. This reactance has a value such that the voltage drop across it corresponds to a voltage drop of ϕ'_{Lf} across the associated reactance in the dynamic analogue. Reactance X_2 is given by the following expression

$$X_2 = \frac{2\pi f\ \phi'_{Lf}}{\frac{N_f\ I'_f\ A_1}{P}} \times \frac{1.91\ A_{d1}}{P} \times (T_{ph}\ K_{w1})^2$$

Substituting from equation 5.10 in the above expression, we have,

$$X_2 = \frac{2.7\ A_{d1}\ T_{ph}\ K_{w1}}{A_1\ N_f} \times \frac{I_a}{I'_f} \times 2.1$$

$$= \frac{1}{n} \times \frac{I_a}{I'_f} \times 2.1 \qquad (5.11)$$

The turns-ratio n is the ratio of the armature and field currents which establish the same fundamental air-gap flux.

If both sides of equation 5.6 are multiplied by the term $2\pi f T_{ph} K_{w1} / \sqrt{2} I_f'$, the left hand side becomes the fundamental voltage induced in an armature phase by unit field current. Hence it can be replaced by n X_{uns}. The other two terms can be written as follows.

$$nX_{uns} = \left[\frac{2\pi f T_{ph} K_{w1}}{\sqrt{2} I_a} \times \frac{1}{S_g} \times F_a \times 0.877 \right] \times \frac{I_a}{I_f'} \times \frac{0.953}{1.02} - \frac{2\pi f T_{ph} K_{w1}}{\sqrt{2} I_f'} \times \frac{\phi_{Lf}'}{1.02}$$

$$\text{i.e. } nX_{uns} = X_{uns} \times \frac{I_a}{I_f'} \times \frac{0.953}{1.02} - \frac{2\pi f T_{ph} K_{w1} \times \phi_{Lf}'}{\sqrt{2} I_f' \times 1.02} \qquad (5.12)$$

Substituting from equation 5.10 for the term involving ϕ_{Lf}', equation 5.12 becomes

$$nX_{uns} = \left[X_{uns} \times \frac{0.953}{1.02} - \frac{2.1}{1.02} \right] \frac{I_a}{I_f'} \qquad (5.13)$$

Reactance X_2 can now be determined by eliminating I_a/I_f' between equations 5.11 and 5.13. A value of X_2 = 2.4 ohms is obtained from the two equations.

The general expression for X_2 derived by the above procedure is as follows.

$$X_2 = \frac{\left[X - X_{uns} \left(1 - \frac{K_1}{K_\phi}\right) \right] K_\phi \times X_{uns}}{(X_{uns} - X)} \qquad (5.14)$$

The constants describing the air-gap **flux density** distribution in machine B are: $A_1 = 0.865$, $K_\phi = 0.95$, $A_{d1} = 0.767$ and $K_1 = 0.9$. Employing a turns-ratio of 7.6, the reactance X_{uns} becomes 61 ohms. Using the minimum Potier reactance of 3.3 ohms as the armature leakage reactance, X becomes 6.4 ohms. Equation 5.14 then yields a value of $X_2 = 3.37$ ohms.

For comparison, the values of X_2 have also been calculated by using the expression for X derived in reference 40. These calculations yield the values of $X_2 = 2.3$ ohms and $X_2 = 2.5$ ohms for machines A and B respectively. The difference between these reactances and the corresponding reactances evaluated as above arises from the different approximations employed for their calculation. In reference 40, the expression for reactance X is derived by assuming that only a part of the space fundamental of flux established by F_a links the field winding. The flux linking the field winding is evaluated by first determining the rectangular distribution of m.m.f. of which F_a forms the fundamental component. The constant A_1 is then used to determine the fundamental flux established by the rectangular m.m.f. This flux forms the left hand side of an equation the right hand side of which is similar to equation 5.5. The expression for ϕ_g is the same as in equation 5.7. Thus, the expression for reactance X is derived in reference 40 by ignoring the linkages with the field winding due to the space-harmonic components of flux established by F_a. Besides the fundamental component F_a, the rectangular m.m.f. referred to above also has harmonic components. Some of these components establish fundamental air-gap fluxes. The linkages of such fluxes with the field winding are also ignored in reference 40. On the other hand, the method described in the preceding paragraphs is based on the assumption that all the fluxes established by F_a link the field winding. It has been pointed out in section 5.4.1 that this assumption is justified for the two machines considered. It would be less so when considering practical machines in which the ratio of pole-arc to pole-pitch is smaller than in the test machines. In the practical machines, the linkages with the field winding established by the harmonic components of the air-gap flux due to F_a would be small. Hence the expression derived in reference 40 would be more appropriate for such machines.

As an additional check, the referred reactance X_2 was approximately calculated from design data. Referring to Fig. 5.1a, the leakage flux passing between the pole sides was calculated by considering the field winding to be located in partially-closed slots. The slots were regarded as being composed of three sections, as shown in Fig. 5.19. The field winding was considered to be formed by a wedge-shaped arrangement of uniformly distributed conductors having a negligible cross-section. The leakage flux existing at the ends of the pole system was evaluated by adopting the simplified representation of the flux paths used in reference 42 (p 42). This flux does not contribute materially to the total field leakage flux. An approximate representation of the paths of this flux is therefore justified. The calculations yielded the values of $X_2 = 1.86$ ohms and $X_2 = 3.0$ ohms for machines A and B respectively. In spite of the approximate nature of the calculations, these values offer reasonable checks on the reactances determined from the terminal measurements.

Reactance X_2 has to be employed in a linear Tee circuit describing the steady-state operation of the unsaturated machine. Transformation of this Tee circuit yields an equivalent Pi circuit. Using the value of $X_2 = 2.4$ ohms, reactance X_3 in the equivalent Pi circuit of machine A becomes 6.1 ohms. The reactance X_3 in the corresponding equivalent Pi circuit of machine B is 6.8 ohms. If the effect of different distributions of the armature and field windings is ignored, x_2 becomes the referred field leakage reactance in the equivalent

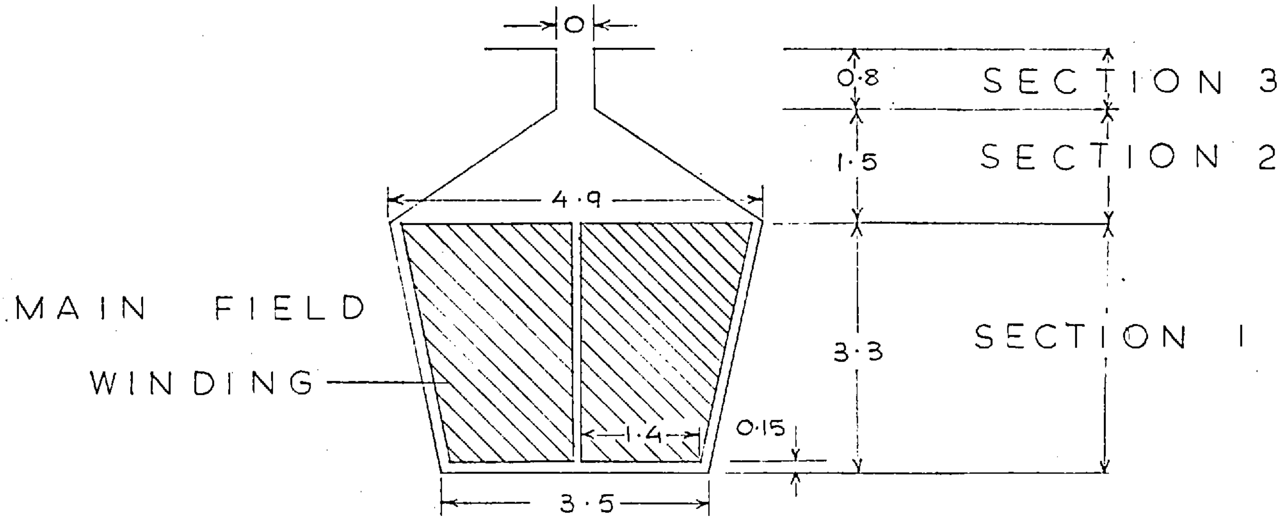

OPENING O — 1.5 Cm. IN MACHINE A; 0.5 cm. IN MACHINE B

CORE LENGTH = 10.7 cm.

ALL DIMENSIONS ARE IN cm.

FIG. 5.19 SIMPLIFIED REPRESENTATION OF THE SLOT SHOWN IN FIG. 5.1a

Tee circuit. Reactance x_2 is evaluated by equating X to the parallel combination of X_{uns} and x_2. The values of x_2 for machines A and B are 4.7 and 7.16 ohms respectively. The values of X_3 in the corresponding Pi circuits, derived by transformation, are 8.72 ohms and 10.8 ohms respectively. The unsaturated values of reactances X_1' and X_2' in the two Pi circuits differ. The two values of X_3 differ by 43 per cent in the case of machine A and 60 per cent in the case of machine B. (The percentage values quoted are based on the 'actual' value of X_3).

Calculations were performed to determine the reactances X_2 and x_2 of the equivalent Tee circuit of machine C. The reactance X_2 was evaluated also taking into account the small proportion of linkages (with the field winding) due to the third harmonic component of flux established by the field m.m.f. The winding factors of the field winding were calculated on the basis of the disposition of the rotor slots shown in Fig.5.1b. The reactance X_2 derived by calculation includes the referred overhang leakage reactance of the field winding. Only the flux linkages, with the field winding, established by the fundamental component of armature-reaction m.m.f. were taken into account. This component of m.m.f. acts on an air-gap of uniform length (except for the influence of slot-openings) and establishes a fundamental air-gap flux. The small flux set up by the harmonic components of armature-reaction m.m.f. forms the differential leakage flux of the armature. The minimum Potier reactance of 3.7 ohms and the corresponding turns-ratio of 6.34 were employed for the calculations, the calculations being similar to those explained in connection with machine A. The calculations yielded the values of X_2 = 1.26 ohms and x_2 = 2.4 ohms. The corresponding values of X_3 are 5.03 ohms and 6.24 ohms respectively. The difference between these two values of X_3 is 24 per cent. This difference is smaller than the difference between the two values of X_3 of machines A and B mainly because in the case of machine C, the reactances x_2 and X_2 form less significant parts of X_3.

The results indicate that the direct use of the measured transient reactance for evaluating the parameters of the equivalent Pi circuit is not strictly correct. However, both the test measurements and calculations are simplified if the measured transient reactance is directly employed. Therefore, the performance of the Pi circuit derived on the basis of the measured transient reactance is examined in the following section. A comparison of the performance of this Pi circuit with that of the more "exact" Pi circuit is also made in the following section.

5.6.2. Performance of the equivalent Pi circuits of the machines

Assuming that the transient reactance X_d' is the reactance measured at terminals 1-1 of the circuit drawn in Fig. 5.20 with terminals 2-2 short-circuited, we have

$$X_d' = \frac{X_1' \, X_3}{X_1' + X_3} \tag{5.15}$$

The reactances of the equivalent Pi circuit can be determined by solving equation 5.15 and equations similar to equation 3.14 and 3.16. The method by which the saturation characteristics of reactances X_1' and X_2' can be obtained has been explained in section 3.4.2.

The open-circuit characteristics of the three machines along with the zero power factor characteristics marked a were employed for calculating the characteristics of X_1' and X_2'. The values of n used for these calculations are 8.16, 7.6 and 6.34 for machines A, B and C respectively. The calculated characteristics are drawn in Figs. 5.20, 5.21a and 5.22.

The calculated characteristics of X_1' and X_2' are influenced by experimental errors such as an error in the measurement of the field current at short-circuit. To indicate the influence of these errors, two sets of graphs are drawn in Fig. 5.21a. Graphs a and a' show the characteristics of X_1' and X_2' calculated by using the

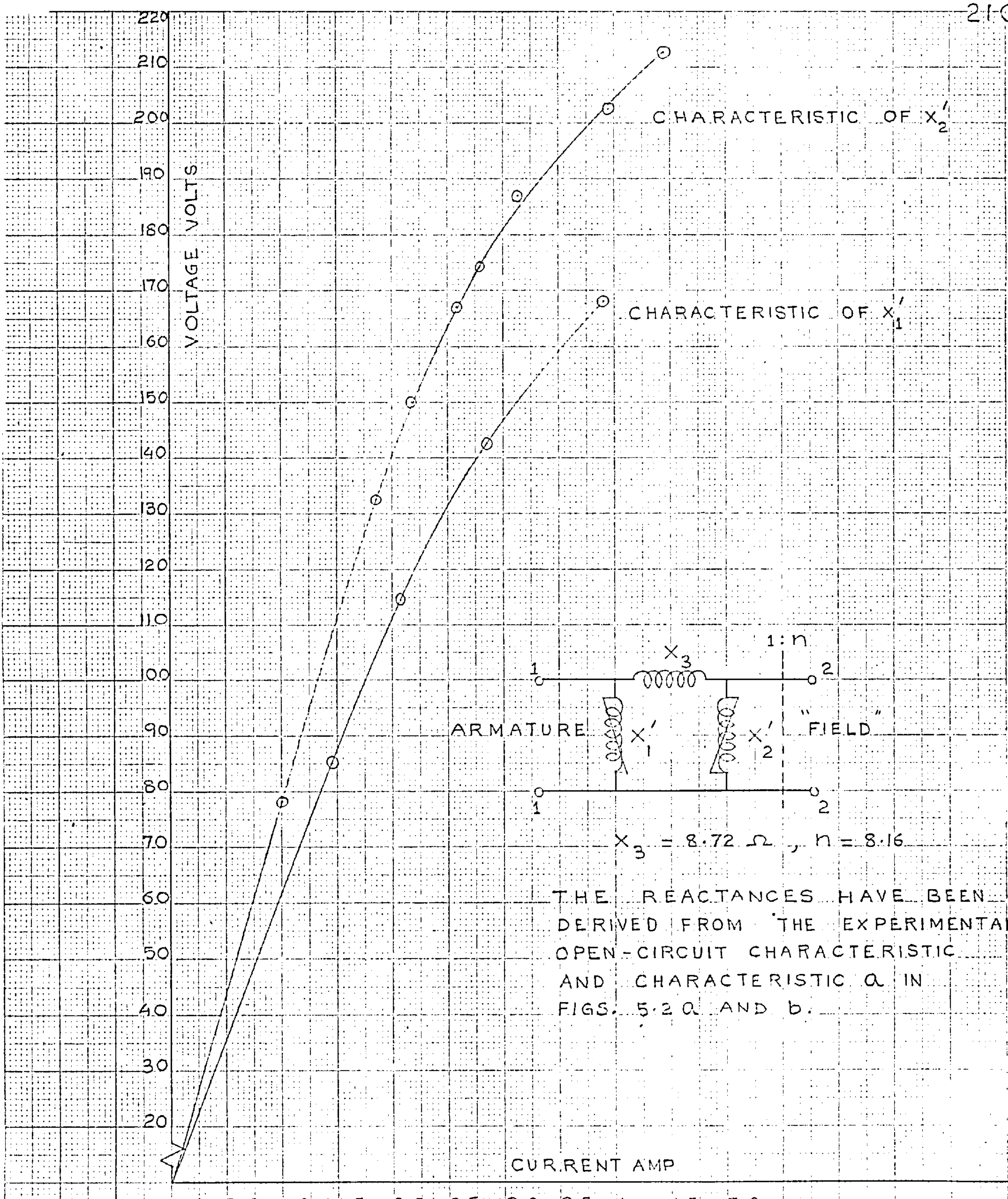

FIG. 5.20 PARAMETERS OF THE EQUIVALENT PI CIRCUIT OF MACHINE A

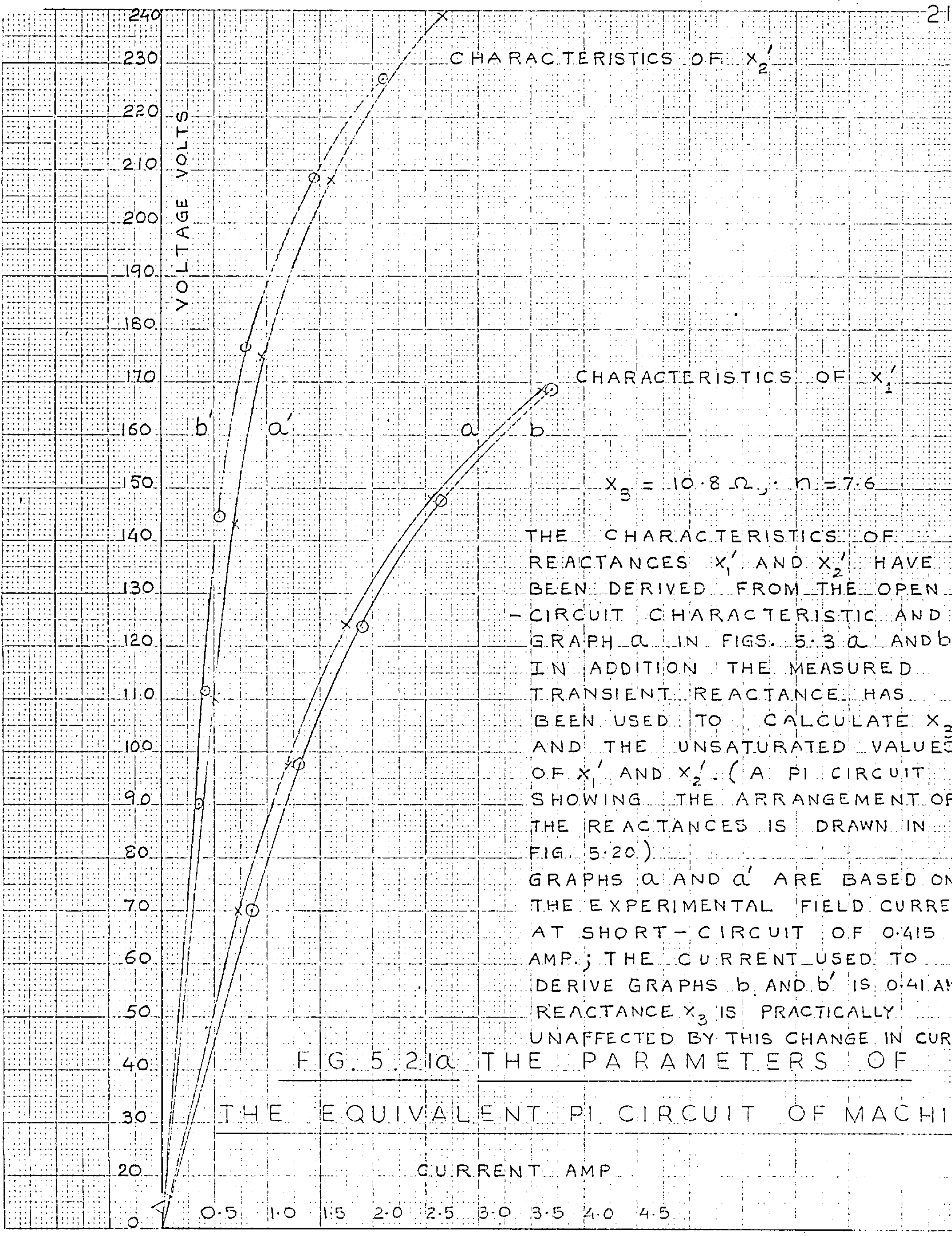

$X_3 = 10{\cdot}8\ \Omega$, $n = 7{\cdot}6$

THE CHARACTERISTICS OF REACTANCES X_1' AND X_2' HAVE BEEN DERIVED FROM THE OPEN-CIRCUIT CHARACTERISTIC AND GRAPH a IN FIGS. 5·3 a AND b. IN ADDITION THE MEASURED TRANSIENT REACTANCE HAS BEEN USED TO CALCULATE X_3 AND THE UNSATURATED VALUES OF X_1' AND X_2'. (A PI CIRCUIT SHOWING THE ARRANGEMENT OF THE REACTANCES IS DRAWN IN FIG. 5·20.)

GRAPHS a AND a' ARE BASED ON THE EXPERIMENTAL FIELD CURRENT AT SHORT-CIRCUIT OF 0·415 AMP.; THE CURRENT USED TO DERIVE GRAPHS b AND b' IS 0·41 AMP. REACTANCE X_3 IS PRACTICALLY UNAFFECTED BY THIS CHANGE IN CURRENT

FIG. 5.21a THE PARAMETERS OF THE EQUIVALENT PI CIRCUIT OF MACHINE B

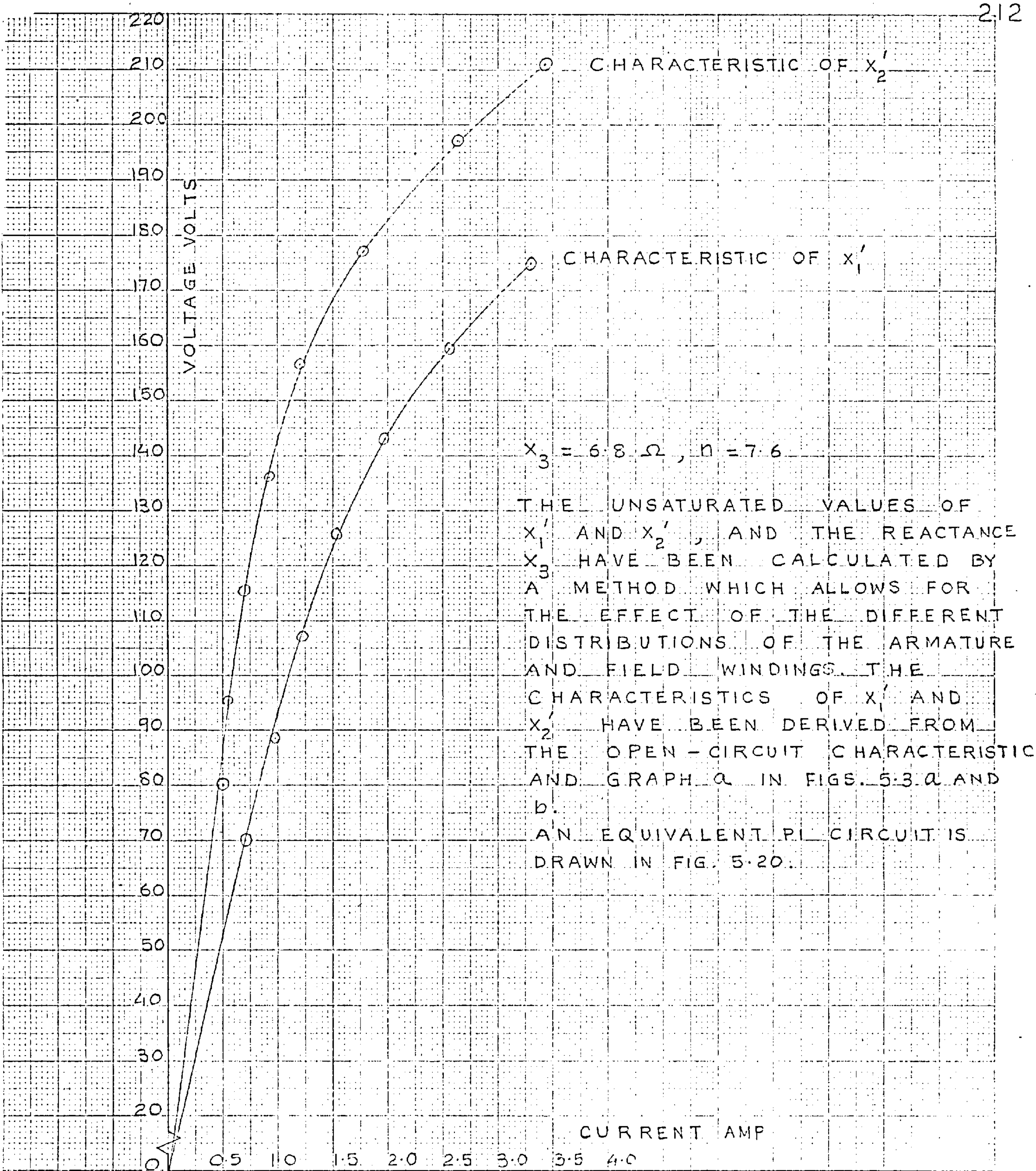

FIG 5.21b PARAMETERS OF THE EQUIVALENT PI CIRCUIT OF MACHINE B

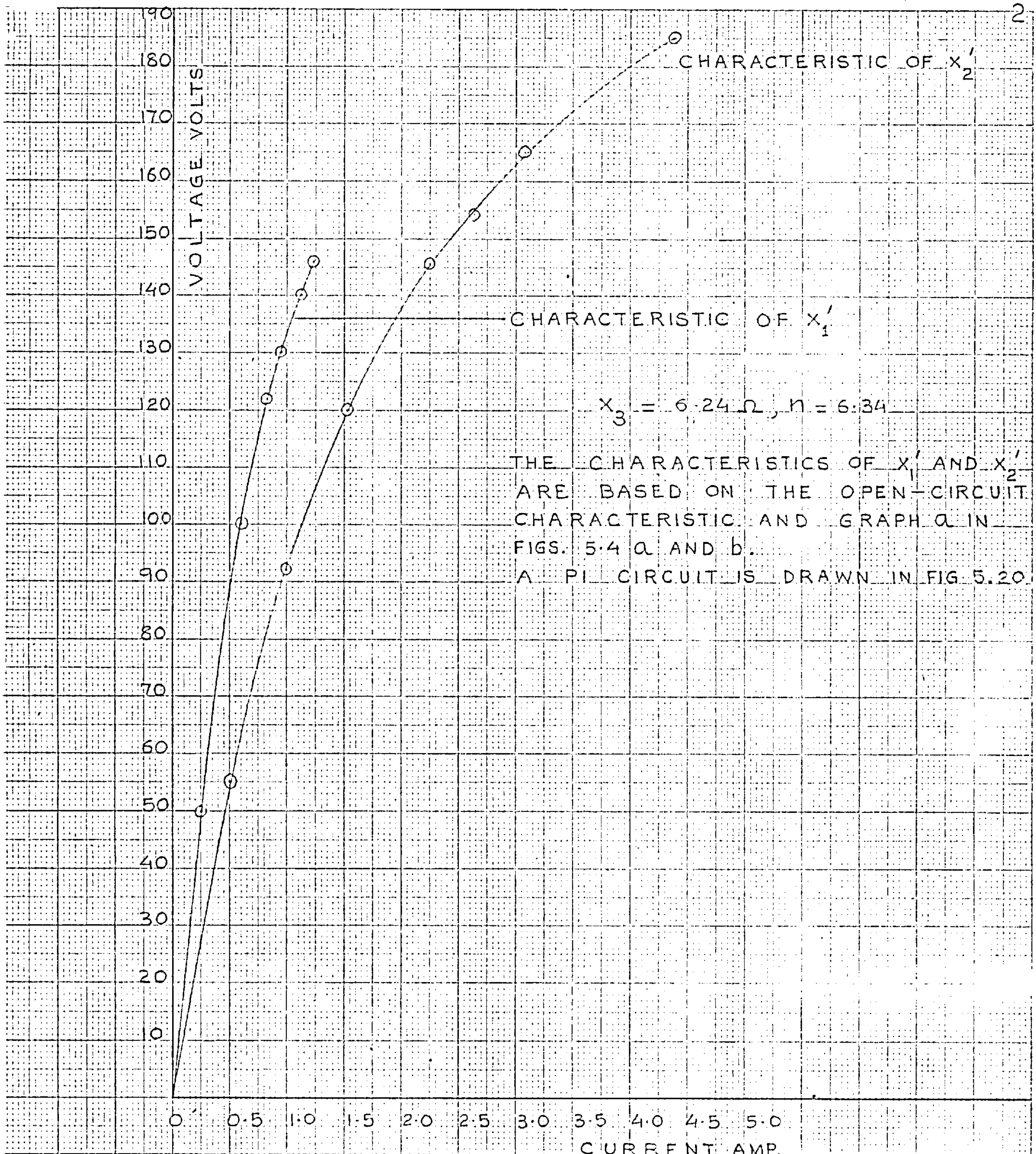

FIG. 5.22 PARAMETERS OF THE EQUIVALENT PI CIRCUIT OF MACHINE C

experimental value of the field current at short-circuit (0.415 amp); b and b' are the characteristics evaluated by using a field current of 0.41 amp. The difference between the two field currents is 1.2 per cent. The influence of an error in X_1' and X_2' on the prediction of field excitation is small. This is seen by a comparison of points on the characteristic marked (ii) with the points enclosed in squares in Fig. 5.3b. The former points represent calculated field currents based on graphs a and a' in Fig. 5.21a while the latter are based on graphs b and b'. The entire range of graph a, Fig. 5.3b has been utilised to determine the characteristics of X_2'. The characteristics of X_2' do not cover a range wide enough to permit the determination of values on graph (ii) above 140 volts. (The graph referred to is that associated with graph c, Fig. 5.3b.) However, the part of graph (ii) shown is sufficient to establish the trend of the graph. The graphs associated with graph c, Fig. 5.3a show that errors in X_1' and X_2' perceptibly influence the predicted field currents at operating points located in the unsaturated region of the calculated zero power factor characteristics.

Additional graphs marked (ii) are drawn in Figs. 5.2b and 5.3b. These graphs are based on the characteristics of X_1' and X_2' shown in Fig. 5.20 and in graphs a and a',

Fig. 5.21a. The calculated graph (ii) corresponding to graph b, Fig. 5.2b is almost coincident with graph (i). Since the unsaturated regions of the operating characteristics are not of much interest, similar graphs marked (ii) are not drawn in Figs. 5.2a and 5.3a. (This remark excepts the two graphs mentioned in the preceding paragraph).

The difference between graphs (i) and (ii) in Figs. 5.2b and 5.3b is largely accounted for as follows. The minimum Potier reactance and the corresponding turns-ratio have been employed for calculating the graphs marked (i). Both these quantities are influenced by experimental errors. As mentioned in section 5.4.1, the possible error in Potier reactance is 0.3 ohm . The average value of Potier reactance based on graph (ii) and the field current at short-circuit given by graph c, Figs. 5.2a and 5.3a, is 4.0 ohms for both the machines. Some of the values of Potier reactance shown in graph a, Fig. 5.5 are nearly equal to 4.0 ohms. Therefore, the difference between calculated characteristics (i) and (ii) associated with graph c, Fig. 5.2b could largely arise from experimental errors. The Potier reactance shown in graph a, Fig. 5.6 is more consistent than that shown in graph a, Fig. 5.5. Hence the difference between graphs (i) and (ii), Fig. 5.3b represents a slight increase in the accuracy of prediction (of the field excitation) achieved by the use of the Pi circuit. The maximum difference between the field currents in graphs (i) and (ii) associated with graph c, Fig. 5.3b is 3.5 per cent. The corresponding difference between the field currents in the two graphs associated with graph b, Fig. 5.3b is about 1 per cent.

Additional characteristics of reactances X_1' and X_2' of the equivalent Pi circuit of machine B are drawn in Fig. 5.21b. These characteristics correspond to the "actual" reactance X_3 = 6.8 ohms (section 5.6.1). The characteristics shown in Fig. 5.21b are derived from the open-circuit characteristic and zero power factor characteristic a in Figs. 5.3a and b. These characteristics of X_1' and X_2' have been used to calculate the zero power factor characteristics for 5.0 and 7.0 amp . The calculated characteristics are found to be in in close agreement with the corresponding characteristics marked (i) in Fig. 5.3b.

Referring to the characteristics of machine B, the difference between the two zero power factor characteristics (associated with experimental characteristic c) calculated by using the two Pi circuits is small. Therefore additional calculations were performed to ensure that the difference between the two calculated characteristics represented the effect of using different values of X_3, X_1' and X_2'. These calculations were performed on a hypothetical Pi circuit. The characteristics of reactors 1 and 2, described in appendix B, were suitably modified and used as the characteristics of X_1' and X_2'. The reactance X_3 was chosen to be equal to 1 ohm . The terminals of reactance X_2' were assumed to form the "field" terminals. The open-circuit characteristic of the Pi circuit and its zero power factor characteristic for a load current of 2.0 amp were calculated. Using these calculated terminal characteristics, the characteristics of X_1' and X_2' corresponding to an arbitrarily increased value of X_3 = 2.0 ohms were determined. The original Pi circuit (with X_3 = 1.0 ohm) and the Pi circuit with X_3 = 2.0 ohms were then employed to "predict" zero power factor characteristics for a higher load current. It was found that the "field" current determined by using the Pi circuit with X_3 = 2.0 ohms was clearly larger than that determined by using the original Pi circuit.

The factors causing the difference between experimental characteristic c and graph (i), Fig. 5.3b have been indicated in section 5.4.1. Of the factors discussed there, the influence of additional saturation due to changes in the distribution of air-gap flux density can not be accounted for in an equivalent circuit. Further more, both the Tee and Pi circuits are only approximate forms of the equivalent circuit of Fig. 2.12c. Both these factors account for the major part of the difference between graphs (i) and (ii) and graph c. The close agreement, referred to previously, between characteristics (i) in Fig. 5.3(b) and the characteristics calculated by employing the Pi circuit with X_3 = 6.8 ohms must be expected in view of the small difference between characteristics (i) and (ii).

The direct use of the measured transient reactance for calculating the reactances of the Pi circuit is not entirely correct. Therefore, the slight increase in accuracy achieved by the use of this Pi circuit (with X_3 = 10.8 ohms) must be regarded as being empirical in nature. The extent of this increase would depend upon the pole-profile.

The characteristics of reactances X_1' and X_2' of the equivalent Pi circuit of machine C are shown in Fig. 5.22. Points on the zero power factor characteristics for 7.0 amp calculated by using the Pi circuit representation are enclosed by squares in Fig. 5.4 b. The field currents in graph (i) associated with graph c, Fig. 5.4b are within 1 per cent of the experimental field currents. Both these factors indicate that the

Tee and Pi circuits constitute equally satisfactory representations of the machine.

5.7. Test on machine B at power factors other than zero

The results of a real-load test on machine B are presented in this section. These results are mainly used to briefly indicate the method of calculating load-angle and field excitation when a Pi circuit representation of the direct-axis is employed. The quadrature-axis is represented by reactance X_q.

The load test on machine B was performed by operating the machine as a synchronous motor. The d.c. machine coupled to it was operated as a generator supplying a variable resistive load. The load angle δ was measured on a calibrated disc by means of a stroboscopic arrangement. Table 5.2 shows the test results.

Vector diagrams referring to the operation of machine B as an over-excited synchronous motor are drawn in Fig. 5.23. To secure uniformity of presentation, the machine is shown operating as a generator in the accompanying direct-axis equivalent circuits.

Referring to Fig. 5.23, the maximum phase-shift introduced by the resistance of an armature phase is about a degree. The maximum voltage drop due to this

Table 5.2. : Load Test on Salient-Pole Machine B.

					From Test.		From Tee circuit.		From Pi circuit
Phase Voltage Volts.	Load Current Amp	Power Input Kilo-watts.	Power Factor.	Power Output of D.C.Machine Kilo-watts.	Field Current I_f amp.	Load Angle δ	Field Current I_f amp	Load Angle δ	Field Current I_f amp
125	6.28	2.265	0.962 (lag)	1.81	0.75	59°	0.743	$60^\circ 30'$	0.74
124.8	5.52	2.072	1.00	1.655	0.75	49°	0.73	$51^\circ 6'$	0.73
125.1	4.44	1.596	0.955 (lead)	1.261	0.75	34°	0.745	$36^\circ 6'$	0.73
127.0	3.36	0.84	0.656 (lead)	0.575	0.75	18°	0.775	$17^\circ 24'$	0.75
127.2	2.92	0.248	0.222 (lead)	0	0.75	7°	0.76	$5^\circ 6'$	0.75

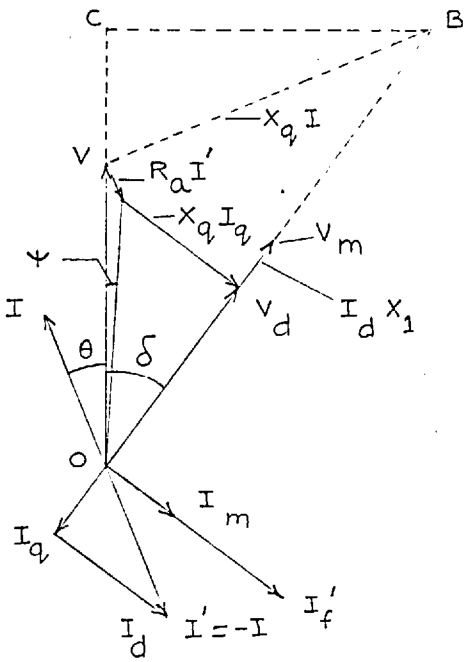

I = CURRENT DRAWN BY THE MOTOR

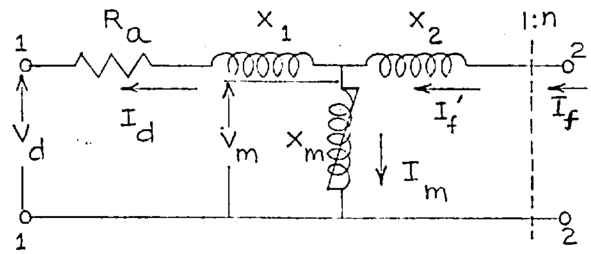

TERMINALS 1-1 ARMATURE
TERMINALS 2-2 "FIELD"

THE DOTTED LINES SHOW THE CONSTRUCTION THAT COULD BE EMPLOYED TO DETERMINE δ IF THE DROP $R_a I'$ IS IGNORED

a. DIRECT-AXIS REPRESENTED BY A TEE CIRCUIT

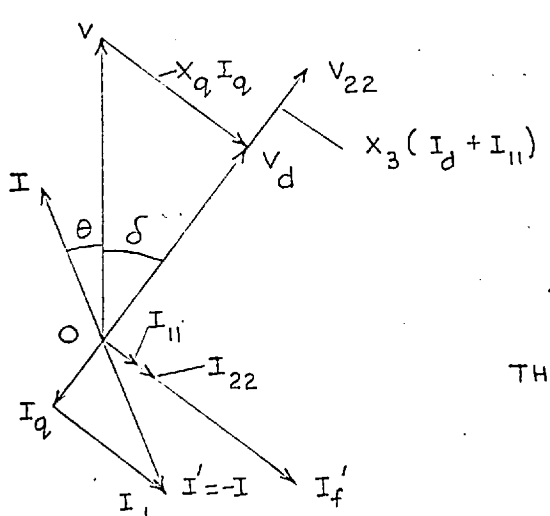

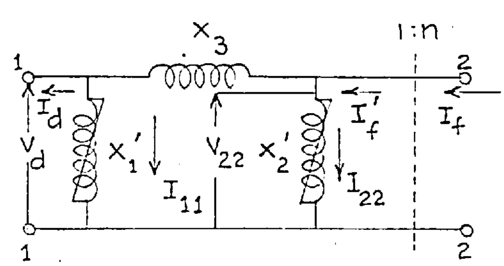

TERMINALS 1-1 ARMATURE
TERMINALS 2-2 "FIELD"
THE RESISTANCE R_a IS NEGLECTED

b. DIRECT-AXIS REPRESENTED BY A PI CIRCUIT

FIG. 5.23 VECTOR DIAGRAMS OF A SYNCHRONOUS MOTOR OPERATING AT A LEADING POWER FACTOR resistance is 1 volt. In view of the small magnitudes of both these quantities, the following calculations have been performed neglecting the resistance of an armature phase. The iron loss in the machine is also ignored.

From Fig. 5.23(a), the load-angle δ is given by the expression,

$$\tan \delta = \frac{CB}{OC} = \frac{IX_q \cos \theta}{V + IX_q \sin \theta} \qquad (5.16)$$

The reactance X_q was determined from a slip test (Ref. 39, p. 1334). An unsaturated value of 28 ohms was obtained from this test. The reactance X_q does not saturate at the rated terminal voltage.

The calculated values of δ are given in Table 5.2. The difference of about 2 degrees between the experimental and calculated values of δ arises from small errors in the measurement of power. These errors result in errors in the angle θ. An additional factor that may be mentioned is that the minimum load angle that could be measured on the calibrated disc was 2 degrees. Further, the possible error in the experimental value of reactance X_q is of the order of an ohm. Considering all these factors the agreement between the measured and calculated angles can be regarded as satisfactory. The voltage V_d across the terminals of the direct-axis equivalent circuits and the current I_d can now be calculated employing the following expressions.

$$V_d = V \cos\delta \tag{5.17}$$

$$I_d = I \sin (\delta + \theta) \tag{5.18}$$

The method of calculation of field excitation has been indicated on the vector diagrams. A Potier reactance of 3.3 ohms and the corresponding turns-ratio of 7.6 were employed for calculations based on the Tee circuit representation. The characteristics of reactances X_1' and X_2' corresponding to a reactance X_3 of 10.8 ohms were employed for calculations using the Pi circuit representation of the direct-axis. The calculated values of the field excitation are given in Table 5.2.

It can be seen from the table that almost similar values of field excitation are obtained from calculations based on either representation. These values are in agreement with the experimental field currents.

It may be mentioned that the maximum internal voltage across the reactance X_m of the equivalent Tee circuit is 135 volts. The open-circuit characteristic in Fig. 5.3(b) shows that the magnetic circuit is only slightly saturated at this voltage. It has been found in the previous section that the difference between the field currents predicted with the two circuits is small at much higher levels of saturation. Hence the agreement between the two calculated field excitations in Table 5.2 has to be expected.

CHAPTER 6

Conclusions

The experimental work described in the previous chapters has amply illustrated the novel methods of determination of the parameters of the equivalent Tee and Pi circuits of a two-winding transformer. Only the turns-ratio of the associated ideal transformer and two of the three reactances of the equivalent Tee circuit have to be employed for the prediction of the steady-state performance of a synchronous machine. A novel method of determining the turns-ratio and the two reactances has been discussed and illustrated by tests on the model synchronous machine. Theoretical considerations show that a synchronous machine can be more fully represented by a Pi circuit which is in general not equivalent to the Tee circuit. The parameters of this Pi circuit can be determined by the additional measurement of the transient reactance. This additional measurement can be also used to determine the third reactance (referred field leakage reactance) in the equivalent Tee circuit of the machine. It is clear that the novel methods referred to above could also be used to derive the equivalent circuits of a slip-ring induction motor.

It is seen that when the cylindrical-rotor synchronous machine is represented by the equivalent Tee circuit, the values of the armature leakage reactance determined by the method proposed in this thesis and by the Potier method are in good agreement. This agreement is secured in spite of the fact that the reactances evaluated from the test characteristics could be greatly influenced by small errors in measurement. However, the test results indicate that by any of the methods a reliable value of armature leakage reactance can be obtained only from the highly saturated regions of the test characteristics.

The proposed method of derivation of the relevant parameters of the equivalent Tee circuit thus forms a useful alternative to the Potier method of determining armature leakage reactance. However, the main utility of the method is that it leads to a better understanding and a direct exposition of the basis of the Potier method.

In the case of the salient-pole machine, it is seen that the influence of a non-uniform length of the air-gap causes the value of armature leakage reactance determined by the novel method to be smaller than the minimum Potier reactance. This value of the Potier reactance is approximately equal to the armature leakage reactance. The test results illustrate the need for a suitable choice of load current in the Potier test.

If too low a value of this current is used, the reactance determined from tests is subject to considerable experimental errors. On the other hand, if too high a value is employed, there is additional saturation of the magnetic circuit due to field leakage flux and changes in the distribution of air-gap flux. This saturation is seen to result in an increased value of Potier reactance.

In both the salient-pole and cylindrical-rotor machines, the distributions of the field and armature windings are, in general, different. It is found that owing to this difference in distributions, the referred field leakage reactance in the equivalent Tee circuit, and the reactances of the Pi circuit can be only approximately determined from terminal tests. An equivalent Pi circuit, representing the direct-axis of the machines, could be derived, ignoring the difference in distributions of the two windings. In the case of the model synchronous machine with the cylindrical rotor, the results of tests indicate that this Pi circuit and the Tee circuit constitute equally satisfactory representations of the machine. The representation of the direct-axis of the model machine with a salient-pole rotor by this Pi circuit is found to result in a slight improvement in accuracy over that achieved with the Tee circuit representation. Another Pi circuit could be derived by approximately allowing for the difference in distributions of the armature and field windings. However, for the model machine with a salient-pole rotor, the use of this Pi circuit is found to result in no perceptible improvement in accuracy over that achieved by the use of the Tee circuit representation. Thus, the former Pi circuit is found to be a better representation of the direct-axis than the latter. The improvement in accuracy achieved by the use of the former Pi circuit depends upon certain design factors of individual machines and is empirical in nature. Therefore, tests on a range of larger machines employed in practice would be useful in determining the significance of the improvement achieved by the use of the former Pi circuit.

The parameters of the equivalent Tee and Pi circuits could be calculated from design data by the method outlined in appendix C. The calculation of these parameters is facilitated by adopting the systematic approach to the derivation of an equivalent circuit outlined in appendix A.

REFERENCES

1. Electrical Engineering Staff, Massachusetts Institute of Technology, : "Magnetic Circuits and Transformers", (Book) (John Wiley, 1961), pp. 455-461
2. ibid, p. 462
3. Morris, D. :"Some Tests of an Exact Practical Theory of the Transformer", Proc. I.E.E., 1950, Vol. 97, Pt. II, p. 19
4. Dahl, O.G.C. :"Separate Leakage Reactance of Transformer Windings", Trans. A.I.E.E, 1925, Vol. XLIV, p. 787
5. Boyajian, A. :"Resolution of Transformer Reactance into Primary and Secondary Reactances", ibid, p. 808
6. Stirzaker, E.G. : "Determination of Separated Leakage Reactances of Transformer from No-load Test", Bulletin of Electrical Engineering Education, 1960, Vol. 24, p. 42
7. Reference 1, pp. 339, 353
8. Langsdorf, A.S. : "Theory of Alternating-Current Machinery", (Book) (Mcgraw-Hill, 1955), p.404
9. ibid, p. 166
10. Bean, R.L. et al : "Transformers for the Electric Power Industry", (Book) (Mcgraw-Hill, 1959), pp. 113-115

11. Reference 1, p. 457

12. Blume, L.F. et al: "Transformer Engineering", (Book) (John Wiley, 1961), p. 70

13. March, L.A. and Crary, S.B.: "Armature Leakage Reactance of Synchronous Machines", Trans. A.I.E.E, 1935, Vol. 54, pp. 378-81

14. Beckwith, S.: "Approximating Potier Reactance", Trans. A.I.E.E., 1937, Vol. 56, p. 813

15. Mikhail, Saad L.: "Potier Reactance for Salient-Pole Synchronous Machines", Trans. A.I.E.E., 1950, Vol. 69, Part I, p. 235

16. Schuisky, W.: "Vor aus bestimmung der Erregung von Synchron Machinen", ETZ-A, 1963, Vol. 84, p. 317 (English Electric Translation no. 847)

17. Cherry, E.C.: "The Duality of Interlinked Electric and Magnetic Circuits and the Formation of Transformer Equivalent circuits", Proc. Physical Society, 1949, B, Vol. 62, p. 101

18. Cherry, E.C.: "Duality, Partial Duality and Contact Transformation", Proc. of the Symposium on Modern Network Synthesis, Polytechnic Institute of Brooklyn, 1955, p. 331.

19. Morris, D.G.O.: "The Topology of Circuits and Fields", Spring Term Lecture Course, Imperial College, 1963.

20. Macfadyen, K.: "Vector Permeability", J.I.E.E., 1947, Vol. 94, Part III, No. 32, p. 407

21. Slemon, G.R.: "A Method of Approximate Steady-State Analysis for Non-Linear Networks", Proc. I.E.E., 1953, Part c, p. 280

22. Slemon, G.R.: "Equivalent Circuits for Transformers and Machines Including Non-Linear Effects", Proc. I.E.E., 1953, Part c, p. 132

23. Morris, D.: "Some Practical Equivalent Circuits for Multi-Circuit Transformers", Proc. I.E.E, 1951, Vol. 98, Part II, p. 260 (appendix 9.1)

24. Reference 22, p. 130

25. Guillemin, E.A.: "Introductory Circuit Theory", (Book) (John Wiley, 1953), p. 163

26. Say, M.G.: "The Performance and Design of Alternating Current Machines", (Book) (Pitman, 1961), p. 149

27. Reference 12, p. 71 and Reference 10, p. 115

28. Kron, G.: "Equivalent Circuits of Electric Machinery", (Book) (John Wiley, 1951), p. 95

29. Reference 8, p. 419

30. Reference 26, p. 569

31. Wieseman, R.W.: "Graphical Determination of Magnetic Fields", Trans. A.I.E.E., 1927, Vol. XLVI, p. 141

32. Still, A. and Siskind, C.S.: "Elements of Electrical Machine Design", (Book) (Mcgraw-Hill, 1954), p. 210

33. Hamdi-Sepen, D.: "Saturation Effects in Synchronous Machines", Trans. A.I.E.E., 1954, Vol. 73, p. 1349

34. Dalal, M.K.: "The Two Reactions of a Synchronous Machine", Thesis for M.Sc. (ENG), London University, 1957

35. "Instructions and Operating Manual for Type FRA - 2 and FRA-2T Wave-Analyser", Radiometer, Denmark.

36. Harris, Forest, K.: "Electrical Measurements", (Book) (John Wiley, 1956), p. 420

37. Robert, M.R.: "Le Microréseau, Modele Dynamique de Réseaux", Bulletin de la Société Francaise de Electriciens, 1954, Vol. 4, No. 38, p. 67

38. Stephen, D.D.: "Testing Synchronous Machines", Electrical Times, 23rd August 1962, p. 257

39. Wright, S.H.: "Determination of Synchronous Machine Constants by Test", Trans. A.I.E.E., 1931, Vol. 50, p. 1336

40. Kilgore, L.A.: "Calculation of Synchronous Machine Constants", ibid, p. 1208

41. Foster Transformers, London: "Technical College Equipment", T.C.Q.1, page 2; Drawing opposite p. 4; List no. 2600 (88882) and illustrations No. G 1111 and 1112.

42. Clayton, A.E. and Hancock, N.N.: "The Performance and Design of Direct Current Machines", (Book)(Pitman, 1961), p. 48.

APPENDIX A

Some factors influencing the choice of the turns-ratio associated with the equivalent circuit of a cylindrical-rotor machine

The requirement that the conditions at the terminals of an equivalent circuit should correspond to the conditions at the terminals of the actual machine imposes certain restrictions on the dynamic analogue. To prevent confusion, these restrictions are discussed in the following paragraphs and not in the main body of the thesis.

To illustrate the restrictions involved, the equivalent Tee circuit of an unsaturated cylindrical-rotor machine is derived in this Appendix. The m.m.f. required by the iron paths is ignored. Resistances of the windings and iron losses are also neglected. For convenience, the armature is assumed to be wound with a single-layer winding. The machine is assumed to be operating at zero power factor.

A magnetic circuit describing the machine consists of the fundamental components of armature-reaction and field m.m.f.s acting on the reluctance of the air-gap. The circuit also includes reluctances representing slot leakage flux paths in the machine.

The amplitudes of the fundamental components of armature-reaction and field m.m.f.s are derived from a harmonic analysis of the stepped waveforms of these m.m.f.s. The following formulae follow from the analysis. (Ref. 26, P.227)

$$F_a = 1.5 \times \frac{4}{\pi} \times \frac{\sqrt{2}\, T_{ph}\, K_{w1} I_a}{P}$$

$$= \frac{1.91 \sqrt{2}\, T_{ph}\, K_{w1} I_a}{P} \qquad \text{A.1}$$

$$F_f = \frac{4}{\pi}\ \frac{N_f K_w I_f}{P} \qquad \text{A.2}$$

The reluctance of the air-gap is defined so as to relate the total flux per pole set up by the armature and field m.m.f.s. to the peak values of the two m.m.f.s. The reluctance then becomes,

$$S_g = \frac{\pi}{2} \times \frac{l_g}{\mu_o a} \qquad \text{A.3}$$

l_g is the effective length of the air-gap, and a is the product of the pole-pitch and the length of the core.

The reluctances representing slot leakage flux paths have to be chosen such that the leakage fluxes in the machine and the magnetic circuit are equal in magnitude. The peak value of the armature slot leakage flux set up by a phase is given by the expression,

$$\phi_{sL} = \frac{4\, T_{ph} \sqrt{2}\, I_a}{Pg}\ \mu_o \lambda L_c \qquad \text{A.4}$$

λ is the specific slot permeance and g is the number of slots per pole per phase. L_c is the length of the core.

Assuming that the slot leakage flux at all sections of the core has the above value, the equivalent reluctance in the magnetic circuit becomes,

$$S_{sL} = \frac{F_a}{\phi_{sL}} \qquad \text{A.5}$$

A similar expression can be derived for the reluctance S_{sLf} representing the rotor slot leakage flux paths. Fig. A.1(a) shows the resulting magnetic circuit. The dynamic analogue of this circuit is shown in Fig. A.1(b). The inductances in the analogue are the inverse of the corresponding reluctances in the magnetic circuit; currents in the analogue are equal in magnitude to the respective m.m.f.s.

To obtain an equivalent circuit in which the currents in an armature phase and the field winding are the terminal quantities, two ideal transformers are interposed as shown in Fig. A.2(a). The turns-ratios of these transformers follow from eqns. A.1 and A.2.

Referred to terminals 1-1, the open-circuit voltage across the reactance $\frac{\omega}{S_g}$ becomes,

$$V_1 = \omega \times \frac{1.91\ T_{ph}\ K_{w1}}{P} \times \frac{1}{S_g} \times \frac{F_f}{\sqrt{2}} \qquad \text{A.6}$$

The open-circuit voltage generated in an armature phase

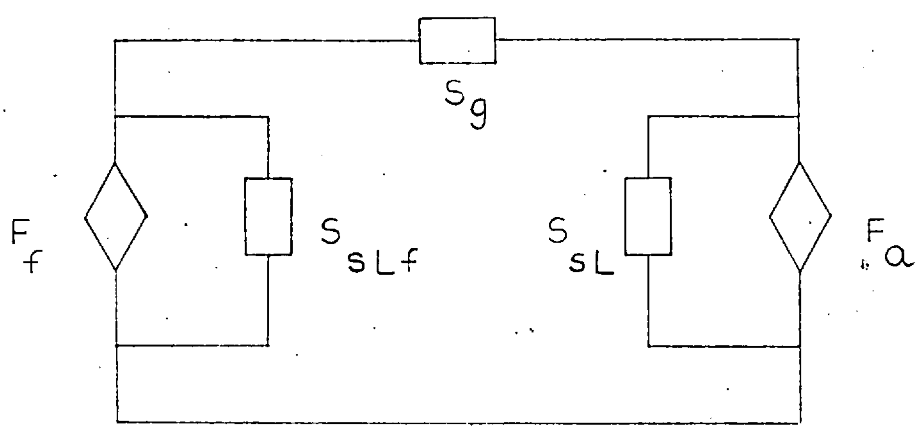

THE SIGNIFICANCE OF THE SYMBOLS IS AS STATED IN FIG. 2.7a

FIG.A1a MAGNETIC CIRCUIT

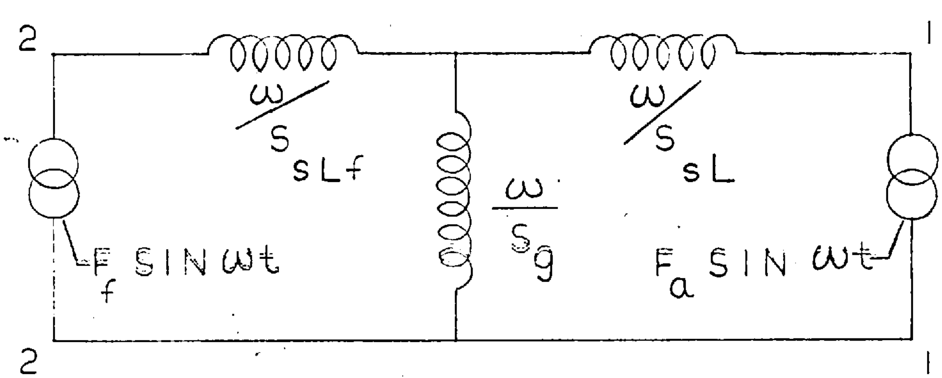

FIG. A.1 b DYNAMIC ANALOGUE

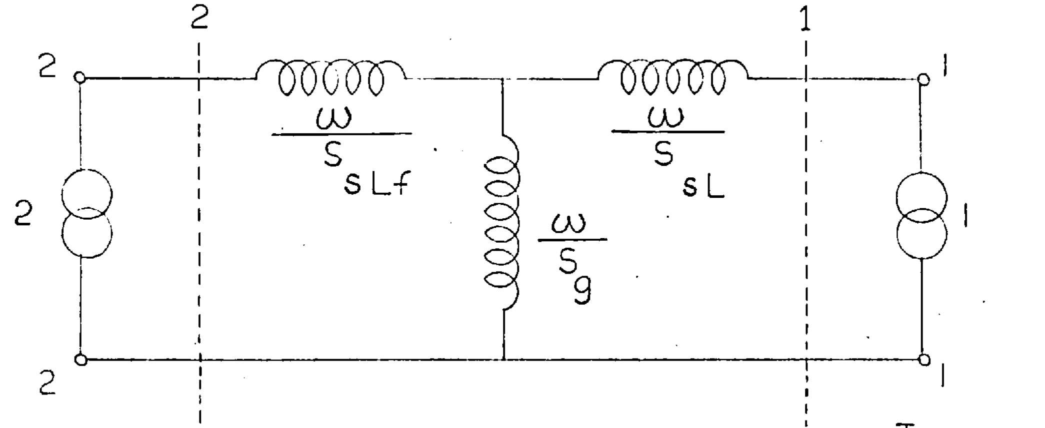

$\frac{4}{\pi}\cdot\frac{N_f}{p}\cdot K_w : 1$ $\qquad$ $1 : 1.91\,\frac{T_{ph} K_{w1}}{p}$

SOURCE 1—$\sqrt{2}\, I_a \sin\omega t$

SOURCE 2 — $I_f \sin\omega t$

FIG. A 2 a

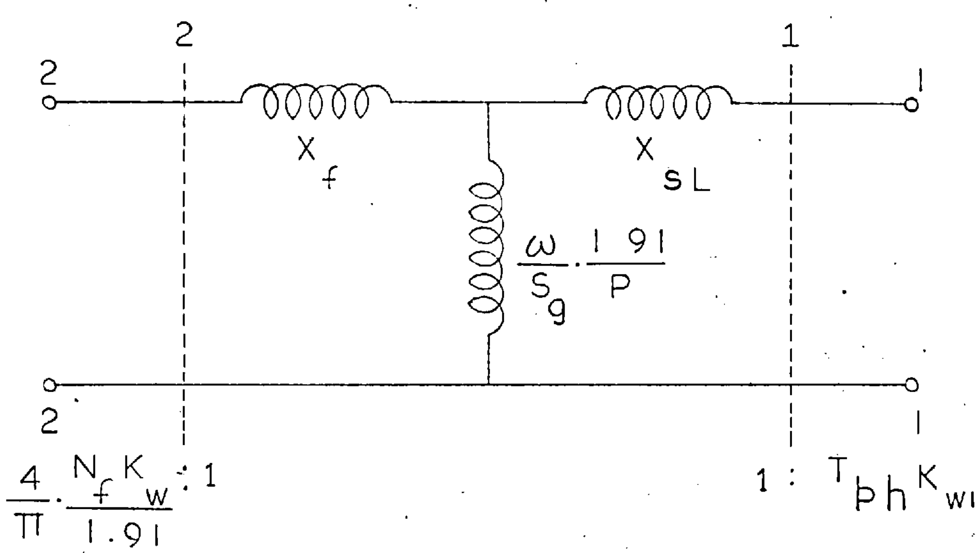

$$X_f = \frac{\omega}{S_{sLf}}\cdot\frac{1.91}{P} \quad ; \quad X_{sL} = \frac{\omega}{S_{sL}}\cdot\frac{1.91}{P}$$

SOURCES REMAIN AS IN FIG. A2 a

FIG. A.2 b

has the following magnitude

$$E_1 = \omega \times T_{ph} K_{w1} \times \frac{1}{S_g} \times \frac{F_f}{\sqrt{2}} \qquad \text{A.7}$$

Therefore, if it is required that the equivalent circuit should have the armature voltage as a terminal quantity, the values of various elements in Fig. A.2(a) have to be modified to those shown in Fig. A.2(b). The currents in the 'dynamic analogue' section of Fig. A.2(b) are not equal to the fundamental m.m.f.s in the magnetic circuit. The fundamental flux set up by given currents I_a and I_f is, however, maintained at the value in the magnetic circuit.

To maintain the slot leakage fluxes at their original values, the two reactances are modified to X_{sL} and X_f in Fig. A.2(b). X_{sL} and X_f are given by:

$$X_{sL} = \frac{\omega}{S_{sL}} \times \frac{1.91}{P} \qquad \text{A.8}$$

$$X_f = \frac{\omega}{S_{sLf}} \times \frac{1.91}{P} \qquad \text{A.9}$$

The ideal transformer coupling the analogue to terminals 1-1 in Fig. A.2(b) may now be removed by referring the reactances to the primary side of the transformer. The resulting circuit is drawn in Fig. A.2(c). The turns-ratio of ideal transformer 2 is altered to preserve the relationship between open-circuit voltage and field current. The turns-ratio is also adjusted to directly

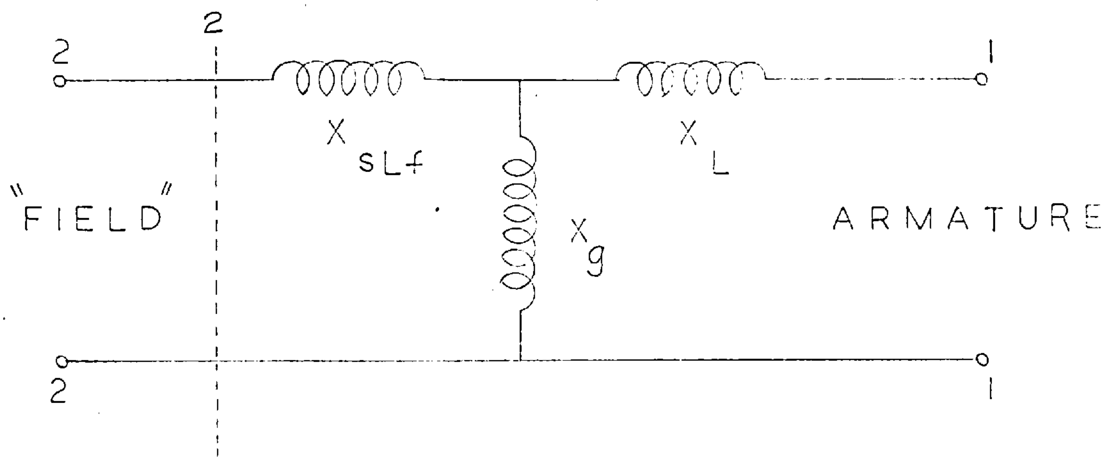

$$\frac{4}{\pi} \cdot \frac{N_f K_w}{2.7} : T_{ph} K_{w1}$$

CURRENT AT TERMINALS 2-2 — $\sqrt{2}\, I_f \sin \omega t$

CONDITIONS AT TERMINALS 1-1 ARE THE SAME AS AT THE TERMINALS OF A ARMATURE PHASE.

$$X_{sLf} = X_f \left(T_{ph} K_{w1}\right)^2 \; ; \; X_L = X_{sL} \left(T_{ph} K_{w1}\right)^2$$

$$X_g = \omega / s_g \cdot \frac{1.91}{p} \cdot \left(T_{ph} K_{w1}\right)^2$$

FIG. A2C EQUIVALENT CIRCUIT OF THE CYLINDRICAL-ROTOR MACHINE relate the field current I_f to the r.m.s. open-circuit voltage. This adjustment is the division of the expression for turns-ratio in Fig. A.2(b) by $\sqrt{2}$.

The terminals 1-1 of the equivalent circuit of Fig. A.2(c) can now be properly termed as the "armature" terminals. The voltage across terminals 2-2 has no significance in as far as the actual field winding is concerned. However, the current at terminals 2-2 being the same as the actual field current, the terminals can be termed the "field" terminals.

Reactance X_{sL} in Fig. A.2(b) has a value such that the voltage drop across it is equal to the slot leakage flux associated with an armature phase of the machine. Therefore, when the analogue represents a machine having a single-layer armature winding, or a double-layer winding with full-pitch coils, the voltage drop across X_L in Fig. A.2(c) is less than the actual voltage drop due to slot leakage flux by the factor K_{w1}. When the winding is of the fractional-pitch type, some of the slots contain conductors belonging to different phases. The above relationship between the two voltage drops has to be modified to take this factor into account. If reactance X_L is made equal to the actual armature slot leakage reactance, the voltage drop across the corresponding reactance ω/S_{sL} in Fig. A.1(b) becomes larger than the slot leakage flux associated with an armature phase. The representation of the actual slot leakage flux in various sections of the armature core by the reluctance S_{sL} [Fig. A.1(a)] is only approximate. Consequently little additional error is involved in choosing this reluctance so as to make X_L in Fig. A.2(c) equal to the actual slot leakage reactance. The reactance X_L has to be increased to include the overhang and differential leakage components of armature reactance. The total leakage reactance of an armature phase is denoted by X_{La}.

Under normal operating conditions, no voltage is induced in the field winding by the field leakage flux. Therefore reactance X_f in Fig. A.2(b) can be chosen such that the voltage drop across it represents the slot leakage flux associated with the field winding.

The turns-ratio of the ideal transformer in Fig. A.2(c) is equal to the ratio of armature and field currents obtained by equating the expressions for F_a and F_f.

APPENDIX B

The impossibility of determining explicitly the parameters of the equivalent Pi circuit

B1 Basic approach to the determination of an explicit value of n

The fact that the turns-ratio associated with a non-linear Tee circuit can be determined explicitly suggests, at first sight, that an explicit value of n could also be determined from terminal measurements on the Pi circuit of Fig. 3.3(P. 81). It would appear that this value of n can be obtained by utilising the non-linear nature of reactances X_1' and X_2' as an additional condition. The condition that must be satisfied is that the reactance X_1' (or X_2') must have the same value at a given voltage across its terminals, regardless of whether the voltage is applied across it as in Fig. 3.3 or is induced in it as in Fig. 3.4. The values of reactance X_1' under these two test conditions are given by the following expressions.

$$X_1' = \frac{V_1}{I_1 - \frac{(V_1 - nV_2)}{X_3}} \qquad \text{B.1}$$

and

$$X_1' = \frac{V_1' \ (= V_1)}{\frac{(nV_2' - V_1')}{X_3}} \qquad \text{B.2}$$

Equating the currents in the above expressions, we have

$$I_1 - \frac{(V_1 - nV_2)}{X_3} = \frac{(nV_2' - V_1')}{X_3}$$

or $$X_3/n = \frac{(V_2' - V_2)}{I_1} \qquad \text{B.3}$$

Equation B.3 may also be expressed as

$$X_3/n = \frac{(V_{d2} + V_{d1})}{I_1} \qquad \text{B.4}$$

where $V_{d2} = (V_2' - V_1)$ and $V_{d1} = (V_1 - V_2)$

Both X_3 and n are constant quantities. Therefore the relationship (between the terminal quantities) contained in equation B.3 can be satisfied by a number of Pi circuits with various values of X_3 and n. However, all these values would be in the constant ratio given by equation B.3. An expression similar to equation B.3 can be derived by equating the two expressions for reactance X_2'. It then follows that a number of Pi circuits can be derived from the characteristics obtained from open-circuit tests on the actual Pi circuit. All these Pi circuits would be equivalent in so far as the reactances measured at their terminals are concerned. All other terminal tests on the actual circuit are essentially similar to the open-circuit tests. Hence an explicit determination of the parameters of the Pi circuit by terminal tests on the circuit is not possible.

B2 Experimental Verification

Tests were performed on a Pi circuit formed by two iron-cored reactors and an air-cored reactor. The iron-cored reactors employed consisted of two similar "Foster Experimental Transformer" cores.[41] Each of these cores was wound with a coil of 100 turns having a resistance of 0.1ohm. The terminal characteristics of the reactors are shown in Fig. B.1(a).

A variable air-cored reactor formed the reactance X_3. This reactor was one out of the set of three similar air-cored reactors described in section 4.3.3. (P 91). The sections of the two coils forming the reactor and the two coils themselves were connected in parallel. The mutual inductance between the two coils was adjusted to obtain a total reactance of 2 ohms at the terminals of the reactor. The resistance measured at the terminals of the reactor was 0.09 ohm.

The terminals of the coils placed on the two "experimental transformer" cores were connected to the terminals of the air-cored reactor in the manner shown in Fig. B.1(b). The "actual" turns-ratio of a hypothetical ideal transformer placed between terminals 2-2 and the terminals of the coil on core 2 was therefore unity.

The variable voltage supply required for the tests was derived from a "Variac" auto-transformer. The

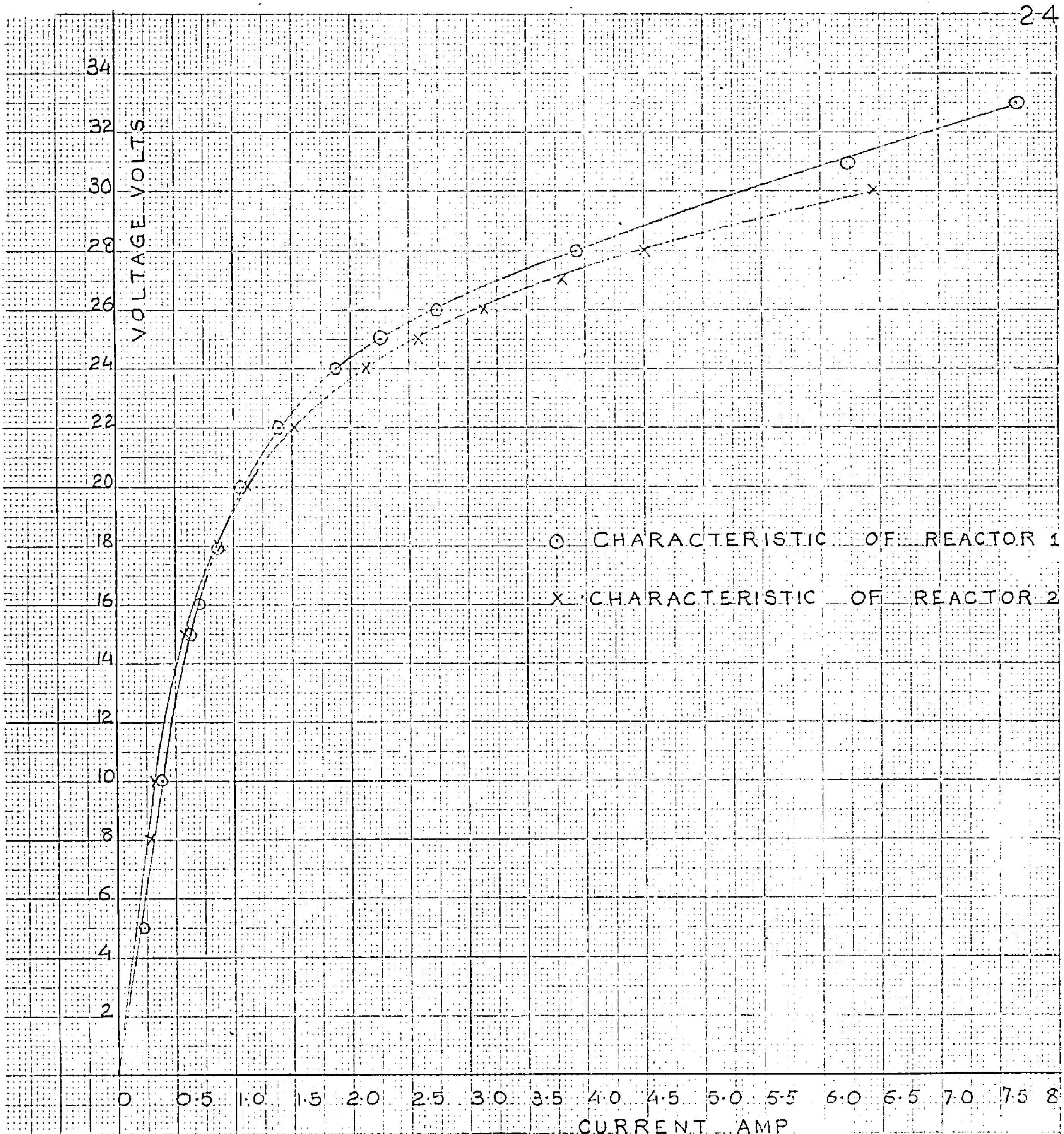

FIG. B1a CHARACTERISTICS OF THE SATURABLE REACTORS OF THE PI CIRCUIT

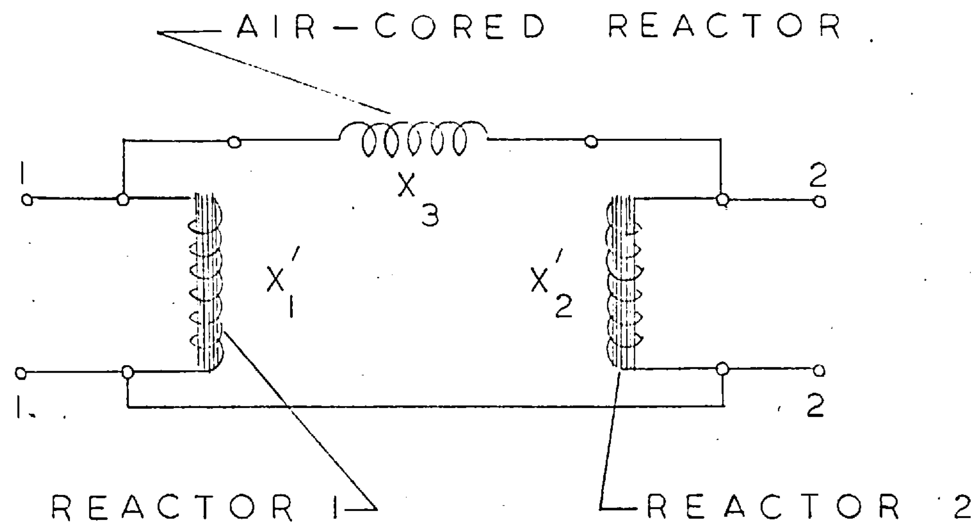

FIG. B1b ARRANGEMENT OF THE PI CIRCUIT.

specifications of this transformer are given in section 4.3.2 of chapter 4. The fundamental components of various voltages were measured with the 'Radiometer' wave-analyser.[35] The currents at the terminals of the Pi circuit were measured with a precision multi-range moving-iron meter capable of measuring currents upto 15 amp to within $\frac{1}{2}$ per cent of the maximum value of the range.

B3 Value of X_3/n of the Pi circuit

Open-circuit tests as per Figs. 3.3 and 3.4 were performed on the Pi circuit. For better accuracy, the fundamental difference voltages V_{d1} and V_{d2} (equation B.4) were directly measured. These voltages and the current I_1 are plotted in Fig. B.2 as functions of the fundamental voltage V_1. At low values of V_1, both the difference voltages and the current are small. The reactance X_3/n calculated from such values of V_{d1}, V_{d2} and I_1 is consequently considerably influenced by experimental errors. Therefore only the values of V_{d1}, V_{d2} and I_1 for voltage V_1 above 12 volts are shown in Fig. B.2.

The calculated values of X_3/n are plotted in Fig. B.3 as a function of voltage V_1. The value of X_3/n = 2.02 ohms obtained for V_1 below 18 volts is in good agreement with the actual value of X_3 = 2.0 ohms. The decrease in X_3/n at higher values of V_1 can be explained as follows.

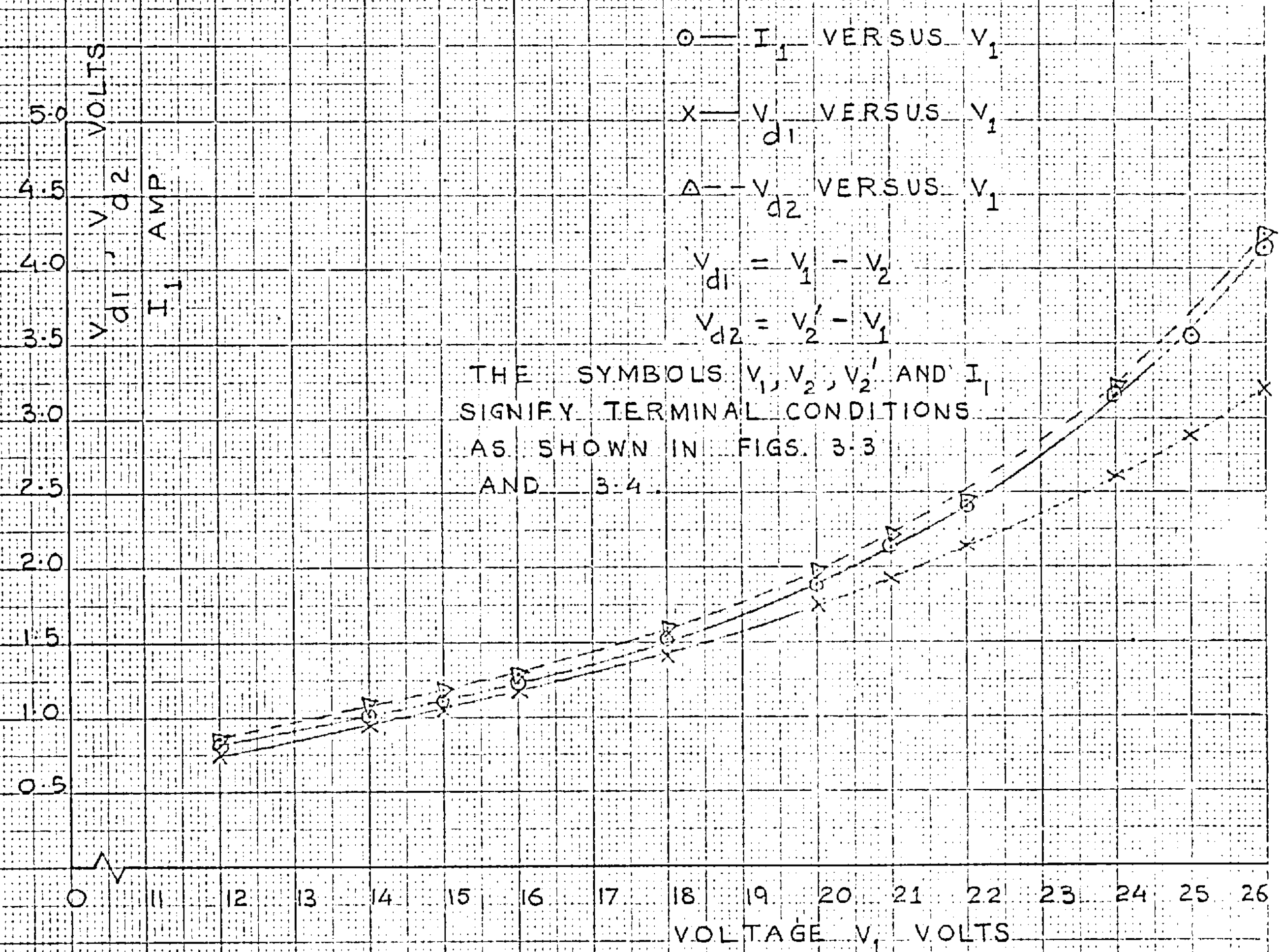

FIG B2 RESULTS OF TESTS ON THE PI CIRCUIT

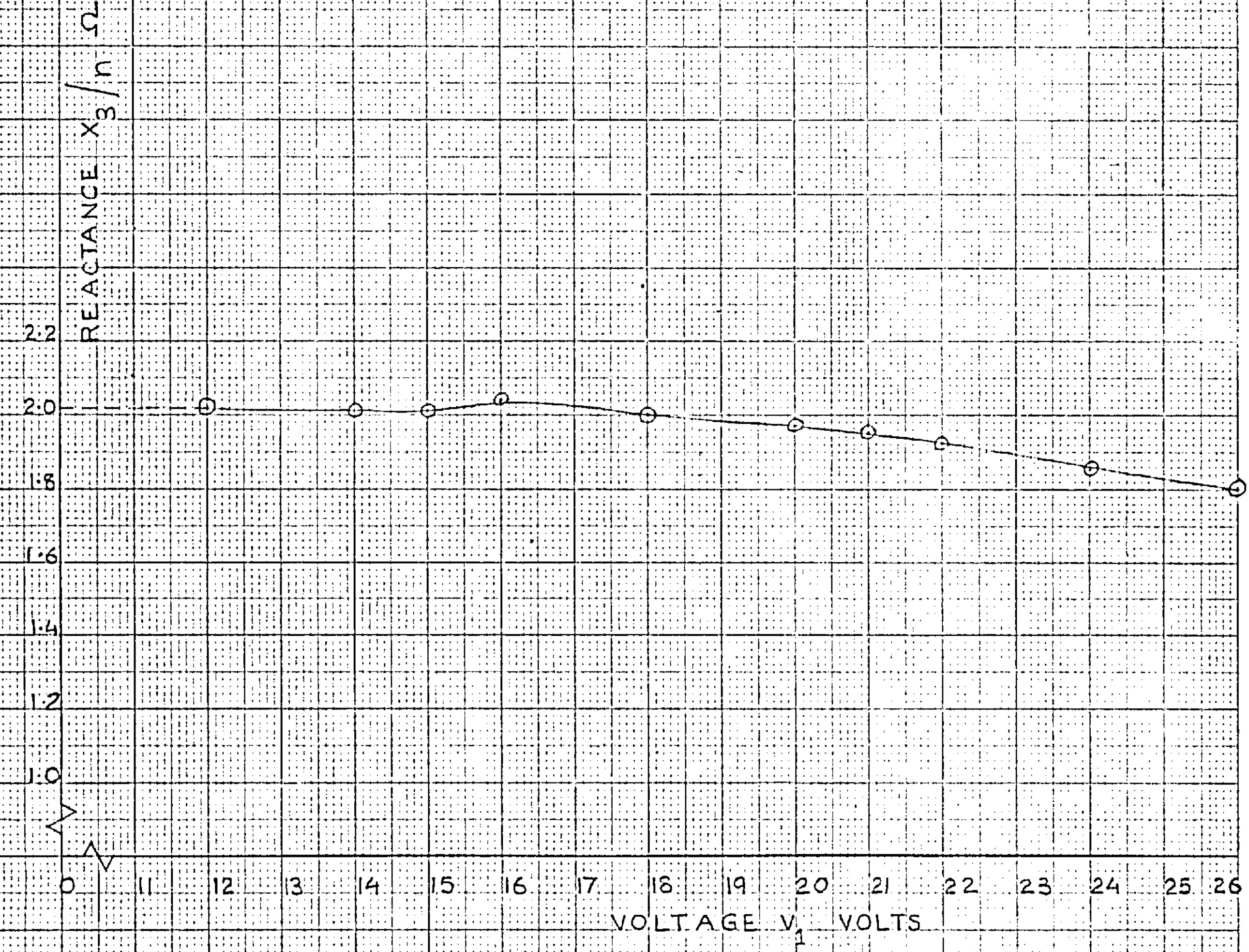

FIG. B3 REACTANCE X_3/n OF THE PI CIRCUIT

As shown in reference 21, the fundamental reactance of a non-linear reactor depends not only on the fundamental component of the voltage across its terminals but also on the waveform of this voltage. For a given fundamental voltage, the reactance is least when the terminal voltage is sinusoidal and maximum when the current through the reactor is sinusoidal. The waveform of the voltage across reactor 1 can be assumed to be nearly sinusoidal when the circuit is excited as per Fig. 3.3. On the other hand, when the circuit is excited as in Fig. 3.4, the third harmonic voltage drop across X_3 causes the voltage across reactor 1 to be peaked. The current through the reactor is however more sinusoidal for this test condition than when the circuit is excited as in Fig. 3.3. For the same fundamental voltage $V_1'(= V_1)$, the fundamental reactance X_1' is consequently larger for the test condition of Fig. 3.4. The voltage drop V_{d2} is therefore reduced. This reduction in V_{d2} causes a corresponding reduction in X_3/n. The influence of changes in the waveform of the terminal voltage on the fundamental reactance X_1' becomes more pronounced with increasing saturation of reactor 1. The reactance X_3/n in Fig. B.3 therefore progressively reduces as shown.

As pointed out in reference 21, the variation of fundamental reactance with the waveform of the terminal voltage is much reduced if the magnetic state of a reactor is defined by the fundamental current through it. Additional calculations have been performed to illustrate this point. The characteristics of reactor 1 were calculated from equations B.1 and B.2 by employing the values of X_3 = 2.00 ohms and n = 1. These characteristics are shown in Fig. B.4. Graph a relates the fundamental voltage V_1 to the fundamental current given by the denominator of equation B.1. Graph b relates V_1 to the fundamental current given by the denominator of equation B.2. The fundamental reactances obtained by dividing V_1 by the currents at points (i) and (ii) in Fig.B.4 are 12 and 13.6 ohms respectively. The reactances corresponding to points (i) and (iii) are 12 and 12.4 ohms respectively. Thus by defining the magnetic state of reactor 1 by the fundamental current, the difference between the two values of X_1' is considerably reduced.

The above results are presented in a slightly different fashion in Fig. B.5. The graphs drawn in this figure show the values of X_1' at a voltage V_1 of 25 volts. These values have been calculated by employing the ratio X_3/n = 2.0 ohms and various assumed values of n. Graphs a and b show the values based on equations B.1 and B.2 respectively. The voltage V_2' used to calculate the values shown in graph b is the sum of V_1 and the voltage

GRAPH a —⊙ CHARACTERISTIC SHOWING THE VOLTAGE ACROSS REACTOR 1 AS A FUNCTION OF THE CURRENT (THROUGH IT) CALCULATED BY EMPLOYING THE EXPRESSION FOR CURRENT IN EQUATION B1.

GRAPH b---x CHARACTERISTIC SHOWING THE VOLTAGE ACROSS REACTOR 1 AS A FUNCTION OF THE CURRENT (THROUGH IT) CALCULATED BY EMPLOYING THE EXPRESSION FOR CURRENT IN EQUATION B2.

BOTH CHARACTERISTICS ARE BASED ON THE VALUES OF $X_3/n = 2{\cdot}0\,\Omega$ AND $n=1$.

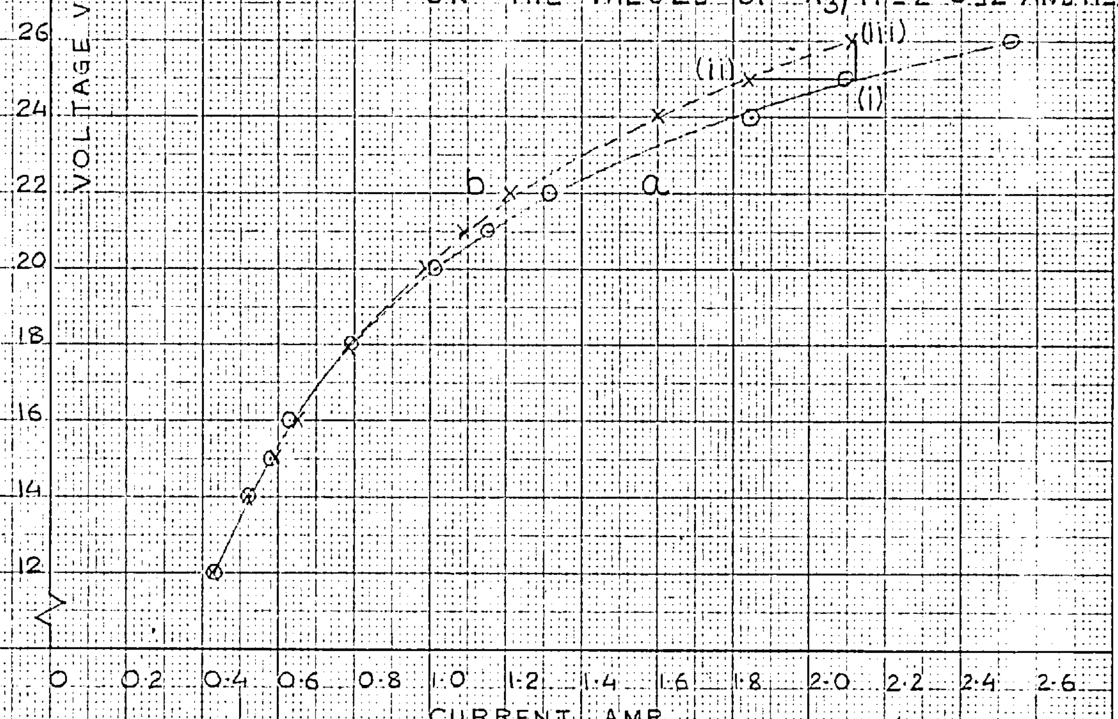

FIG B4 CALCULATED CHARACTERISTICS OF REACTOR 1

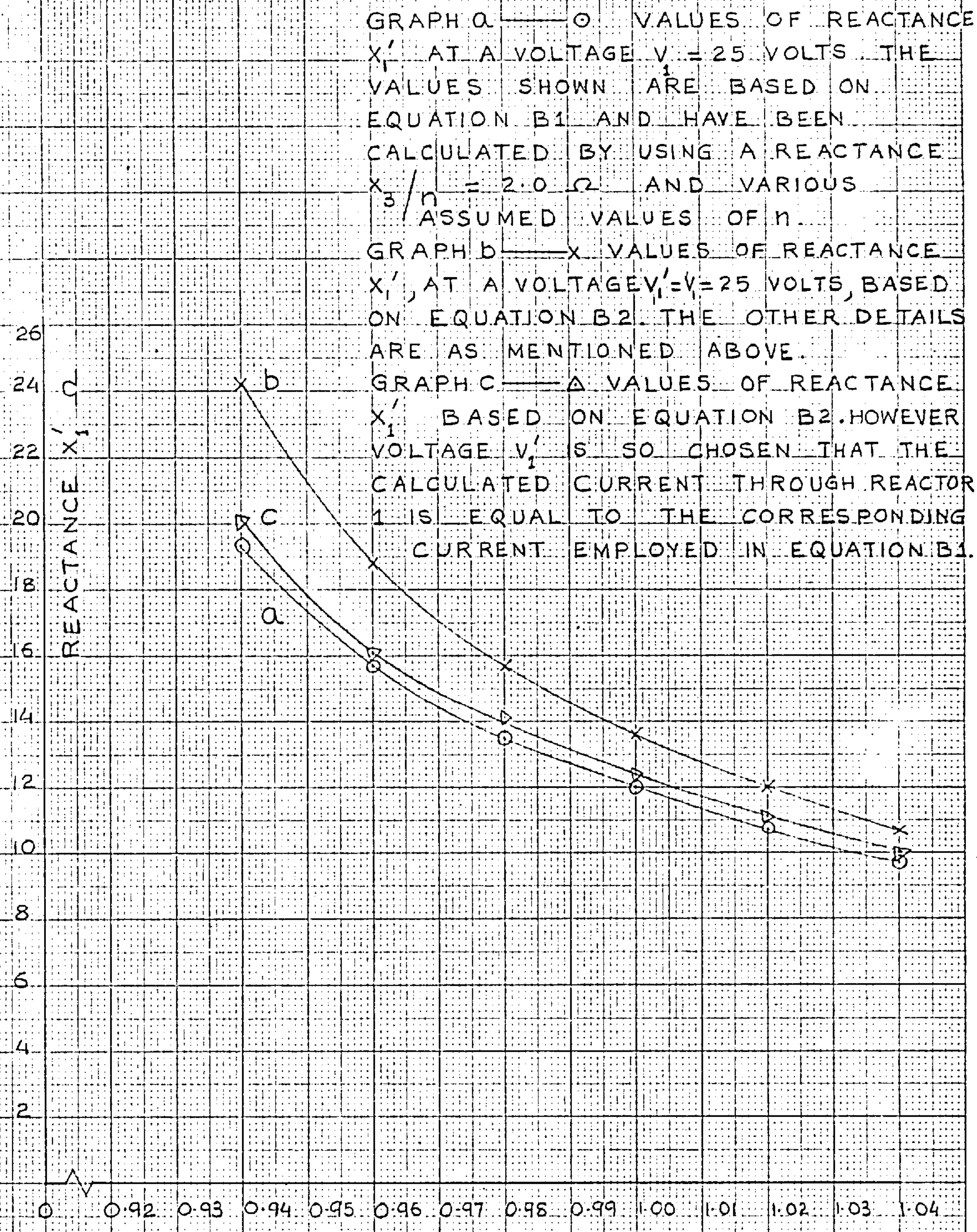

FIG. B5 REACTANCE X_1' OF THE PI CIRCUIT

V_{d2} at a voltage V_1 of 25 volts. Graph c also shows the reactance X_1' obtained from equation B.2. The values of X_1' in graph c have been calculated by employing a voltage V_1' at which the fundamental current through reactor 1 is equal to the corresponding current calculated from the denominator of equation B.1. The definition of the magnetic state of reactor 1 by the fundamental current through it can be seen to result in a more consistent value of X_1'.

The fair agreement that exists between graphs a and c, Fig. B.5 shows that irrespective of the value of n chosen, the same value of reactance X_1' is obtained from both the open-circuit tests on the circuit. This result can be further extended to include all values of the operating voltage V_1. Similar arguments can also be employed to relate the two values of X_2'. By this means it can be seen that a unique value of n can not be determined from terminal tests on the Pi circuit.

APPENDIX C

Some observations on the calculation of the equivalent Tee and Pi circuits from design data

Though the thesis is primarily concerned with the experimental determination of the parameters of the equivalent circuits, some observations on the derivation of these circuits from design data are included in the following sections. These observations refer to a salient-pole synchronous machine. A similar procedure, with some modifications, has to be adopted in the case of a cylindrical-rotor machine.

The equivalent Tee and Pi circuits can be derived from the calculated open-circuit and zero power factor characteristics of the machine. The calculation of these characteristics can be based on the magnetic circuit of Fig. 2.12a (P. 63). Owing to the complex nature of the magnetic system of the machine, the open-circuit and zero power factor characteristics can be only approximately calculated from design data. The calculation of these characteristics amounts to little more than the determination of the total ampere-turns required to establish a given fundamental flux in the air-gap. One of the difficulties in an exact calculation of these ampere-turns is that the distribution of air-gap flux density is not known. Hence the total flux corresponding to a given fundamental flux can not be calculated. Consequently the ampere-turns required by various parts of the magnetic circuit can not be exactly determined. Another factor which has been mentioned previously is that the mutual flux follows paths of various lengths in the stator core (and in the rotor core of a cylindrical-rotor machine). This factor also influences the distribution of air-gap flux density.

Considering the machine on open-circuit, the m.m.f. required to establish a given fundamental air-gap flux may be approximately calculated as follows. It can be assumed that the reluctance of all the flux paths in the stator core is identical. The field m.m.f. is determined by considering a flux path passing through the polar-axis. For an assumed value of B_g, the actual air-gap flux-density at the polar-axis, the m.m.f. required by a tooth located at the polar-axis is calculated on the basis of the flux contained in a slot-pitch. The flux density in this slot-pitch is equal to B_g. The presence of parallel magnetic paths through the adjoining slots is taken into account in the calculation of the m.m.f. The m.m.f. required by the air-gap is calculated on a similar basis, using Carter's coefficients to allow for the fringing of flux at the tooth-tips. The m.m.f.s required by the tooth and air-gap are plotted as functions of B_g, as shown in graphs (i) and (ii), Fig. C.1.

The reluctance of all the flux paths through the stator core is assumed to be identical. The flux lines follow nearly similar paths in the pole system. Therefore, the distribution of air-gap flux density can be determined by assuming that the same total m.m.f. is applied along all the flux paths in the stator teeth and in the region of the air-gap inside the pole-arc.[42] For an operating point P in Fig. C.1, the m.m.f. applied along the paths referred to above is represented by the length (EP + EF). This m.m.f. is applied to one such path, the air-gap flux density along which is represented by point Q. The m.m.f. required by a tooth located along this path is represented by DC. Therefore the m.m.f. required by the air-gap is represented by the difference ($\overline{EP + EF}$ - DC). Knowing the air-gap length at the polar-axisand the m.m.f. EP required to establish the flux density corresponding to point P, the length of the air-gap associated with m.m.f. ($\overline{EP + EF}$ - DC) can be calculated. The angular position with respect to the polar-axis at which the length of the air-gap is equal to this calculated length is determined from a knowledge of the pole-profile. As a reasonable approximation, the pattern of the fringe flux outside the pole-arc can be assumed to be unaffected

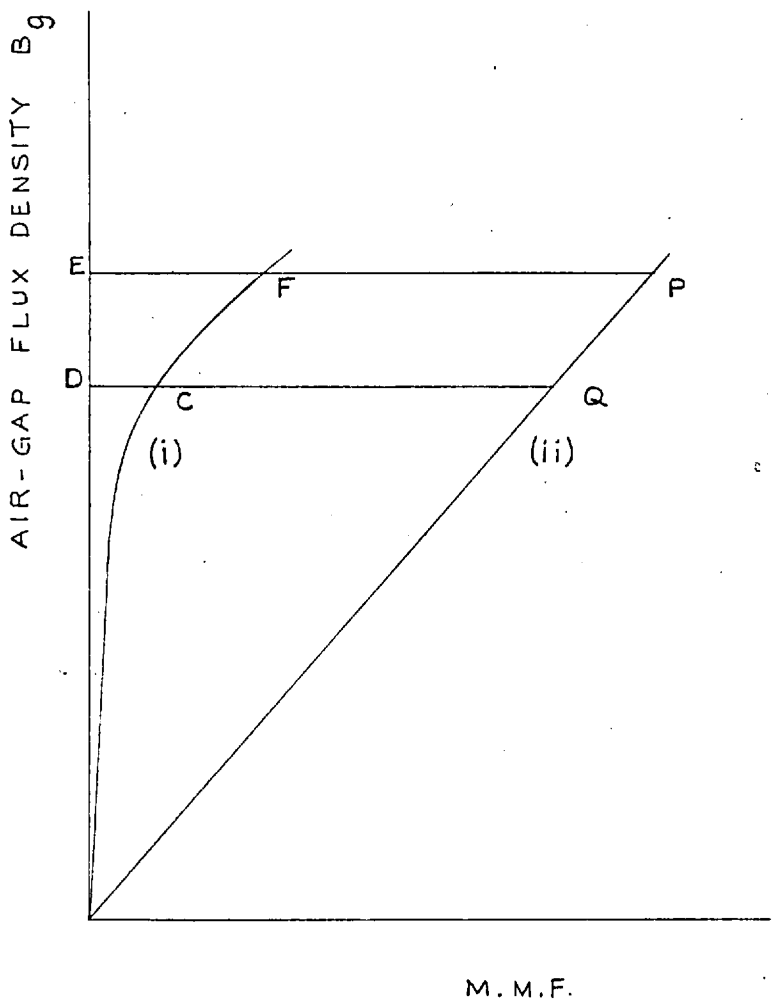

(i) M.M.F REQUIRED BY THE TEETH

(ii) M.M.F REQUIRED BY THE AIR-GAP

FIG. C1 M.M.F REQUIRED BY THE TEETH AND AIR-GAP by saturation of the magnetic circuit. This pattern is determined from flux plots.[31] The total mutual flux per pole and the fundamental component of this flux may now be calculated. Based on this total flux, the m.m.f. required by the stator core is determined next.

The total flux prevailing at a cross-section at any point on the axis of the pole is the sum of the total mutual flux per pole and the field leakage flux at the section. The distribution of field leakage flux does change with saturation of the field system. For usual calculations, this change is ignored. The distribution of field leakage flux determined from flux plots based on an unsaturated magnetic circuit[31] can then be used to calculate the field leakage flux at any section. The m.m.f. required by the pole is obtained on the basis of this distribution of leakage flux. An equivalent leakage flux linking the entire field winding could also be determined from this distribution of field leakage flux.

Using a number of assumed values of B_g, calculations performed as above yield the magnetisation characteristics of the machine. For the unsaturated machine, the coefficients describing the distribution of air-gap flux established by the direct-axis armature m.m.f. alone can be most simply calculated by employing the constants given in reference 31. These coefficients and the coefficients describing the flux distribution due to field m.m.f. alone may be employed to determine the effective turns-ratio. The reactances of the equivalent Tee circuit of the unsaturated machine are calculated by a method similar to that outlined in appendix A. This circuit is transformed to yield the corresponding Pi circuit.

The zero power factor characteristics could be calculated by a procedure similar to that described above. A simplification can be adopted for obtaining approximate equivalent circuits. This simplification consists in neglecting the influence of changes in the distribution of air-gap flux density. Calculations are then based on the distribution of air-gap flux density that prevails at the same fundamental flux in the machine on open-circuit.

The reactance X (section 5.6.1) is determined by employing the expression derived by Kilgore.[40] This reactance can be directly used to derive a Pi circuit, ignoring the different distributions of the armature and field windings. The details of this procedure follow from the discussion in section 5.6.1. The saturation characteristics of the reactances of the Pi circuit can be readily derived from the calculated open-circuit and zero power factor characteristics.

The procedure for calculating the open-circuit characteristic outlined in the previous paragraphs is based on the most simple approach. For closer accuracy, the influence of the different paths of flux in the stator core on the distribution of air-gap flux density has to be considered. The problem at once becomes complicated and only approximate solutions are possible.